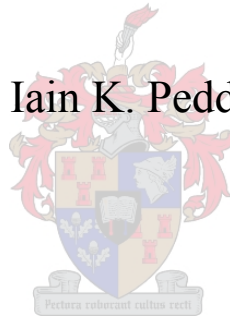


Acceleration Based Manoeuvre Flight Control System for Unmanned Aerial Vehicles

Iain K. Peddle



Dissertation presented for the degree of Doctor of Philosophy in Engineering at
Stellenbosch University

Promoter: Prof. T. Jones

December 2008

Declaration

By submitting this dissertation electronically, I declare that the entirety of the work contained therein is my own, original work, that I am the owner of the copyright thereof (unless to the extent explicitly otherwise stated) and that I have not previously in its entirety or in part submitted it for obtaining any qualification.

Date: 1 September 2008

Copyright © 2008 Stellenbosch University

All rights reserved

Abstract

A strategy for the design of an effective, practically feasible, robust, computationally efficient autopilot for three dimensional manoeuvre flight control of Unmanned Aerial Vehicles is presented. The core feature of the strategy is the design of attitude independent inner loop acceleration controllers. With these controllers implemented, the aircraft is reduced to a point mass with a steerable acceleration vector when viewed from an outer loop guidance perspective. Trajectory generation is also simplified with reference trajectories only required to be kinematically feasible. Robustness is achieved through uncertainty encapsulation and disturbance rejection at an acceleration level.

The detailed design and associated analysis of the inner loop acceleration controllers is carried out for the case where the airflow incidence angles are small. For this case it is shown that under mild practically feasible conditions the inner loop dynamics decouple and become linear, thereby allowing the derivation of closed form pole placement solutions. Dimensional and normalised non-dimensional time variants of the inner loop controllers are designed and their respective advantages highlighted. Pole placement constraints that arise due to the typically weak non-minimum phase nature of aircraft dynamics are developed.

A generic, aircraft independent guidance control algorithm, well suited for use with the inner loop acceleration controllers, is also presented. The guidance algorithm regulates the aircraft about a kinematically feasible reference trajectory. A number of fundamental basis trajectories are presented which are easily linkable to form complex three dimensional manoeuvres. Results from simulations with a number of different aircraft and reference trajectories illustrate the versatility and functionality of the autopilot.

Key words: Aircraft control, Autonomous vehicles, UAV flight control, Acceleration control, Aircraft guidance, Trajectory tracking, Manoeuvre flight control.

Opsomming

'n Strategie vir die ontwerp van 'n effektiewe, prakties haalbaar, robuuste, rekenkundig effektiewe outoloods vir drie dimensionele maneuer vlugbeheer van onbemande vliegtuie word voorgestel. Die kerneienskap van die strategie is die ontwerp van oriëntasie-onafhanklike binnelus-versnellingbeheerders. Hierdie beheerders stel die navigasie buitelus in staat om die voertuig as 'n puntmassa met 'n stuurbare versnellingsvektor te beskou. Trajekgenerasie is ook vereenvoudig deurdat verwysingstrajekte slegs kinematies haalbaar hoef te wees. Robuustheid word verkry deur onsekerhede en versteuringsverwerping op 'n versnellingsvlak te hanteer.

Die gedetailleerde ontwerp en saamhangende analise van die binnelus versnellingsbeheerders word uitgevoer vir die geval waar die invalshoeke klein is. Dit word aangetoon dat, onder praktiese omstandighede, die binnelus dinamika ontkoppel kan word en lineêr word, wat die afleiding van geslotevorm poolplasingoplossings toelaat. Dimensionele en genormaliseerde, nie-dimensionele tydvariante van die binnelusbeheerders word ontwerp en hul onderskeidelike voordele word uitgewys. Poolplasing beperkings, wat ontstaan as gevolg van die tipiese geringe nie-minimum fasegedrag van voertuigdinamika, word ontwikkel.

'n Gepaste generiese, voertuig onafhanklike navigasiebeheer algoritme vir gebruik saam met die binnelus-versnellingsbeheerders word voorgestel. Die voertuig word om 'n kinematies haalbare verwysingstrajek deur hierdie navigasie algoritme gereguleer. 'n Aantal fundamentele trajekte word voorgestel wat maklik gekombineer kan word om komplekse drie dimensionele maneuvres te vorm. Die veelsydigheid en funksionaliteit van die outoloods word deur simulasiresultate met 'n verskeidenheid voertuie en verwysingstrajekte gedemonstreer.

Slutelwoorde: Vliegtuigbeheer, Outonome voertuie, Onbemande vliegtuig vlugbeheer, Versnellingsbeheer, Trajekvolging, Maneuver vlugbeheer.

Acknowledgements

I would like to extend my gratitude to the following people/organisations for their contributions towards this dissertation,

- Prof. Thomas Jones for his support, guidance and advice throughout the course of this project. Your work ethic is inspiring and your friendship is also very much valued.
- My lovely wife Laura for listening and pretending to understand! Thank you for being there to support me through the tough times and rejoice with me in the good times. You have helped me unbelievably in this project.
- My mum, dad and sister, for the support network and loving family environment that has allowed me to achieve all that I have today.
- All the UAV research students for the constructive, friendly, highly enjoyable research environment they have played a part in creating. In particular to Steven, Deon, Rudi, Ruan and Bernard for the feedback they provided when applying the algorithms of this thesis to their specific Masters projects. Also to Wihan, A.M. and Jeanne Marie for their help in translating the abstract.
- The UAV research funding partners, in particular Armscor for their financial support, and the CSIR for their variable stability aircraft concept that served as a particularly interesting application of this thesis work.
- Prof. Garth Milne who sadly passed away in May 2007 for his invaluable practical insights into aircraft dynamics.
- All of my friends for distracting me from my work when I really needed to be and also when I didn't!

Contents

List of Figures	x
Nomenclature	xiii
Chapter 1 – Introduction	1
1.1 Background	1
1.1.1 History of UAVs	1
1.1.2 Motivation for a manoeuvre autopilot	2
1.1.3 Manoeuvre autopilot research at Stellenbosch University	3
1.2 Manoeuvre autopilot discussion	4
1.2.1 Literature study	4
1.2.2 A novel approach	6
1.3 Thesis overview	7
Chapter 2 – Manoeuvre Autopilot Architecture	9
2.1 Initial discussion and fundamental thoughts	9
2.2 Six degree of freedom equations of motion	11
2.2.1 Point mass dynamics	11
2.2.2 Rigid body rotational dynamics	13
2.2.3 Forces and moments	16
2.2.4 Summary of equations of motion	18
2.3 Development of the manoeuvre autopilot architecture	19
2.3.1 Initial formulation of the manoeuvre autopilot	20
2.3.2 Addressing the conditions required by the autopilot	22
2.3.3 Estimation of the states required by the autopilot	24
2.3.4 Summary of the manoeuvre autopilot architecture	25
2.4 Conclusion	26
Chapter 3 – Small Incidence Angle Simplifications	27
3.1 Force and moment model	27
3.1.1 Aerodynamic model	28
3.1.2 Thrust model	30
3.1.3 Gravitational model	31
3.2 Towards linearisation and decoupling of the dynamics	32
3.2.1 Trigonometric simplifications	32
3.2.2 Thrust coupling simplifications	34
3.2.3 Analysing the coupling of lift into drag	35
3.2.4 Summary of simplified dynamics	38
3.3 Handling the inertial cross coupling terms	38

3.3.1 Static inversion of the inertial cross coupling terms	39
3.3.2 Direct force feed-through analysis	40
3.4 The linear decoupled rigid body rotational dynamics.....	43
3.4.1 Normal dynamics and the Short Period mode.....	45
3.4.2 Lateral dynamics and the Roll/Dutch-Roll modes	45
3.5 Conclusion	46
<u>Chapter 4 – Inner Loop Controllers: Axial and Normal Dynamics</u>	48
4.1 Axial specific acceleration controller.....	48
4.2 Normal specific acceleration controller	51
4.2.1 Natural normal specific acceleration dynamics	52
4.2.2 Analysis of the NMP dynamics case	54
4.2.3 Frequency bounds on the normal specific acceleration controller	59
4.2.4 Normal specific acceleration controller design.....	61
4.2.5 Placing the closed loop poles	63
4.2.6 NNDT normal specific acceleration controller design.....	65
4.2.7 Integrator pole placement.....	69
4.3 Conclusion	70
<u>Chapter 5 – Inner Loop Controllers: Lateral Dynamics</u>	71
5.1 Analysis of natural lateral dynamics	71
5.1.1 Aileron to roll rate transfer function.....	73
5.1.2 Rudder to yaw rate transfer function.....	74
5.1.3 Rudder to lateral specific acceleration transfer function.....	75
5.1.4 Summary of results	75
5.2 Roll rate controller	77
5.2.1 Roll rate controller design	77
5.2.2 Selection of the closed loop poles	78
5.2.3 NNDT roll rate controller design	78
5.2.4 Integrator pole placement.....	79
5.3 Lateral specific acceleration controller.....	80
5.3.1 Natural lateral specific acceleration dynamics.....	80
5.3.2 Lateral specific acceleration controller design.....	84
5.3.2.1 Directional stability augmentation	85
5.3.2.2 Lateral specific acceleration regulation.....	87
5.3.3 Selection of the closed loop poles	88
5.3.4 NNDT lateral specific acceleration controller design	89
5.4 Conclusion	93
<u>Chapter 6 – Outer Loop Guidance Controllers</u>	95
6.1 Investigation of the guidance level dynamics.....	95
6.2 Guidance controller design strategies	103
6.2.1 Receding horizon predictive control	103
6.2.2 Linearisation and successive linearisation control	104
6.2.3 Specific acceleration matching.....	105

6.3 Specific acceleration matching controller design	105
6.3.1 Normal specific acceleration vector direction controller	108
6.3.1.1 Taking the inner loop roll rate dynamics into account	112
6.3.2 Specific acceleration transformation algorithm	114
6.3.3 Velocity and position controllers	118
6.3.4 Summary	120
6.4 Conclusion	121
Chapter 7 – Reference Trajectories	123
7.1 Reference trajectory dynamics.....	123
7.1.1 Reference trajectories for the SAM guidance controller.....	124
7.2 Building block reference trajectories	127
7.2.1 Straight line flight.....	128
7.2.1.1 Linking the trajectory	129
7.2.1.2 Flight orientation reference vector	131
7.2.2 Vertical arc.....	131
7.2.2.1 Linking the trajectory	133
7.2.2.2 Flight orientation reference vector	137
7.2.3 Horizontal spiral arc	137
7.2.3.1 Linking the trajectory	139
7.2.3.2 Flight orientation reference vector	142
7.3 Conclusion	142
Chapter 8 – Simulation of Example Applications	143
8.1 Manoeuvre control of an aerobatic aircraft.....	144
8.1.1 Application of the manoeuvre autopilot	144
8.1.1.1 Axial specific acceleration controller design.....	145
8.1.1.2 Normal specific acceleration controller design	146
8.1.1.3 Analysis of the lateral dynamics.....	148
8.1.1.4 Roll rate controller design	149
8.1.1.5 Lateral specific acceleration controller design	150
8.1.1.6 The actual closed loop lateral dynamics.....	153
8.1.1.7 Error angle controller design	154
8.1.1.8 Velocity and position controller designs.....	155
8.1.2 Simulation	155
8.1.2.1 Dynamic responses.....	155
8.1.2.2 Reference trajectory flight.....	158
8.1.3 Comments	164
8.2 Stabilisation and control of a variable stability aircraft	164
8.2.1 Application of the manoeuvre autopilot.....	164
8.2.1.1 Axial specific acceleration controller design.....	165
8.2.1.2 Normal specific acceleration controller design	165
8.2.1.3 Analysis of the lateral dynamics.....	168
8.2.1.4 Combined roll rate and error angle controller design.....	169
8.2.1.5 Lateral specific acceleration controller design	169
8.2.1.6 Velocity and position controller designs.....	170
8.2.2 Simulation	171

8.2.2.1 Dynamic responses	171
8.2.2.2 Reference trajectory flight	174
8.2.3 Comments	177
8.3 Transition control of a VTOL aircraft	177
8.3.1 Application of the manoeuvre autopilot	178
8.3.1.1 Axial specific acceleration controller design	179
8.3.1.2 NNDT normal specific acceleration controller design	179
8.3.1.3 Analysis of the lateral dynamics	182
8.3.1.4 NNDT roll rate controller design	182
8.3.1.5 NNDT lateral specific acceleration controller design	184
8.3.1.6 Error angle controller design	186
8.3.1.7 Velocity and position controller designs	187
8.3.2 Simulation	187
8.3.2.1 Dynamic responses	187
8.3.2.2 Reference trajectory flight	190
8.3.3 Comments	195
8.4 Conclusion	195
Chapter 9 – Conclusion	196
9.1 Summary	196
9.2 Contributions to the field	198
9.3 Further research	199
Appendix A – Rigid Body Dynamics	202
A.1 Preliminaries	202
A.1.1 Axis systems, vectors and coordinate vectors	202
A.1.2 The dot and cross product operators	203
A.1.3 Time derivative of a vector	204
A.1.4 Coordinate vector transformations	205
A.1.4.1 A useful special case of the transformation matrix	207
A.1.4.2 Transforming the elements of a cross product matrix	208
A.2 Kinematics	208
A.2.1 The motion of a point through space	208
A.2.2 Attitude parameterisations	211
A.2.2.1 Euler angles	211
A.2.2.2 Quaternions	213
A.3 Kinetics	214
A.3.1 Newton’s laws of motion for mass particles	214
A.3.2 Modelling a rigid body	214
A.3.2.1 Insight into the linear and angular momentum integrals	218
Appendix B – Detailed Derivations	221
B.1 Non-minimum phase system analysis	221
B.2 Normal dynamics	223
B.2.1 Characteristic equation for the poles	224
B.2.2 Characteristic equation for the zeros	224

B.2.3 Normal specific acceleration controller design	225
B.2.4 Deriving the NNDT normal dynamics	229
B.2.5 Characteristic equation for the NNDT poles	230
B.2.6 Characteristic equation for the NNDT zeros	231
B.2.7 NNDT normal specific acceleration controller design	231
B.3 Lateral dynamics	235
B.3.1 Characteristic equation for the poles	235
B.3.2 Aileron to roll rate zeros characteristic equation	236
B.3.3 Rudder to yaw rate zeros characteristic equation	237
B.3.4 Rudder to lateral specific acceleration zeros characteristic equation	238
B.4 Roll dynamics	238
B.4.1 Roll rate controller design	239
B.4.2 Rudder to roll rate disturbance transfer function	240
B.5 Directional dynamics	240
B.5.1 Directional dynamics gravity coupling transfer function	241
B.5.2 Analysis of adverse yaw static inversion	242
B.5.3 Directional stability augmentation	244
B.5.4 Steady state gain from rudder to lateral specific acceleration	247
B.5.5 Deriving the NNDT directional dynamics	248
B.5.6 Characteristic equation for the NNDT poles	250
B.5.7 Characteristic equation for the NNDT zeros	250
B.5.8 NNDT directional stability augmentation	251
B.5.9 NNDT rudder to lateral specific acceleration steady state gain	254

Appendix C – Example Aircraft Data 256

C.1 Aerobatic aircraft	256
C.2 Variable stability aircraft	257
C.3 VTOL aircraft	258

Bibliography 261

List of Figures

Figure 2.1 – Block diagram of the six degree of freedom equations of motion in a form well suited for the design of a manoeuvre autopilot.....	20
Figure 3.1 – Block diagram overview of the manoeuvre autopilot control system to be designed.....	47
Figure 4.1 – Maximum undershoot of a 2 nd order system as a function of the normalised RHP zero frequency for various damping ratios	56
Figure 4.2 – Lower bound on the sensitivity function magnitude as a function of the RHP zero frequency normalised to the natural frequency.....	58
Figure 4.3 – Feasible pole placement region constrained by NMP upper bound and timescale separation lower bound.....	60
Figure 6.1 – Block diagram overview of the SAM guidance controller	121
Figure 8.1 – Picture of the aerobatic aircraft.....	144
Figure 8.2 – Bode magnitude plot of the actual and approximated return disturbance transfer function and its constituents	146
Figure 8.3 – Actual and approximated open loop poles, desired and actual closed loop poles and upper and lower normal specific acceleration frequency bounds	147
Figure 8.4 – Normalised normal specific acceleration controller gains as a function of the RHP zero position normalised to the desired natural frequency.....	148
Figure 8.5 – Open and closed loop rudder coupling gain into roll rate over frequency	150
Figure 8.6 – Desired and actual closed loop directional dynamics	152
Figure 8.7 – Open and closed loop aileron and attitude parameter coupling gains into lateral specific acceleration over frequency	153
Figure 8.8 – Desired and actual closed loop lateral dynamics poles.....	154
Figure 8.9 – Desired and actual closed loop error angle dynamics poles	155
Figure 8.10 – Simulated and expected step responses of inner loop controllers.....	156
Figure 8.11 – Simulated and expected error angle response to a 10 degree error.....	157
Figure 8.12 – Simulated and expected inertial velocity coordinate step responses	157
Figure 8.13 – Simulated and expected inertial position coordinate step responses	158
Figure 8.14 – Aerobatic aircraft reference trajectory	159

Figure 8.15 – Reference trajectory and actual trajectory flown	161
Figure 8.16 – Position and velocity errors relative to the reference trajectory	162
Figure 8.17 – Commanded and actual inner loop signals over the reference trajectory	163
Figure 8.18 – Actuator signals over the reference trajectory	163
Figure 8.19 – Design diagram of Sekwa superimposed on a background	164
Figure 8.20 – Open loop poles and zeros, desired and actual closed loop poles, additional closed loop zero and upper and lower pole placement frequency bounds	167
Figure 8.21 – Simulated and expected step responses of inner loop controllers with the centre of mass in its most forward position.....	172
Figure 8.22 – Simulated step responses of the inner loop normal specific acceleration controller with the centre of mass in various positions.....	173
Figure 8.23 – Simulated and expected error angle response to a 10 degree error.....	173
Figure 8.24 – Simulated and expected step responses of the velocity and position inertial coordinates	174
Figure 8.25 – Variable stability aircraft reference trajectory.....	174
Figure 8.26 – Reference trajectory and actual trajectory flown.....	175
Figure 8.27 – Position and velocity errors relative to the reference trajectory	176
Figure 8.28 – Commanded and actual inner loop signals over the reference trajectory.....	176
Figure 8.29 – Actuator signals over the reference trajectory	177
Figure 8.30 – Schematic diagram of the VTOL aircraft [16].....	178
Figure 8.31 – Corresponding dimensional normal dynamics poles for various velocities.....	181
Figure 8.32 – Corresponding dimensional roll dynamics poles for various velocities.....	183
Figure 8.33 – Corresponding dimensional directional dynamics poles for various velocities.....	186
Figure 8.34 – Simulated and expected step responses of the NNDT inner loop controllers with corresponding dimensional time responses.....	188
Figure 8.35 – Simulated and expected inertial velocity coordinate step responses with roll-to-turn implemented.....	189
Figure 8.36 – Simulated and expected inertial velocity coordinate step responses with skid-to-turn implemented.....	189
Figure 8.37 – VTOL aircraft reference trajectory	190
Figure 8.38 – Reference trajectory and actual trajectory flown.....	191
Figure 8.39 – Position and velocity errors relative to the reference trajectory	192

Figure 8.40 – Velocity magnitude, angle of attack and angle of sideslip over the reference trajectory	193
Figure 8.41 – Commanded and actual inner loop signals over the reference trajectory	194
Figure 8.42 – Actuator signals over the reference trajectory	195

Nomenclature

General

- t, s Time and Laplace variable respectively.
- I, B, W, R Denote the inertial, body, wind and reference axis systems respectively.

Vector and matrix

- i, j, k Basis unit vectors of the superscripted axis system.
- J, A, V, P Jerk, acceleration, velocity and position vectors.
- α, ω Angular acceleration and velocity vectors.
- L, H Linear and angular momentum vectors.
- F, M Force and moment vectors.
- Σ, G Specific and gravitational acceleration vectors.
- DCM, S, T, I_B Direction cosine matrix, cross product matrix, single axis rotation transformation matrix and moment of inertia matrix.

Coordinate vector

- X, Y, Z Axial, lateral and normal force vector coordinates in the subscripted axis system. If the subscript is omitted, body axes is implied.
- A, B, C Axial, lateral and normal specific acceleration vector coordinates in the subscripted axis system. If the subscript is omitted, body axes is implied.
- L, M, N Roll, pitch and yaw moment coordinates in the subscripted axis system. If the subscript is omitted, body axes is implied.
- P, Q, R Roll, pitch and yaw rate of the subscripted axis system with respect to inertial space. When the subscript is omitted, body axes is implied.
- \bar{V}, α, β Velocity magnitude, angle of attack and angle of sideslip.
- P_x, P_y, P_z Inertial axes position coordinates.

$e_{()}^{()}$ DCM parameter. The subscript indicates its position in the DCM matrix while the superscript indicates the axis systems involved in the DCM transformation.

Modelling

\bar{V}_a, ρ, q Airspeed magnitude, air density and dynamic pressure.

S, \bar{c}, b Wing area, mean aerodynamic chord and wing span.

A, e Aspect ratio and Oswald efficiency factor.

L, D, R_{LD} Lift, drag and ratio of lift to drag.

C_{L_0}, C_{m_0} Static lift and pitching moment coefficients.

C_L, C_D, C_y Aerodynamic lift, drag and side force coefficients.

C_l, C_m, C_n Aerodynamic roll, pitch and yaw moment coefficients.

$\delta_A, \delta_E, \delta_R$ Aileron, elevator and rudder control deflections.

T, T_C Thrust variable and thrust command variable.

ε_T, m_T Thrust setting angle and moment arm.

g Gravitational force per unit mass.

$m, I_{()}$ Mass and moment of inertia parameter.

Control

p, z Poles and zeros.

ω_n, ζ, τ Natural frequency, damping ratio and time constant.

$K_{()}, \gamma$ Feedback gain and return disturbance gain.

$S, \Delta C_W$ Sensitivity function and return disturbance transfer function.

k_Q, k_R, k_x, k_y, k_z Non-dimensional constants used in the NNDDT controllers.

r Natural frequency to RHP zero position ratio.

ϕ Error angle.

ε Threshold used in SAM guidance controller to switch between roll-to-turn and skid-to-turn modes.

r_x, r_y, r_z Roll, pitch and yaw radii of gyration.

l_T, l_D, l_N	Effective length to the tail-plane, damping arm length and length to the neutral point. The normalised lengths are denoted with an accent.
l_F, l_D, l_W	Effective length to the fin, damping arm length and weathercock arm length. The normalised lengths are denoted with an accent.

Acronyms

3D	Three Dimensional
DCM	Direction Cosine Matrix
GPS	Global Positioning System
LQR	Linear Quadratic Regulator
LTI	Linear Time Invariant
LTV	Linear Time Varying
MIMO	Multiple Input Multiple Output
NED	North-East-Down
NMP	Non-Minimum Phase
NNDT	Normalised Non-Dimensional Time
NTI	Nonlinear Time Invariant
PI	Proportional-Integral
RHP	Right Half Plane
RHPC	Receding Horizon Predictive Control
RPV	Remotely Piloted Vehicle
SAM	Specific Acceleration Matching
SU	Stellenbosch University
TUAV	Tactical Unmanned Aerial Vehicle
UAV	Unmanned Aerial Vehicle
UCAV	Unmanned Combat Aerial Vehicle
VTOL	Vertical Take-Off and Landing

Chapter 1

Introduction

This chapter begins by providing background information relating to the research presented in this thesis. After a brief history of Unmanned Aerial Vehicles (UAVs) is presented, motivation for the design of a manoeuvre autopilot is provided together with a description of how this type of research fits in with previous research conducted at Stellenbosch University. A literature study investigating manoeuvre autopilot design strategies precedes a brief description of the novel design strategy presented in this thesis. The chapter concludes with an overview of the thesis structure.

1.1 Background

1.1.1 History of UAVs

Depending on the exact definition of UAVs, it is difficult to pinpoint the precise date of their inception. Unmanned balloons loaded with bombs date back long before the Wright Brothers introduced manned flight [1]. However, most historical texts credit the Sperry “Flying Bomb” and the “Kettering Bug” developed during World War One, as the first ‘real’ UAVs [1-3]. These simple UAVs were gyroscope stabilised biplanes programmed to fly a predetermined distance before diving to the earth and exploding.

After World War One, UAV development was quiet until the 1930’s when fear of a second world war once again spurred on development. However, this time UAVs were developed primarily for target practice. These “Target Drones” were typically remotely piloted and thus are more commonly referred to as Remotely Piloted Vehicles (RPVs). The most prominent and feared UAV during World War Two was the German V-1 Buzz Bomb, a small, pulse-jet powered drone pre-programmed to hold a certain altitude and direction before detonation [3]. The USA also operated UAVs during the Second World War in the form of modified B-17s loaded with explosives [4].

The 1950’s and 1960’s saw significant technological advances in aircraft control systems and in turn the development of the legendary Firebee UAV [1,3]. This UAV was used very effectively as a target drone as well as for surveillance during the Cold War and Vietnam.

While USA investments into UAVs slowed after Vietnam, developments in other countries around the world started to rise. Most particularly, the 1970's and 1980's saw Israel pioneer the development of several new UAVs and successfully and effectively integrate these aircraft into their Air Force [1]. This success spurred other countries to emulate Israel's use of UAVs and many of today's modern UAVs such as Hunter, Pioneer and Seeker (South African) are direct derivatives of Israeli Systems [3].

Recent conflicts in Iraq and Afghanistan have provided UAVs and their applications with widespread media coverage. UAVs such as the US Air Force's Predator and Global Hawk, the US Navy's Pioneer (to be replaced by the Fire Scout) and the US Army's Hunter (to be replaced by the Shadow) are all well know. The 1990's also saw the rise of civil applications for UAVs, initially for the purpose of research and now too for government and commercial applications. Typical civil applications include maritime surveillance, law enforcement, search and rescue, and fire monitoring to name but a few.

Recent UAV developments include the introduction of tactical and combat unmanned aerial vehicles (TUAVs andUCAVs respectively). These UAVs are expected to display high levels of autonomy and manoeuvrability for weapons delivery and avoidance of enemy fire. CurrentUCAV and TUAV programmes include among others Boeing's X-45 technology demonstrator, EADS's Barracuda and the French Dassault Neuron. For an overview of current and future mainstream UAV programs see [5].

According to [1], there are estimated to be between 200 and 300 models of UAVs in existence worldwide (depending on the definition of a UAV), operating in at least 41 countries. South Africa's contribution to UAVs is primarily through Denel Aerospace's Seeker II surveillance system and their high speed target drone SKUA, as well as ATE's (Advanced Technologies and Engineering) Vulture system used to perform target detection, localisation and artillery fire adjustment.

1.1.2 Motivation for a manoeuvre autopilot

From a military perspective, according to [4], UAVs are best suited to “dull, dirty and dangerous” missions. Dull missions are those that are long and tedious, where human pilot and aircrew fatigue play a significant role. Dirty missions refer to those that involve investigation of hazardous sites such as after nuclear or chemical fallout. Dangerous missions are those where the risk of loosing a pilot's life is high, such as during suppression of enemy air defences. From a civil perspective UAV missions typically involve surveillance and reconnaissance of some form to serve a particular government or commercial need.

The typical UAV mission types described above, with the possible exception of the “dangerous” military missions, all involve very relaxed flight path trajectories and demand little manoeuvring from the aircraft. As such, classic linearised straight and level flight type

autopilots provide a sufficient degree of autonomy for most UAV missions. In cases where the flight range needs to be extended in altitude and airspeed, simple control techniques such as gain scheduling can be effectively employed without influencing the design strategy. Present day UAVs conducting “dangerous” missions also do not display high levels of autonomous manoeuvrability and are instead either considered disposable (e.g. HARPY by Israel Aircraft Industries) or can be remotely operated by a human pilot in dangerous situations (e.g. Predator).

Future TUAVs and UCAVs are however expected to be highly manoeuvrable and highly autonomous. Furthermore, from a civil perspective, if UAVs are ever to become fully integrated into the lives of humans, they will need to operate autonomously with at least the degree of precision and manoeuvrability offered by a human pilot. This level of autonomy would provide UAVs with the ability to navigate in constrained environments such as over/through complex terrain and even between buildings. Furthermore, high levels of autonomy would also improve safety by allowing UAVs to take evasive action faster and recover from large disturbances that would otherwise have placed them outside of their traditional domain of convergence. Thus it can be seen that there is a very strong drive towards higher levels of flight control autonomy in UAVs.

The desire to significantly improve the flight control autonomy levels of UAVs calls for the design of what will be referred to in this dissertation as a *manoeuvre autopilot*. A manoeuvre autopilot should be capable of adequately guiding an aircraft through precision manoeuvres such as landing approaches, high bank angle turns, aggressive climbs and aerobatic manoeuvres. This capability would allow the UAV to navigate effectively in three dimensional (3D) space and in so doing make better use of the airframe and allow tasks to be completed more efficiently. From a military perspective this type of autopilot would for example allow a UCAV to avoid threats by performing standard aerobatic type evasive manoeuvres. Improved levels of safety, capability, precision and efficiency would also make UAVs an even more attractive technology for civil applications.

1.1.3 Manoeuvre autopilot research at Stellenbosch University

To place this research in context with the ongoing UAV research at Stellenbosch University (SU), a short review of SU’s UAV activities is provided with the focus steered towards work done on manoeuvre autopilot design.

SU’s UAV activities formally began in 2001 with a project aimed at automating the hover flight of a small electrically powered unmanned helicopter [6]. The following year research into autonomous flight of a methanol powered fixed wing aircraft began [7,8]. Helicopter, fixed wing and the associated modelling, simulation and avionics systems research continued over the years [9-15] together with a new branch of research into control of experimental aircraft. These experimental aircraft include a tail-sitter Vertical Takeoff and Landing (VTOL)

aircraft [16,17] and a coaxial, counter rotating, thrust vectored ducted fan [18].

On the fixed wing side, after practical autonomous waypoint navigation was demonstrated in [7,8], the conventional flight autopilot was successfully extended to handle automatic takeoff and landing too [11,12]. A second branch of fixed wing UAV research began in 2004 with the aim of advancing the state of the art in flight control through the design of an autopilot capable of performing aerobatic manoeuvres. Research by [13] led to the successful practical demonstration of autonomous aileron roll, loop and Immelmann manoeuvres. However, the controller designed in [13] involved Receding Horizon Predictive Control (RHPC) of the linearised aircraft model about the reference trajectory and as such was very computationally demanding. Furthermore, the use of an optimisation based control algorithm made the selection of appropriate weights in the cost function particularly difficult. Fine tuning of these weights was required for each trajectory. Trajectory design was also complicated by having to find a reference trajectory for every single state for a particular manoeuvre. The generation of mathematically feasible reference trajectories then became an optimal control task of its own with a potential complexity greater than that of the regulation problem itself. This complexity was avoided in [13] by using near feasible trajectories and considering trajectory errors as disturbances to be rejected by the regulation control law.

With regard to the history of UAV research at SU, the manoeuvre autopilot research presented in this thesis stems from the desire to advance the state of the art in UAV flight control. More specifically, it is desired to develop a flight control algorithm capable of guiding a UAV through the full kinematic flight envelope while at the same time addressing outstanding issues such as controller complexity, computational burden, ease of reference trajectory generation and robustness. The results presented in this thesis are seen to adequately address all of these issues and provide an effective, elegant solution to the 3D manoeuvre flight control problem for a very wide class of UAVs.

1.2 Manoeuvre autopilot discussion

Given the desire to design a manoeuvre autopilot, this section begins by providing a literature review on the subject of manoeuvre autopilot design strategies. Thereafter, a brief description of the novel manoeuvre autopilot design strategy of this thesis is presented.

1.2.1 Literature study

The design of autopilots for conventional flight UAVs is a mature field of research with a myriad of published control system design strategies [8,19-24]. However, common to most of these design strategies is linearisation about a trim flight condition and the use of basic steady state near trim flight kinematic relationships to simplify control law design [19,20]. To ensure stability this class of controllers typically imposes significant limitations on the aircraft's allowable attitude, velocity and altitude deviations.

Gain scheduling is a commonly used method to expand the airspeed and altitude flight envelopes of aircraft without changing the control system design strategy above [19,25]. Gain scheduling involves linearisation of the plant model at a number of different operating points and interpolation of the feedback gains for flight conditions between these points. Variations exist on the number of operating points to use and the interpolation methods to employ [25]. Operating points are however usually limited to different airspeed and altitude combinations since these two variables change slowly relative to the aircraft's flight dynamics i.e. a timescale separation exists.

It is however also feasible to linearise the aircraft model about more complex manoeuvre trajectories and again apply gain scheduling. This is equivalent to converting a problem involving control of a nonlinear plant to one involving control of a Linear Time Varying (LTV) one. Great care needs to be taken when using gain scheduling in this manner since ensuring that the linearised system's poles remain within the left half of the s-plane at all times is not a sufficient condition for stability of a LTV system [26]. Thus, although gain scheduling is desirable from a simplicity of design point of view, the time consuming nature of the design and the fact that it is typically only useful at extending the airspeed and altitude flight envelopes, make it neither an effective nor elegant method for the design of a manoeuvre autopilot.

Dynamic inversion [26] has recently become a popular design strategy for manoeuvre flight control of UAVs and manned aircraft [27-30]. However, when directly applied, this promising strategy suffers from two major drawbacks. Firstly, due to the open loop nature of the inversion and the uncertainty associated with aircraft dynamics, controller robustness is a concern. This concern is explicitly addressed in [30] and [31], through the design of a structured singular value synthesis outer loop controller. The second drawback arises due to the slightly Non-Minimum Phase (NMP) nature of most aircraft dynamics. In this case, direct application of dynamic inversion not only results in an impractical controller with large counterintuitive control signals [30,32], but also in undesired internal dynamics whose stability must be investigated explicitly [26]. Although techniques to address these issues have been developed [32,33], dynamic inversion may not necessarily provide a very practical solution to the 3D flight control problem and should ideally only be used in the presence of relatively certain minimum phase dynamics.

Receding Horizon Predictive Control (RHPC) has also been theoretically applied to the manoeuvring flight control problem [34-36], and similarly to missile control [37]. This control approach involves solving for the control input that minimises a cost function of state and control errors (actual relative to feasible reference trajectory provided) over a finite time horizon while adhering to any constraints. The optimal control input is then utilised for a finite time period (typically far less than the horizon) before the process is repeated again. Feedback is incorporated into the controller by beginning each optimisation from the aircraft's

measured/estimated state. The controller thus allows all aircraft and kinematic nonlinearities to be taken into account including hard constraints such as actuator clipping and slew rates limits.

Although this strategy is conceptually very promising and has been successfully practically applied to the slower dynamics plants of the process control industry [38,39], it is less popular in the field of aircraft control due to the associated computational burden. This is particularly so in the field of low cost UAV automation where processing power is limited. In [13], a RHPC algorithm was investigated for guidance of a low cost UAV through a number of aerobatic manoeuvres. It was found that only a 0.2s prediction horizon could be achieved using the aircraft's onboard Pentium-3 300MHz processor when the control was executed at 50Hz. Although much can be done to improve the computational performance of this type of system and thereby lengthen the horizon, it does clearly illustrate the potential computation burden associated with RHPC type controllers. This fact is again highlighted in [36] where computationally feasible prediction horizons of 0.1s and 1.0s were used and compared. For this reason, and so as not to exclude low cost UAVs from the benefits of a manoeuvre autopilot, RHPC is also not considered an ideal design strategy for the task.

1.2.2 A novel approach

In light of the above discussion, a novel strategy for the design of a manoeuvre flight control system is presented in this thesis. The design strategy does not make use of novel, fundamentally different mathematical methods for design of the control system. Rather, the complexity of the manoeuvre autopilot design is reduced by appropriately formulating the aircraft dynamics and carefully selecting the states to be controlled. In this way, the complexity of the manoeuvre autopilot design is dramatically reduced and existing control system design techniques can be applied to elegantly, efficiently and robustly solve the manoeuvre control problem.

The core of the control strategy involves the design of attitude independent inner loop acceleration controllers. Although acceleration controllers are commonly used in missile applications [19], the attitude independence extension of this type of controller and its application to aircraft manoeuvre flight control is novel. The attitude independence of the controllers means that the same set of acceleration controllers can be used throughout the entire 3D flight envelope. It is for the design of these attitude independent acceleration controllers that the appropriate formulation of the aircraft dynamics is crucial.

With the acceleration controllers in place the aircraft is then reduced to a point mass with a steerable acceleration vector from a guidance perspective. This in turn greatly simplifies control at this level, allowing for aircraft independent guidance. Furthermore, reference trajectory generation is simplified enormously since trajectories need only be kinematically feasible and not dynamically feasible as in most other manoeuvre autopilot designs.

In terms of attributes, the control system architecture is argued to be inherently robust due to the inner loop regulation at an acceleration level. Regulation at this level means that all aircraft specific uncertainty will remain encapsulated behind the typically high bandwidth acceleration controllers. Thus, the effect of such uncertainty on the rest of the dynamics will be greatly reduced. Furthermore, with disturbance rejection also at an acceleration level, control action can be taken before disturbances manifest themselves into position, velocity and attitude errors. Practical feasibility and computational efficiency will also be seen later in this thesis to be attributes of a manoeuvre autopilot based on this design strategy.

It must be noted that in [40] an acceleration based control algorithm was also employed for manoeuvre flight control. However, there are several fundamental differences between the strategy presented in this thesis and that of [40]. Firstly, in [40] the method of transforming the desired inertial acceleration to body axes is iterative whereas a closed form solution is presented here. From a computational intensity point of view an iterative solution is undesirable. Secondly and most importantly, given the desired acceleration coordinates in body axes, the actuator commands are generated in an open loop fashion through inversion of the aircraft specific dynamics. Although feedback control of the measured accelerations is enforced, the damage of the open loop inversion through uncertain dynamics is already done. It is thus expected that the performance of this control technique will be very sensitive to the accuracy of the aircraft parameters. In contrast, the strategy presented in this thesis makes use of feedback control at all times when uncertainty is present. Desired accelerations are thus presented as reference commands to acceleration controllers that in turn command the actuators. Finally, in [40] the use of Euler 3-2-1 angles for attitude parameterisation will result in singularity problems during some manoeuvres. In contrast, a generalised attitude parameterisation with no singularities is employed in this thesis.

The few paragraphs above are intended only to provide a brief conceptual overview of the autopilot design strategy and its inherent attributes. The concepts and arguments presented above will be thoroughly addressed and expanded upon in the body of the thesis and then concisely summarised in the conclusion. The precise layout of this thesis is the topic of the following section.

1.3 Thesis overview

In Chapter 2 the manoeuvre autopilot design strategy is formally presented and mathematically supported. To maintain generality no specific form is assigned to the aircraft's force and moment model e.g. linear aerodynamics, thrust profiles etc. Only typical dependencies are made use of to illustrate the general applicability of the design strategy. Chapter 3 continues by enforcing an appropriate structure to the aircraft's aerodynamic and thrust models for the case when the incidence angles are small. This structure allows further detailed analysis of the open loop system and shows that under mild conditions the dynamics

for the acceleration controller designs decouple and become linear.

The detailed acceleration controller designs and their associated analyses are carried out in Chapters 4 and 5. The analysis focuses on conditions for practical application of the controllers. Normalised, non-dimensional time variants of the acceleration controllers are also presented and contrasted with their dimensional counterparts. Chapter 6 discusses a number of possible guidance strategies to interface with the acceleration controllers of the previous chapters. A novel closed form guidance control system particularly suited for use with the acceleration controllers is presented in detail.

The topic of reference trajectory generation is handled in Chapter 7 and a number of building block reference trajectories are created to reduce the parameter space when designing complex trajectories. These trajectories are used in the simulation examples of Chapter 8. Here, the manoeuvre autopilot is applied to a number of example aircraft, each with very different mission profiles and/or flying qualities. The purpose of this chapter is to illustrate the range of aircraft and trajectories that the autopilot can handle.

The thesis concludes with Chapter 9. The fundamental results are summarised and the novel contributions of this thesis to the field of aircraft dynamics, control and guidance are highlighted. Potential future research that stems directly from the results presented is also discussed.

Chapter 2

Manoeuvre Autopilot Architecture

This chapter describes the general architecture of the manoeuvre autopilot to be designed. It begins with an initial discussion describing the fundamental thoughts that shape the autopilot architecture. It then moves on to develop the six degree of freedom equations of motion in a form that provides an appropriate mathematical hold on the aircraft dynamics for the effective design of a manoeuvre autopilot. The force and moment models are kept general to illustrate that the architecture of the autopilot can be applied to a wide class of aircraft under a set of practically feasible conditions. The chapter concludes by highlighting the many advantages of the manoeuvre autopilot architecture.

2.1 Initial discussion and fundamental thoughts

For most UAV autopilot design purposes, an aircraft is well modelled as a six degree of freedom rigid body with specific and gravitational forces and their corresponding moments acting on it. The specific forces typically include aerodynamic and propulsion forces and arise due to the form and motion of the aircraft itself. On the other hand the gravitational force is universally applied to all bodies in proportion to their mass, assuming an equipotential gravitational field. The sum of the specific and gravitational forces determines the aircraft's total acceleration. It is desirable to be able to control the aircraft's acceleration as this would leave only simple outer control loops to regulate further kinematic states.

Of the total force vector only the specific force component is controllable, with the gravitational force component acting as a well modelled bias on the system. Thus, with a predictable gravitational force component, control of the total force vector can be achieved through control of the specific force vector. Modelling the specific force vector as a function of the aircraft states and control inputs is an involved process that introduces almost all of the uncertainty into the total aircraft model. Thus, to ensure robust control of the specific force vector a pure feedback control solution is desirable. As a result, regulation techniques such as dynamic inversion, which although typically also make use of outer feedback loops, are avoided due to the open loop nature of the inversion and the uncertainty associated with the specific force model.

Considering the specific force vector in more detail the following important observation is made from an autopilot design simplification point of view. Unlike the gravitational force vector which remains inertially aligned (or varies slowly with position depending on the exact distribution of the gravitational field in inertial space), the components that make up the specific force vector tend to remain aircraft aligned. This alignment is a consequence of the specific force arising as a result of the form and motion of the aircraft itself. For example, the aircraft's thrust vector acts along the same aircraft fixed action line at all times while the lift vector tends to remain close to perpendicular to the wing depending on the specific angle of attack. The observation is thus that the coordinates of the specific force vector in a body fixed axis system are independent of the gross attitude of the aircraft. Thus, if the specific force coordinates in body axes could also be measured independently of the aircraft's gross attitude then the design of attitude independent specific force controllers would be possible. Of course, appropriately mounted accelerometers provide just this measurement, normalised to the aircraft's mass, thus practically enabling the control strategy through specific acceleration instead.

With gross attitude independent specific acceleration controllers in place, the remainder of a full 3D manoeuvre flight autopilot design is greatly simplified. From a guidance perspective the aircraft reduces to a point mass with a steerable acceleration vector. Due to the acceleration interface, the guidance dynamics will be purely kinematic and the only uncertainty present will be that associated with gravitational acceleration. The highly certain nature of the guidance dynamics thus allows amongst others, techniques such as dynamic inversion and RHPC to be effectively implemented at a guidance level.

In addition to the associated autopilot simplifications, acceleration based control also provides for a robust autopilot solution. All aircraft specific uncertainty will remain encapsulated behind a wall of high bandwidth specific acceleration controllers. Furthermore, high bandwidth specific acceleration controllers would be capable of providing fast disturbance rejection at an acceleration level, allowing action to be taken before the disturbances manifest themselves into attitude, velocity and position errors.

To take advantage of the potential of regulating the specific acceleration independently of the aircraft's gross attitude, requires the equations of motion to be written in an appropriate form that provides a mathematical hold on the problem. The motion of the aircraft needs to be split into the motion of a reference frame relative to inertial space, that captures the gross attitude of the vehicle, and the superimposed motion of the aircraft relative to the reference frame. With this mathematical split, it is expected that the specific acceleration coordinates in the reference and body frames will remain independent of the attitude of the reference frame. An obvious and appropriate choice for the reference frame is the commonly used wind axis system as defined in Appendix A. With this choice, the aircraft's motion is split into a gross point mass motion with a superimposed rotational motion relative to the wind axes (velocity vector).

In section 2.2 the detailed mathematics of this split dynamics modelling process will be presented. A general aircraft force and moment model will be introduced to complete the six degree of freedom aircraft dynamics. Then, with the appropriate mathematical foundation developed and available to support further arguments, the precise architecture and the accompanying advantages of the proposed manoeuvre autopilot will be discussed in section 2.3, with concluding remarks in section 2.4.

2.2 Six degree of freedom equations of motion

This section develops the six degree of freedom equation of motion for a rigid body in a form that explicitly highlights the ideas presented in the previous section. The strategy is to describe the total motion of the body as the superposition of the body's point mass motion and its rigid body rotational motion. The point mass motion is maintained through the position and attitude of the wind axis system over time. The total rigid body motion of the aircraft is then described by maintaining the attitude of the body axis system with respect to the wind axis system.

It should be noted that the final form of the equations of motion derived in this section (or at least one very similar to it) can be found in the literature [41]. However, in the literature this particular form is not derived with the manoeuvre autopilot concepts of the previous section in mind and thus is simply presented as another of the many forms of the equations of motion. Deriving this particular form within the context of the proposed acceleration based manoeuvre autopilot architecture provides a novel perspective on the form, explicitly highlighting the numerous autopilot design advantages associated with it.

Finally, note that the notation standards used in the mathematics to follow are described in Appendix A.

2.2.1 Point mass dynamics

This section investigates the dynamics of the aircraft's centre of mass. There is a kinematic relationship between the acceleration, velocity and position of the aircraft's centre of mass with respect to inertial space (I). Since by definition the origin of the wind axis system (W) corresponds with the aircraft's centre of mass the kinematic relationships can be written as follows,

$$\left. \frac{d}{dt} \mathbf{P}^{wi} \right|_I = \mathbf{V}^{wi} \quad (2.1)$$

$$\left. \frac{d}{dt} \mathbf{V}^{wi} \right|_I = \mathbf{A}^{wi} \quad (2.2)$$

where, \mathbf{A}^{wi} , \mathbf{V}^{wi} and \mathbf{P}^{wi} are the acceleration, velocity and position vectors of the wind axis system with respect to inertial space respectively. There is a kinetic relationship between the aircraft's linear momentum (\mathbf{L}) and the applied resultant force vector (\mathbf{F}),

$$\mathbf{F} = \frac{d}{dt} \mathbf{L} \Big|_I = \frac{d}{dt} m \mathbf{V}^{WI} \Big|_I = m \frac{d}{dt} \mathbf{V}^{WI} \Big|_I = m \mathbf{A}^{WI} \quad (2.3)$$

where it has been assumed that the mass (m) is a time invariant parameter. Substituting for the acceleration vector into equation (2.2) gives,

$$\frac{d}{dt} \mathbf{V}^{WI} \Big|_I = \frac{1}{m} \mathbf{F} \quad (2.4)$$

For the purposes of illustrating the manoeuvre autopilot design concepts introduced in the previous section, it is more desirable to work with the velocity magnitude and the attitude of the wind axis system when describing the velocity vector. Thus, the derivative of the velocity vector in equation (2.4) is converted to a derivative with respect to wind axes by making use of equation (A.20) in Appendix A,

$$\frac{d}{dt} \mathbf{V}^{WI} \Big|_W = -\boldsymbol{\omega}^{WI} \times \mathbf{V}^{WI} + \frac{1}{m} \mathbf{F} \quad (2.5)$$

Here $\boldsymbol{\omega}^{WI}$ is the angular velocity of the wind axis system with respect to inertial space. The angular velocity vector is defined by equation (A.18) in Appendix A. Since use has been made of the wind axis system it is necessary to maintain its attitude with respect to inertial space. By definition, the angular velocity vector is related to the time rate of change of the wind axis system basis vectors ($\mathbf{i}^W, \mathbf{j}^W, \mathbf{k}^W$) with respect to inertial space. Equation (A.41) of Appendix A summarises the vector relationship in a matrix form and is restated below for the wind-inertial axis system case,

$$\frac{d}{dt} \begin{bmatrix} \mathbf{i}^W & \mathbf{j}^W & \mathbf{k}^W \end{bmatrix} \Big|_I = \boldsymbol{\omega}^{WI} \times \begin{bmatrix} \mathbf{i}^W & \mathbf{j}^W & \mathbf{k}^W \end{bmatrix} \quad (2.6)$$

Equations (2.1), (2.5) and (2.6) are vector equations describing the position, velocity and attitude dynamics of the wind axis system with respect to inertial space. Coordinating all of the vectors except those involved in the position dynamics into wind axes, and using the relationships of equations (A.25) and (A.37) in Appendix A gives,

$$\dot{\mathbf{P}}_I^{WI} = \left[\mathbf{DCM}^{WI} \right]^T \mathbf{V}_W^{WI} \quad (2.7)$$

$$\dot{\mathbf{V}}_W^{WI} = -\mathbf{S}_{\boldsymbol{\omega}^{WI}} \mathbf{V}_W^{WI} + m^{-1} \mathbf{F}_W \quad (2.8)$$

$$\frac{d}{dt} \left[\mathbf{DCM}^{WI} \right] = -\mathbf{S}_{\boldsymbol{\omega}^{WI}} \left[\mathbf{DCM}^{WI} \right] \quad (2.9)$$

with,

$$\left[\mathbf{DCM}^{WI} \right] = \left[\mathbf{DCM}^{IW} \right]^T = \begin{bmatrix} \mathbf{i}_I^W & \mathbf{j}_I^W & \mathbf{k}_I^W \end{bmatrix}^T \quad (2.10)$$

and the attitude kinematics constraint equation from equation (A.29),

$$[\mathbf{DCM}^{WI}][\mathbf{DCM}^{WI}]^T = \mathbf{I} \quad (2.11)$$

The \mathbf{S} matrix above implements a cross product and is defined in equation (A.10). Equations (2.7), (2.8) and (2.9) are the point mass dynamics in coordinate vector form. They are provided in expanded form below,

$$\begin{bmatrix} \dot{e}_{11}^{WI} & \dot{e}_{12}^{WI} & \dot{e}_{13}^{WI} \\ \dot{e}_{21}^{WI} & \dot{e}_{22}^{WI} & \dot{e}_{23}^{WI} \\ \dot{e}_{31}^{WI} & \dot{e}_{32}^{WI} & \dot{e}_{33}^{WI} \end{bmatrix} = - \begin{bmatrix} 0 & -R_W & Q_W \\ R_W & 0 & -P_W \\ -Q_W & P_W & 0 \end{bmatrix} \begin{bmatrix} e_{11}^{WI} & e_{12}^{WI} & e_{13}^{WI} \\ e_{21}^{WI} & e_{22}^{WI} & e_{23}^{WI} \\ e_{31}^{WI} & e_{32}^{WI} & e_{33}^{WI} \end{bmatrix} \quad (2.12)$$

$$\left[\dot{\bar{V}} \right] = \frac{1}{m} [X_W] \quad (2.13)$$

$$\begin{bmatrix} \dot{P}_x \\ \dot{P}_y \\ \dot{P}_z \end{bmatrix} = \begin{bmatrix} e_{11}^{WI} \\ e_{12}^{WI} \\ e_{13}^{WI} \end{bmatrix} \bar{V} \quad (2.14)$$

and generate the two algebraic constraint equations,

$$\begin{bmatrix} Q_W \\ R_W \end{bmatrix} = \frac{1}{m\bar{V}} \begin{bmatrix} -Z_W \\ Y_W \end{bmatrix} \quad (2.15)$$

Note that \bar{V} is the velocity magnitude and is the only non-zero coordinate of the velocity vector in wind axes. The attitude of the wind axis system with respect to inertial space is maintained through Direction Cosine Matrix (DCM) parameters (e_{ij}^{WI}) at this stage to keep the analysis general. The attitude and the attitude dynamics could be simplified using any common attitude parameterisation as discussed in Appendix A. P_W , Q_W and R_W are the roll, pitch and yaw rates of the wind axis system with respect to inertial space, while X_W , Y_W and Z_W are the axial, lateral and normal coordinates of the force vector in wind axes. P_x , P_y and P_z are the position coordinates of the wind axis system in inertial space.

Finally, note how the point mass equations of motion accept the coordinates of the force vector in wind axes (X_W, Y_W, Z_W) together with the roll rate of the wind axis system with respect to inertial space (P_W) as inputs.

2.2.2 Rigid body rotational dynamics

The equations of motion developed thus far govern the motion of the aircraft's centre of mass through inertial space. The motion of the centre of mass was maintained by maintaining the motion of the wind axis system over time. However, with the aircraft modelled as a rigid body, there can also be rotational motion of the body axis system relative to the wind axes as a result of the point of application of the total force vector. This section investigates the equations of

motion that govern the rigid body rotational dynamics of the aircraft. These dynamics together with the point mass dynamics then completely describe the six degree of freedom motion of the aircraft.

The rotational motion arises due to the point of application of the force vector i.e. the moment applied to the aircraft about its centre of mass. As shown in Appendix A, there is a kinetic relationship between this applied external moment vector (\mathbf{M}) and the aircraft's angular momentum about the centre of mass (\mathbf{H}),

$$\mathbf{M} = \frac{d}{dt} \mathbf{H} \Big|_I \quad (2.16)$$

where,

$$\mathbf{H} = \int_V \mathbf{P}^{dmB} \times (\boldsymbol{\omega}^{BI} \times \mathbf{P}^{dmB}) dm \quad (2.17)$$

and $\boldsymbol{\omega}^{BI}$ is the angular velocity of the body axis system (B) with respect to inertial space. The vector \mathbf{P}^{dmB} is the position of an arbitrary mass element dm , relative to the centre of mass (origin of the body axis system), within the volume of the rigid body V . The angular momentum vector takes on its simplest form when coordinated into body axes since the moment arms to all mass elements are fixed and independent of other motion variables. Applying the vector derivative relationship of equation (A.20) to equation (2.16) yields,

$$\mathbf{M} = \frac{d}{dt} \mathbf{H} \Big|_B + \boldsymbol{\omega}^{BI} \times \mathbf{H} \quad (2.18)$$

Substituting equation (2.17) into equation (2.18), coordinating all vectors into body axes and assuming the aircraft inertia properties remain constant gives the rearranged coordinate vector differential equation,

$$\dot{\boldsymbol{\omega}}_B^{BI} = \mathbf{I}_B^{-1} \left(-\mathbf{S}_{\boldsymbol{\omega}_B^{BI}} \mathbf{I}_B \boldsymbol{\omega}_B^{BI} + \mathbf{M}_B \right) \quad (2.19)$$

Here \mathbf{I}_B is the moment of inertia matrix referenced to the body axis system defined in equation (A.89). The above equation governs the angular velocity (rotational motion) of the body axis system with respect to inertial space as a function of the applied moment vector. However, the rotational motion of the body axis system can be thought of as the superposition of the angular velocity of the wind axis system with respect to inertial space and the angular velocity of the body axis system with respect to the wind axes ($\boldsymbol{\omega}^{BW}$). Mathematically, this can be written as follows,

$$\boldsymbol{\omega}^{BI} = \boldsymbol{\omega}^{BW} + \boldsymbol{\omega}^{WI} \quad (2.20)$$

Note that the angular velocity of the body axis system with respect to the wind axis system is

constrained, since by definition the wind axis system's normal unit vector must lie in the aircraft's plane of symmetry at all times. The constraint can be written mathematically as follows,

$$\mathbf{k}^W \cdot \mathbf{j}^B = 0 \quad \forall t \quad (2.21)$$

where \mathbf{j}^B is the body axis system lateral unit vector. Because this condition must hold for all time (t), the time derivative of equation (2.21) must also be zero. The derivative of a scalar quantity can be taken with respect to an axis system of choice. Taking the time derivative with respect to wind axes simplifies the result,

$$\begin{aligned} \left. \frac{d}{dt} \mathbf{k}^W \cdot \mathbf{j}^B \right|_W &= 0 \\ &= \mathbf{k}^W \cdot \left. \frac{d}{dt} \mathbf{j}^B \right|_W + \left. \frac{d}{dt} \mathbf{k}^W \right|_W \cdot \mathbf{j}^B \\ &= \mathbf{k}^W \cdot \left[\left. \frac{d}{dt} \mathbf{j}^B \right|_B + \boldsymbol{\omega}^{BW} \times \mathbf{j}^B \right] \\ &= \mathbf{k}^W \cdot \left[\boldsymbol{\omega}^{BW} \times \mathbf{j}^B \right] \end{aligned} \quad (2.22)$$

The above constraint only holds when $\boldsymbol{\omega}^{BW}$ takes on the following form,

$$\boldsymbol{\omega}^{BW} = a\mathbf{j}^B + b\mathbf{k}^W \quad a, b \in \mathbb{R} \quad (2.23)$$

Equation (2.23) implies that $\boldsymbol{\omega}^{BW}$ must lie in the two dimensional plane spanned by the basis vectors \mathbf{j}^B and \mathbf{k}^W . This constraint is enforced by the appropriate selection of the variable P_w which was shown in section 2.2.1 to be a free input into the point mass dynamics. By definition, the angle of attack (α) and angle of sideslip (β) are related to the parameters a and b of equation (2.23) as follows,

$$\begin{aligned} a &= +\dot{\alpha} \\ b &= -\dot{\beta} \end{aligned} \quad (2.24)$$

Combining equations (2.20), (2.23) and (2.24) yields,

$$\boldsymbol{\omega}^{BI} = \dot{\alpha}\mathbf{j}^B - \dot{\beta}\mathbf{k}^W + \boldsymbol{\omega}^{WI} \quad (2.25)$$

Analysing the above equation in body axes gives,

$$\begin{aligned} \boldsymbol{\omega}_B^{BI} &= \dot{\alpha}\mathbf{j}_B^B - \dot{\beta}\mathbf{k}_B^W + \boldsymbol{\omega}_B^{WI} \\ &= \dot{\alpha}\mathbf{j}_B^B - \dot{\beta}\mathbf{T}_a^2\mathbf{T}_\beta^3\mathbf{k}_W^W + \mathbf{T}_a^2\mathbf{T}_\beta^3\boldsymbol{\omega}_W^{WI} \end{aligned} \quad (2.26)$$

where the transformation matrices (\mathbf{T}) used in the above equation are defined in Appendix A. Expanding equation (2.26) gives,

$$\begin{bmatrix} P \\ Q \\ R \end{bmatrix} = \begin{bmatrix} 0 & \sin \alpha \\ 1 & 0 \\ 0 & -\cos \alpha \end{bmatrix} \begin{bmatrix} \dot{\alpha} \\ \dot{\beta} \end{bmatrix} + \begin{bmatrix} \cos \alpha \cos \beta & -\cos \alpha \sin \beta & -\sin \alpha \\ \sin \beta & \cos \beta & 0 \\ \sin \alpha \cos \beta & -\sin \alpha \sin \beta & \cos \alpha \end{bmatrix} \begin{bmatrix} P_w \\ Q_w \\ R_w \end{bmatrix} \quad (2.27)$$

where P , Q and R are the roll, pitch and yaw rate of the body axis system with respect to inertial space respectively. Making $\dot{\alpha}$, $\dot{\beta}$ and P_w the subject of the equation and substituting for Q_w and R_w from the algebraic constraint of equation (2.15) gives,

$$\begin{bmatrix} \dot{\alpha} \\ \dot{\beta} \\ P_w \end{bmatrix} = \begin{bmatrix} -\cos \alpha \tan \beta & 1 & -\sin \alpha \tan \beta \\ \sin \alpha & 0 & -\cos \alpha \\ \cos \alpha \sec \beta & 0 & \sin \alpha \sec \beta \end{bmatrix} \begin{bmatrix} P \\ Q \\ R \end{bmatrix} + \frac{1}{m\bar{V}} \begin{bmatrix} \sec \beta & 0 \\ 0 & 1 \\ -\tan \beta & 0 \end{bmatrix} \begin{bmatrix} Z_w \\ Y_w \end{bmatrix} \quad (2.28)$$

Note that the first two dynamic equations above arise as a result of the kinematic relationship between the angular velocity and attitude of the body axis system with respect to the wind axis system. The third equation is a constraint on P_w that ensures that equation (2.21) holds for all time. Expanding equation (2.19) and combining it with equation (2.28) gives the rigid body rotational dynamics,

$$\begin{bmatrix} \dot{\alpha} \\ \dot{\beta} \end{bmatrix} = \begin{bmatrix} -\cos \alpha \tan \beta & 1 & -\sin \alpha \tan \beta \\ \sin \alpha & 0 & -\cos \alpha \end{bmatrix} \begin{bmatrix} P \\ Q \\ R \end{bmatrix} + \frac{1}{m\bar{V}} \begin{bmatrix} \sec \beta & 0 \\ 0 & 1 \end{bmatrix} \begin{bmatrix} Z_w \\ Y_w \end{bmatrix} \quad (2.29)$$

$$\begin{bmatrix} \dot{P} \\ \dot{Q} \\ \dot{R} \end{bmatrix} = \begin{bmatrix} I_{xx} & -I_{xy} & -I_{xz} \\ -I_{xy} & I_{yy} & -I_{yz} \\ -I_{xz} & -I_{yz} & I_{zz} \end{bmatrix}^{-1} \left(- \begin{bmatrix} 0 & -R & Q \\ R & 0 & -P \\ -Q & P & 0 \end{bmatrix} \begin{bmatrix} I_{xx} & -I_{xy} & -I_{xz} \\ -I_{xy} & I_{yy} & -I_{yz} \\ -I_{xz} & -I_{yz} & I_{zz} \end{bmatrix} \begin{bmatrix} P \\ Q \\ R \end{bmatrix} + \begin{bmatrix} L \\ M \\ N \end{bmatrix} \right) \quad (2.30)$$

with,

$$P_w = \begin{bmatrix} \cos \alpha \sec \beta & 0 & \sin \alpha \sec \beta \end{bmatrix} \begin{bmatrix} P \\ Q \\ R \end{bmatrix} + \frac{1}{m\bar{V}} \begin{bmatrix} -\tan \beta & 0 \end{bmatrix} \begin{bmatrix} Z_w \\ Y_w \end{bmatrix} \quad (2.31)$$

The dynamics above are seen to maintain the attitude of the body axes with respect to the wind axes over time (α and β), as a function of the applied moment vector coordinates in body axes (L, M, N) and the lateral and normal force vector coordinates in wind axes.

2.2.3 Forces and moments

In this section, models for the force and moment vectors are investigated. However, no formal structure is applied to the force and moment model. Instead the model is kept very general with only typical dependencies highlighted. This is done to allow the general applicability of the manoeuvre autopilot architecture to be illustrated in the sections that follow. Note, to simplify the discussions below, only the forces acting on an aircraft will be considered since moments simply arise as a function of a force's action point.

The total force vector can be written as the sum of a specific force component (F^S) and a gravitational force component (F^G),

$$F = F^S + F^G \quad (2.32)$$

The specific force component can again typically be divided into two parts i.e. aerodynamic (F^A) and propulsion forces (F^T). The aerodynamic forces are typically a function of the dynamic pressure, the attitude of the body axis system with respect to the wind axis system, the angular velocity of the body axis system with respect to inertial space and the aerodynamic control actuator inputs [42]. This relationship can be written mathematically as follows,

$$F^A = f^A(\alpha, \beta, P, Q, R, \delta_{(\cdot)}, \bar{V}, \rho) \quad (2.33)$$

where ρ is the air density and $\delta_{(\cdot)}$ represents the various aerodynamic actuators. Depending on the complexity of the propulsion source, the propulsion force vector can be dependent on a number of state and control variables. Typical variables include the velocity magnitude, air density and thrust command (T_C). This can be written mathematically as follows,

$$F^T = f^T(T_C, \bar{V}, \rho) \quad (2.34)$$

Combining the aerodynamic and propulsion dependencies, the typical specific force vector dependencies can be written as follows,

$$\begin{aligned} F^S &= F^A + F^T \\ &= f^A + f^T \\ &= f^S(\alpha, \beta, P, Q, R, \delta_{(\cdot)}, T_C, \bar{V}, \rho) \end{aligned} \quad (2.35)$$

Assuming an equipotential gravitational field over the volume of the aircraft, the gravitational force vector is a function only of the aircraft's mass and can be written as follows,

$$F^G = f^G(m) \quad (2.36)$$

Considering the dependencies of the externally applied moment vector, it is firstly noted that because the moment vector is referenced to the aircraft's centre of mass, it is only contributed towards by the specific force vector. The moment vector thus simply arises due to the action point of the specific force vector. It therefore is dependent on the same state and control variables as the specific force vector,

$$M = f^M(\alpha, \beta, P, Q, R, \delta_{(\cdot)}, T_C, \bar{V}, \rho) \quad (2.37)$$

The equations of motion derived in sections 2.2.1 and 2.2.2 require the force vector coordinated in wind axes and the moment vector coordinated in body axes. Since transforming between these two axis systems involves only the angle of attack and the angle of sideslip, no

further dependencies are added to the specific force and moment vectors when coordinated into their respective axis systems. Thus, the total force and moment vectors coordinated in wind and body axes respectively can be written as follows,

$$\mathbf{F}_w = \mathbf{F}_w^\Sigma + \mathbf{F}_w^G = \mathbf{f}_w^\Sigma(\alpha, \beta, P, Q, R, \delta_0, T_c, \bar{V}, \rho) + [\mathbf{DCM}^{wI}] \mathbf{f}_I^G(m) \quad (2.38)$$

$$\mathbf{M}_B = \mathbf{f}_B^M(\alpha, \beta, P, Q, R, \delta_0, T_c, \bar{V}, \rho) \quad (2.39)$$

Note that as previously argued in section 2.1, the coordinates of the specific force and moment vectors above are not a function of the gross attitude of the aircraft. This is because the specific force vector arises due to the form and motion of the aircraft itself and thus moves with the aircraft. However, the typically inertially fixed (or slowly inertially varying) gravitational force vector is seen to be a function of the gross attitude of the aircraft when coordinated into wind axes. This issue will need to be addressed in the manoeuvre autopilot formulation.

2.2.4 Summary of equations of motion

The dynamic equations developed in the previous sections are summarised below in a slightly modified form that explicitly reveals the manoeuvre autopilot design concepts promoted in section 2.1. The total acceleration vector has been divided into a specific acceleration component (Σ) and a gravitational acceleration component (G) and related to the total force vector using equation (2.32) as follows,

$$\mathbf{F} = \mathbf{F}^\Sigma + \mathbf{F}^G = m(\Sigma + G) \quad (2.40)$$

Working with the specific and gravitational accelerations instead is important because it allows the mass parameter to be removed from the point mass dynamics, leaving these dynamics purely kinematic. The motivation for writing the equations of motion in the form provided below will be fully clarified in the following section.

Rigid body rotational dynamics:

$$\begin{bmatrix} \dot{\alpha} \\ \dot{\beta} \end{bmatrix} = \begin{bmatrix} -\cos \alpha \tan \beta & 1 & -\sin \alpha \tan \beta \\ \sin \alpha & 0 & -\cos \alpha \end{bmatrix} \begin{bmatrix} P \\ Q \\ R \end{bmatrix} + \frac{1}{\bar{V}} \begin{bmatrix} \sec \beta & 0 \\ 0 & 1 \end{bmatrix} \begin{bmatrix} C_w \\ B_w \end{bmatrix} + \frac{1}{\bar{V}} \begin{bmatrix} \sec \beta & 0 \\ 0 & 1 \end{bmatrix} \begin{bmatrix} g_w^z \\ g_w^y \end{bmatrix} \quad (2.41)$$

$$\begin{bmatrix} \dot{P} \\ \dot{Q} \\ \dot{R} \end{bmatrix} = \begin{bmatrix} I_{xx} & -I_{xy} & -I_{xz} \\ -I_{xy} & I_{yy} & -I_{yz} \\ -I_{xz} & -I_{yz} & I_{zz} \end{bmatrix}^{-1} \left(- \begin{bmatrix} 0 & -R & Q \\ R & 0 & -P \\ -Q & P & 0 \end{bmatrix} \begin{bmatrix} I_{xx} & -I_{xy} & -I_{xz} \\ -I_{xy} & I_{yy} & -I_{yz} \\ -I_{xz} & -I_{yz} & I_{zz} \end{bmatrix} \begin{bmatrix} P \\ Q \\ R \end{bmatrix} + \begin{bmatrix} L \\ M \\ N \end{bmatrix} \right) \quad (2.42)$$

with,

$$\begin{bmatrix} A_w \\ B_w \\ C_w \end{bmatrix} = \Sigma_w = \frac{1}{m} \mathbf{f}^\Sigma (\alpha, \beta, P, Q, R, \delta_0, T_C, \bar{V}, \rho) \quad (2.43)$$

$$\begin{bmatrix} L \\ M \\ N \end{bmatrix} = \mathbf{M}_B = \mathbf{f}^M (\alpha, \beta, P, Q, R, \delta_0, T_C, \bar{V}, \rho) \quad (2.44)$$

$$[P_w] = [\cos \alpha \sec \beta \quad 0 \quad \sin \alpha \sec \beta] \begin{bmatrix} P \\ Q \\ R \end{bmatrix} + \frac{1}{\bar{V}} [-\tan \beta] [C_w] + \frac{1}{\bar{V}} [-\tan \beta] [g_w^z] \quad (2.45)$$

Point mass kinematics:

$$\begin{bmatrix} \dot{e}_{11}^{wI} & \dot{e}_{12}^{wI} & \dot{e}_{13}^{wI} \\ \dot{e}_{21}^{wI} & \dot{e}_{22}^{wI} & \dot{e}_{23}^{wI} \\ \dot{e}_{31}^{wI} & \dot{e}_{32}^{wI} & \dot{e}_{33}^{wI} \end{bmatrix} = - \begin{bmatrix} 0 & -R_w & Q_w \\ R_w & 0 & -P_w \\ -Q_w & P_w & 0 \end{bmatrix} \begin{bmatrix} e_{11}^{wI} & e_{12}^{wI} & e_{13}^{wI} \\ e_{21}^{wI} & e_{22}^{wI} & e_{23}^{wI} \\ e_{31}^{wI} & e_{32}^{wI} & e_{33}^{wI} \end{bmatrix} \quad (2.46)$$

$$\left[\frac{\dot{\bar{V}}}{\bar{V}} \right] = [g_w^x] + [A_w] \quad (2.47)$$

$$\begin{bmatrix} \dot{P}_x \\ \dot{P}_y \\ \dot{P}_z \end{bmatrix} = \begin{bmatrix} e_{11}^{wI} \\ e_{12}^{wI} \\ e_{13}^{wI} \end{bmatrix} \bar{V} \quad (2.48)$$

with,

$$\begin{bmatrix} Q_w \\ R_w \end{bmatrix} = \frac{1}{\bar{V}} \begin{bmatrix} -g_w^z \\ g_w^y \end{bmatrix} + \frac{1}{\bar{V}} \begin{bmatrix} -C_w \\ B_w \end{bmatrix} \quad (2.49)$$

$$\begin{bmatrix} g_w^x \\ g_w^y \\ g_w^z \end{bmatrix} = \begin{bmatrix} e_{11}^{wI} & e_{12}^{wI} & e_{13}^{wI} \\ e_{21}^{wI} & e_{22}^{wI} & e_{23}^{wI} \\ e_{31}^{wI} & e_{32}^{wI} & e_{33}^{wI} \end{bmatrix} \mathbf{G}_1 \quad (2.50)$$

2.3 Development of the manoeuvre autopilot architecture

In section 2.1 it was argued that because the specific acceleration vector moves with the aircraft, feedback from aircraft fixed accelerometers to aircraft fixed control surfaces would allow the specific acceleration vector to be controlled independently of the aircraft's gross attitude. Furthermore, it was argued that with the specific acceleration controlled, all further dynamics would be purely kinematic, thus allowing for simple outer loop controllers to be designed based on highly certain dynamics. These arguments led to the development of a specific form of the equations of motion in section 2.2. This form is summarised in section 2.2.4 and depicted graphically in Figure 2.1 below.

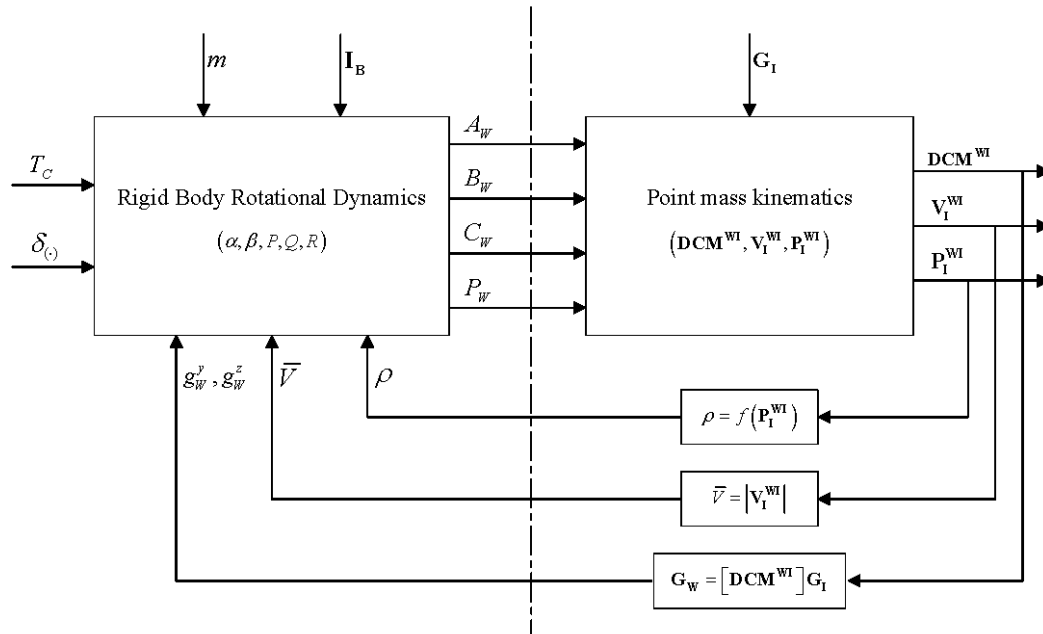


Figure 2.1 – Block diagram of the six degree of freedom equations of motion in a form well suited for the design of a manoeuvre autopilot

The complete mathematics of section 2.2 and the corresponding diagram of Figure 2.1 indicate that the initial arguments of section 2.1 were in fact correct but that some subtleties still need to be addressed. These subtleties are addressed in the initial formulation of the manoeuvre autopilot discussed in the subsection to follow. The formulated autopilot architecture is based on a few assumptions which are addressed in section 2.3.2. In section 2.3.3 issues concerning the feedback signals required by the autopilot are addressed. Finally, section 2.3.4 summarises the manoeuvre autopilot architecture. The proposed manoeuvre autopilot architecture forms the primary contribution of this dissertation to the field of aircraft flight control.

It must be noted that the arguments presented in this section are qualitative of nature, particularly those justifying the practical feasibility of the assumptions required by the manoeuvre autopilot in section 2.3.2. The analysis is forced to remain qualitative while the force and moments models remain general functions of the aircraft states. The purpose of the arguments in this section is to describe the general structure of the manoeuvre autopilot and illustrate qualitatively that the autopilot is practically feasible for a large class of aircraft. In Chapter 3, the force and moment models will be structured which in turn will allow a thorough theoretical analysis of the manoeuvre autopilot for that specific structure.

2.3.1 Initial formulation of the manoeuvre autopilot

Considering the summarised aircraft dynamics of section 2.2.4 and the corresponding block diagram of Figure 2.1, it is clear that the aircraft dynamics can be split into two sections. On the right hand side of the border in Figure 2.1 (dash-dotted vertical line), are the point mass

kinematics which describe the gross motion of the aircraft. As expected, these dynamics are completely aircraft independent and are driven by the coordinates of the specific acceleration vector in wind axes (A_w, B_w, C_w) as well as the roll rate about the velocity vector (P_w). The only inherent uncertainty in this section of the dynamics is that introduced through the gravitational acceleration model. However, as previously argued, the gravitational acceleration model is usually of a high fidelity, thus introducing very little uncertainty.

On the left hand side of the border are the rigid body rotational dynamics. These dynamics contain all of the aircraft specific parameters and thus all of the aircraft specific uncertainty. It is thus clear that by writing the equations of motion in the form presented in section 2.2.4, a natural split along an uncertainty boundary is revealed in the aircraft dynamics. Furthermore, as expected, the specific force and moment models are largely a function of the rigid body rotational dynamics states and are independent of the gross attitude of the vehicle. However, it is clear that the wind axis system attitude couples kinematically into the rigid body rotational dynamics via gravitational acceleration. If this feedback connection could be blocked, then the ideal of designing attitude independent specific acceleration controllers could be realised.

Upon further consideration of the dynamics, it is clear that the only other point mass kinematics states that couple back into the rigid body rotational dynamics are the velocity magnitude and air density (altitude). These terms couple back into the rigid body rotational dynamics because they play a direct role in determining the magnitude of the specific forces and moments. If the dynamic effect of these feedback connections could also be blocked or ignored, then the rigid body rotational dynamics would be completely dynamically independent of the point mass kinematics. Assuming all states were available for feedback, this would then allow for a single set of inner loop controllers to be designed to regulate the four signals that drive into the point mass kinematics with an invariant dynamic response for all point mass kinematics states. With these ‘virtual actuators’ and their invariant dynamic responses, all further outer control loops would then be completely aircraft independent, thereby greatly decreasing the remaining complexity of the manoeuvre autopilot design.

Further to decreasing the complexity of the autopilot design, these typically high bandwidth controllers would encapsulate all of the aircraft specific uncertainty. This wall of inner loop controllers would thus serve to desensitise the point mass kinematics to the adverse effects of uncertainty in the aircraft model. Thus, the point mass kinematics would retain their highly certain nature and model dependent control techniques such as dynamic inversion and RHPC could be practically applied at a guidance level. The control architecture also provides enormous potential for disturbance rejection since the inner control loops would provide regulation at an acceleration and angular rate level. Thus, disturbance rejection would take place before disturbances even manifested themselves into attitude, velocity and position errors.

2.3.2 Addressing the conditions required by the autopilot

The controller architecture discussed above requires the dynamic coupling from the point mass kinematics back into the rigid body rotational dynamics to be negated. This section analyses the conditions under which these couplings can be ignored. It argues that the conditions are practically feasible and can be met by a large class of aircraft.

Considering the velocity magnitude and air density feedback couplings first. The velocity magnitude bandwidth will be determined by the outer loop velocity magnitude control system. For all practical purposes this bandwidth need not be exceptionally high since aircraft, due to their streamlined nature, are not particularly susceptible to axial disturbances and attitude induced axial accelerations can be compensated for through feed-forward. The maximum rate of change of the air density is determined by the aircraft's maximum velocity and the change in air density with altitude. Given the very slow change in air density with altitude, this rate of change is low.

For typical aircraft parameters, the states involved in the rigid body rotational dynamics operate on a much shorter timescale than the controlled velocity magnitude and air density states do. Furthermore, if the aircraft parameters result in rigid body rotational dynamics that do not operate at a high enough bandwidth, then their natural bandwidth can be increased through feedback control. A timescale separation argument can thus be used to handle the dynamic coupling of the velocity magnitude and air density terms into the rigid body rotational dynamics. With a significant timescale separation between the dynamics, the velocity magnitude and air density can be considered parameters in the rigid body rotational dynamics instead of states. This is equivalent to saying that over the timescales of interest in the rigid body rotational dynamics, the velocity magnitude and air density must remain very close to constant.

Placing a timescale separation condition between the rigid body rotational dynamics and the velocity magnitude and air density dynamics is not in general a practically limiting condition. The condition is often naturally met and can otherwise be enforced through feedback. The upper bandwidth of the rigid body rotational dynamics is of course limited by practical factors such as actuator saturation and structural limitations. A further consideration is the speed of the axial specific acceleration dynamics. Since the propulsion source is often significantly bandwidth-limited (referred to as band-limited from this point forward), the bandwidth of the axial specific acceleration dynamics can often not be increased to the point where a timescale separation condition holds. However, it will be shown in the following chapter that there need not exist a timescale separation between the axial specific acceleration dynamics and the velocity magnitude dynamics for the velocity magnitude and air density to be regarded as parameters in the rigid body rotational dynamics. Finally, the designer also has the option of limiting the velocity magnitude bandwidth and maximum rate of climb/descent with outer

control loops to ease the minimum bandwidth constraints on the rigid body rotational dynamics.

Before continuing, it should be noted that the border in Figure 2.1 not only represents a separation of uncertainty in the aircraft model but as previously argued, for typical aircraft parameters also highlights a natural timescale separation of the dynamics. Thus, the dynamic coupling of the wind axis system attitude into the rigid body rotational dynamics could also be argued away through a timescale separation argument. However, although the wind axis system attitude parameters will have slower dynamics than the rigid body rotational dynamics, it is desirable for the manoeuvre autopilot to be capable of guiding the aircraft through gross attitude changes in short time periods. Furthermore, an aircraft can typically roll about its velocity vector very quickly implying that the attitude parameters quantifying the direction of the wind axis system normal and lateral unit vectors will have fast dynamics. Thus, placing a timescale separation condition between the rigid body rotational dynamics and the point mass kinematics attitude parameters would require the rigid body rotational dynamics to operate at speeds that could only be realised by a very limited class of aircraft.

To keep the manoeuvre autopilot's architecture applicable to a very general class of aircraft, an alternative method of negating the wind axis system's attitude coupling is sought. The wind axis system attitude parameters couple into the rigid body rotational dynamics via the typically well modelled gravitational acceleration vector. Since the coupling is well modelled, its effect on the rigid body rotational dynamics could be cancelled via dynamic inversion if it is assumed that high bandwidth actuators exist that are capable of performing the inversion. Equations (2.41) and (2.45) show that the wind axis system attitude parameters only couple back into the rigid body rotational dynamics through accelerations normal to the velocity vector. Thus, there need only be high bandwidth actuators capable of either directly producing or dynamically inducing accelerations in the plane normal to the velocity vector to perform the dynamic inversion. For reasonable angles of attack and sideslip, this is not a practically limiting assumption since standard aerodynamic actuators would suffice.

Adopting the approach of dynamic inversion over timescale separation to block the dynamic coupling of the wind axis system attitude parameters keeps the architecture of the manoeuvre autopilot applicable to a wide class of aircraft. It does however, require knowledge of the wind axis system orientation (i.e. gross attitude) to perform the inversion and thus would be dependent on attitude estimation accuracies in practice. Furthermore, since dynamic inversion is an open loop process, the effectiveness of the inversion is dependent on the accuracy of the aircraft model. However, the objective of the inversion is to remove the bulk of the coupling such that the inner loop controllers can be designed without regard for it. It thus forms only a small part of an otherwise purely feedback based inner loop control system, which will also naturally reject any remaining coupling, particularly given the timescale separation arguments above.

2.3.3 Estimation of the states required by the autopilot

Although throughout this thesis it will be assumed that all states are available for feedback, it is prudent to briefly investigate the feasibility of estimating the signals that will typically be required by the manoeuvre autopilot. This is important from the perspective of designing dynamically invariant inner loop controllers. Furthermore, from a future research perspective, it will be highlighted how the split in the aircraft dynamics depicted in Figure 2.1 can be used to potentially reduce the computational burden of estimating the aircraft's state vector.

The proposed inner loop controllers require feedback from the specific acceleration coordinates in wind axes and the roll rate about the velocity vector. Typical sensors available to measure inner loop states are angular rate gyroscopes and accelerometers. Appropriately mounted angular rate gyroscopes are capable of directly measuring three of the rigid body rotational dynamics states. As previously discussed, accelerometers mounted at the aircraft's centre of mass are capable of measuring the specific acceleration coordinates in body axes. These coordinates are related to the coordinates in wind axes through a transformation involving the angle of attack and angle of sideslip, both of which are states of the rigid body rotational dynamics. One possible estimation technique for the rigid body rotational dynamics is thus to adapt equation (2.41) slightly to accept the easily measurable angular rate and specific acceleration coordinates in body axes as follows,

$$\begin{bmatrix} \dot{\alpha} \\ \dot{\beta} \end{bmatrix} = \begin{bmatrix} -\cos \alpha \tan \beta & 1 & -\sin \alpha \tan \beta \\ \sin \alpha & 0 & -\cos \alpha \end{bmatrix} \begin{bmatrix} P \\ Q \\ R \end{bmatrix} + \frac{1}{V} \begin{bmatrix} -\sin \alpha \sec \beta & 0 & \cos \alpha \sec \beta \\ -\cos \alpha \sin \beta & \cos \beta & -\sin \alpha \sin \beta \end{bmatrix} \begin{bmatrix} A \\ B \\ C \end{bmatrix} + \frac{1}{V} \begin{bmatrix} g_w^z \sec \beta \\ g_w^y \end{bmatrix} \quad (2.51)$$

If the velocity magnitude and wind axis system attitude parameters could be obtained (this will be addressed in the next paragraph) then a purely kinematic rigid body rotational dynamics based estimator could be designed to estimate the angles of attack and sideslip. These estimates could be used to convert the body coordinated measurements of angular rate and specific acceleration to wind axes as desired. Although a number of other rigid body rotational dynamics state estimators could be designed, including aircraft specific model based estimators, the above argument serves to illustrate the feasibility of estimating the signals required in a computationally efficient manner.

At a point mass kinematics level, a standard Global Positioning System (GPS) receiver is capable of providing inertially coordinated (albeit in a polar form), position and velocity vector information directly. Thus, with reference to the definition of the wind axis system, only the orientation of the normal and lateral unit vectors in the plane perpendicular to the velocity vector cannot be directly sensed. However, a point mass kinematics based estimator could be designed to estimate the wind axis system attitude. This estimator would accept estimates of specific acceleration and roll rate from the rigid body rotational dynamics estimator and use GPS and magnetometer measurements to bound propagated state estimates.

Note that this outer estimator would then in turn be responsible for providing the rigid body rotational dynamics estimator with velocity magnitude and wind axis system attitude information. The timescale separation between the two estimators would allow this split in design.

The discussion above makes it clear that practically feasible options do exist for estimating the states required by the manoeuvre autopilot and that the split dynamics of Figure 2.1 in fact reveal further estimation potential. As previously stated however, the estimation problem will not be pursued further in this thesis and instead all states will be considered available for feedback.

2.3.4 Summary of the manoeuvre autopilot architecture

The manoeuvre autopilot architecture has been presented over the course of the previous subsections and is summarised below.

Firstly, the following assumptions about the aircraft and its dynamics are made,

- A timescale separation exists between the rigid body rotational dynamics and the velocity magnitude and air density dynamics.
- The dynamic coupling of the wind axis system attitude parameters into the rigid body rotational dynamics can be negated through dynamic inversion.

In section 2.3.2 it was argued that these two assumptions are practically feasible for a general class of aircraft. If these two assumptions hold then the velocity magnitude and the air density can be treated as parameters in the rigid body rotational dynamics, and the dynamic coupling of the wind axis system attitude parameters into the rigid body rotational dynamics can be ignored. The rigid body rotational dynamics then become dynamically independent of the point mass kinematics. With this dynamic independence, it is then assumed that,

- Inner loop controllers can be designed to regulate the specific acceleration coordinates in wind axes and the roll rate about the velocity vector with nominal closed loop dynamics for all point mass kinematics states.

In general, to design dynamically invariant inner loop controllers for all point mass kinematics states would require the full rigid body rotational dynamics state vector to be available. Section 2.3.3 argued that estimating the rigid body rotational dynamics state vector was indeed possible with typically available sensors.

With the specific acceleration and roll rate about the velocity vector regulated, all of the aircraft's uncertainty remains encapsulated behind a wall of inner loop controllers. Furthermore, control at an acceleration and angular rate level will provide for good disturbance rejection since rejection can take place before disturbances manifest themselves into attitude, velocity and position errors.

With the nominal dynamics inner loop controllers designed, aircraft independent guidance level controllers can then be created to regulate the gross motion of the aircraft. Due to the highly certain nature of the dynamics, a number of control system design techniques could be employed at a guidance level, including model dependent techniques such as dynamic inversion and RHPC. Furthermore, the timescale separation assumption above will in many cases allow the nominal inner loop dynamics to simply be ignored and the signals entering the point mass kinematics to be treated as instantaneously commandable ‘virtual actuators’. Although this is not required to reap all the benefits of the manoeuvre autopilot architecture, it would of course greatly simplify the guidance level controllers.

Finally, the guidance controllers mentioned above would be used to regulate the aircraft about a kinematically feasible trajectory. Designing a kinematically feasible reference trajectory is a far less demanding task than that of designing a dynamically feasible trajectory. The former can very often be done by hand while the latter typically involves a complex optimisation problem if an accurate trajectory is desired. Thus, the manoeuvre autopilot architecture is also seen to ease the process of reference trajectory generation.

2.4 Conclusion

This chapter presented the architecture of the manoeuvre autopilot, the primary contribution of this dissertation. It introduced the fundamental arguments that lead to the architecture and mathematically supported these by specifically developing a generalised aircraft model in an appropriate form. The form mathematically illustrated a split in the aircraft dynamics along an uncertainty and timescale separation boundary. Although the particular form of the six degree of freedom equation of motion can be found in the literature, its derivation within the context of the manoeuvre autopilot presented in this chapter provides a novel perspective on the form. With the general equations of motion in place, a set of conditions for the implementation of the manoeuvre autopilot architecture were derived and argued to be practically feasible for a large class of aircraft. The associated robustness, guidance, trajectory generation and estimation benefits provided by the autopilot architecture were also highlighted.

Chapter 3

Small Incidence Angle Simplifications

The developments up to this point have presented the general architecture of the manoeuvre autopilot without enforcing a particular aircraft model structure. In this chapter, a structured force and moment model applicable to a large class of aircraft operating at small incidence angles (pre-stall flight) is presented. It is important to note that although this model is only valid for small incidence angles, the gross attitude angles are not limited in any way.

The structured force and moment model presented in section 3.1 allows for further detailed investigation of the inner loop rigid body rotational dynamics. It is shown in sections 3.2 and 3.3 that under further mild conditions, these dynamics are linear and decouple into axial, normal and lateral systems. With linear decoupled dynamics, the complexity of designing inner loop controllers that yield dynamically invariant closed loop responses is dramatically reduced. Furthermore, the decoupled linear models make a more rigorous analysis of the resulting autopilot possible.

Note that it will be assumed for the remainder of this document that the flight envelope of the aircraft is such that a flat earth reference frame is appropriate and that this reference frame can be considered an inertial reference frame. The greatest benefit of this assumption is the associated equipotential gravitational field. As was seen in the previous chapter, a flat earth assumption was not a necessary condition for the implementation of the manoeuvre autopilot architecture presented. All that was required was that the gravitational force vector be well modelled and at worst vary slowly in inertial space. Making use of the flat earth assumption thus serves primarily to reduce the complexity of the analysis to follow and avoids clutter of the fundamental results.

3.1 Force and moment model

In this section, the aerodynamic, propulsion and gravitational force and moment models introduced in section 2.2.3 are elaborated upon. An aerodynamic model valid for small incidence angles is presented along with a simple propulsion model that captures the major effects of typical propulsion sources. A standard flat earth gravitational force model is also

presented.

3.1.1 Aerodynamic model

In section 2.2.3 of Chapter 2, it was argued that the aerodynamic force vector is typically a nonlinear function of the following variables,

$$\mathbf{F}^A = \mathbf{f}^A(\alpha, \beta, P, Q, R, \delta_{(\cdot)}, \bar{V}, \rho) \quad (3.1)$$

The standard small incidence angle aerodynamic model presented below [43] provides a structure to the functional dependence indicated by equation (3.1) with the aerodynamic forces and moments modelled in wind axes.

$$\begin{bmatrix} X_w^A \\ Y_w^A \\ Z_w^A \end{bmatrix} = qS \begin{bmatrix} -C_D \\ C_y \\ -C_L \end{bmatrix} \quad (3.2)$$

$$\begin{bmatrix} L_w^A \\ M_w^A \\ N_w^A \end{bmatrix} = qS \begin{bmatrix} b & 0 & 0 \\ 0 & \bar{c} & 0 \\ 0 & 0 & b \end{bmatrix} \begin{bmatrix} C_l \\ C_m \\ C_n \end{bmatrix} \quad (3.3)$$

where,

$$q = \frac{1}{2} \rho \bar{V}_a^2 \quad (3.4)$$

Here, q is the dynamic pressure, \bar{V}_a the airspeed magnitude, ρ the air density, S the wing area, \bar{c} the mean aerodynamic chord and b the wing span. The dimensionless coefficients C_L , C_D and C_y are the lift, drag and side force coefficients respectively with C_l , C_m and C_n the dimensionless roll, pitch and yaw moment coefficients respectively. It is common practice to model the aerodynamic forces in wind axes since the lift and drag forces are defined as being perpendicular and parallel to the velocity vector respectively.

The dimensionless coefficients capture the specific aerodynamic properties of the aircraft. Under small incidence angle assumptions (both absolute and induced), the lift, side force and moment coefficients are well modelled as linear in the rigid body rotational dynamics states and their first time derivatives. The drag coefficient however is typically modelled as nonlinear in the rigid body rotational dynamics states, being the sum of parasitic and induced drag. Standard coefficient models are presented below [43].

$$C_D = C_{D_0} + \frac{C_L^2}{\pi A e} \quad (3.5)$$

$$\begin{bmatrix} C_y \\ C_L \end{bmatrix} = \begin{bmatrix} 0 \\ C_{L_0} \end{bmatrix} + \begin{bmatrix} 0 & C_{y\beta} & \frac{b}{2\bar{V}_a} C_{yP} & 0 & \frac{b}{2\bar{V}_a} C_{yR} \\ C_{L\alpha} & 0 & 0 & \frac{\bar{c}}{2\bar{V}_a} C_{LQ} & 0 \end{bmatrix} \begin{bmatrix} \alpha \\ \beta \\ P \\ Q \\ R \end{bmatrix} + \begin{bmatrix} C_{y\delta_A} & 0 & C_{y\delta_R} \\ 0 & C_{L\delta_E} & 0 \end{bmatrix} \begin{bmatrix} \delta_A \\ \delta_E \\ \delta_R \end{bmatrix} \quad (3.6)$$

$$\begin{bmatrix} C_l \\ C_m \\ C_n \end{bmatrix} = \begin{bmatrix} 0 \\ C_{m_0} \\ 0 \end{bmatrix} + \begin{bmatrix} 0 & C_{l\beta} & \frac{b}{2\bar{V}_a} C_{lP} & 0 & \frac{b}{2\bar{V}_a} C_{lR} \\ C_{m\alpha} & 0 & 0 & \frac{\bar{c}}{2\bar{V}_a} C_{mQ} & 0 \\ 0 & C_{n\beta} & \frac{b}{2\bar{V}_a} C_{nP} & 0 & \frac{b}{2\bar{V}_a} C_{nR} \end{bmatrix} \begin{bmatrix} \alpha \\ \beta \\ P \\ Q \\ R \end{bmatrix} + \begin{bmatrix} C_{l\delta_A} & 0 & C_{l\delta_R} \\ 0 & C_{m\delta_E} & 0 \\ C_{n\delta_A} & 0 & C_{n\delta_R} \end{bmatrix} \begin{bmatrix} \delta_A \\ \delta_E \\ \delta_R \end{bmatrix} \quad (3.7)$$

In equation (3.5), C_{D_0} is the parasitic drag coefficient, A the wing's aspect ratio and e the Oswald efficiency factor. In equations (3.6) and (3.7), C_{L_0} and C_{m_0} are the static lift and pitching moment coefficients respectively. The terms of the form,

$$C_{A_B} \equiv \frac{\partial C_A}{\partial B'} \quad (3.8)$$

with,

$$B' = nB \quad (3.9)$$

where n is the appropriate normalising coefficient of B , are the non-dimensional stability and control derivatives. The appropriate normalising coefficient for the incidence angles and the control deflection angles is unity while for the pitch rate it is $\bar{c}/2\bar{V}_a$ and for the roll and yaw rates it is $b/2\bar{V}_a$.

Three standard aerodynamic control actuators have been included in the model i.e. ailerons (δ_A), elevator (δ_E) and rudder (δ_R). It should be noted that the control system design and analysis of this thesis can easily be adapted to handle a number of control surface configurations, provided that the control surfaces combined can generate a three dimensional moment vector. Furthermore, note that the stability derivatives for the first time derivative states have been ignored. Of the first time derivatives however, only the coefficients of $\dot{\alpha}$ are typically significant and quantify effects such as downwash lag and added mass [42]. It would be straightforward to incorporate these coefficients into the model and they would result in only minor changes in the analysis to follow. However they are left out primarily to avoid clutter of the results to follow and also because, depending on the aircraft's configuration, their effect is often negligible for control system design purposes.

In the model presented above it is assumed that the stability and control derivatives are not a function of the rigid body rotational dynamics states i.e. they are parameters in the rigid body rotational dynamics. In practice however, these derivatives can be a function of the rigid body

rotational dynamics states, especially for example when there is a fundamental change in the airflow over the aircraft at certain angles of attack. However, for many aircraft operating in the small incidence angle range, the assumption that the derivatives are independent of the rigid body rotational dynamics states is valid and greatly simplifies the manoeuvre autopilot analysis and design. Note that the derivatives can however still be a function of the point mass kinematics states given a timescale separation between the dynamics associated with these states and the rigid body rotational dynamics. For example, an aircraft's natural yaw damping is dominated by the induced angle of attack on the fin but is also contributed towards by differential drag across the wings. Due to the nonlinear nature of dynamic pressure, the damping component due to differential drag will be a function of the velocity magnitude. However, with timescale separation arguments in place, this velocity magnitude dependency is not of concern and the rigid body rotational dynamics remain dynamically decoupled from the point mass kinematics.

To conclude this section, it is noted that the rigid body rotational dynamics require the moment vector to be coordinated in body axes and not wind axes. Applying the appropriate transformation relationship yields the desired result,

$$\begin{bmatrix} L_B^A \\ M_B^A \\ N_B^A \end{bmatrix} = \mathbf{T}_a^2 \mathbf{T}_p^3 \begin{bmatrix} L_w^A \\ M_w^A \\ N_w^A \end{bmatrix} = \begin{bmatrix} \cos \alpha \cos \beta & -\cos \alpha \sin \beta & -\sin \alpha \\ \sin \beta & \cos \beta & 0 \\ \sin \alpha \cos \beta & -\sin \alpha \sin \beta & \cos \alpha \end{bmatrix} \begin{bmatrix} L_w^A \\ M_w^A \\ N_w^A \end{bmatrix} \quad (3.10)$$

3.1.2 Thrust model

In section 2.2.3 of Chapter 2 it was argued that the propulsion force vector is typically a function of the following variables,

$$\mathbf{F}^T = \mathbf{f}^T(T_C, \bar{V}, \rho) \quad (3.11)$$

Depending on the specific propulsion source, many different propulsion models exist. In this section a very simple propulsion model that captures the main effects of a typical propulsion source is presented.

Firstly, most propulsion sources have a significantly band-limited response. This can easily be modelled as a first order lag (low pass filter) from thrust command to thrust output. Secondly, the propulsion source is often dependent on the velocity magnitude. For example, in propeller driven aircraft, the angle of attack on the propeller blades is reduced with an increase in the velocity magnitude. However, the dynamic effect of the velocity coupling is often fairly negligible and can if necessary be dynamically inverted. For these reasons the velocity magnitude dependency is ignored in the model presented. Similar arguments could be applied to ignore air density dependence as well as any other low bandwidth dependencies such as temperature. Thus the propulsion source is simply modelled as a low pass filtered thrust vector

as shown below,

$$\dot{T} = -\frac{1}{\tau}T + \frac{1}{\tau}T_c \quad (3.12)$$

Assuming the thrust vector acts in the aircraft's plane of symmetry, with a setting angle relative to the body axis system axial unit vector ε_T (a positive setting angle is defined as one that results in a pitched up thrust vector relative to the aircraft), and with a moment arm to the centre of mass m_r (a positive moment arm is defined as one that would result in a positive pitching moment), then the thrust force and moment coordinates take on their simplest form when written in body axes,

$$\begin{bmatrix} X_B^T \\ Y_B^T \\ Z_B^T \end{bmatrix} = \begin{bmatrix} \cos \varepsilon_T \\ 0 \\ -\sin \varepsilon_T \end{bmatrix} T \quad (3.13)$$

$$\begin{bmatrix} L_B^T \\ M_B^T \\ N_B^T \end{bmatrix} = \begin{bmatrix} 0 \\ m_r \\ 0 \end{bmatrix} T \quad (3.14)$$

The rigid body rotational dynamics however require the force vector to be coordinated in wind axes. Applying the necessary transformation yields the result,

$$\begin{bmatrix} X_W^T \\ Y_W^T \\ Z_W^T \end{bmatrix} = \mathbf{T}_\beta^3 \mathbf{T}_\alpha^2 \begin{bmatrix} X_B^T \\ Y_B^T \\ Z_B^T \end{bmatrix} = \begin{bmatrix} \cos(\alpha + \varepsilon_T) \cos \beta \\ -\cos(\alpha + \varepsilon_T) \sin \beta \\ -\sin(\alpha + \varepsilon_T) \end{bmatrix} T \quad (3.15)$$

3.1.3 Gravitational model

In section 2.2.3 of Chapter 2, it was argued that the gravitational force vector is a function only of the aircraft's mass,

$$\mathbf{F}^G = \mathbf{f}^G(m) \quad (3.16)$$

Assuming an equipotential gravitational field, a standard flat earth model for the gravitational force vector is,

$$\mathbf{F}^G = mg\mathbf{k}^I \quad (3.17)$$

where g is the gravitational force per unit mass. Due to its inertially fixed alignment, the gravitational force vector takes on its simplest form when coordinated into inertial axes as shown below,

$$\begin{bmatrix} X_I^G \\ Y_I^G \\ Z_I^G \end{bmatrix} = \begin{bmatrix} 0 \\ 0 \\ mg \end{bmatrix} \quad (3.18)$$

However, the rigid body rotational dynamics require the gravitational force vector to be coordinated in wind axes. Applying the appropriate coordinate transformation yields the desired result,

$$\begin{bmatrix} X_W^G \\ Y_W^G \\ Z_W^G \end{bmatrix} = [\mathbf{DCM}^{WI}] \begin{bmatrix} X_I^G \\ Y_I^G \\ Z_I^G \end{bmatrix} = \begin{bmatrix} e_{13}^{WI} \\ e_{23}^{WI} \\ e_{33}^{WI} \end{bmatrix} mg \quad (3.19)$$

Of course, with a uniform gravitational field, the moments produced by the gravitational force about the centre of mass are all zero.

3.2 Towards linearisation and decoupling of the dynamics

The purpose of this section is to analyse the nonlinearities and undesired couplings in the rigid body rotational dynamics. Arguments involving small incidence angles and typically weak couplings will be used to show that to a good approximation, almost all of the dynamics are linear and furthermore, that they can be decoupled into three distinct systems. The final step towards making the rigid body rotational dynamics completely linear will be discussed in section 3.3.

The section begins by considering the trigonometric simplifications that result when the incidence angles are small and then analyses and illustrates the weakness of the remaining small angle couplings. It then moves on to analyse the nonlinear drag model where it is shown that under certain practically feasible controller design constraints, the effect of lift coupling into drag can be ignored.

3.2.1 Trigonometric simplifications

Equations (2.41) and (2.45) of the rigid body rotational dynamics and equations (3.10) and (3.15) of the aerodynamic moment and thrust force models respectively are all restated below with standard trigonometric small angle assumptions. The small angles are the two incidence angles, together with the thrust vector setting angle. Furthermore the assumption that products of small angles are negligible has also been made.

$$\begin{bmatrix} \dot{\alpha} \\ \dot{\beta} \end{bmatrix} = \begin{bmatrix} -\beta & 1 & 0 \\ \alpha & 0 & -1 \end{bmatrix} \begin{bmatrix} P \\ Q \\ R \end{bmatrix} + \frac{1}{\bar{V}} \begin{bmatrix} 1 & 0 \\ 0 & 1 \end{bmatrix} \begin{bmatrix} C_w \\ B_w \end{bmatrix} + \frac{1}{\bar{V}} \begin{bmatrix} 1 & 0 \\ 0 & 1 \end{bmatrix} \begin{bmatrix} g_w^z \\ g_w^y \end{bmatrix} \quad (3.20)$$

$$[P_w] = [1 \quad 0 \quad \alpha] \begin{bmatrix} P \\ Q \\ R \end{bmatrix} + \frac{1}{\bar{V}} [-\beta][C_w] + \frac{1}{\bar{V}} [-\beta][g_w^z] \quad (3.21)$$

$$\begin{bmatrix} L_B^A \\ M_B^A \\ N_B^A \end{bmatrix} = \begin{bmatrix} 1 & -\beta & -\alpha \\ \beta & 1 & 0 \\ \alpha & 0 & 1 \end{bmatrix} \begin{bmatrix} L_w^A \\ M_w^A \\ N_w^A \end{bmatrix} \quad (3.22)$$

$$\begin{bmatrix} X_w^T \\ Y_w^T \\ Z_w^T \end{bmatrix} = \begin{bmatrix} 1 \\ -\beta \\ -\alpha - \varepsilon_T \end{bmatrix} T \quad (3.23)$$

Considering now the remaining nonlinear couplings through the angle of attack and sideslip above. Firstly, it is noted that if the angle of sideslip is maintained negligibly small, then a number of the nonlinear couplings are removed. Most aircraft are designed to fly coordinated turns (i.e. zero lateral specific acceleration), which in turn typically implies very small angles of sideslip. Under the condition that the control system enforces coordinated turns, the angle of sideslip can be assumed negligibly small and the nonlinear couplings can thus reasonably be ignored.

Continuing, the nonlinear couplings through angle of attack are considered individually. Firstly, in the angle of sideslip dynamics, the roll rate couples in through the angle of attack. This term can become significant when the angle of attack approaches the limits of the small angle range e.g. 10 to 15 deg (note these angles will be referred to as high or large for the arguments that follow), or when the roll rate is particularly high. Large angles of attack occur during high g (refers to large normal accelerations expressed in units of g) manoeuvring flight or when flying at low speed. When flying slowly, high roll rates are not common, since the aerodynamic moments produced by the ailerons reduce with dynamic pressure. Furthermore, it is not common to roll fast during high g manoeuvres since the aircraft would tend to be pulled in the direction of the large lift vector during the roll. Thus, if the flight envelope of the aircraft is limited such that large roll rates do not commonly occur during high angle of attack flight, then ignoring the nonlinear coupling becomes acceptable.

Considering the coupling of the yaw moment into the roll rate dynamics and the roll moment into the yaw rate dynamics. The couplings again only become significant at high angles of attack. At 12 deg of angle of attack, there is approximately a 20% cross coupling. This cross coupling will manifest itself in a Dutch Roll type motion. Thus, if the lateral controllers are designed to over-damp Dutch Roll type motions, then it is acceptable to simply neglect these terms. A second strategy would be to cancel the cross coupling through static inversion, by noting that aerodynamic actuators capable of directly producing both roll and yaw moments do exist. The adverse effect of the static inversion control law would be the excitement of the angle of sideslip dynamics through the force produced by the rudder. However, this force

would typically be negligible relative to the weathercock force of the entire fin and thus the adverse effects could arguably be ignored.

The yaw rate couples into the wind axis system roll rate output through the angle of attack. Again, the coupling will only be significant at low speeds or during high g manoeuvres when the angle of attack is large. During low speed flight, the yaw rate is typically low due to the reduced control authority. During high g manoeuvres, an aircraft does not typically yaw at high rates e.g. during a steeply banked turn, the normal acceleration is high but the yaw rate is low due to the bank angle required to maintain a coordinated turn. Thus, limiting the flight envelope of the aircraft such that high yaw rates do not commonly occur simultaneously with high angles of attack, allows for the nonlinear coupling terms to be ignored.

The nonlinear thrust couplings of equation (3.23) will be addressed in the following subsection.

3.2.2 Thrust coupling simplifications

With the angle of sideslip argued to be negligibly small, the thrust force in wind axes and thrust moment in body axes can be written as follows,

$$\begin{bmatrix} X_W^T \\ Y_W^T \\ Z_W^T \end{bmatrix} = \begin{bmatrix} 1 \\ 0 \\ -\alpha - \varepsilon_T \end{bmatrix} T \quad (3.24)$$

$$\begin{bmatrix} L_B^T \\ M_B^T \\ N_B^T \end{bmatrix} = \begin{bmatrix} 0 \\ m_T \\ 0 \end{bmatrix} T \quad (3.25)$$

The coupling of the thrust force into the angle of attack dynamics (via the normal force) is undesirable both from a linearity and decoupling point of view. However, the coupling can be shown to be negligibly weak by considering the following two points together. Firstly, the thrust force couples into the total normal force via the sum of two small angles. With a total coupling angle of 20 deg for example (a fairly extreme example), approximately 35% of the thrust magnitude moves through to disturb the normal force. Secondly, the thrust is largely responsible for countering the drag in the system and thus its magnitude is on the order of that of the drag force. On the other hand, the normal force is dominated by lift which for most aircraft is an order of magnitude greater than the drag. Assuming a lift to drag ratio of approximately 10 (which is fairly poor for most aircraft), the effective thrust disturbance to the normal force is then 3.5%. In most flight conditions, it will be significantly less than this figure. The disturbance coupling is seen to be small thus justifying its neglect.

The thrust force couples linearly into the pitch rate dynamics via the thrust moment arm. Although the coupling is linear, it is still undesirable from a decoupling point of view. There

are a number of possibilities that allow the coupling to be ignored. Firstly, the thrust moment arm for a large number of aircraft is negligibly small, thus solving the problem immediately. Secondly, the pitching moment drives into the dynamics that govern the normal specific acceleration. The normal specific acceleration can typically be regulated at a much higher bandwidth than that of the propulsion source. Thus, the coupling can simply be treated as a disturbance within the normal specific acceleration controller bandwidth to be rejected by the controller. Finally, the effect of the coupling can be removed through dynamic inversion using the elevator. Although the dynamic inversion control law will disturb the angle of attack dynamics through the direct force produced by the elevator, the disturbance is typically negligible and can be analysed on a case by case basis. Thus, if it is assumed that the aircraft to be controlled meets at least one of the three criteria listed above then the coupling can be ignored.

3.2.3 Analysing the coupling of lift into drag

With the small incidence angle simplifications, the wind axis system axial acceleration can be written as follows,

$$A_w = \left[\frac{1}{m} \right] T - \left[\frac{1}{m} \right] D \quad (3.26)$$

where,

$$D = -X_w^A = qSC_D \quad (3.27)$$

The axial specific acceleration is seen to be the difference between the thrust acceleration and the drag acceleration. The thrust component can be controlled via the thrust command variable while from equations (3.5) and (3.6), the drag component is a nonlinear function of the angle of attack, pitch rate, elevator deflection and dynamic pressure. From a decoupling point of view it would be desirable to ignore the effect of the drag term in equation (3.26). This would decouple the axial specific acceleration dynamics from the rest of the rigid body rotational dynamics.

Considering the drag coupling in more detail, the low frequency portion could simply be viewed as a disturbance to the axial specific acceleration. Using the band-limited thrust actuator, an axial specific acceleration controller could be designed to provide sufficient disturbance rejection of the drag term up to some particular frequency. Assuming that effective low frequency disturbance rejection can take place up to the bandwidth of the thrust actuator, then only drag disturbance frequencies beyond this would leak through and influence the axial specific acceleration.

Considering the point mass kinematics, it is clear from equation (2.47) that the axial specific acceleration drives solely into the velocity magnitude dynamics. Thus high frequency drag

disturbances will move directly into the velocity magnitude dynamics and result in changes in the velocity magnitude. These changes will in turn couple back into the rest of the rigid body rotational dynamics both kinematically and through the dynamic pressure.

However, the natural integration process of the velocity magnitude dynamics will filter the high frequency part of the drag coupling. Thus, given acceptable deviations in the velocity magnitude, the thrust actuator need only reject enough of the low frequency portion of the drag disturbance for its total effect on the velocity magnitude to be acceptable. By acceptable it is meant that the velocity magnitude perturbations are small enough to result in a negligible coupling into the rigid body rotational dynamics.

To obtain a mathematical hold on the above arguments, consider the closed loop transfer function from the normalised drag input to the axial specific acceleration output,

$$S_D(s) \equiv \frac{A_w(s)}{D(s)/m} \quad (3.28)$$

Through proper control system design, the gain of the output sensitivity transfer function above can be kept below a certain threshold within the controller bandwidth. The bandwidth of the axial specific acceleration controller will however typically be limited to that of the propulsion source for actuator saturation reasons. For frequencies above the controller bandwidth, the sensitivity transfer function will display some form of transient and then settle to unity gain. Considering the velocity magnitude dynamics of equation (2.47), the total transfer function of the normalised drag input to velocity magnitude is then,

$$\frac{V(s)}{D(s)/m} = \frac{S_D(s)}{s} \quad (3.29)$$

Note that the integrator introduced by the natural velocity dynamics will result in diminishing high frequency gains. Equation (3.29) can be used to determine whether drag perturbations will result in acceptable velocity magnitude perturbations. Conversely, given the expected drag perturbations and the acceptable level of velocity magnitude perturbations, the specifications on the sensitivity transfer function can be determined.

To ease the process of determining acceptable levels of velocity magnitude perturbations and expected levels of drag perturbations, it is convenient to write these both in terms of normal specific acceleration. The return disturbance in normal specific acceleration due to a normal specific acceleration perturbation can then be used to specify acceptable coupling levels. To this end, the following useful relationship is stated,

$$L = -Z_w^A = qSC_L \quad (3.30)$$

where L is the aircraft's lift. As a result of the thrust simplification arguments of the previous section, the above equation can be well approximated as follows,

$$L \approx -mC_w \quad (3.31)$$

Relating now the normalised drag to the normal specific acceleration the following result is obtained,

$$\frac{D/m}{C_w} = -\frac{1}{R_{LD}} \quad (3.32)$$

where R_{LD} is the aircraft's lift to drag ratio. Equation (3.30) can then be used to capture the dominant relationship between velocity perturbations and the resulting normal specific acceleration perturbations. Partially differentiating equation (3.30) with respect to the velocity magnitude yields the desired result,

$$\frac{\partial C_w}{\partial \bar{V}} = \frac{\partial}{\partial \bar{V}} \frac{-qSC_L}{m} \approx \frac{-\rho \bar{V} SC_L}{m} = 2 \frac{C_w}{\bar{V}} \quad (3.33)$$

Combining equations (3.29), (3.32) and (3.33) yields the *return disturbance* transfer function,

$$\begin{aligned} \Delta C_w(s) &\equiv \frac{\partial C_w}{\partial \bar{V}} \cdot \frac{V(s)}{D(s)/m} \cdot \frac{D/m}{C_w} \\ &= -2 \frac{C_w}{\bar{V} R_{LD}} \frac{S_D(s)}{s} \end{aligned} \quad (3.34)$$

Given an acceptable return disturbance level, the specifications of the sensitivity transfer function of equation (3.28) can be determined for a particular flight condition. With the velocity magnitude and lift to drag ratio forming part of the denominator of equation (3.34), the resulting constraints on the sensitivity function are mild for low operating values of normal specific acceleration. Only during very high g manoeuvres does the sensitivity specification become more difficult to practically realise. The mildness of the sensitivity function constraint will be further highlighted in Chapter 4 during the design of the associated inner loop controller and in Chapter 8 where a number of example aircraft are considered.

With the above arguments, the drag coupling into the axial specific acceleration dynamics can be ignored if the associated sensitivity function constraint is adhered to when designing the axial specific acceleration control system. Furthermore, ignoring the effect of drag coupling and adopting the sensitivity function constraint does not significantly limit the practical applicability of the decoupled model. Finally, note that with the drag term ignored in the axial specific acceleration dynamics, the dynamics become independent of the velocity magnitude and the air density. Thus, there is no need for the axial specific acceleration controller to operate on a timescale much faster than these variables. Considering the significantly band-limited nature of most thrust actuators, this greatly improves the practical viability of designing an axial specific acceleration control system.

3.2.4 Summary of simplified dynamics

With the nonlinear cross couplings terms discussed in the above subsections removed, the rigid body rotational dynamics can be written as follows,

$$\begin{bmatrix} \dot{\alpha} \\ \dot{\beta} \end{bmatrix} = \begin{bmatrix} 0 & 1 & 0 \\ 0 & 0 & -1 \end{bmatrix} \begin{bmatrix} P \\ Q \\ R \end{bmatrix} + \frac{1}{\bar{V}} \begin{bmatrix} 1 & 0 \\ 0 & 1 \end{bmatrix} \begin{bmatrix} C_W \\ B_W \end{bmatrix} + \frac{1}{\bar{V}} \begin{bmatrix} 1 & 0 \\ 0 & 1 \end{bmatrix} \begin{bmatrix} g_W^z \\ g_W^y \end{bmatrix} \quad (3.35)$$

$$\begin{bmatrix} \dot{P} \\ \dot{Q} \\ \dot{R} \end{bmatrix} = \begin{bmatrix} I_{xx} & -I_{xy} & -I_{xz} \\ -I_{xy} & I_{yy} & -I_{yz} \\ -I_{xz} & -I_{yz} & I_{zz} \end{bmatrix}^{-1} \left(- \begin{bmatrix} 0 & -R & Q \\ R & 0 & -P \\ -Q & P & 0 \end{bmatrix} \begin{bmatrix} I_{xx} & -I_{xy} & -I_{xz} \\ -I_{xy} & I_{yy} & -I_{yz} \\ -I_{xz} & -I_{yz} & I_{zz} \end{bmatrix} \begin{bmatrix} P \\ Q \\ R \end{bmatrix} + \begin{bmatrix} L \\ M \\ N \end{bmatrix} \right) \quad (3.36)$$

with,

$$\begin{bmatrix} A_W \\ B_W \\ C_W \end{bmatrix} = \frac{qS}{m} \begin{bmatrix} -C_D \\ C_y \\ -C_L \end{bmatrix} + \frac{1}{m} \begin{bmatrix} 1 \\ 0 \\ 0 \end{bmatrix} T \quad (3.37)$$

$$\begin{bmatrix} L \\ M \\ N \end{bmatrix} = qS \begin{bmatrix} b & 0 & 0 \\ 0 & \bar{c} & 0 \\ 0 & 0 & b \end{bmatrix} \begin{bmatrix} C_l \\ C_m \\ C_n \end{bmatrix} \quad (3.38)$$

$$[P_W] = \begin{bmatrix} 1 & 0 & 0 \\ Q \\ R \end{bmatrix} \quad (3.39)$$

where the coefficient of drag term has been left in the axial specific acceleration dynamics but its dependence on lift will be ignored. Barring the inertial cross coupling (or gyroscopic coupling) terms in equation (3.36), the dynamics presented above are completely linear. Furthermore, the arguments made in this section have shown that the assumptions required to linearise and decouple the dynamics up to this point do not significantly reduce the flight envelope of the aircraft or impose unachievable practical constraints on it. These arguments, particularly the lift into drag coupling arguments and analysis of section 3.2.3, serve as a contribution of this dissertation to the field of aircraft dynamics. In the following section, the inertial cross coupling terms are addressed.

3.3 Handling the inertial cross coupling terms

This section focuses on removing the nonlinear inertial cross coupling terms from the angular rate dynamics. It begins by developing a static inversion control law to feedback linearise the nonlinearities. Section 3.3.2 then provides a novel analysis of the adverse effects caused by the control law due to the direct forces that the aerodynamic actuators also produce. It is illustrated that the adverse effects are typically negligible except under extreme flight conditions where the cross coupling terms would instead have to be explicitly taken into

account in the rigid body rotational dynamics control laws.

3.3.1 Static inversion of the inertial cross coupling terms

A control law to feedback linearise the inertial cross coupling terms is made feasible by the assumption that aerodynamics actuators capable of producing moments about all three body axis unit vectors exist and that the angular rate coordinates in body axes can be measured/estimated. Begin by rewriting moment equation (3.7) as follows,

$$\begin{bmatrix} C_l \\ C_m \\ C_n \end{bmatrix} = \begin{bmatrix} 0 \\ C_{m_0} \\ 0 \end{bmatrix} + \begin{bmatrix} 0 & C_{l_\beta} & \frac{b}{2\bar{V}_a} C_{l_p} & 0 & \frac{b}{2\bar{V}_a} C_{l_r} \\ C_{m_\alpha} & 0 & 0 & \frac{\bar{c}}{2\bar{V}_a} C_{m_q} & 0 \\ 0 & C_{n_\beta} & \frac{b}{2\bar{V}_a} C_{n_p} & 0 & \frac{b}{2\bar{V}_a} C_{n_r} \end{bmatrix} \begin{bmatrix} \alpha \\ \beta \\ P \\ Q \\ R \end{bmatrix} + \begin{bmatrix} C_{l_{\delta_A}} & 0 & C_{l_{\delta_R}} \\ 0 & C_{m_{\delta_E}} & 0 \\ C_{n_{\delta_A}} & 0 & C_{n_{\delta_R}} \end{bmatrix} \begin{bmatrix} \delta_A + \delta'_A \\ \delta_E + \delta'_E \\ \delta_R + \delta'_R \end{bmatrix} \quad (3.40)$$

where the aerodynamic control inputs have been written as the sum of accented and non-accented variables. The accented variables will be used to invert the inertial cross coupling terms through feedback. The above equation can be written in matrix form as follows,

$$\mathbf{C}_M = \mathbf{C}_{M_0} + \mathbf{C}_{M_x} \mathbf{x} + \mathbf{C}_{M_\delta} \boldsymbol{\delta} + \mathbf{C}_{M_\delta'} \boldsymbol{\delta}' \quad (3.41)$$

where the matrix assignment is obvious. The moment vector coordinated in body axes can be written as follows,

$$\begin{aligned} \mathbf{M}_B &= q\mathbf{S}\mathbf{L}\mathbf{C}_M \\ &= q\mathbf{S}\mathbf{L}(\mathbf{C}_{M_0} + \mathbf{C}_{M_x} \mathbf{x} + \mathbf{C}_{M_\delta} \boldsymbol{\delta}) + q\mathbf{S}\mathbf{L}(\mathbf{C}_{M_\delta'} \boldsymbol{\delta}') \\ &= \bar{\mathbf{M}}_B + \mathbf{M}'_B \end{aligned} \quad (3.42)$$

where,

$$\bar{\mathbf{M}}_B = q\mathbf{S}\mathbf{L}(\mathbf{C}_{M_0} + \mathbf{C}_{M_x} \mathbf{x} + \mathbf{C}_{M_\delta} \boldsymbol{\delta}) \quad (3.43)$$

$$\mathbf{M}'_B = q\mathbf{S}\mathbf{L}(\mathbf{C}_{M_\delta'} \boldsymbol{\delta}') \quad (3.44)$$

and where \mathbf{L} is the diagonal matrix with reference lengths as used in equation (3.3). The rotational dynamics of equation (2.19) can thus be rewritten as follows,

$$\begin{aligned} \dot{\boldsymbol{\omega}}_B^{BI} &= \mathbf{I}_B^{-1} \left(-\mathbf{S}_{\omega_B^{BI}} \mathbf{I}_B \boldsymbol{\omega}_B^{BI} + \bar{\mathbf{M}}_B + \mathbf{M}'_B \right) \\ &= \mathbf{I}_B^{-1} (\bar{\mathbf{M}}_B) \end{aligned} \quad (3.45)$$

if,

$$-\mathbf{S}_{\omega_B^{BI}} \mathbf{I}_B \boldsymbol{\omega}_B^{BI} + \mathbf{M}'_B = \mathbf{0} \quad (3.46)$$

Substituting for $\mathbf{M}_B^{B'}$ from equation (3.44) gives the static inversion control law,

$$\delta' = \frac{1}{qS} \mathbf{C}_{M_{\delta'}}^{-1} \mathbf{L}^{-1} \mathbf{S}_{\omega_B^{BI}} \mathbf{I}_B \omega_B^{BI} \quad (3.47)$$

This control law removes the nonlinear inertial cross coupling terms from the angular velocity dynamics and in so doing reduces these dynamics to those of equation (3.45). Note that the inversion process is open loop (as with all inversion control laws) with the primary purpose of removing most of the cross coupling given that the system parameters and state estimates will display uncertainty. From equation (3.47), the aircraft parameters of primary importance for effective inversion are the control derivatives and the moments of inertia. However, it should be noted that for a large number of manoeuvre autopilot applications an inertial cross coupling inversion control law will not be necessary. This is because the control law responds to second order terms in the angular velocity components and thus only tends to produce significant actuator signals at very high angular rates or combinations thereof. With an appropriately limited angular rate flight envelope the inertial cross coupling terms can instead simply be ignored as negligible higher order terms.

3.3.2 Direct force feed-through analysis

The control law developed in the previous section removes the inertial cross coupling terms from the angular velocity dynamics. However, because the aerodynamic actuators not only produce moments but also produce direct forces on the aircraft, implementation of the control law will introduce disturbance inputs to the angle of incidence dynamics. However, for conventional aircraft the moment produced by the aerodynamic actuators is far more dominant than the force and as a result the disturbances introduced are expected to be negligible except in extreme angular velocity cases. This section analyses the direct force coupling as a result of the static inversion control law and in so doing provides a novel mathematical hold to determine the limiting angular rates for acceptable coupling.

To begin the analysis the static inversion control law of equation (3.47) is written out in full below,

$$\begin{bmatrix} \delta'_A \\ \delta'_E \\ \delta'_R \end{bmatrix} = \frac{1}{qS} \begin{bmatrix} C_{l_{\delta_A}} & 0 & C_{l_{\delta_R}} \\ 0 & C_{m_{\delta_E}} & 0 \\ C_{n_{\delta_A}} & 0 & C_{n_{\delta_R}} \end{bmatrix}^{-1} \begin{bmatrix} b & 0 & 0 \\ 0 & \bar{c} & 0 \\ 0 & 0 & b \end{bmatrix}^{-1} \begin{bmatrix} 0 & -R & Q \\ R & 0 & -P \\ -Q & P & 0 \end{bmatrix} \begin{bmatrix} I_{xx} & 0 & -I_{xz} \\ 0 & I_{yy} & 0 \\ -I_{xz} & 0 & I_{zz} \end{bmatrix} \begin{bmatrix} P \\ Q \\ R \end{bmatrix} \quad (3.48)$$

where the moment of inertia matrix has been simplified by noting that the aircraft is symmetrical about the body axes XZ-plane. To simplify the analysis to follow, it is first assumed that the following cross coupling terms in equation (3.48) are negligible,

$$I_{xz} = C_{n_{\delta_A}} = C_{l_{\delta_R}} = 0 \quad (3.49)$$

These are reasonable assumptions for conventional aircraft since the inertia cross product is often negligibly small and the two aerodynamic control derivatives are usually not dominant (they typically quantify adverse yaw and adverse roll respectively). Note that these terms have only been assumed negligible for clarity of the analysis to follow and will not be neglected, unless otherwise stated, for the remainder of this document. With the simplifications of equation (3.49) in place the control law can be written as follows,

$$\begin{bmatrix} \delta'_A \\ \delta'_E \\ \delta'_R \end{bmatrix} = \frac{1}{qS} \begin{bmatrix} \frac{1}{bC_{l_{\delta_A}}} QR(I_{zz} - I_{yy}) \\ \frac{1}{\bar{c}C_{m_{\delta_E}}} PR(I_{xx} - I_{zz}) \\ \frac{1}{bC_{n_{\delta_R}}} PQ(I_{yy} - I_{xx}) \end{bmatrix} \quad (3.50)$$

From the aerodynamic force equation of (3.2) and with reference to equations (3.6) and (3.5), it is clear that the aerodynamic actuators couple directly into the normal and lateral force coordinates in wind axes and indirectly into the axial force through drag. Ignoring the changes in drag, based on the arguments of section 3.2.3, and noting that the lateral force due to aileron deflection is negligible, the following result is obtained,

$$\begin{bmatrix} Z'_W \\ Y'_W \end{bmatrix} = qS \begin{bmatrix} -C_{L_{\delta_E}} & 0 \\ 0 & C_{y_{\delta_R}} \end{bmatrix} \begin{bmatrix} \delta'_E \\ \delta'_R \end{bmatrix} \quad (3.51)$$

where the accented force variables indicate a perturbation to the respective variable. Substituting the elevator and rudder components of the feedback linearisation control law and normalising the forces to the aircraft's mass gives,

$$\begin{bmatrix} C'_W \\ B'_W \end{bmatrix} = \begin{bmatrix} -\frac{C_{L_{\delta_E}}(I_{xx} - I_{zz})}{C_{m_{\delta_E}} m \bar{c}} PR \\ \frac{C_{y_{\delta_R}}(I_{yy} - I_{xx})}{C_{n_{\delta_R}} mb} PQ \end{bmatrix} = \begin{bmatrix} \frac{(I_{xx} - I_{zz}) PR}{l_T m} \\ \frac{(I_{xx} - I_{yy}) PQ}{l_F m} \end{bmatrix} \quad (3.52)$$

where l_T is the effective length to the tail-plane and l_F is the effective length to the fin with the following relationship to the control derivatives,

$$\frac{l_T}{\bar{c}} = -\frac{C_{m_{\delta_E}}}{C_{L_{\delta_E}}} \quad (3.53)$$

$$\frac{l_F}{b} = -\frac{C_{n_{\delta_R}}}{C_{y_{\delta_R}}} \quad (3.54)$$

For most aircraft the effective length to the tail-plane and fin are very similar and for the

purposes of simplifying the analysis they will be considered equal and be denoted by l . Substituting the relationship into equation (3.52) and writing the moments of inertia in terms of mass and the roll, pitch and yaw radii of gyration (r_x , r_y and r_z respectively) yields,

$$\begin{bmatrix} C'_w \\ B'_w \end{bmatrix} = \begin{bmatrix} \frac{(r_x^2 - r_z^2)}{l} PR \\ \frac{(r_x^2 - r_y^2)}{l} PQ \end{bmatrix} \quad (3.55)$$

Now,

$$\begin{bmatrix} C'_w \\ B'_w \end{bmatrix} = \begin{bmatrix} \frac{(r_x^2 - r_z^2)}{l} PR \\ \frac{(r_x^2 - r_y^2)}{l} PQ \end{bmatrix} \leq \begin{bmatrix} l \left(\frac{r_z}{l} \right)^2 PR \\ l \left(\frac{r_y}{l} \right)^2 PQ \end{bmatrix} \leq l \left(\frac{r_{y/z}}{l} \right)^2 \begin{bmatrix} PR \\ PQ \end{bmatrix} \quad (3.56)$$

where $r_{y/z}$ is the greater of the pitch and yaw radius of gyration. Equation (3.56) can be used to determine bounds on the products PR and PQ that will result in acceptable normal and lateral specific acceleration coupling levels. For conventional aircraft the squared term in parenthesis is typically small and so the acceptable products tend to be large. Using the parameters for a standard 5 kg aerobatic UAV (see Appendix A), it can be shown that for less than 0.1 g of direct acceleration disturbance coupling, the angular rate products are limited to be less than 6.5 (rad/s)^2 . This constraint thus defines two hyperbolic boundaries in state space in the two angular rate products.

To gain further insight into the above constraint the steady state case where the body and wind axis systems rotate together can be considered. Here the angular velocity relationship of equation (2.49) for the wind axis system can be used to substitute for the pitch and yaw angular velocities in equation (3.56). Doing this yields,

$$\begin{bmatrix} C'_w \\ B'_w \end{bmatrix} \leq l \left(\frac{r_{y/z}}{l} \right)^2 \left\| \frac{P}{\bar{V}} \begin{bmatrix} B_w + g e_{23}^{wI} \\ -C_w - g e_{33}^{wI} \end{bmatrix} \right\| \quad (3.57)$$

The lateral specific acceleration is usually regulated very close to zero so that the aircraft flies coordinated turns. Furthermore, each of the attitude parameters in equation (3.57) is bounded between plus and minus one. The maximum normal specific acceleration is bounded by the airframe limits and is most often significantly larger than g. Thus, to a good approximation equation (3.57) can be written as follows,

$$\begin{bmatrix} C'_w \\ B'_w \end{bmatrix} \leq l \left(\frac{r_{y/z}}{l} \right)^2 \left\| \frac{P}{\bar{V}} \begin{bmatrix} B_w + g e_{23}^{wI} \\ -C_w - g e_{33}^{wI} \end{bmatrix} \right\| \approx l \left(\frac{r_{y/z}}{l} \right)^2 \left\| \frac{P}{\bar{V}} \begin{bmatrix} g e_{23}^{wI} \\ -C_w \end{bmatrix} \right\| \quad (3.58)$$

and so,

$$\begin{bmatrix} C'_w \\ B'_w \end{bmatrix} \leq \left| \left(\frac{r_{y/z}}{l} \right)^2 \frac{gl}{\bar{V}} \begin{bmatrix} 1 \\ n_{\max} \end{bmatrix} P \right| \quad (3.59)$$

where n_{\max} is the maximum normal specific acceleration measured in g's. The above equation reveals that the lateral acceleration perturbation resulting from direct force feed-through from the static inversion control law is potentially the most prominent. It is thus the most likely limiting factor for the implementation of the static inversion control law used to remove the inertial cross coupling terms. Analysing this equation it is noted that because the first squared term in parenthesis is usually small and \bar{V} usually large, large roll rate commands are required before the lateral specific acceleration perturbations start to become significant. For example, using the aircraft data from Appendix C for a typical aerobatic UAV travelling at 30 m/s with a maximum normal specific acceleration of 5 g's, the relationship of equation (3.59) becomes,

$$|B'_w| \leq \left| \frac{n_{\max} g}{200} P \right| \quad (3.60)$$

If the maximum limit on the lateral acceleration perturbation is set to 0.1 g's then roll rates of up to 4 rad/s can be handled when the aircraft is experiencing maximum normal acceleration (an extremely unlikely event in itself). Equation (3.59) thus provides a second useful measure as to whether the static inversion control law of equation (3.47) will cause unacceptable direct feed-through acceleration disturbances. The analysis however suggests that for all but very extreme flight conditions the acceleration disturbances will be negligible and the inertial cross coupling terms can either be effectively inverted or simply ignored from the rigid body rotational dynamics.

3.4 The linear decoupled rigid body rotational dynamics

With the linearising and decoupling simplifications of section 3.2 and the feedback linearisation control law and associated arguments of section 3.3, the rigid body rotational dynamics and the force and moment models can be combined and written as three sets of linear decoupled dynamic equations. The three sets are listed below and will be referred to as the axial, normal and lateral dynamics respectively,

Axial:

$$\dot{T} = \begin{bmatrix} -1 \\ \tau_T \end{bmatrix} T + \begin{bmatrix} 1 \\ \tau_T \end{bmatrix} T_C \quad (3.61)$$

$$A_w = \begin{bmatrix} 1 \\ m \end{bmatrix} T + \begin{bmatrix} -qS \\ m \end{bmatrix} C_D \quad (3.62)$$

Normal:

$$\begin{bmatrix} \dot{\alpha} \\ \dot{Q} \end{bmatrix} = \begin{bmatrix} -\frac{qS}{m\bar{V}} C_{L_\alpha} & 1 - \frac{qS}{m\bar{V}} \frac{\bar{c}}{2\bar{V}_a} C_{L_Q} \\ \frac{qS\bar{c}}{I_{yy}} C_{m_\alpha} & \frac{qS\bar{c}}{I_{yy}} \frac{\bar{c}}{2\bar{V}_a} C_{m_Q} \end{bmatrix} \begin{bmatrix} \alpha \\ Q \end{bmatrix} + \begin{bmatrix} -\frac{qS}{m\bar{V}} C_{L_{\delta_E}} \\ \frac{qS\bar{c}}{I_{yy}} C_{m_{\delta_E}} \end{bmatrix} \delta_E + \begin{bmatrix} -\frac{qS}{m\bar{V}} C_{L_0} \\ \frac{qS\bar{c}}{I_{yy}} C_{m_0} \end{bmatrix} + \begin{bmatrix} \frac{g}{\bar{V}} \\ 0 \end{bmatrix} e_{33}^{WI} \quad (3.63)$$

$$C_W = \begin{bmatrix} -\frac{qS}{m} C_{L_\alpha} & -\frac{qS}{m} \frac{\bar{c}}{2\bar{V}_a} C_{L_Q} \end{bmatrix} \begin{bmatrix} \alpha \\ Q \end{bmatrix} + \begin{bmatrix} -\frac{qS}{m} C_{L_{\delta_E}} \\ -\frac{qS}{m} C_{L_0} \end{bmatrix} \delta_E + \begin{bmatrix} -\frac{qS}{m} C_{L_0} \end{bmatrix} \quad (3.64)$$

Lateral:

$$\begin{bmatrix} \dot{\beta} \\ \dot{P} \\ \dot{R} \end{bmatrix} = \begin{bmatrix} \frac{qS}{m\bar{V}} C_{y_\beta} & \frac{qS}{m\bar{V}} \frac{b}{2\bar{V}_a} C_{y_P} & \frac{qS}{m\bar{V}} \frac{b}{2\bar{V}_a} C_{y_R} - 1 \\ \frac{qSb}{I_{xx}} \bar{C}_{l_\beta} & \frac{qSb}{I_{xx}} \frac{b}{2\bar{V}_a} \bar{C}_{l_P} & \frac{qSb}{I_{xx}} \frac{b}{2\bar{V}_a} \bar{C}_{l_R} \\ \frac{qSb}{I_{zz}} \bar{C}_{n_\beta} & \frac{qSb}{I_{zz}} \frac{b}{2\bar{V}_a} \bar{C}_{n_P} & \frac{qSb}{I_{zz}} \frac{b}{2\bar{V}_a} \bar{C}_{n_R} \end{bmatrix} \begin{bmatrix} \beta \\ P \\ R \end{bmatrix} + \begin{bmatrix} \frac{qS}{m\bar{V}} C_{y_{\delta_A}} & \frac{qS}{m\bar{V}} C_{y_{\delta_R}} \\ \frac{qSb}{I_{xx}} \bar{C}_{l_{\delta_A}} & \frac{qSb}{I_{xx}} \bar{C}_{l_{\delta_R}} \\ \frac{qSb}{I_{zz}} \bar{C}_{n_{\delta_A}} & \frac{qSb}{I_{zz}} \bar{C}_{n_{\delta_R}} \end{bmatrix} \begin{bmatrix} \delta_A \\ \delta_R \end{bmatrix} + \begin{bmatrix} \frac{g}{\bar{V}} \\ 0 \\ 0 \end{bmatrix} e_{23}^{WI} \quad (3.65)$$

$$\begin{bmatrix} B_W \\ P_W \end{bmatrix} = \begin{bmatrix} \frac{qS}{m} C_{y_\beta} & \frac{qS}{m} \frac{b}{2\bar{V}_a} C_{y_P} & \frac{qS}{m} \frac{b}{2\bar{V}_a} C_{y_R} \\ 0 & 1 & 0 \end{bmatrix} \begin{bmatrix} \beta \\ P \\ R \end{bmatrix} + \begin{bmatrix} \frac{qS}{m} C_{y_{\delta_A}} & \frac{qS}{m} C_{y_{\delta_R}} \\ 0 & 0 \end{bmatrix} \begin{bmatrix} \delta_A \\ \delta_R \end{bmatrix} \quad (3.66)$$

The barred stability and control derivatives of the lateral model are defined below as a function of the original aircraft stability derivatives and the moment and product of inertia terms,

$$\bar{C}_{l_0} \equiv \left(C_{l_0} + \frac{I_{xz}}{I_{zz}} C_{n_0} \right) \Delta \quad (3.67)$$

$$\bar{C}_{n_0} \equiv \left(C_{n_0} + \frac{I_{xz}}{I_{zz}} C_{l_0} \right) \Delta \quad (3.68)$$

with,

$$\Delta = \frac{I_{xx} I_{zz}}{I_{xx} I_{zz} - I_{xz} I_{xz}} \quad (3.69)$$

where the terms in parenthesis in equations (3.67) and (3.68) are taken from the set of states and controls,

$$S = \{ \beta, P, R, \delta_A, \delta_R \} \quad (3.70)$$

Being able to both linearise and decouple the rigid body rotational dynamics greatly simplifies the task of designing inner loop controllers to regulate the specific acceleration and angular rate signals of interest with dynamically invariant closed loop responses. Note that all terms

that form part of the system matrices above have been argued to display a timescale separation to the rigid body rotational dynamics and as a result can be considered parameters in the model. With linear, decoupled inner loop dynamics, the possibility of designing simple, closed form pole placement type control laws to provide exponential inner loop stability is opened up.

3.4.1 Normal dynamics and the Short Period mode

Considering the normal dynamics further, it is clear that barring the final gravitational coupling term, they are simply the dynamics generated by the standard Short Period mode approximation [43]. Arriving at the standard Short Period mode approximation dynamics in this unconventional manner illustrates the gross attitude independent nature of this mode of motion and forms part of the contribution of this dissertation to the field of aircraft dynamics. At any particular wind axis system attitude, the gravity term simply acts as a bias input to the normal dynamics. Thus, it can be seen that the Short Period mode approximation is valid for all gross attitudes. Intuitively this makes sense since the physical phenomenon that manifests itself into what is classically referred to as the Short Period mode is not gross attitude dependent. Whether an aircraft is flying straight and level, inverted or climbing steeply, the short period motion of the aircraft relative to the wind axis system remains the same, biased only through the gravity coupling term.

Thus, the normal dynamics can simply be thought of as the short period mode dynamics. Typically these dynamics are fast, reasonably well damped and stable. Thus, as previously argued, these dynamics will most often naturally meet the timescale separation condition of Chapter 2. If however they do not, then the speed of these dynamics can be increased through feedback. There are however limitations on the upper bandwidth of the system, which will be discussed further in the chapters to follow.

3.4.2 Lateral dynamics and the Roll/Dutch-Roll modes

When considering the lateral dynamics, it is clear that barring the gravitational coupling term, these are simply the standard Roll/Dutch-Roll approximation dynamics [43]. Again, arriving at the standard Roll/Dutch-Roll mode approximation dynamics in this unconventional manner illustrates the gross attitude independent nature of these modes of motion and forms part of the contribution of this dissertation to the field of aircraft dynamics. The attitude dependent gravitational force term acts as a bias input to the dynamics for a particular gross attitude. Thus, the Roll/Dutch-Roll approximation is shown to be valid for all gross attitudes and the lateral dynamics can simply be thought of as describing these modes of motion. The gross attitude independence of the modes again makes intuitive sense when considering the phenomena that manifest themselves into the Roll/Dutch-Roll modes. These phenomena are not gross attitude dependent but rather are a function of the aircraft's attitude relative to the wind axis system.

The Roll and Dutch Roll modes are also typically fast relative to the bandwidth (or desired bandwidth) of the outer loop point mass kinematics states. The speed of both modes however can be increased through feedback control. For example, the frequency of the typically oscillatory Dutch Roll mode may need to be artificially increased to meet timescale separation requirements. Limitations on the upper bandwidths of these systems will be explored in the chapters that follow.

3.5 Conclusion

This chapter began by expanding and structuring the force and moment models of Chapter 2. A standard aerodynamic model for small incidence angle flight was presented together with a simple thrust and standard flat earth gravitational model. The nonlinearities and cross couplings inherent in the rigid body rotational dynamics were then analysed. After small angle trigonometric assumptions were used to simplify the dynamics, cross coupling terms were removed by arguing that their effects would only become dominant during unlikely or very extreme flight conditions. The nonlinear coupling of lift into drag and in turn into the axial dynamics was replaced by a practically feasible sensitivity function constraint on the closed loop axial dynamics. The analysis of the nonlinear cross couplings and in particular the lift into drag coupling, forms part of the contribution of this dissertation to the field of aircraft dynamics.

With the nonlinear and cross coupling terms removed, a feedback linearisation control law was derived to negate the inertial cross coupling terms. A novel analysis showed that the adverse effects of the control law's direct force feed-through is typically negligible except under extreme flight conditions. With all of the above steps taken, the rigid body rotational dynamics were shown to be linear and to decouple into axial, normal and lateral dynamics. The normal dynamics were shown to be equivalent to those generated by the classical Short Period mode approximation barring the biasing gravitational acceleration term. Similarly, the lateral dynamics were shown to be equivalent to those generated by the classical Roll/Dutch-Roll mode approximation. Obtaining the Short Period and Roll/Dutch-Roll mode approximations in this alternative manner highlights the attitude independent nature of these modes of motion and serves as another contribution of this dissertation to the field of aircraft dynamics.

With all of the initial mathematics in place, it is prudent to provide a graphical overview of the thesis content still to come. Figure 3.1 provides a block diagram overview of the individual controllers to be designed and analysed in the chapters that follow. On the right hand side of the dash-dotted line in Figure 3.1 are the inner loop, aircraft specific controllers. Over the course of Chapters 4 and 5, decoupled controllers will be designed to regulate the axial, normal and lateral specific acceleration as well as the roll rate about the velocity vector. The controller designs will be based on the linear, decoupled dynamics derived in this chapter. The linear dynamics significantly aid the design and associated analysis of the inner loop

controllers.

In Chapter 6, the focus shifts to the design of an outer loop guidance controller, shown in the centre of Figure 3.1. This outer loop controller design is based on the point mass kinematics only and is thus aircraft independent. As illustrated in the figure, the guidance controller interfaces with the actual aircraft via the four inner loop controllers. The inner loop controllers thus serve to create virtual actuators for use at a guidance level. The guidance controller accepts a feasible reference trajectory and is responsible for using the virtual actuators to regulate the aircraft onto the trajectory. The generation of feasible reference trajectories will be the topic of Chapter 7 as denoted by the left most block of Figure 3.1. Chapter 8 provides the results of a number of application examples where the control structure of Figure 3.1 is applied to the aircraft. Finally, conclusions are drawn in Chapter 9.

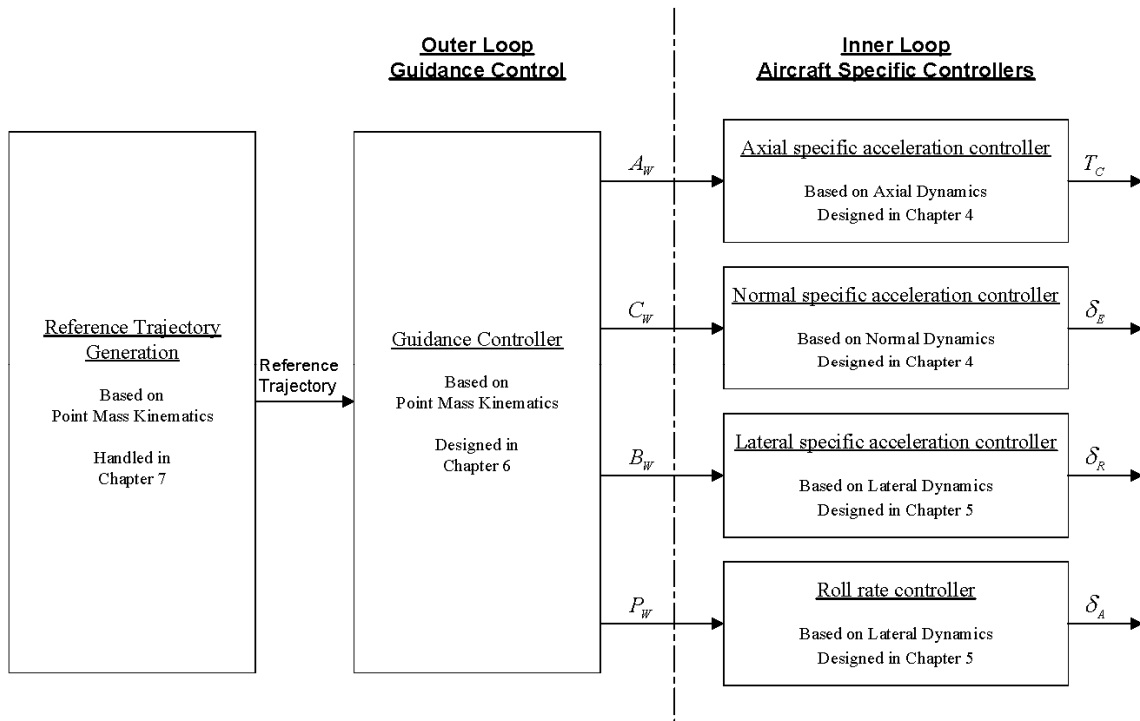


Figure 3.1 – Block diagram overview of the manoeuvre autopilot control system to be designed

Chapter 4

Inner Loop Controllers: Axial and Normal Dynamics

The detailed design and associated analysis of the inner loop axial and normal specific acceleration controllers is presented in this chapter. The controller designs are based on the linear, decoupled rigid body rotational dynamics models derived in the previous chapter. Pole placement is used to ensure stability, performance and an invariant dynamic response of the closed loop system. Guidelines for pole placement are also investigated, driven by either enforced or inherent constraints on the systems. A novel normalised non-dimensional time control system for normal specific acceleration is also introduced specifically to better handle inherent system performance constraints. All controllers are made generic by designing the control laws as a function of the aircraft parameters. This allows them to be easily applied to different aircraft as illustrated in Chapter 8.

4.1 Axial specific acceleration controller

In this section a controller capable of regulating the axial specific acceleration is designed. Attention will also be given to the closed loop sensitivity function constraint of equation (3.34) for a specific return disturbance level. Rewriting the axial dynamics of equations (3.61) and (3.62) below for convenience,

$$\dot{T} = \begin{bmatrix} -1 \\ \tau_T \end{bmatrix} T + \begin{bmatrix} 1 \\ \tau_T \end{bmatrix} T_C \quad (4.1)$$

$$A_W = \begin{bmatrix} 1 \\ m \end{bmatrix} T + \begin{bmatrix} -1 \\ m \end{bmatrix} D \quad (4.2)$$

Define now the following Proportional-Integral (PI) control law with enough degrees of freedom to allow for arbitrary closed loop pole placement,

$$T_c = -K_A A_W - K_E E_A \quad (4.3)$$

$$\dot{E}_A = A_W - A_{W_g} \quad (4.4)$$

where A_{w_r} is the reference axial specific acceleration command. The integrator in the controller is essential for robustness towards uncertain steady state drag and thrust actuator offsets. Substituting the control law into the engine lag dynamics,

$$\begin{aligned}\dot{T} &= -\frac{1}{\tau_T}T + \frac{1}{\tau_T}[-K_A A_w - K_E E_A] \\ &= \left[-\frac{1}{\tau_T} - \frac{K_A}{m\tau_T}\right]T + \left[-\frac{K_E}{\tau_T}\right]E_A + \left[\frac{K_A}{m\tau_T}\right]D\end{aligned}\quad (4.5)$$

Substituting the axial specific acceleration into the integrator dynamics and writing the integrator dynamics and thrust dynamics in state space form,

$$\begin{bmatrix} \dot{T} \\ \dot{E}_A \end{bmatrix} = \begin{bmatrix} -\frac{1}{\tau_T} - \frac{K_A}{m\tau_T} & -\frac{K_E}{\tau_T} \\ \frac{1}{m} & 0 \end{bmatrix} \begin{bmatrix} T \\ E_A \end{bmatrix} + \begin{bmatrix} 0 \\ -1 \end{bmatrix} A_{w_r} + \begin{bmatrix} \frac{K_A}{m\tau_T} \\ -\frac{1}{m} \end{bmatrix} D\quad (4.6)$$

The characteristic equation of the closed loop system is,

$$s^2 + \left(\frac{1}{\tau_T} + \frac{K_A}{m\tau_T}\right)s + \frac{K_E}{m\tau_T} = 0\quad (4.7)$$

Given the desired characteristic equation,

$$\alpha_c(s) = s^2 + \alpha_1 s + \alpha_0\quad (4.8)$$

the feedback gains become,

$$K_A = m(\tau_T \alpha_1 - 1)\quad (4.9)$$

$$K_E = m\tau_T \alpha_0\quad (4.10)$$

These simple, closed form solution gains will ensure an invariant closed loop axial specific acceleration dynamic response as desired. The controller design freedom is reduced to that of selecting appropriate closed loop poles bearing in mind factors such as actuator saturation and the sensitivity function constraint of section 3.2.3. To investigate the closed loop sensitivity function for this particular control law, the feedback gains above are substituted back into equation (4.6),

$$\begin{bmatrix} \dot{T} \\ \dot{E}_A \end{bmatrix} = \begin{bmatrix} -\alpha_1 & -m\alpha_0 \\ \frac{1}{m} & 0 \end{bmatrix} \begin{bmatrix} T \\ E_A \end{bmatrix} + \begin{bmatrix} 0 \\ -1 \end{bmatrix} A_{w_r} + \begin{bmatrix} \alpha_1 - \tau_T^{-1} \\ -\frac{1}{m} \end{bmatrix} D\quad (4.11)$$

$$A_w = \begin{bmatrix} \frac{1}{m} & 0 \end{bmatrix} \begin{bmatrix} T \\ E_A \end{bmatrix} + \begin{bmatrix} -\frac{1}{m} \end{bmatrix} D\quad (4.12)$$

Using the definition of the drag sensitivity function in equation (3.28) yields the following result,

$$\begin{aligned}
S_D(s) &\equiv \frac{A_w(s)}{D(s)/m} \\
&= \frac{m \begin{bmatrix} 1 & 0 \\ m & 0 \end{bmatrix} \begin{bmatrix} s & -m\alpha_0 \\ 1 & s + \alpha_1 \end{bmatrix} \begin{bmatrix} \alpha_1 - \tau_T^{-1} \\ -\frac{1}{m} \end{bmatrix}}{s^2 + \alpha_1 s + \alpha_0} - 1 \\
&= \frac{(\alpha_1 - \tau_T^{-1})s + \alpha_0}{s^2 + \alpha_1 s + \alpha_0} - 1 \\
&= -\frac{s}{\tau_T \alpha_0} \left(\frac{\tau_T s + 1}{1} \frac{\alpha_0}{s^2 + \alpha_1 s + \alpha_0} \right)
\end{aligned} \tag{4.13}$$

For actuator saturation reasons the closed loop axial dynamics bandwidth is typically limited to being close to that of the open loop thrust actuator and thus for reasonable closed loop damping ratios the second order term in parenthesis in the sensitivity function above can be well approximated by a first order model to simplify the sensitivity function as follows,

$$S_D(s) \approx -\frac{s}{\tau_T \alpha_0} \frac{1}{\tau_A s + 1} \tag{4.14}$$

Here,

$$\tau_A = \frac{1}{\tau_T \alpha_0} \tag{4.15}$$

is the approximating time constant and is calculated to match the actual and approximated high frequency sensitivity function asymptotes. Note that the approximate sensitivity function of equation (4.14) will not capture the extra overshoot experienced close to the bandwidth of the closed loop system that is required to satisfy Bode's sensitivity function integrals. However, with well damped, stable closed loop poles and no right half plane zeros in the system, the extra overshoot will be negligible and the sensitivity function of equation (4.14) is expected to yield a good approximation to that of equation (4.13). The return disturbance transfer function of equation (3.34) can then be calculated by substituting equation (4.14) into equation (3.34) to yield,

$$\begin{aligned}
\Delta C_w(s) &= -2 \frac{C_w}{\bar{V} R_{LD}} \frac{S_D(s)}{s} \\
&= 2 \frac{C_w}{\bar{V} R_{LD} \tau_T \alpha_0} \frac{1}{\tau_A s + 1}
\end{aligned} \tag{4.16}$$

Given the maximum allowable gain of the return disturbance transfer function γ , a lower bound constraint on the natural frequency (ω_n) of the closed loop axial control system can be

calculated,

$$\alpha_0 = \omega_n^2 \geq \left[\frac{2C_W}{\bar{V}R_{LD}\tau_T\gamma} \right]_{\max} \quad (4.17)$$

where the subscript max in the above equation implies the maximum value of the right hand term above. Thus,

$$\frac{\omega_n}{\omega_T} \geq \sqrt{\left[\frac{2C_W\tau_T}{\bar{V}R_{LD}\gamma} \right]_{\max}} \quad (4.18)$$

where,

$$\omega_T = \frac{1}{\tau_T} \quad (4.19)$$

is the open loop bandwidth of the thrust actuator. The novel sensitivity function based frequency constraint of equation (4.18) can be used to determine the minimum allowable closed loop axial specific acceleration bandwidth relative to the open loop thrust actuator bandwidth for a desired return disturbance level. For example, given that an aircraft is to fly with a minimum velocity of 20 m/s with a maximum normal acceleration of 4 g's and a minimum lift to drag ratio of 10. Then, for more than 20 dB's of return disturbance rejection, the natural frequency of the closed loop system should have the following relationship to the open loop thrust bandwidth,

$$\frac{\omega_n}{\omega_T} \geq 2\sqrt{\tau_T} \quad (4.20)$$

For this specific example, thrust actuators with a bandwidth of below 4 rad/s (time constant of greater than 0.25 s) will require that the closed loop natural frequency is greater than that of the thrust actuator. Despite the fairly extreme nature of this example (low velocity magnitude, high g's and low lift to drag ratio), thrust time constants on the order of 0.25 s are still practically feasible for UAVs. The deduction is thus that the axial specific acceleration controller will be practically applicable to most UAVs.

4.2 Normal specific acceleration controller

The normal dynamics are restated below for convenience using dimensional stability derivative notation,

$$\begin{bmatrix} \dot{\alpha} \\ \dot{Q} \end{bmatrix} = \begin{bmatrix} -\frac{L_\alpha}{m\bar{V}} & 1 - \frac{L_Q}{m\bar{V}} \\ \frac{M_\alpha}{I_{yy}} & \frac{M_Q}{I_{yy}} \end{bmatrix} \begin{bmatrix} \alpha \\ Q \end{bmatrix} + \begin{bmatrix} -\frac{L_{\delta_E}}{m\bar{V}} \\ \frac{M_{\delta_E}}{I_{yy}} \end{bmatrix} \delta_E + \begin{bmatrix} -\frac{L_0}{m\bar{V}} \\ \frac{M_0}{I_{yy}} \end{bmatrix} + \begin{bmatrix} \frac{g}{\bar{V}} \\ 0 \end{bmatrix} e_{33}^{w1} \quad (4.21)$$

$$C_w = \begin{bmatrix} -\frac{L_\alpha}{m} & -\frac{L_Q}{m} \end{bmatrix} \begin{bmatrix} \alpha \\ Q \end{bmatrix} + \begin{bmatrix} -\frac{L_{\delta_E}}{m} \\ -\frac{L_0}{m} \end{bmatrix} \delta_E + \begin{bmatrix} -\frac{L_0}{m} \end{bmatrix} \quad (4.22)$$

The dimensional stability and control derivative notation is standard as defined below,

$$A_B \equiv qS(l) \frac{\partial C_A}{\partial B'} n \quad (4.23)$$

where the length term l in parenthesis is unity for the force derivatives, \bar{c} for the pitch moment derivatives and b for the roll and yaw moment derivatives. The term n is the non-dimensionalising coefficient taken from equation (3.9).

This section presents the design and associated analysis of a normal specific acceleration controller that yields an invariant dynamic response for all point mass kinematics states. As argued in section 2.3.1 the design of such a controller is dramatically simplified if the velocity magnitude and air density can be considered parameters in the normal dynamics and the coupling of the flight path angle can be rejected using dynamic inversion. To consider the velocity magnitude and air density as parameters rather than dependant variables, requires a timescale separation to exist between these two quantities and the normal dynamics. Therefore, it is important to investigate any upper limits on the allowable bandwidth of the normal dynamics as this will in turn clamp the upper bandwidth of the velocity magnitude and the air density (altitude) dynamics. Furthermore, it is important to investigate the eligibility of the normal dynamics for effective dynamic inversion of the gravity coupling term. Thus, before continuing with the normal specific acceleration controller design, the natural normal dynamics are analysed in more detail.

4.2.1 Natural normal specific acceleration dynamics

Consider the dynamics from the elevator control input to the normal specific acceleration output. The direct feed-through term in the normal specific acceleration output implies that the associated transfer function has as many zeros as it does poles. Investigating the poles first, Appendix B derives the standard [43] characteristic equation for the normal dynamics (Short Period mode) poles shown below,

$$p(s) = s^2 + \left(\frac{L_\alpha}{m\bar{V}} - \frac{M_Q}{I_{yy}} \right) s - \left(\frac{L_\alpha}{m\bar{V}} \frac{M_Q}{I_{yy}} + \frac{M_\alpha}{I_{yy}} \right) \quad (4.24)$$

where it has been assumed that,

$$\left| \frac{L_Q}{m\bar{V}} \right| \ll 1 \quad (4.25)$$

Note that this assumption is valid for almost all aircraft and is commonly made in analysing

aircraft dynamics [43]. Considering equation (4.24) it is important to note that the normal dynamics poles are not influenced by the lift due to pitch rate or elevator deflection. The importance of this will be made clear later on in this section. The zeros from the elevator input to the normal specific acceleration output are shown in Appendix B to be the roots of the characteristic equation,

$$s^2 - \frac{L_Q}{I_{yy}} \left(\frac{M_Q}{L_Q} - \frac{M_{\delta_E}}{L_{\delta_E}} \right) s - \frac{L_\alpha}{I_{yy}} \left(\frac{M_\alpha}{L_\alpha} - \frac{M_{\delta_E}}{L_{\delta_E}} \right) = 0 \quad (4.26)$$

Note that in obtaining the novel result above, use was made of equation (4.25). Now define the following relationships,

$$l_N \equiv -\frac{M_\alpha}{L_\alpha} \quad (4.27)$$

$$l_T \equiv -\frac{M_{\delta_E}}{L_{\delta_E}} \quad (4.28)$$

$$l_D \equiv -\frac{M_Q}{L_Q} \quad (4.29)$$

where l_N is the length to the neutral point, l_T is the effective length to the tail-plane, l_D is the effective damping arm length and all lengths are relative to the centre of mass. The characteristic equation for the zeros can then be written as follows,

$$s^2 - \frac{L_Q}{I_{yy}} (l_T - l_D) s - \frac{L_\alpha}{I_{yy}} (l_T - l_N) = 0 \quad (4.30)$$

Completing the square to find the roots of equation (4.30) gives,

$$\left[s - \frac{1}{2} \frac{L_Q}{I_{yy}} (l_T - l_D) \right]^2 = \left[\frac{1}{2} \frac{L_Q}{I_{yy}} (l_T - l_D) \right]^2 + \frac{L_\alpha}{I_{yy}} (l_T - l_N) \quad (4.31)$$

For most aircraft the effective length to the tail-plane and effective damping arm lengths are very similar. This is because most of the damping arises from the tail-plane which is also typically home to the elevator control surface. Thus the moment arm lengths for pitch rate and elevator deflection induced forces are very similar. As a result, the first term on the right hand side of equation (4.31) is most often negligibly small and to a good approximation, the zeros from elevator input to normal specific acceleration output are,

$$z_{1,2} \approx \frac{1}{2} \frac{L_Q}{I_{yy}} (l_T - l_D) \pm \sqrt{\frac{L_\alpha}{I_{yy}} (l_T - l_N)} \quad (4.32)$$

Analysis of equation (4.32) reveals that the only effect of the lift due to pitch rate derivative on

the zeros is that of producing an offset along the real axis. As previously argued, the effective tail-plane and damping arms are typically very similar and as a result the offset is usually small. Thus, it can be seen that to a good approximation, the lift due to pitch rate plays no role in determining the elevator to normal specific acceleration dynamics.

On the other hand, the effective length to the tail-plane and the length to the neutral point typically differ significantly. With this difference scaled by the lift due to angle of attack (which is typically far greater than the lift due to pitch rate) it can be seen that the second term in equation (4.32) will dominate the first in determining the zero positions. Thus although the lift due to elevator deflection played no role in determining the system poles, it plays a large role in determining the zeros. Knowing the positions of the zeros is important from a controller design point of view since not only will they affect the dynamic response of the system but they may also impose controller independent limitations on the practically achievable system bandwidth.

To further illustrate this point, consider a conventional statically stable aircraft where the effective length to the tail-plane is many times greater than the length to the neutral point and very similar in magnitude to the effective damping arm length. In this situation, the first term in equation (4.32) is typically negligible and the second term is large and positive thus giving rise to two real zeros of opposite sign. The result, as intuitively expected, is that the dynamics from the elevator to normal specific acceleration are Non-Minimum Phase (NMP) since a Right Half Plane (RHP) zero exists. A RHP zero places severe restrictions on the practically attainable upper bandwidth of the closed loop normal specific acceleration dynamics. These restrictions are independent of the controller architecture employed [44,45]. Furthermore, designing a dynamic inversion control law in a system with NMP dynamics, will result in an impractical solution with internal dynamics that may or may not be stable [26,32].

Since this NMP dynamics case is by far the most common for aircraft, the limits imposed by it shall be investigated further in the following subsection. The goal of the investigation is to seek a set of conditions under which the effects of a RHP zero become negligible, equivalently allowing the NMP nature of a system to be ignored. With these conditions identified and satisfied, the design of the normal specific acceleration controller can continue based on a set of simplified dynamics that do not capture the NMP nature of the system.

4.2.2 Analysis of the NMP dynamics case

Ignoring the real axis offset term in the typical position of the zeros in equation (4.32), the transfer function from the elevator input to the normal specific acceleration is of the form,

$$G(s) = k \frac{\omega_n^2}{s^2 + 2\zeta\omega_n s + \omega_n^2} \frac{z_0^2 - s^2}{z_0^2} \quad (4.33)$$

However, the dynamic effect of the left half plane zero is of less interest and is furthermore

most often largely negated by un-modelled dynamics such as those introduced through servo lag. Thus, in the analysis to follow, the transfer function will be approximated as follows,

$$G(s) \approx k \frac{\omega_n^2}{s^2 + 2\zeta\omega_n s + \omega_n^2} \frac{z_0 - s}{z_0} \quad (4.34)$$

The transfer function of equation (4.34) can be written as follows,

$$\begin{aligned} G(s) &= G_n(s) \frac{z_0 - s}{z_0} \\ &= G_n(s) - \frac{s}{z_0} G_n(s) \end{aligned} \quad (4.35)$$

where,

$$G_n(s) = k \frac{\omega_n^2}{s^2 + 2\zeta\omega_n s + \omega_n^2} \quad (4.36)$$

is a nominal second order transfer function with no zeros. Equation (4.35) makes it clear that as the position of the zero tends to infinity, so the total system transfer function converges towards $G_n(s)$. The purpose of the analysis to follow is to investigate more precisely, the conditions under which $G(s)$ can be well approximated by $G_n(s)$. To this end, two analysis methods are employed. The first is based on a time domain analysis while the second involves a frequency domain sensitivity function analysis. The results of the analyses form part of the contribution of this dissertation to the field of control systems.

Beginning with the time response analysis, consider the Laplace transform of the system's step response,

$$\begin{aligned} Y(s) &= G_n(s) \frac{1}{s} - G_n(s) \frac{1}{z_0} \\ &= Y_n(s) - G_n(s) \frac{1}{z_0} \end{aligned} \quad (4.37)$$

where $Y_n(s)$ is the step response of the nominal system without any zeros. Equation (4.37) makes it clear that the total step response is the nominal step response less the impulse response of the system scaled by the inverse of the zero frequency. Since the nominal response gradient is always zero at the time of the step, the system must always exhibit undershoot. The level of undershoot will depend of the damping and speed of response of the system as well as the zero frequency. If the level of undershoot is small relative to unity then it is equivalent to saying that the second term of equation (4.37) has a negligible effect. Thus, by investigating the system undershoot further, conditions can be developed under which the total system response is well approximated by the nominal system response.

A closed form solution for the exact level of undershoot experienced in response to a step

command for a system of the form presented in equation (4.34) is derived in Appendix B and simply stated below,

$$y_{\min} = 1 - \frac{\sin \theta}{\sin \phi} e^{-\left(\frac{\theta - \phi}{\tan \theta}\right)} \quad (4.38)$$

where,

$$\theta = \cos^{-1}(\zeta) \quad (4.39)$$

$$\phi = \tan^{-1} \left(\frac{\sqrt{1 - \zeta^2}}{\zeta + r} \right) \quad (4.40)$$

$$r = \frac{\omega_n}{z_0} \quad (4.41)$$

Derivation of equations (4.38) through (4.41) involves inverse Laplace transforming equation (4.37) and finding the time response minima through calculus. The above equations make it clear that the undershoot is only a function of the ratio between the system's natural frequency and the zero frequency (r) and the system's damping ratio (ζ). Figure 4.1 below provides a plot of the maximum percentage undershoot as a function of r^{-1} for various damping ratios.

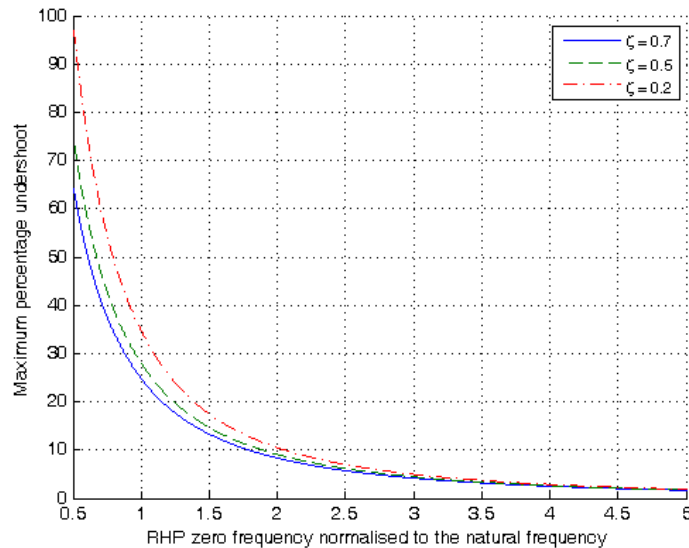


Figure 4.1 – Maximum undershoot of a 2nd order system as a function of the normalised RHP zero frequency for various damping ratios

It is clear from the figure that for low percentage undershoots, the damping ratio has very little influence. Thus, the primary factor determining the level of undershoot is the ratio of the system's natural frequency to the zero frequency. Furthermore, it is clear that for less than 5% maximum undershoot, the natural frequency should be kept at least three times lower than the frequency of the zero. With only 5% undershoot, the response of the total system will be well

approximated by the response of the nominal system with no zero. Thus, by making use of the maximum undershoot as a measure of the NMP nature of the system, the following frequency domain design rule is proposed,

$$\omega_n < \frac{z_0}{3} \quad (4.42)$$

for the NMP nature of the system to be considered negligible. This rule implies that the system poles must lie within a circle of radius $z_0/3$ in the s-plane. Thus, an upper bound is placed on the natural frequency of the system if its NMP nature is to be ignored.

Being able to ignore the NMP nature of a system is essential for the dynamic inversion part of the normal specific acceleration control law. If this cannot be done, the dynamic inversion control law will attempt to negate the effect of the gravity coupling term by making direct use of the lift generated by elevator deflection. Not only is this practically infeasible, but as previously stated it will also result in first order internal dynamics that may or may not be stable. The frequency domain analysis to follow however also shows that if the natural frequency ω_n approaches that of the zero frequency, then a poor control system with practically infeasible actuator commands will result. This result is illustrated through analysis of one of Bode's sensitivity function integrals [44,46]. By adapting the results presented in [45] to this specific case, it can be shown that the sensitivity function of a system with a real, right half plane zero and all poles strictly in the left half plane, must satisfy the following integral constraint,

$$2 \int_0^{\infty} \ln |S(j\omega)| \frac{z_0}{z_0^2 + \omega^2} d\omega = 0 \quad (4.43)$$

Continuing to present results from [45], given that the sensitivity function magnitude is to satisfy,

$$|S(j\omega)| < \varepsilon < 1 \quad \omega \in [0, \omega_t] \quad (4.44)$$

then a lower bound for the sensitivity function magnitude peak can be found such that the integral constraint of equation (4.43) is satisfied. Splitting the integration interval of equation (4.43) into two parts the following result is obtained,

$$\begin{aligned}
2 \int_0^{\infty} \ln |S(j\omega)| \frac{z_0}{z_0^2 + \omega^2} d\omega &= 0 \\
&= 2 \int_0^{\omega_l} \ln |S(j\omega)| \frac{z_0}{z_0^2 + \omega^2} d\omega + 2 \int_{\omega_l}^{\infty} \ln |S(j\omega)| \frac{z_0}{z_0^2 + \omega^2} d\omega \\
&< 2 \ln \varepsilon \int_0^{\omega_l} \frac{z_0}{z_0^2 + \omega^2} d\omega + 2 \ln S_{lb} \int_{\omega_l}^{\infty} \frac{z_0}{z_0^2 + \omega^2} d\omega \\
&= 2 \ln \varepsilon \left[\tan^{-1} \left(\frac{\omega_l}{z_0} \right) \right] + 2 \ln S_{lb} \left[\pi - \tan^{-1} \left(\frac{\omega_l}{z_0} \right) \right]
\end{aligned} \tag{4.45}$$

Thus,

$$\ln S_{lb} > \frac{2 |\ln \varepsilon| \tan^{-1}(r)}{\pi - 2 \tan^{-1}(r)} \tag{4.46}$$

where use has been made of the fact that $\varepsilon < 1$ and it has been assumed that the frequency range over which equation (4.44) holds is up to the natural frequency. A plot of the lower bound of the sensitivity function versus the ratio of the RHP zero frequency to the natural frequency (r^{-1}) is provided in Figure 4.2 below. Here it has been assumed that the sensitivity magnitude is upper bounded by $\varepsilon = 1 - 1/\sqrt{2}$ i.e. the complementary sensitivity lies between 0 and -3 dB up to the natural frequency.

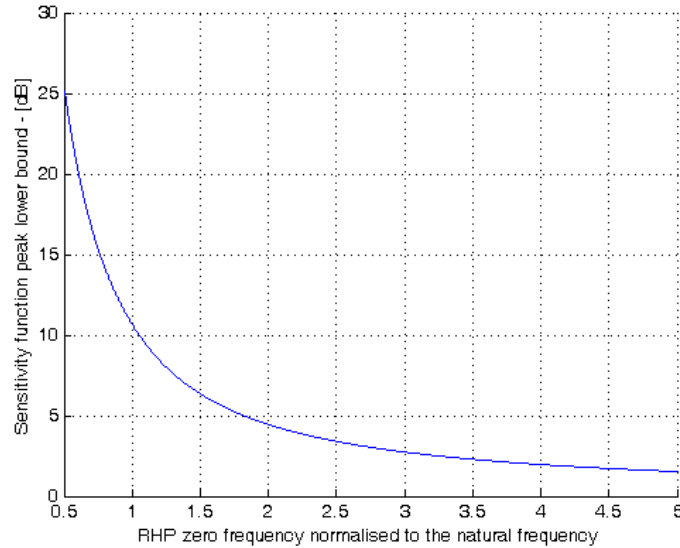


Figure 4.2 – Lower bound on the sensitivity function magnitude as a function of the RHP zero frequency normalised to the natural frequency

In Figure 4.2 it is seen that as the RHP zero frequency approaches that of the natural frequency, the lower bound on the sensitivity function peak rises dramatically. Thus, disturbances with frequencies just greater than the natural frequency of the closed loop system (from sensor noise for example) will be significantly amplified and the control signals

commanded in response to these disturbances will saturate most actuators. When the RHP zero frequency is three times greater than the natural frequency then the lower bound on the sensitivity function peak is reduced to approximately 2.5 dB (amplification gain of approximately 1.33). This RHP zero to natural frequency ratio suggests a practically feasible design and supports the frequency domain design rule of equation (4.42).

The situation worsens further when there are unstable plant poles. For more details on this specific situation see [44,45]. The clear result of the above analysis however is that restricting the natural frequency to well below the zero frequency is important not only for dynamic inversion purposes but for practical controller design reasons too. From Figures 4.1 and 4.2 and their corresponding arguments, it is seen that enforcing the upper bound of equation (4.42) on the natural frequency of the system will allow the NMP nature of the system to be ignored and result in the design of a practically feasible control system.

4.2.3 Frequency bounds on the normal specific acceleration controller

Given the results of the previous two subsections, the upper bound on the natural frequency of the normal specific acceleration controller becomes,

$$\omega_n < \frac{1}{3} \left| \sqrt{\frac{L_\alpha}{I_{yy}} (l_T - l_N)} \right| \quad (4.47)$$

where the offset in the zero positions in equation (4.32) has been ignored. Adhering to this simple to calculate upper bound will allow the NMP nature of the system to be ignored and will thus ensure both practically feasible dynamic inversion of the flight path angle coupling and no large sensitivity function peaks in the closed loop system.

It is important to note that the upper bound applies to both the open loop and closed loop normal specific acceleration dynamics. If the open loop poles violate the condition of equation (4.47) then moving them through control application to within the acceptable frequency region will require taking into account the effect of the system zeros. Thus, for an aircraft to be eligible for the normal specific acceleration controller of the next subsection, its open loop normal dynamics poles must at least satisfy the bound of equation (4.47). If they do not then an aircraft specific normal specific acceleration controller would have to be designed. However, most aircraft tend to satisfy this bound in the open loop because open loop poles outside the frequency bound of equation (4.47) would yield an aircraft with poor natural flying qualities i.e. the aircraft would be too statically stable and display significant undershoot and lag when performing elevator based manoeuvres. The frequency bound can thus also be utilised as a design rule for determining the forward centre of mass position of an aircraft.

In terms of lower bounds, the normal dynamics must be timescale separated from the velocity magnitude and air density dynamics. Of these two signals, the velocity magnitude typically

has the highest bandwidth and is thus considered the limiting factor. Given the desired velocity magnitude bandwidth (where it is assumed here that the given bandwidth is achievable with the available axial actuator), then as a practical, commonly used design rule the normal dynamics bandwidth should be at least five times greater than this for sufficient timescale separation. Note that unlike in the upper bound case, only the closed loop poles need satisfy the lower bound constraint. However, if the open loop poles are particularly slow, then it will require a large amount of control effort to meet the lower bound constraint in the closed loop. This may result in actuator saturation and thus a practically infeasible controller. However, for typical aircraft parameters the open loop poles tend to already satisfy the timescale separation lower bound.

With the timescale separation lower bound and the NMP zero upper bound, the natural frequency of the normal specific acceleration controller is constrained to lying within a circular band in the s -plane as shown in Figure 4.3 below. Note that the obvious stability constraints have not been illustrated. Note too that although the upper bound of equation (4.47) may be superseded by other upper bounds such as those introduced by actuator saturation, these too have been neglected from the figure.

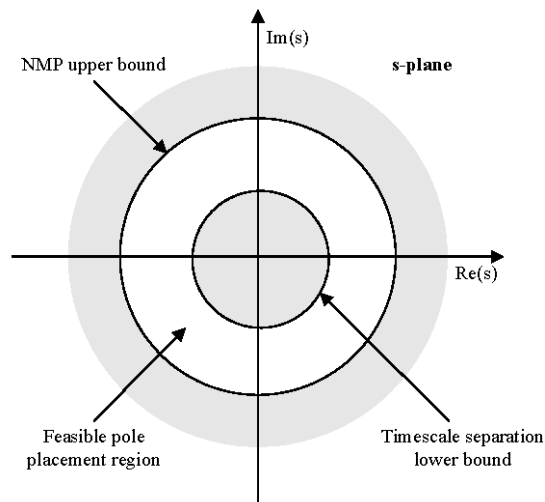


Figure 4.3 – Feasible pole placement region constrained by NMP upper bound and timescale separation lower bound

The width of the circular band in Figure 4.3 is an indication of the eligibility of a particular airframe for the application of the normal specific acceleration controller to be designed in the following subsection. For most aircraft this band is acceptably wide and the control system to be presented can be directly applied. For less conventional aircraft, the band can become very narrow and the two constraint boundaries may even cross. In this case, the generic control system to be presented cannot be directly applied. One solution to this problem is to design an aircraft specific normal specific acceleration controller. However, this solution is typically not

desirable since the closeness of the bounds suggests that the desired performance of the particular airframe will not easily be achieved practically. Instead, redesign of the airframe and/or reconsideration of the outer loop performance bandwidths will constitute a more practical solution.

4.2.4 Normal specific acceleration controller design

Assuming that the frequency bounds of the previous section are met, the design of a practically feasible normal specific acceleration controller can proceed based on the following reduced normal dynamics,

$$\begin{bmatrix} \dot{\alpha} \\ \dot{Q} \end{bmatrix} = \begin{bmatrix} -\frac{L_\alpha}{m\bar{V}} & 1 \\ \frac{M_\alpha}{I_{yy}} & \frac{M_Q}{I_{yy}} \end{bmatrix} \begin{bmatrix} \alpha \\ Q \end{bmatrix} + \begin{bmatrix} 0 \\ \frac{M_{\delta_E}}{I_{yy}} \end{bmatrix} \delta_E + \begin{bmatrix} -\frac{L_0}{m\bar{V}} \\ \frac{M_0}{I_{yy}} \end{bmatrix} + \begin{bmatrix} \frac{g}{\bar{V}} \\ 0 \end{bmatrix} e_{33}^{WT} \quad (4.48)$$

$$C_w = \begin{bmatrix} -\frac{L_\alpha}{m} & 0 \end{bmatrix} \begin{bmatrix} \alpha \\ Q \end{bmatrix} + [0] \delta_E + \begin{bmatrix} -\frac{L_0}{m} \end{bmatrix} \quad (4.49)$$

The simplifications in the dynamics above arise from the analysis of subsection 4.2.1 where it was shown that to a good approximation, the lift due to pitch rate and elevator deflection only play a role in determining the zeros from elevator to normal specific acceleration. Under the assumption that the upper bound of equation (4.47) is satisfied, the zeros effectively move to infinity and correspondingly these two terms become zero. Thus, the simplified normal dynamics above will yield identical approximated poles to those of equation (4.24), but will display no finite zeros from elevator to normal specific acceleration. The design of a controller to dynamically invert the gravity coupling term and provide enough degrees of freedom to allow for arbitrary placement of the closed loop normal dynamics poles for all point mass kinematics states now follows. Only an abbreviated design is provided in this section with the detailed derivation provided in Appendix B.

To dynamically invert the effect of the flight path angle coupling on the normal specific acceleration dynamics requires differentiating the output of interest until the control input appears in the same equation. The control can then be used to directly cancel the undesirable terms. Differentiating the normal specific acceleration output of equation (4.49) once with respect to time yields,

$$\dot{C}_w = \begin{bmatrix} -\frac{L_\alpha}{m\bar{V}} \end{bmatrix} C_w + \begin{bmatrix} -\frac{L_\alpha}{m} \end{bmatrix} Q + \begin{bmatrix} -\frac{L_\alpha g}{m\bar{V}} \end{bmatrix} e_{33}^{WT} \quad (4.50)$$

where the angle of attack dynamics of equation (4.48) have been used in the result above. Differentiating the normal specific acceleration a second time gives,

$$\ddot{C}_W = \left[\frac{M_Q}{I_{yy}} - \frac{L_\alpha}{m\bar{V}} \right] \dot{C}_W + \left[\frac{M_\alpha}{I_{yy}} + \frac{L_\alpha M_Q}{m\bar{V}I_{yy}} \right] C_W + \left[-\frac{L_\alpha M_{\delta_E}}{mI_{yy}} \right] \delta_E + \left[\frac{L_0 M_\alpha}{mI_{yy}} - \frac{L_\alpha M_0}{mI_{yy}} \right] + \left[\frac{L_\alpha g}{m\bar{V}} \left(\frac{M_Q}{I_{yy}} e_{33}^{WI} - e_{33}^{WI} \right) \right] \quad (4.51)$$

where use has been made of equations (4.48) to (4.50) in obtaining the result above. The elevator control input could now be used to cancel the effect of the attitude angle coupling terms on the normal specific acceleration dynamics. However, the output feedback control law to be implemented will make use of pitch rate feedback. Upon analysis of equation (2.28), it is clear that pitch rate feedback will reintroduce flight path angle coupling terms into the normal specific acceleration dynamics. Thus, the feedback control law is first defined and substituted into the dynamics, and then the dynamic inversion is carried out. A PI control law with enough degrees of freedom to place the closed loop poles arbitrarily and allow for dynamic inversion (through $\delta_{E_{DI}}$) is defined below,

$$\delta_E = -K_Q Q - K_C C_W - K_E E_C + \delta_{E_G} \quad (4.52)$$

$$\dot{E}_C = C_W - C_{W_R} \quad (4.53)$$

with C_{W_R} the reference normal specific acceleration command. The integral action of the control law is introduced to ensure that the normal specific acceleration is robustly tracked with zero steady state error. Offset disturbance terms such as those due to static lift and pitching moment can thus be ignored in the design to follow. It is best to remove the effect of terms such as these with integral control since they are not typically known to a high degree of accuracy and thus cannot practically be inverted along with the flight path angle coupling. Upon substitution of the control law above into the normal specific acceleration dynamics of equation (4.51), the closed loop normal dynamics become,

$$\ddot{C}_W = \left[\frac{M_Q}{I_{yy}} - \frac{L_\alpha}{m\bar{V}} - \frac{M_{\delta_E}}{I_{yy}} K_Q \right] \dot{C}_W + \left[\frac{M_\alpha}{I_{yy}} + \frac{L_\alpha M_Q}{m\bar{V}I_{yy}} + \frac{L_\alpha M_{\delta_E}}{mI_{yy}} K_C - \frac{L_\alpha M_{\delta_E}}{m\bar{V}I_{yy}} K_Q \right] C_W + \left[\frac{L_\alpha M_{\delta_E}}{mI_{yy}} K_E \right] E_C \quad (4.54)$$

$$\dot{E}_C = C_W - C_{W_R} \quad (4.55)$$

when,

$$\delta_{E_G} = \frac{g}{\bar{V}} \left[\left(\frac{M_Q}{M_{\delta_E}} - K_Q \right) e_{33}^{WI} - \frac{I_{yy}}{M_{\delta_E}} e_{33}^{WI} \right] \quad (4.56)$$

and the static offset terms are ignored. Note that the dynamic inversion part of the control law is still a function of the yet to be determined pitch rate feedback gain. Given the desired closed loop characteristic equation for the normal dynamics,

$$\alpha_c(s) = s^3 + \alpha_2 s^2 + \alpha_1 s + \alpha_0 \quad (4.57)$$

the closed form solution feedback gains can be calculated by matching characteristic equation coefficients to yield,

$$K_Q = \frac{I_{yy}}{M_{\delta_E}} \left(\alpha_2 + \frac{M_Q}{I_{yy}} - \frac{L_\alpha}{m\bar{V}} \right) \quad (4.58)$$

$$K_C = -\frac{mI_{yy}}{L_\alpha M_{\delta_E}} \left(\alpha_1 + \frac{M_\alpha}{I_{yy}} - \frac{L_\alpha}{m\bar{V}} \left(\alpha_2 - \frac{L_\alpha}{m\bar{V}} \right) \right) \quad (4.59)$$

$$K_E = -\frac{mI_{yy}}{L_\alpha M_{\delta_E}} \alpha_0 \quad (4.60)$$

Substituting the pitch rate feedback gain into equation (4.56) gives,

$$\delta_{E_G} = \frac{g}{\bar{V}} \frac{I_{yy}}{M_{\delta_E}} \left[\left(\frac{L_\alpha}{m\bar{V}} - \alpha_2 \right) e_{33}^{WI} + \left(\frac{C_W + g e_{33}^{WI}}{\bar{V}} \right) e_{13}^{WI} + P_W e_{23}^{WI} \right] \quad (4.61)$$

where use has been made of equation (2.46) to remove the attitude parameter derivative. The controller design freedom is reduced to that of placing the three poles that govern the closed loop normal dynamics. The control system will work to keep these poles fixed for all point mass kinematics states and in so doing yield a dynamically invariant normal specific acceleration response at all times. Guidelines for placing the closed loop poles are provided in the following subsection.

4.2.5 Placing the closed loop poles

There are a number of factors that influence the selection of the closed loop normal dynamics poles. A lower bound constraint on the frequency of the closed loop poles exists to ensure a timescale separation between the closed loop normal dynamics and the velocity magnitude and air density dynamics. Upper bounds on the pole positions are imposed through the NMP zero constraint of equation (4.47) as well as actuator saturation and slew rate limits. Of course for the normal specific acceleration controller design to be feasible, these upper and lower bounds should not cross in the frequency domain as discussed in section 4.2.3.

Considering the NMP zero upper frequency bound constraint further, it is clear from equation (4.47) that as the dynamic pressure is decreased, so the upper frequency bound constraint tightens. Thus, if a designer were to select a nominal fixed set of closed loop normal dynamics poles then the constraint of equation (4.47) would at some point be violated as the dynamic pressure is decreased. Intuitively, this is because the normal specific acceleration controller would attempt to obtain the nominal dynamic response at reduced dynamic pressures which becomes less and less feasible as dynamic pressure is reduced. This problem promotes two fundamentally different pole placement strategies for the normal specific acceleration controller.

The first strategy involves selecting appropriate closed loop poles for a particular dynamic pressure, in the knowledge that the aircraft to be controlled will continuously operate close to this nominal dynamic pressure. The normal specific acceleration controller would then work to ensure the same dynamic response for all dynamic pressure variations. This would provide a simple, clean interface to the outer guidance level controllers. A second strategy is to schedule the pole positions with the dynamic pressure (or in some other appropriate fashion) to ensure that the constraint of equation (4.47) is never violated, thus ensuring a practically feasible design. However, by scheduling the speed of the normal specific acceleration controller, its interface with the guidance level controllers is complicated since the closed loop response would no longer be dynamically invariant. This complication could however be handled through complementary scheduling of the outer guidance level controller bandwidths.

Each of the pole placement strategies described above has its benefits. The fixed pole placement strategy is better suited to aircraft whose mission profile is to navigate and manoeuvre about a constant dynamic pressure. Adopting this strategy would provide the simplest interface to the guidance level controllers and consequently the simplest guidance level controllers. On the other hand, the variable pole placement strategy is better suited to aircraft that need to operate over a wide dynamic pressure range. This strategy constantly changes the normal specific acceleration speed of response so as not to violate the physical constraints imposed by the aircraft. Of course, a combination of the two strategies may provide the best solution to a specific problem. An aircraft that is accelerating up to speed and altitude could initially use variable pole placement. Once at the desired operating point, it could switch over to fixed pole placement to ensure that it operates consistently about the nominal flight condition. Once its mission has been completed it could revert back to variable pole placement for its return to base.

The controller design of the previous section makes both the fixed and variable pole placement strategies feasible. For fixed pole placement a single set of characteristic equation coefficients would be selected and used throughout the flight. For variable pole placement, these coefficients would have to be appropriately updated during flight and then used to update the controller gains. One method for adjusting the pole positions (and thus characteristic equation coefficients) would be to schedule the natural frequency of the closed loop poles such that they remain a constant factor of the NMP zero frequency constraint of equation (4.47). This would ensure that the frequency constraint is never violated and thus provide a practically feasible design barring any other constraint violations.

A second more direct method for implementing the variable pole placement strategy is described in the subsection that follows. Although the method involves more complicated concepts than those involved in the implementation method above, it presents a particularly elegant solution to the variable pole placement problem. The method involves normalising the states, controls and outputs of the normal dynamics and most importantly non-

dimensionalising time. It is thus referred to as the Normalised Non-Dimensional Time (NNDT) variant of the normal specific acceleration controller. By appropriately non-dimensionalising time, and consequently frequency, it will be seen that the transformed open loop normal dynamics become largely invariant with dynamic pressure. As a result, the NMP frequency bound constraint remains fixed in the non-dimensional frequency plane thus allowing for a fixed pole placement design for the NNDT system. The end result is a control law that implements variable pole placement for the dimensional system without the need to explicitly schedule poles.

4.2.6 NNDT normal specific acceleration controller design

Consider the normal dynamics of equations (4.21) and (4.22). Define the normalised states, controls, outputs, time and gravitational acceleration respectively,

$$\alpha' \equiv \alpha \quad (4.62)$$

$$Q' \equiv \frac{\bar{c}}{2\bar{V}_a} Q \quad (4.63)$$

$$\delta'_E \equiv \delta_E \quad (4.64)$$

$$C'_W \equiv \frac{m}{qS} C_W \quad (4.65)$$

$$t' \equiv \frac{qS}{m\bar{V}} t \quad (4.66)$$

$$g' \equiv \frac{m}{qS} g \quad (4.67)$$

Then define the derivative of a variable with respect to normalised time as follows,

$$\bar{x} \equiv \frac{dx}{dt'} = \frac{dx}{d\frac{qS}{m\bar{V}}t} = \frac{m\bar{V}}{qS} \frac{dx}{dt} = \frac{m\bar{V}}{qS} \dot{x} \quad (4.68)$$

With these definitions in place, the NNDT normal dynamics are shown in Appendix B to be,

$$\begin{bmatrix} \bar{\alpha}' \\ \bar{Q}' \end{bmatrix} = \begin{bmatrix} -C_{L_\alpha} & k_Q \\ k_y C_{m_\alpha} & k_y C_{m_Q} \end{bmatrix} \begin{bmatrix} \alpha' \\ Q' \end{bmatrix} + \begin{bmatrix} -C_{L_{\delta_E}} \\ k_y C_{m_{\delta_E}} \end{bmatrix} \delta'_E + \begin{bmatrix} -C_{L_0} \\ k_y C_{m_0} \end{bmatrix} + \begin{bmatrix} g' \\ 0 \end{bmatrix} e_{33}^{mT} \quad (4.69)$$

$$\begin{bmatrix} C'_W \\ Q' \end{bmatrix} = \begin{bmatrix} -C_{L_\alpha} & -C_{L_Q} \\ 0 & 1 \end{bmatrix} \begin{bmatrix} \alpha' \\ Q' \end{bmatrix} + \begin{bmatrix} -C_{L_{\delta_E}} \\ 0 \end{bmatrix} \delta'_E + \begin{bmatrix} -C_{L_0} \\ 0 \end{bmatrix} \quad (4.70)$$

where,

$$k_Q = 4m'_Q \bar{V}' \quad (4.71)$$

$$k_y = \frac{1}{2} \frac{\bar{V}'}{r_y'^2} \quad (4.72)$$

and,

$$m'_Q = \frac{m}{\rho S \bar{c}} \quad (4.73)$$

$$\bar{V}' = \frac{\bar{V}}{\bar{V}_a} \quad (4.74)$$

$$r_y' = \frac{r_y}{\bar{c}} \quad (4.75)$$

with,

$$r_y = \sqrt{\frac{I_{yy}}{m}} \quad (4.76)$$

In equations (4.71) and (4.72), m'_Q is the aircraft's mass normalised to a longitudinal reference air mass, \bar{V}' is the relative ground to airspeed magnitude and r_y' is the normalised pitch radius of gyration. Note that it has been assumed that,

$$|C_{L_Q}| \ll |k_Q| \quad (4.77)$$

which is equivalent to the standard aircraft assumption of equation (4.25). When the ground speed magnitude and the airspeed magnitude are equivalent, then k_y is constant and the normal dynamics are only a function of the air density through the gain k_Q . Investigation of the characteristic equation for the NNDT open loop poles is shown in Appendix B to yield,

$$p(s') = (s')^2 + (C_{L_\alpha} - k_y C_{m_Q}) s' - k_y (C_{m_Q} C_{L_\alpha} + k_Q C_{m_\alpha}) \quad (4.78)$$

From equation (4.78), it is clear that when the ground speed and airspeed magnitudes are equal (zero wind conditions) the NNDT normal dynamics poles are not a function of the velocity magnitude and that only the natural frequency of the open loop NNDT normal dynamics poles changes with the air density. Because air density changes slowly with altitude, the open loop NNDT normal dynamics poles can be thought of as fixed in the NNDT frequency plane when operating about a nominal altitude. Investigating the zeros from elevator to normal specific acceleration, the calculations in Appendix B show that the characteristic equation for the zeros is,

$$z(s') = (s')^2 - k_y C_{L_Q} \left(\frac{C_{m_Q}}{C_{L_Q}} - \frac{C_{m_{\delta E}}}{C_{L_{\delta E}}} \right) s' - k_Q k_y C_{L_\alpha} \left(\frac{C_{m_\alpha}}{C_{L_\alpha}} - \frac{C_{m_{\delta E}}}{C_{L_{\delta E}}} \right) \quad (4.79)$$

Define now the following normalised characteristic lengths,

$$l'_N \equiv -\frac{C_{m\alpha}}{C_{L\alpha}} \quad (4.80)$$

$$l'_T \equiv -\frac{C_{m\delta_E}}{C_{L\delta_E}} \quad (4.81)$$

$$l'_D \equiv -\frac{C_{m\dot{Q}}}{C_{L\dot{Q}}} \quad (4.82)$$

where l'_N is the normalised length to the neutral point, l'_T is the effective normalised length to the tail-plane, l'_D is the effective normalised damping arm length and all lengths are relative to the centre of mass. Completing the square on equation (4.79) and making use of the characteristic lengths defined above and the arguments provided in section 4.2.1, the zero positions in the NNDT frequency plane are shown in Appendix B to be,

$$z'_{1,2} = \frac{1}{2}k_y C_{L\dot{Q}} (l'_T - l'_D) \pm \sqrt{k_Q k_y C_{L\alpha} (l'_T - l'_N)} \quad (4.83)$$

Note that again, for typical aircraft parameters the second term in equation (4.83) tends to dominate the first. Investigation of equation (4.83) shows that similarly to the pole positions under zero wind conditions, the zero positions do not depend on the velocity magnitude and depend only on the air density through the gain k_Q . Thus, about a nominal altitude, the zero positions remain largely unchanged. With reference to the analysis done in section 4.2.2, the NMP upper bound imposed on the natural frequency of the NNDT normal dynamics poles is,

$$\omega'_n < \frac{1}{3} \left| \sqrt{k_Q k_y C_{L\alpha} (l'_T - l'_N)} \right| \quad (4.84)$$

Analysis of the natural elevator to normal specific acceleration dynamics shows that the frequency of the open loop poles and zeros changes only with the inverse of the square root of the air density. Thus, fixing the normal dynamics poles appropriately in the NNDT frequency plane would result in a practically feasible dimensional time normal specific acceleration controller for large dynamic pressure ranges. Fixed NNDT normal dynamics poles would only result in physical constraint violations if the air density was to change significantly. However, large dynamic pressure changes are most often due to large changes in airspeed magnitude (due to the quadratic relationship) and not to large changes in air density (since air density changes slowly with altitude). Thus for a large class of aircraft/mission combinations, fixed NNDT closed loop normal dynamics poles would be acceptable for the entire flight envelope. In aircraft where the altitude is to change significantly, the closed loop NNDT poles could be scheduled slowly with air density.

Before continuing with the details of the control system design, note that a feedback control

law designed to fix the closed loop normal dynamics poles in the NNDT frequency plane would in general be a function of the air density. However, under the assumption that the flight envelope of interest is limited such that air density changes do not significantly affect the open loop NNDT normal dynamics, then a control law that fixes poles in the NNDT frequency plane would involve constant feedback gains that could be calculated offline. In comparison, a dimensional time pole scheduling technique would require a fair amount of online computation to determine the desired pole positions and varying feedback gains. Thus employing a controller that fixes the closed loop poles in the NNDT frequency plane provides a particularly simple, elegant solution to the variable pole placement problem.

To design the NNDT controller the PI control law with freedom for dynamic inversion is defined below,

$$\delta'_E = -K'_Q \mathcal{Q}' - K'_C C'_W - K'_E E'_C + \delta'_{E_g} \quad (4.85)$$

$$\bar{E}'_C = C'_{W_r} - C'_{W_z} \quad (4.86)$$

where C'_{W_r} is the NNDT normal specific acceleration reference command. The control law has enough degrees of freedom to place the closed loop poles arbitrarily in the NNDT frequency plane. Appendix B shows that given the desired closed loop characteristic equation,

$$\alpha_c(s') = (s')^3 + \alpha_2 (s')^2 + \alpha_1 (s') + \alpha_0 \quad (4.87)$$

the feedback gains that will result in the desired poles are,

$$K'_Q = \frac{\alpha_2 + k_y C_{m_Q} - C_{L_\alpha}}{k_y C_{m_{\delta_E}}} \quad (4.88)$$

$$K'_C = -\frac{\alpha_1 + k_Q k_y C_{m_\alpha} - C_{L_\alpha} (\alpha_2 - C_{L_\alpha})}{k_Q k_y C_{L_\alpha} C_{m_{\delta_E}}} \quad (4.89)$$

$$K'_E = -\frac{\alpha_0}{k_Q k_y C_{L_\alpha} C_{m_{\delta_E}}} \quad (4.90)$$

with the dynamic inversion term,

$$\delta'_{E_g} = \frac{\mathbf{g}'}{k_Q k_y C_{m_{\delta_E}}} \left[(C_{L_\alpha} - \alpha_2) e_{33}^{WI} + \left[(C'_W + e_{33}^{WI} \mathbf{g}') e_{13}^{WI} + P'_W e_{23}^{WI} \right] \right] \quad (4.91)$$

where,

$$P'_W = \frac{m \bar{V}}{qS} P_W \quad (4.92)$$

To implement the control law, the signals required for feedback are normalised using equations

(4.63), (4.65), (4.67) and (4.92). The feedback gains of equations (4.88), (4.89) and (4.90) can be updated if the air density changes significantly or if the airspeed and ground speed magnitudes differ greatly. If these factors can be neglected then these feedback gains remain constant (where it is assumed the non-dimensional stability derivatives are constant). Given the NNDT normal specific acceleration reference command, the control law of equations (4.85) and (4.86) can be implemented to calculate the normalised elevator deflection. Equation (4.64) would then be used to calculate the dimensional elevator deflection. The end result is an elegant and efficient solution to the variable pole placement problem as will be illustrated in one of the simulation examples of Chapter 8.

4.2.7 Integrator pole placement

Both the dimensional time and non-dimensional time control laws discussed previously introduce the reference input signal via the integrator state. Doing this requires the closed loop integrator dynamics to be fast since they directly influence the system's speed of response to a reference input. However, practically it is often not desirable to have an integrator with very fast dynamics. To allow for a slower integrator, it is straightforward to show that if the control law of equation (4.52) is changed to incorporate a feed-forward term as follows,

$$\delta_E = -K_Q Q - K_C C_W - K_E E_C + N_C C_{W_R} + \delta_{E_G} \quad (4.93)$$

$$\dot{E}_C = C_W - C_{W_R} \quad (4.94)$$

then the effect is to introduce a zero at,

$$s = -\frac{K_E}{N_C} \quad (4.95)$$

in the closed loop system from the reference input to the output. Similarly for the NNDT system if the control law of equation (4.85) is changed to,

$$\delta'_E = -K'_Q Q' - K'_C C'_W - K'_E E'_C + N'_C C'_{W_R} + \delta'_{E_G} \quad (4.96)$$

$$\bar{E}'_C = C'_W - C'_{W_R} \quad (4.97)$$

then the effect is to introduce a zero at,

$$s' = -\frac{K'_E}{N'_C} \quad (4.98)$$

in the NNDT frequency plane of the closed loop system from the reference input to the output. Selecting the feed-forward gain such that the zero lies on top of the closed loop integrator pole will have the effect of removing the closed loop integrator dynamics from the reference to output system. In turn this allows the closed loop integrator pole to be placed at a much lower

frequency than the two remaining dominant poles. Note that feed-forward cancellation of closed loop integrator dynamics is not a novel concept [47] and merely serves as a standard variation on the novel control laws introduced in sections 4.2.4 and 4.2.6.

From a timescale separation point of view, slowing the closed loop integrator dynamics and cancelling them from the reference input via feed-forward is acceptable since the outer guidance level controllers interface with the inner loop controllers via the reference input. Note however that the slow closed loop integrator dynamics will be visible from disturbance inputs. Disturbances due to parameter uncertainty, un-modelled dynamics and wind will take longer to be fully rejected with a slow integrator than they would if the integrator was fast. Thus, although slowing down the integrator pole will result in a more practically manageable control system, it will decrease the disturbance rejection capabilities of the controller. The designer should consider both of these factors when selecting the integrator pole location and adopt the option best suited to the particular application.

4.3 Conclusion

This chapter covered the detailed design and associated analysis of the axial and normal specific acceleration controllers (top two controllers on the right hand side of Figure 3.1). These controllers and the analysis associated with their design forms part of the primary contribution of this dissertation to the field of aircraft flight control. In terms of analysis, of particular importance is the sensitivity function analysis of section 4.1, the analytical determination of the elevator to normal specific acceleration zeros in section 4.2.1 and the determination of the associated frequency bound constraints of section 4.2.3 through the NMP system analysis of section 4.2.2.

To allow the controllers to be readily applied to different aircraft, closed form parameterised control laws were developed. Pole placement was the primary method used in the control system design together with a limited amount of dynamic inversion to handle the gravity coupling into the normal dynamics. Pole placement discussions for the normal specific acceleration controller lead to the concept of fixed and variable pole placement strategies. A novel NNDT variant of the normal specific acceleration control system was presented as an elegant solution to the variable pole placement problem. Finally, a variant of the normal dynamics control laws was presented to allow for slower closed loop integrator dynamics using standard feed-forward techniques.

Chapter 5

Inner Loop Controllers: Lateral Dynamics

In the previous chapter, inner loop controllers for axial and normal specific acceleration were designed. This chapter continues in a similar vein with the design of controllers for the lateral dynamics. After analysing the lateral dynamics in section 5.1 it is shown that under certain conditions, typically met by most conventional aircraft, the lateral dynamics can be decoupled into roll and directional dynamics. Two independent inner loop controllers are then designed based on the decoupled dynamics to regulate roll rate about the velocity vector and lateral specific acceleration. Pole placement for both controllers is considered which similarly to the previous chapter leads to a NNDT version of each controller.

5.1 Analysis of natural lateral dynamics

The lateral dynamics are restated below for convenience,

$$\begin{bmatrix} \dot{\beta} \\ \dot{P} \\ \dot{R} \end{bmatrix} = \begin{bmatrix} \frac{Y_\beta}{m\bar{V}} & \frac{Y_P}{m\bar{V}} & \frac{Y_R}{m\bar{V}} - 1 \\ \frac{\bar{L}_\beta}{I_{xx}} & \frac{\bar{L}_P}{I_{xx}} & \frac{\bar{L}_R}{I_{xx}} \\ \frac{\bar{N}_\beta}{I_{zz}} & \frac{\bar{N}_P}{I_{zz}} & \frac{\bar{N}_R}{I_{zz}} \end{bmatrix} \begin{bmatrix} \beta \\ P \\ R \end{bmatrix} + \begin{bmatrix} \frac{Y_{\delta_A}}{m\bar{V}} & \frac{Y_{\delta_R}}{m\bar{V}} \\ \frac{\bar{L}_{\delta_A}}{I_{xx}} & \frac{\bar{L}_{\delta_R}}{I_{xx}} \\ \frac{\bar{N}_{\delta_A}}{I_{zz}} & \frac{\bar{N}_{\delta_R}}{I_{zz}} \end{bmatrix} \begin{bmatrix} \delta_A \\ \delta_R \end{bmatrix} + \begin{bmatrix} \frac{g}{\bar{V}} \\ 0 \\ 0 \end{bmatrix} e_{23}^{WI} \quad (5.1)$$

$$\begin{bmatrix} B_W \\ P_W \end{bmatrix} = \begin{bmatrix} \frac{Y_\beta}{m} & \frac{Y_P}{m} & \frac{Y_R}{m} \\ 0 & 1 & 0 \end{bmatrix} \begin{bmatrix} \beta \\ P \\ R \end{bmatrix} + \begin{bmatrix} \frac{Y_{\delta_A}}{m} & \frac{Y_{\delta_R}}{m} \\ 0 & 0 \end{bmatrix} \begin{bmatrix} \delta_A \\ \delta_R \end{bmatrix} \quad (5.2)$$

where standard dimensional stability derivative notation has been used to avoid clutter as described by equation (4.23). The lateral dynamics constitute a Multiple Input Multiple Output (MIMO) system where it is desired to regulate the roll rate about the velocity vector and the lateral specific acceleration coordinate in wind axes. These two signals need to be regulated using the rudder and aileron control inputs and should display invariant dynamic responses for all point mass kinematics states. To gain insight into the lateral dynamics for control system design purposes they are investigated further.

In Appendix B, standard systems theory mathematics shows that the open loop poles of the lateral dynamics (Roll/Dutch-Roll modes) are the roots of the characteristic equation,

$$\alpha_p(s) = \left[s^2 - \left(\frac{\bar{L}_p}{I_{xx}} + \frac{\bar{N}_R}{I_{zz}} \right) s + \frac{\bar{L}_p \bar{L}_R}{I_{xx} I_{zz}} \left(\frac{\bar{N}_R}{\bar{L}_R} - \frac{\bar{N}_p}{\bar{L}_p} \right) \right] \left(s - \frac{Y_\beta}{m\bar{V}} \right) + \left[\frac{\bar{N}_\beta}{I_{zz}} s - \frac{\bar{L}_p \bar{L}_\beta}{I_{xx} I_{zz}} \left(\frac{\bar{N}_\beta}{\bar{L}_\beta} - \frac{\bar{N}_p}{\bar{L}_p} \right) \right] \quad (5.3)$$

where only the following standard aircraft assumptions [43] have been made,

$$Y_p \approx 0 \quad (5.4)$$

$$\left| \frac{Y_R}{m\bar{V}} \right| \ll 1 \quad (5.5)$$

Appendix B also shows that when the following additional, novel conditions hold,

$$\left| \frac{\bar{C}_{n_p}}{\bar{C}_{l_p}} \right| \ll \left| \frac{\bar{C}_{n_R}}{\bar{C}_{l_R}} \right| \quad (5.6)$$

$$\left| \frac{\bar{C}_{n_p}}{\bar{C}_{l_p}} \right| \ll \left| \frac{\bar{C}_{n_\beta}}{\bar{C}_{l_\beta}} \right| \quad (5.7)$$

the lateral dynamics characteristic equation can be further simplified to,

$$\alpha_p(s) \approx \left[s^2 - \left(\frac{Y_\beta}{m\bar{V}} + \frac{\bar{N}_R}{I_{zz}} \right) s + \left(\frac{Y_\beta}{m\bar{V}} \frac{\bar{N}_R}{I_{zz}} + \frac{\bar{N}_\beta}{I_{zz}} \right) \right] \left(s - \frac{\bar{L}_p}{I_{xx}} \right) \quad (5.8)$$

The conditions of equations (5.6) and (5.7) are satisfied by most aircraft as supported by the arguments to follow. Note that the arguments assume the remaining cross product of inertia is negligible and thus that with reference to equations (3.67) and (3.68), barred stability derivatives are equivalent to un-barred derivatives.

Consider the stability derivative ratio on the left hand side of equations (5.6) and (5.7). The roll moment due to roll rate in the denominator is due primarily to the differential lift caused by the induced angle of incidence across the aircraft's wingspan as it rolls. The yaw moment due to roll rate in the numerator is primarily due to the differential drag across the wing as a result of the differential lift above. There is also a small contribution to the yaw moment due to the induced angle of incidence on the fin during a roll manoeuvre. However, ignoring this latter typically negligible effect, the following is true to a good approximation,

$$\left| \frac{\bar{C}_{n_p}}{\bar{C}_{l_p}} \right| \approx \left| \frac{1}{R_{LD}} \right| \quad (5.9)$$

Thus, for most aircraft and flight conditions,

$$\left| \frac{\bar{C}_{n_p}}{\bar{C}_{l_p}} \right| \ll 1 \quad (5.10)$$

The terms on the right hand side of equations (5.6) and (5.7) are typically greater than unity or at least very close. In equation (5.6), the yaw damping coefficient is often of a very similar magnitude to the roll moment due to yaw rate coefficient. The yaw damping is dominated by the induced angles of incidence on the fin during yaw rate motion. The roll moment on the other hand is due to the differential lift across the wings caused by the yaw rate induced differential velocity as well as the roll axis offset of the yaw damping forces. In equation (5.7), the yaw moment due to sideslip is often very closely matched to the roll moment due to sideslip. In aircraft with a high wing, a large amount of dihedral and/or a large amount of wing sweep, this term can become significantly less than unity and the condition of equation (5.7) may not hold well. However for a very large class of aircraft this constraint will hold.

It is important to note that with the conditions of equations (5.4) to (5.7), the natural modes of motion in the lateral dynamics are described by a set of typically complex poles (the Dutch Roll mode) and a single real pole (the Roll mode). Also notice that only the directional derivatives play a role in determining the complex set of poles while only the roll derivatives determine the location of the real pole. It thus seems feasible that the lateral dynamics could be decoupled into roll and directional dynamics. To investigate this possible decoupling further, three transfer functions are investigated in detail. Note that the analysis to follow is novel, in particular the analytic determination of the actuator to output zeros and the associated simplifying conditions, and forms part of the contribution of this dissertation to the field of aircraft dynamics.

5.1.1 Aileron to roll rate transfer function

The zeros from the aileron input to the roll rate are shown in Appendix B to be the roots of the following characteristic equation,

$$\alpha_z(s) = \left[\left(s - \frac{Y_\beta}{m\bar{V}} \right) \left(s - \frac{\bar{N}_R}{I_{zz}} \right) + \frac{\bar{N}_\beta}{I_{zz}} \right] \frac{\bar{L}_{\delta_A}}{I_{xx}} + \left[\frac{\bar{L}_R}{I_{xx}} \left(s - \frac{Y_\beta}{m\bar{V}} \right) + \frac{\bar{L}_\beta}{I_{xx}} \right] \frac{\bar{N}_{\delta_A}}{I_{zz}} \quad (5.11)$$

where only the following commonly made aircraft assumption [43] has been made,

$$Y_{\delta_A} \approx 0 \quad (5.12)$$

Analysing equation (5.11) further, it is shown in Appendix B that under the conditions,

$$\left| \frac{\bar{C}_{n_{\delta_A}}}{\bar{C}_{l_{\delta_A}}} \right| \ll \left| \frac{\bar{C}_{n_R}}{\bar{C}_{l_R}} \right| \quad (5.13)$$

$$\left| \frac{\bar{C}_{n\delta_A}}{\bar{C}_{l\delta_A}} \right| \ll \left| \frac{\bar{C}_{n\beta}}{\bar{C}_{l\beta}} \right| \quad (5.14)$$

the characteristic equation for the zeros reduces to,

$$\alpha_z(s) = \frac{\bar{L}_{\delta_A}}{I_{xx}} \left[s^2 - \left(\frac{Y_\beta}{m\bar{V}} + \frac{\bar{N}_R}{I_{zz}} \right) s + \left(\frac{Y_\beta}{m\bar{V}} \frac{\bar{N}_R}{I_{zz}} + \frac{\bar{N}_\beta}{I_{zz}} \right) \right] \quad (5.15)$$

The conditions of equations (5.13) and (5.14) are typically met by a very large class of aircraft. This can be seen by noting that the yaw to roll moment ratio due to aileron deflection on the left hand side of equations (5.13) and (5.14) is related through an inverse lift to drag ratio and thus satisfies the relationship,

$$\left| \frac{\bar{C}_{n\delta_A}}{\bar{C}_{l\delta_A}} \right| \ll 1 \quad (5.16)$$

Following the arguments used in the analysis of equations (5.6) and (5.7), the relationship between the derivatives on the right hand side of equations (5.13) and (5.14) is typically close to unity thus supporting the argument above. When the conditions of equations (5.4) to (5.7) and (5.12) to (5.14) hold, the zeros of equation (5.15) cancel the directional poles of equation (5.8) and the transfer function from aileron deflection to roll rate reduces to the intuitive result,

$$\frac{P_W(s)}{\delta_A(s)} = \frac{\bar{L}_{\delta_A}/I_{xx}}{s - \bar{L}_p/I_{xx}} \quad (5.17)$$

Thus, if the conditions referred to above hold then to a good approximation, feedback from roll rate to ailerons will not affect the directional dynamics poles.

5.1.2 Rudder to yaw rate transfer function

The zeros from the rudder input to the yaw rate are shown in Appendix B to be the roots of the following characteristic polynomial,

$$\alpha_z(s) = \frac{Y_{\delta_R}}{m\bar{V}} \left[\frac{\bar{N}_\beta}{I_{zz}} \left(s - \frac{\bar{L}_p}{I_{xx}} \right) + \frac{\bar{L}_\beta}{I_{xx}} \frac{\bar{N}_p}{I_{zz}} \right] + \frac{\bar{L}_{\delta_R}}{I_{xx}} \frac{\bar{N}_p}{I_{zz}} \left(s - \frac{Y_\beta}{m\bar{V}} \right) + \frac{\bar{N}_{\delta_R}}{I_{zz}} \left(s - \frac{Y_\beta}{m\bar{V}} \right) \left(s - \frac{\bar{L}_p}{I_{xx}} \right) \quad (5.18)$$

where only the standard aircraft approximations of equations (5.4) and (5.5) have been used. It is also shown in Appendix B that under the condition of equation (5.7) and the following condition,

$$\left| \frac{\bar{C}_{n_p}}{\bar{C}_{l_p}} \right| \ll \left| \frac{\bar{C}_{n_{\delta_R}}}{\bar{C}_{l_{\delta_R}}} \right| \quad (5.19)$$

that the characteristic equation reduces to,

$$z(s) = \frac{\bar{N}_{\delta_R}}{I_{zz}} \left[s - \frac{Y_\beta}{m\bar{V}} \frac{Y_{\delta_R}}{\bar{N}_{\delta_R}} \left(\frac{\bar{N}_{\delta_R}}{Y_{\delta_R}} - \frac{\bar{N}_\beta}{Y_\beta} \right) \right] \left(s - \frac{\bar{L}_P}{I_{xx}} \right) \quad (5.20)$$

Considering equation (5.10), the condition of equation (5.19) requires that the yaw to roll moment ratio as a result of rudder deflections must be close to or greater than unity. This condition is easily satisfied by conventional aircraft where the yaw moment arm length to the rudder is far greater than the roll moment arm length. When the conditions of equations (5.4) to (5.7) and (5.19) hold then the transfer function from the rudder input to the yaw rate reduces to,

$$\frac{R(s)}{\delta_R(s)} = \frac{\bar{N}_{\delta_R}}{I_{zz}} \frac{s - \frac{Y_\beta}{m\bar{V}} \frac{Y_{\delta_R}}{\bar{N}_{\delta_R}} \left(\frac{\bar{N}_{\delta_R}}{Y_{\delta_R}} - \frac{\bar{N}_\beta}{Y_\beta} \right)}{s^2 - \left(\frac{Y_\beta}{m\bar{V}} + \frac{\bar{N}_R}{I_{zz}} \right) s + \left(\frac{Y_\beta}{m\bar{V}} \frac{\bar{N}_R}{I_{zz}} + \frac{\bar{N}_\beta}{I_{zz}} \right)} \quad (5.21)$$

due to the pole-zero cancellation of the roll mode. Thus to a good approximation, feedback from yaw rate to rudder will not influence the roll dynamics.

5.1.3 Rudder to lateral specific acceleration transfer function

The zeros from the rudder input to the lateral specific acceleration output are shown in Appendix B to be the roots of the following polynomial,

$$\alpha_z(s) = \frac{Y_{\delta_R}}{m} \left[s^2 - \frac{Y_R}{I_{zz}} \left(\frac{\bar{N}_R}{Y_{\delta_R}} - \frac{\bar{N}_{\delta_R}}{Y_R} \right) s + \frac{Y_\beta}{I_{zz}} \left(\frac{\bar{N}_\beta}{Y_\beta} - \frac{\bar{N}_{\delta_R}}{Y_{\delta_R}} \right) \right] \left(s - \frac{\bar{L}_P}{I_{xx}} \right) \quad (5.22)$$

under the conditions of equations (5.4) to (5.7) and (5.19). Under these conditions, there is pole-zero cancellation of the Roll mode and the transfer function from the rudder input to the lateral specific acceleration output can be written as follows,

$$\frac{B_W(s)}{\delta_R(s)} = \frac{Y_{\delta_R}}{m} \frac{s^2 + \frac{Y_R}{I_{zz}} \left(\frac{\bar{N}_{\delta_R}}{Y_{\delta_R}} - \frac{\bar{N}_R}{Y_R} \right) s + \frac{Y_\beta}{I_{zz}} \left(\frac{\bar{N}_\beta}{Y_\beta} - \frac{\bar{N}_{\delta_R}}{Y_{\delta_R}} \right)}{s^2 - \left(\frac{Y_\beta}{m\bar{V}} + \frac{\bar{N}_R}{I_{zz}} \right) s + \left(\frac{Y_\beta}{m\bar{V}} \frac{\bar{N}_R}{I_{zz}} + \frac{\bar{N}_\beta}{I_{zz}} \right)} \quad (5.23)$$

Thus, to a good approximation, feedback from lateral specific acceleration to rudder will not influence the roll dynamics.

5.1.4 Summary of results

In this section, it has been shown that under the conditions of equations (5.4) to (5.7), (5.12) to (5.14) and (5.19), feedback from roll rate to ailerons will only affect the roll dynamics and

feedback from both yaw rate and lateral specific acceleration to rudder will only affect the directional dynamics. Thus, for control system design purposes, the lateral dynamics can be split into roll and directional dynamics and the lateral closed loop poles can be positioned separately through feedback involving the inputs and outputs investigated in the transfer functions above. It is important to note however that the conditions above do not fully decouple the lateral dynamics and that aileron deflections will still stimulate the directional dynamics (adverse yaw) and rudder deflections will still stimulate the roll dynamics (rudder induced roll). However, the transfer function results above do show that these cross couplings will only occur via the direct input terms i.e. the side force and yaw moment due to ailerons and the roll moment due to rudder, and not indirectly through the roll and directional dynamics couplings.

With the results of the novel analysis of the previous subsections in place, the lateral dynamics can be written as follows,

Roll dynamics:

$$\dot{P} = \begin{bmatrix} \bar{L}_p \\ I_{xx} \end{bmatrix} P + \begin{bmatrix} \bar{L}_{\delta_A} \\ I_{xx} \end{bmatrix} \delta_A + \begin{bmatrix} \bar{L}_{\delta_R} \\ I_{xx} \end{bmatrix} \delta_R \quad (5.24)$$

$$P_w = P \quad (5.25)$$

Directional dynamics:

$$\begin{bmatrix} \dot{\beta} \\ \dot{R} \end{bmatrix} = \begin{bmatrix} \frac{Y_\beta}{m\bar{V}} & -1 \\ \frac{\bar{N}_\beta}{I_{zz}} & \frac{\bar{N}_R}{I_{zz}} \end{bmatrix} \begin{bmatrix} \beta \\ R \end{bmatrix} + \begin{bmatrix} \frac{Y_{\delta_R}}{m\bar{V}} \\ \frac{\bar{N}_{\delta_R}}{I_{zz}} \end{bmatrix} \delta_R + \begin{bmatrix} 0 \\ \frac{\bar{N}_{\delta_A}}{I_{zz}} \end{bmatrix} \delta_A + \begin{bmatrix} \frac{g}{\bar{V}} \\ 0 \end{bmatrix} e_{23}^{wI} \quad (5.26)$$

$$B_w = \begin{bmatrix} \frac{Y_\beta}{m} & \frac{Y_R}{m} \\ \frac{\bar{N}_\beta}{I_{zz}} & \frac{\bar{N}_R}{I_{zz}} \end{bmatrix} \begin{bmatrix} \beta \\ R \end{bmatrix} + \begin{bmatrix} \frac{Y_{\delta_R}}{m} \\ \frac{\bar{N}_{\delta_R}}{I_{zz}} \end{bmatrix} \delta_R \quad (5.27)$$

Aileron and rudder couplings into the directional and roll dynamics respectively will be considered disturbances. These disturbances will be examined explicitly when designing the roll rate and lateral specific acceleration controllers. By splitting the lateral dynamics into roll and directional dynamics, the complexity of designing a generic controller to regulate the roll rate and lateral specific acceleration is greatly decreased. Furthermore, as shall be seen, splitting the dynamics allows for a greater degree of insight into the lateral aircraft motion. Of course, if the parameters of a particular aircraft violate any of the conditions derived in this section then either active decoupling techniques should be employed or an aircraft specific MIMO controller should be designed. Conversely, the conditions listed above could be used as aircraft design constraints to ensure that the generic lateral controller to be developed in this chapter can be applied.

In the following two sections, controllers for roll rate and lateral specific acceleration will be designed.

5.2 Roll rate controller

The design of a controller capable of regulating the roll rate using the ailerons is presented in this section. The closed loop rudder to roll rate disturbance transfer function is also investigated. All design details are provided in Appendix B.

5.2.1 Roll rate controller design

With reference to the roll rate dynamics of equation (5.24), define a PI control law to provide the design freedom for the desired closed loop dynamic response and to counter any steady state disturbances due to asymmetry in the aircraft,

$$\delta_A = -K_p P - K_E E_p \quad (5.28)$$

$$\dot{E}_p = P - P_R \quad (5.29)$$

where P_R is the reference roll rate command. The closed loop dynamics in state space form are then,

$$\begin{bmatrix} \dot{P} \\ \dot{E}_p \end{bmatrix} = \begin{bmatrix} \bar{L}_p - \bar{L}_{\delta_A} K_p & -\bar{L}_{\delta_A} K_E \\ \frac{\bar{L}_{\delta_A}}{I_{xx}} & 0 \end{bmatrix} \begin{bmatrix} P \\ E_p \end{bmatrix} + \begin{bmatrix} 0 \\ -1 \end{bmatrix} P_R + \begin{bmatrix} \bar{L}_{\delta_R} \\ \frac{\bar{L}_{\delta_R}}{I_{xx}} \\ 0 \end{bmatrix} \delta_R \quad (5.30)$$

Given the desired closed loop characteristic equation,

$$\alpha_c(s) = s^2 + \alpha_1 s + \alpha_0 \quad (5.31)$$

matching of the coefficients yields the following feedback gains,

$$K_p = \frac{1}{\bar{L}_{\delta_A}} (\bar{L}_p + I_{xx} \alpha_1) \quad (5.32)$$

$$K_E = \frac{I_{xx}}{\bar{L}_{\delta_A}} \alpha_0 \quad (5.33)$$

The design freedom is thus reduced to that of selecting suitable closed loop pole locations. Selection of closed loop poles will be discussed in section 5.2.2. To investigate the effects of rudder disturbances on the closed loop system, the rudder to roll rate transfer function is determined. This transfer function is shown in Appendix B to be,

$$\frac{P(s)}{\delta_R(s)} = \frac{\bar{L}_{\delta_R}}{I_{xx}} \frac{s}{s^2 + \alpha_1 s + \alpha_0} \quad (5.34)$$

The transfer function can be investigated in the closed loop to determine whether the rudder input couples unacceptably into the closed loop roll dynamics. However, for typical aircraft parameters and roll dynamics bandwidths, the coupling is negligible across the whole frequency range.

5.2.2 Selection of the closed loop poles

The upper bandwidth of the roll dynamics is typically limited by actuator saturation or slew rate limits and un-modelled structural dynamics. A lower bandwidth limit is imposed through the timescale separation requirement between the roll dynamics and the velocity magnitude and air density. By selecting a fixed set of closed loop roll dynamics poles, the controller will attempt to make the aircraft respond with the same dynamics in roll rate at all dynamic pressures. For aircraft operating about a nominal dynamic pressure flight condition, this strategy is ideal since it provides an invariant interface to the outer guidance level controllers. However, intuitively it is clear that as the dynamic pressure decreases, this strategy will result in very large control deflections and possibly even control surface saturation.

To avoid the problems associated with large dynamic pressure variations, a similar variable pole placement strategy to that proposed in section 4.2.5 can be adopted. The roll dynamics poles can be placed in fixed positions in a NNDT frequency plane which in turn is equivalent to varying pole positions in the dimensional frequency plane. Varying the dimensional time dynamics will ensure that the aircraft's dynamic response in roll is adjusted according to its current flight condition. This will tend to result in the controller utilising the same level of control deflections at all times and consequently will result in an increase in response times as the dynamic pressure decreases.

In practice a combination of the fixed and varying pole placement controllers can be employed depending on the aircraft's mission profile. The following subsection discusses the details of the NNDT pole placement controller for roll rate.

5.2.3 NNDT roll rate controller design

Considering the roll dynamics of equation (5.24), define the following non-dimensional states and controls,

$$P' = \frac{b}{2\bar{V}_a} P \quad (5.35)$$

$$\delta'_A = \delta_A \quad (5.36)$$

Then with the non-dimensional time variable defined by equation (4.66) and the derivative of a variable with respect to non-dimensional time defined by equation (4.68), the roll dynamics can be written in NNDT form as follows,

$$\bar{P}' = [k_x \bar{C}_{l_p}] P' + [k_x \bar{C}_{l_{\delta_A}}] \delta'_A \quad (5.37)$$

where,

$$k_x = \frac{1}{2} \frac{\bar{V}'}{r_x'^2} \quad (5.38)$$

with,

$$r_x' = \frac{r_x}{b} \quad (5.39)$$

$$r_x = \sqrt{\frac{I_{xx}}{m}} \quad (5.40)$$

and \bar{V}' from equation (4.74). In equation (5.39) r_x' is the normalised roll radius of gyration. Notice that under zero wind assumptions, k_x is a constant and the NNDT roll dynamics are time invariant. Define a PI control law of the form,

$$\delta'_A = -K'_p P' - K'_E E'_p \quad (5.41)$$

$$\bar{E}'_p = P' - P'_R \quad (5.42)$$

where P'_R is the non-dimensional reference roll rate command. Given the desired closed loop NNDT characteristic equation,

$$\alpha_c(s') = (s')^2 + \alpha_1 s' + \alpha_0 \quad (5.43)$$

the feedback gains that place the poles in the desired locations are easily shown to be,

$$K'_p = \frac{\alpha_1 + k_x \bar{C}_{l_p}}{k_x \bar{C}_{l_{\delta_A}}} \quad (5.44)$$

$$K'_E = \frac{\alpha_0}{k_x \bar{C}_{l_{\delta_A}}} \quad (5.45)$$

Note that for a fixed set of closed loop NNDT poles and with k_x a constant, the NNDT feedback gains are constant and can be calculated offline. To implement the controller the dimensional roll rate signal is simply normalised using equation (5.35). Then the control law of equations (5.41) and (5.42) is applied and the normalised aileron deflection is converted to its dimensional form using equation (5.36).

5.2.4 Integrator pole placement

Similarly to the normal specific acceleration controller integrator pole, the closed loop roll rate integrator pole need not be placed at timescale separation frequencies if the roll rate control

law is adapted to include a feed-forward term as follows,

$$\delta_A = -K_p P - K_E E_p + N_p P_R \quad (5.46)$$

$$\dot{E}_p = P - P_R \quad (5.47)$$

and in the NNDT case,

$$\delta'_A = -K'_p P' - K'_E E'_p + N'_p P'_R \quad (5.48)$$

$$\bar{E}'_p = P' - P'_R \quad (5.49)$$

The effect of the feed-forward term in the control law is again to add a zero to the closed loop system from the reference input to the output at,

$$s = -\frac{K_E}{N_p} \quad (5.50)$$

and for the NNDT case,

$$s' = -\frac{K'_E}{N'_p} \quad (5.51)$$

If the feed-forward gain is selected such that the zero lies on top of the closed loop integrator pole then the closed loop integrator dynamics will not be visible from the reference input to the output. However, similarly to the normal specific acceleration controller case, the integrator dynamics will be seen from any disturbance input. It is thus the choice of the designer as to whether a slower integrator is desired for practical reasons or whether a faster integrator is desired to quickly fully reject disturbances and the effects of parameter uncertainty.

5.3 Lateral specific acceleration controller

The design of the lateral specific acceleration controller is covered in this section. The natural lateral specific acceleration dynamics are investigated first and the fundamental differences between the directional and normal dynamics are highlighted. These differences force the design of a very different controller to that employed in section 4.2.4. Selection of the closed loop poles is considered and a NNDT version of the controller is also presented.

5.3.1 Natural lateral specific acceleration dynamics

The directional dynamics of equations (5.26) and (5.27) are restated below for convenience,

$$\begin{bmatrix} \dot{\beta} \\ \dot{R} \end{bmatrix} = \begin{bmatrix} \frac{Y_\beta}{m\bar{V}} & -1 \\ \frac{\bar{N}_\beta}{I_{zz}} & \frac{\bar{N}_R}{I_{zz}} \end{bmatrix} \begin{bmatrix} \beta \\ R \end{bmatrix} + \begin{bmatrix} \frac{Y_{\delta_R}}{m\bar{V}} \\ \frac{\bar{N}_{\delta_R}}{I_{zz}} \end{bmatrix} \delta_R + \begin{bmatrix} 0 \\ \frac{\bar{N}_{\delta_A}}{I_{zz}} \end{bmatrix} \delta_A + \begin{bmatrix} \frac{g}{\bar{V}} \\ 0 \end{bmatrix} e_{23}^{WI} \quad (5.52)$$

$$B_W = \begin{bmatrix} \frac{Y_\beta}{m} & \frac{Y_R}{m} \end{bmatrix} \begin{bmatrix} \beta \\ R \end{bmatrix} + \begin{bmatrix} \frac{Y_{\delta_R}}{m} \end{bmatrix} \delta_R \quad (5.53)$$

Ignoring the aileron disturbance to the directional dynamics initially and comparing the directional dynamics to the normal dynamics of equations (4.21) and (4.22), it can be seen that the form of these two sets of dynamics is very similar. However, although the form of the two sets of dynamics is similar, for typical aircraft parameters, the dynamics governing the lateral specific acceleration differ greatly from those governing the normal specific acceleration. This is largely because there is no primary lateral lifting surface on conventional aircraft. As a result, the gain from rudder deflection through to lateral specific acceleration is typically low compared to that from elevator through to normal specific acceleration. Furthermore, with the fin dominating the directional forces and moments, the directional neutral point tends to lie far behind the centre of mass. As shall be seen in the analysis to follow, the position of the directional neutral point and the low rudder to lateral specific acceleration gain result in a significant difference between the directional and normal specific acceleration dynamics. As a result, a different control strategy needs to be employed in order to regulate the lateral specific acceleration.

With reference to the transfer function of equation (5.23) it can be seen that the characteristic equation governing the poles of the directional dynamics is,

$$p(s) = s^2 - \left(\frac{Y_\beta}{m\bar{V}} + \frac{\bar{N}_R}{I_{zz}} \right) s + \left(\frac{Y_\beta}{m\bar{V}} \frac{\bar{N}_R}{I_{zz}} + \frac{\bar{N}_\beta}{I_{zz}} \right) \quad (5.54)$$

For typical aircraft parameters, these Dutch Roll mode poles are usually lightly damped with a frequency on the order of those of the Short Period mode poles. Analysing the transfer function of equation (5.23) further, it can be seen that similarly to the normal specific acceleration dynamics there are two rudder to lateral specific acceleration zeros. Define the following characteristic lengths,

$$l_W \equiv -\frac{\bar{N}_\beta}{Y_\beta} \quad (5.55)$$

$$l_D \equiv -\frac{\bar{N}_R}{Y_R} \quad (5.56)$$

$$l_F \equiv -\frac{\bar{N}_{\delta_R}}{Y_{\delta_R}} \quad (5.57)$$

where l_w is the weathercock arm length, l_D is the damping arm length, l_F is the effective length to the fin and all lengths are relative to the centre of mass. Then, as shown in Appendix B, by completing the square and making similar simplifying assumptions to those made in section 4.2.1, the rudder to lateral specific acceleration zeros are at,

$$z_{1,2} = \frac{1}{2} \frac{Y_R(l_F - l_D)}{I_{zz}} \pm \sqrt{\frac{-Y_\beta(l_F - l_w)}{I_{zz}}} \quad (5.58)$$

In the normal dynamics case, it was argued that the second term in the zeros equation would typically dominate and result in two real zeros centred about a small real axis offset. The analysis of section 4.2.2 showed that the position of these zeros places a strict upper bound on the practically achievable bandwidth of the closed loop system. Comparing the second term of equation (5.58) to the second term of equation (4.32), two major differences are noted. Firstly, the difference in magnitude between the effective length to the fin and the weathercock arm length is typically far smaller than the difference in magnitude between the effective length to the tail-plane and the length to the neutral point. This is because in conventional aircraft, most of the weathercock stiffness arises from the fin surface while the pitch stiffness arises due to a combination of both the wing and the tail-plane surfaces.

Secondly, the latter term of equation (4.32) is scaled by the lift due to angle of incidence dimensional stability derivative while the latter term of equation (5.58) is scaled by the side force due to sideslip dimensional stability derivative. With no primary lateral lifting surface on conventional aircraft, the stability derivative C_{L_α} is typically far greater in magnitude than the stability derivative C_{Y_β} . Thus, ignoring any differences in the moments of inertia it is clear from the arguments above that the rudder to lateral specific acceleration zeros will lie at a far lower frequency than those of the elevator to normal specific acceleration dynamics. As a result, it is typical for the open loop directional dynamics poles to lie outside the frequency bound,

$$\omega_n < \frac{1}{3} \sqrt{\frac{-Y_\beta(l_F - l_w)}{I_{zz}}} \quad (5.59)$$

developed in section 4.2.2 and applied to equation (5.58) with the real axis offset ignored. Consequently, it is necessary to take into account the side force due to rudder deflection and yaw rate when moving these open loop poles thus making the controller design approach presented in section 4.2.4 inappropriate for regulation of the lateral specific acceleration. Furthermore, with the inclusion of these side force terms, dynamic inversion of the gravity coupling term, as was done in section 4.2.4, becomes practically infeasible [26,32]. To handle the gravity coupling problem consider the transfer function, derived in Appendix B, from the wind axis system attitude parameter ($e_{23}^{w'}$) through to the lateral specific acceleration,

$$\frac{B_w(s)}{e_{23}^{wl}(s)} = \frac{g}{\bar{V}} \frac{Y_\beta}{m} \frac{s + \frac{Y_R}{I_{zz}}(l_D - l_w)}{s^2 - \left(\frac{Y_\beta}{m\bar{V}} + \frac{\bar{N}_R}{I_{zz}}\right)s + \left(\frac{Y_\beta}{m\bar{V}} \frac{\bar{N}_R}{I_{zz}} + \frac{\bar{N}_\beta}{I_{zz}}\right)} \quad (5.60)$$

where equations (5.55) and (5.56) have been substituted to provide further insight. Equation (5.60) highlights two important facts regarding the gravity coupling into the lateral specific acceleration. Firstly, it is seen that the magnitude of the coupling is scaled by the side force due to sideslip dimensional stability derivative. In the normal dynamics, this term would be replaced by the lift due to angle of attack. Thus it is clear that the gravity coupling will have far less of an effect on the lateral specific acceleration dynamics than it does on the normal specific acceleration dynamics. Secondly, the damping arm length and the weathercock arm length are typically fairly similar in magnitude with both effects primarily arising from the fin. Thus, with typical Dutch Roll mode natural frequencies the low frequency gain from e_{23}^{wl} to the lateral specific acceleration is usually very small.

The points above show that the same phenomena that cause the rudder to lateral specific acceleration zeros to lie at low frequencies, also cause the gravity coupling into the lateral specific acceleration to be weak. The control strategy adopted in the following section is thus to simply ignore the gravity coupling term in the knowledge that it will act as a small disturbance input to the closed loop system that will ultimately be rejected. Of course the transfer function of equation (5.60) can be used on a case by case basis to determine the level of gravity coupling over frequency. If for a specific aircraft the level of coupling is deemed excessive, then alternative control strategies can be sought.

Before proceeding with the directional controller design, the aileron disturbance coupling in equation (5.52) is considered. The coupling most often manifests itself in adverse yaw and results due to the differential drag across the wings during aileron deflections. Very often, due to the directional stiffness of conventional aircraft, the adverse yaw is negligible and can simply be ignored. In cases where the adverse yaw is not negligible, a human pilot would typically provide a transient rudder input to counter the moment generated by the wings. Motivated by this intuitive solution, a static inversion control law of the form,

$$\delta_R = \delta_{R_i} - \frac{\bar{N}_{\delta_A}}{\bar{N}_{\delta_R}} \delta_A \quad (5.61)$$

could be implemented to cancel the aileron moment disturbance. However, because the rudder also generates a pure side force, the control law does not completely eliminate the aileron coupling and instead results in the following closed loop system,

$$\begin{bmatrix} \dot{\beta} \\ \dot{R} \end{bmatrix} = \begin{bmatrix} \frac{Y_\beta}{m\bar{V}} & -1 \\ \frac{\bar{N}_\beta}{I_{zz}} & \frac{\bar{N}_R}{I_{zz}} \end{bmatrix} \begin{bmatrix} \beta \\ R \end{bmatrix} + \begin{bmatrix} \frac{Y_{\delta_R}}{m\bar{V}} \\ \frac{\bar{N}_{\delta_R}}{I_{zz}} \end{bmatrix} \delta_{R_1} + \begin{bmatrix} -\frac{Y_{\delta_R}}{m\bar{V}} \frac{\bar{N}_{\delta_A}}{\bar{N}_{\delta_R}} \\ 0 \end{bmatrix} \delta_A \quad (5.62)$$

$$B_w = \begin{bmatrix} \frac{Y_\beta}{m} & \frac{Y_R}{m} \\ \frac{\bar{N}_\beta}{m} & \frac{\bar{N}_R}{m} \end{bmatrix} \begin{bmatrix} \beta \\ R \end{bmatrix} + \begin{bmatrix} \frac{Y_{\delta_R}}{m} \\ \frac{\bar{N}_{\delta_R}}{m} \end{bmatrix} \delta_{R_1} + \begin{bmatrix} -\frac{Y_{\delta_R}}{m} \frac{\bar{N}_{\delta_A}}{\bar{N}_{\delta_R}} \\ 0 \end{bmatrix} \delta_A \quad (5.63)$$

where the gravity coupling term has been neglected. Thus, the control law of equation (5.61) is seen to remove the effect of the aileron moment disturbance in exchange for a pure lateral force disturbance. In Appendix B, it is shown that by implementing the static inversion control law, the steady state lateral specific acceleration will be reduced by a factor l_f/l_w per unit of aileron deflection. As previously discussed, the weathercock arm length is often not significantly less than the effective length to the fin. Thus, the percentage reduction in the steady state lateral specific acceleration when the control law of equation (5.61) is implemented is typically quite limited and must be weighed up against the added complexity of implementing the control law at all.

Given the arguments above, the aileron coupling into the directional dynamics will be ignored for the purposes of the lateral specific acceleration control system design. It will be assumed that either the coupling is naturally negligible (or at least constitutes a negligible disturbance to the lateral specific acceleration control system), or its effect can be made negligible by the static inversion control law of equation (5.61). For less conventional aircraft with a significant adverse yaw coupling, an alternative control strategy based on the full MIMO lateral dynamics should be sought.

5.3.2 Lateral specific acceleration controller design

Given the analysis of the previous section, the lateral specific acceleration controller design strategy is as follows. Firstly, with the gravity and aileron disturbances ignored, the full directional dynamics (including side force due to rudder and yaw rate) are used to design a controller that allows the Dutch Roll mode poles to be moved arbitrarily. The purpose of this controller is purely for stability augmentation and it does not seek to regulate the lateral specific acceleration at all. It is assumed that a timescale separation exists or can be enforced through feedback between the velocity magnitude and air density, thus allowing these states to be treated as parameters in the controller.

A second, outer level controller is then designed with the sole purpose of regulating the lateral specific acceleration. The controller also ensures that the closed loop lateral specific acceleration regulation bandwidth does not exceed the frequency bound of equation (5.59), which in turn implies a practically feasible controller. For the design of this control system it is assumed that the stability augmentation controller above places the natural directional

dynamics poles such that a timescale separation exists to the outer regulating controller. This assumption allows the full dynamic model from rudder to lateral specific acceleration to be approximated by the steady state gain. Doing this significantly reduces the complexity of the lateral specific acceleration regulation controller. Furthermore, the assumption does not typically place unreasonable constraints on the stability augmentation controller since as discussed in section 5.3.1 the natural frequency of the Dutch Roll mode poles is typically already greater than the NMP zero frequency.

Although a number of other control strategies do exist for regulating the lateral specific acceleration, the above approach results in a simple, generic control law that is practically feasible for most aircraft. The stability augmentation and regulation phases above could be combined into a single control law where the full directional dynamics model is taken into account at all times. However, this would result in an overly complicated controller with marginal improvement in pole placement accuracy.

5.3.2.1 Directional stability augmentation

Define the stability augmentation control law,

$$\delta_R = -K_R R - K_B B_W + \delta_{R_r} \quad (5.64)$$

where δ_{R_r} will be used as an input for the regulation control law. Substituting the control law into the directional dynamics is shown in Appendix B to give,

$$\begin{bmatrix} \dot{\beta} \\ \dot{R} \end{bmatrix} = \begin{bmatrix} \frac{Y_\beta}{m\bar{V}} - K_B \frac{Y_\beta}{m} \frac{Y_{\delta_R}}{m\bar{V}} X & -1 - K'_R \frac{Y_{\delta_R}}{m\bar{V}} X \\ \frac{\bar{N}_\beta}{I_{zz}} - K_B \frac{Y_\beta}{m} \frac{\bar{N}_{\delta_R}}{I_{zz}} X & \frac{\bar{N}_R}{I_{zz}} - K'_R \frac{\bar{N}_{\delta_R}}{I_{zz}} X \end{bmatrix} \begin{bmatrix} \beta \\ R \end{bmatrix} + \begin{bmatrix} \frac{Y_{\delta_R}}{m\bar{V}} X \\ \frac{\bar{N}_{\delta_R}}{I_{zz}} X \end{bmatrix} \delta_{R_r} \quad (5.65)$$

with,

$$X = \left(1 + K_B \frac{Y_{\delta_R}}{m} \right)^{-1} \quad (5.66)$$

$$K'_R = K_R + K_B \frac{Y_R}{m} \quad (5.67)$$

Appendix B shows that the closed loop poles are well approximated by the roots of the following characteristic equation,

$$\alpha_c(s) = s^2 - \left(\frac{Y_\beta}{m\bar{V}} + \frac{\bar{N}_R}{I_{zz}} - \frac{\bar{N}_{\delta_R}}{I_{zz}} K_R \right) X s + \left[\frac{Y_\beta}{m\bar{V}} \frac{\bar{N}_R}{I_{zz}} + \frac{\bar{N}_\beta}{I_{zz}} + \frac{Y_{\delta_R}}{m} \frac{Y_\beta}{I_{zz}} \left(\frac{\bar{N}_\beta}{Y_\beta} - \frac{\bar{N}_{\delta_R}}{Y_{\delta_R}} \right) K_B \right] X \quad (5.68)$$

given that the following constraints hold,

$$\left| \frac{Y_R}{m} \frac{Y_{\delta_R}}{\bar{N}_{\delta_R}} \left(\frac{\bar{N}_R}{Y_R} - \frac{\bar{N}_{\delta_R}}{Y_{\delta_R}} \right) \frac{K_B}{K_R} \right| \ll 1 \quad (5.69)$$

$$\left| \frac{Y_{\delta_R}}{m\bar{V}} \frac{Y_\beta}{\bar{N}_\beta} \left(\frac{\bar{N}_\beta}{Y_\beta} - \frac{\bar{N}_{\delta_R}}{Y_{\delta_R}} \right) K_R \right| \ll 1 \quad (5.70)$$

These constraints become,

$$\left| \frac{K_B}{K_R} \right| \ll \left| \frac{m}{Y_R} \frac{l_F}{l_D - l_F} \right| \quad (5.71)$$

$$\left| K_R \right| \ll \left| \frac{m\bar{V}}{Y_{\delta_R}} \frac{l_W}{l_W - l_F} \right| \quad (5.72)$$

when the characteristic lengths of equations (5.55) to (5.57) are substituted. Both constraints are typically easily satisfied due to the similar length of the damping arm, weathercock arm and effective length to the fin in conventional aircraft. The similarity in these lengths implies that the denominators of the terms on the right hand side of equations (5.71) and (5.72) are small and thus that the terms themselves are large. Thus, although the designer needs to remain aware of the above bounds on the stability augmentation gains, for typical aircraft parameters and directional dynamics pole locations, these bounds do not come into effect. Continuing with the controller design, given the desired directional dynamics characteristic equation,

$$\alpha_c(s) = s^2 + \alpha_1 s + \alpha_0 \quad (5.73)$$

the coefficients of the characteristic polynomial of equation (5.68) can be matched to yield the stability augmentation feedback gains,

$$K_R = \frac{I_{zz}}{\bar{N}_{\delta_R}} \left[\frac{Y_\beta}{m\bar{V}} + \frac{\bar{N}_R}{I_{zz}} + \alpha_1 \left(1 + K_B \frac{Y_{\delta_R}}{m} \right) \right] \quad (5.74)$$

$$K_B = \frac{\frac{Y_\beta}{m\bar{V}} \frac{\bar{N}_R}{I_{zz}} + \frac{\bar{N}_\beta}{I_{zz}} - \alpha_0}{\frac{Y_{\delta_R}}{m} \left[\alpha_0 - \frac{Y_\beta}{I_{zz}} \left(\frac{\bar{N}_\beta}{Y_\beta} - \frac{\bar{N}_{\delta_R}}{Y_{\delta_R}} \right) \right]} \quad (5.75)$$

A special case of the above control law is obtained when the lateral specific acceleration feedback gain is manually set to zero. When this is done, the characteristic equation of equation (5.68) becomes,

$$\alpha_c(s) = s^2 - \left(\frac{Y_\beta}{m\bar{V}} + \frac{\bar{N}_R}{I_{zz}} - \frac{\bar{N}_{\delta_R}}{I_{zz}} K_R \right) s + \left(\frac{Y_\beta}{m\bar{V}} \frac{\bar{N}_R}{I_{zz}} + \frac{\bar{N}_\beta}{I_{zz}} \right) \quad (5.76)$$

From this equation it is clear that the remaining yaw rate feedback does not affect the natural frequency of the open loop directional dynamics poles and therefore only affects the damping. Thus, this modified control law is particularly attractive when the open loop natural frequency of the directional dynamics is acceptable since it results in a significant reduction in the calculations required for the stability augmentation feedback gains. For typical aircraft, there is little need to change the Dutch Roll mode frequency other than for timescale separation purposes, making the simplified control law an attractive practical approach. Thus, for this special case of the stability augmentation control law, the feedback gains can be written as follows,

$$K_R = \frac{I_{zz}}{\bar{N}_{\delta_R}} \left(\frac{Y_\beta}{m\bar{V}} + \frac{\bar{N}_R}{I_{zz}} + 2\zeta\omega_n \right) \quad (5.77)$$

$$K_B = 0 \quad (5.78)$$

with,

$$\omega_n = \sqrt{\frac{Y_\beta}{m\bar{V}} \frac{\bar{N}_R}{I_{zz}} + \frac{\bar{N}_\beta}{I_{zz}}} \quad (5.79)$$

where the design freedom is left to selecting only the damping ratio (ζ) for the directional dynamics poles. If however, the full controller with feedback gains of equations (5.74) and (5.75) is used then the design freedom is left to fully selecting the desired closed loop pole positions such that the feedback gain constraints of equations (5.71) and (5.72) are satisfied. Selection of the closed loop poles will be discussed further in section 5.3.3.

5.3.2.2 Lateral specific acceleration regulation

With the stability augmentation controller of the previous section in place and the assumption that the closed loop directional dynamics poles operate on a much faster timescale than the lateral specific acceleration regulator will, the transfer function from rudder through to lateral specific acceleration can be well approximated as follows,

$$B_W \approx K_{ss} \delta_{R_r} \quad (5.80)$$

Here, K_{ss} is the steady state gain of the transfer function and is calculated in Appendix B to be,

$$K_{ss} = \frac{Y_{\delta_R}}{m} \frac{Y_\beta}{I_{zz}} \left(\frac{\bar{N}_\beta}{Y_\beta} - \frac{\bar{N}_{\delta_R}}{Y_{\delta_R}} \right) \frac{1}{\alpha_0} \left(1 + K_B \frac{Y_{\delta_R}}{m} \right)^{-1} \quad (5.81)$$

given that the condition of equation (5.72) holds. Note that α_0 in equation (5.81) refers to the final term in the desired characteristic equation of equation (5.73). If the simplified stability augmentation controller with feedback gains of equations (5.77) and (5.78) is used then α_0 in the above equation should be replaced with ω_n^2 from equation (5.79).

An integral controller is designed to regulate the lateral specific acceleration. Integral control will ensure that the closed loop system is insensitive to parameter uncertainty that will corrupt the steady state gain of equation (5.81). The frequency of the closed loop integrator pole is limited by the bound of equation (5.59). This pole will dominate the lateral specific acceleration response and ensure that a practically feasible controller is designed. The stability augmentation controller of the previous section will serve to provide fast disturbance rejection but will not dominate the gross lateral specific acceleration response. Define the control law,

$$\delta_{R_r} = -K_E E_B \quad (5.82)$$

$$\dot{E}_B = B_W - B_{W_r} \quad (5.83)$$

where B_{W_r} is the reference lateral specific acceleration command. The closed loop dynamics are then,

$$\dot{E}_B = [-K_{ss} K_E] E_B + [-1] B_{W_r} \quad (5.84)$$

with closed loop characteristic equation,

$$s + K_{ss} K_E = 0 \quad (5.85)$$

Given the desired characteristic equation or equivalently pole location,

$$\alpha_c(s) = s + \alpha_0 \quad (5.86)$$

the integrator feedback gain can be calculated as follows,

$$K_E = \frac{\alpha_0}{K_{ss}} \quad (5.87)$$

The design freedom is left to choosing the integrator pole bearing in mind the frequency constraint of equation (5.59). It should be noted that the frequency constraint of equation (5.59) will typically enforce a lateral specific acceleration regulation bandwidth that violates the timescale separation condition to velocity magnitude and air density. Practically however, this is not of major concern since the velocity magnitude and air density will be held relatively constant by outer guidance loop controllers. Thus, for the controller designed in this section, the velocity and air density can simply be updated by a low pass filtered version of the actual signal.

5.3.3 Selection of the closed loop poles

With the design freedom reduced to that of pole placement, the controller design of the previous subsections ensures that the closed loop directional dynamics remain invariant for all point mass kinematics states. For aircraft that operate about a nominal dynamic pressure this is

an ideal control strategy since it provides the simplest interface with the outer guidance level controllers. However, as discussed in sections 4.2.5 and 5.2.2, when the dynamic pressure changes significantly (more particularly when it is reduced significantly), then the controller design of the previous section would quickly result in problems such as actuator saturation.

To avoid these problems, fixed and variable pole placement strategies can again be employed. For example, the bandwidth of the stability augmentation directional controller could be scheduled to be some factor (or multiple) of the NMP zero frequency. This would tend to ensure that the closed loop bandwidth remained practically feasible over large dynamic pressure ranges and thus avoid actuator saturation. A second strategy could be to schedule the stability augmentation bandwidth with the open loop natural frequency of the directional dynamics. This would have a very similar result to that of the previously mentioned strategy. However, an added advantage is that it would naturally lend itself to the simplified stability augmentation controller design with gains of equations (5.77) and (5.78).

A final strategy for implementing variable pole placement is again to design the directional controller in a NNDT frequency domain. This strategy was employed for the normal specific acceleration controller in section 4.2.6 and the roll rate controller in section 5.2.3. The analysis of the following subsection will show that by normalising the states, controls, outputs and time, the directional dynamics become largely invariant. This allows a single controller to be designed to place the directional dynamics poles in a NNDT frequency plane which ultimately results in dimensional poles that remain practically feasible.

5.3.4 NNDT lateral specific acceleration controller design

Consider the directional dynamics of equations (5.52) and (5.53). Define the following non-dimensional states, controls and outputs,

$$\beta' \equiv \beta \quad (5.88)$$

$$R' \equiv \frac{b}{2\bar{V}_a} R \quad (5.89)$$

$$\delta'_R \equiv \delta_R \quad (5.90)$$

$$B'_W \equiv \frac{m}{qS} B_W \quad (5.91)$$

Given the non-dimensional time definition of equation (4.66) and the non-dimensional time derivative definition of equation (4.68), the NNDT directional dynamics are shown in Appendix B to be,

$$\begin{bmatrix} \vec{\beta}' \\ \vec{R}' \end{bmatrix} = \begin{bmatrix} C_{y\beta} & -k_R \\ k_z \bar{C}_{n\beta} & k_z \bar{C}_{nR} \end{bmatrix} \begin{bmatrix} \beta' \\ R' \end{bmatrix} + \begin{bmatrix} C_{y\delta_R} \\ k_z \bar{C}_{n\delta_R} \end{bmatrix} \delta'_R + \begin{bmatrix} 0 \\ k_z \bar{C}_{n\delta_A} \end{bmatrix} \delta'_A + \begin{bmatrix} g' \\ 0 \end{bmatrix} e_{33}^{WT} \quad (5.92)$$

$$B'_W = \begin{bmatrix} C_{y\beta} & C_{yR} \end{bmatrix} \begin{bmatrix} \beta' \\ R' \end{bmatrix} + \begin{bmatrix} C_{y\delta_R} \end{bmatrix} \delta'_R \quad (5.93)$$

where,

$$k_R = 4m'_R \bar{V}' \quad (5.94)$$

$$k_z = \frac{1}{2} \frac{\bar{V}'}{r_z'^2} \quad (5.95)$$

with,

$$m'_R = \frac{m}{\rho S b} \quad (5.96)$$

$$r_z' = \frac{r_z}{b} \quad (5.97)$$

$$r_z = \sqrt{\frac{I_{zz}}{m}} \quad (5.98)$$

and g' and \bar{V}' from equations (4.67) and (4.74) respectively. In equations (5.94) and (5.95), m'_R is the aircraft's mass normalised to a lateral reference air mass and r_z' is the normalised pitch radius of gyration. Note that it has been assumed that,

$$|C_{yR}| \ll |k_R| \quad (5.99)$$

which is equivalent to the standard aircraft assumption of equation (5.5). When the ground speed magnitude and the airspeed magnitude are equivalent, then k_z is constant and the directional dynamics are only a function of the air density through the gain k_R . Investigation of the characteristic equation of the NNDT closed loop poles yields,

$$p(s') = (s')^2 - (C_{y\beta} + k_z \bar{C}_{n_R}) s' + k_z (C_{y\beta} \bar{C}_{n_R} + k_R \bar{C}_{n_\beta}) \quad (5.100)$$

From equation (5.100), it is clear that under zero wind conditions the NNDT directional dynamics poles are not a function of the velocity magnitude and that only the natural frequency of the open loop NNDT directional dynamics poles changes with the air density. Because air density changes slowly with altitude, the open loop directional dynamics poles can be thought of as relatively constant about a nominal altitude. Investigating the zeros from rudder to lateral specific acceleration, the calculations in Appendix B show that the characteristic equation for the zeros is,

$$z(s') = (s')^2 - k_z C_{yR} \left(\frac{\bar{C}_{n_R}}{C_{yR}} - \frac{\bar{C}_{n_{\delta R}}}{C_{y\delta R}} \right) s' + k_R k_z C_{y\beta} \left(\frac{\bar{C}_{n_\beta}}{C_{y\beta}} - \frac{\bar{C}_{n_{\delta R}}}{C_{y\delta R}} \right) \quad (5.101)$$

Define now the following normalised characteristic lengths,

$$l'_W \equiv -\frac{\bar{C}_{n\beta}}{C_{Y\beta}} \quad (5.102)$$

$$l'_F \equiv -\frac{\bar{C}_{n\delta_R}}{C_{Y\delta_R}} \quad (5.103)$$

$$l'_D \equiv -\frac{\bar{C}_{nR}}{C_{Y_R}} \quad (5.104)$$

where l'_W is the normalised weathercock arm length, l'_F is the effective normalised length to the fin, l'_D is the effective normalised damping arm length and all lengths are relative to the centre of mass. Completing the square and following the arguments provided in section 5.3.1 yields the following equation for the zero positions in the NNDT frequency plane,

$$z'_{1,2} = \frac{1}{2}k_z C_{y_R} (l'_F - l'_D) \pm \sqrt{-k_R k_z C_{y\beta} (l'_F - l'_W)} \quad (5.105)$$

With reference to the analysis done in section 4.2.2, the NMP upper bound imposed on the natural frequency of the NNDT normal dynamics poles is,

$$\omega'_n < \frac{1}{3} \sqrt{-k_R k_z C_{y\beta} (l'_F - l'_W)} \quad (5.106)$$

Note that under zero wind conditions the zeros and thus the bound, change only with the air density through k_R . Thus, about a nominal altitude, the zeros remain relatively fixed in the NNDT frequency plane. With the rudder to lateral specific acceleration dynamics dependent only on air density i.e. not on velocity magnitude or any other point mass kinematics states, the normalised frequency domain provides a particularly useful design space for what will ultimately be a variable pole placement control system. Fixing the poles in the non-dimensional frequency plane will have the effect of varying the poles appropriately in the dimensional frequency plane such that they remain practically feasible relative to the NMP frequency constraint. Note that when operating about a nominal air density, the feedback gains to fix the poles in the NNDT frequency plane will be constant and can be calculated offline.

A controller of the same form as that designed in section 5.3.2 is designed to place the directional dynamics poles in the NNDT frequency plane. Define the stability augmentation control law,

$$\delta'_R = -K'_R R' - K'_B B'_W + \delta'_{R_r} \quad (5.107)$$

where δ'_{R_r} will be used as an input for the regulation part of the control law. It is shown in Appendix B that given the desired closed loop characteristic equation,

$$\alpha_c(s') = (s')^2 + \alpha_1 s' + \alpha_0 \quad (5.108)$$

the feedback gains that result in the desired poles are,

$$K'_R = \frac{1}{k_z \bar{C}_{n\delta_R}} \left[C_{y\beta} + k_z \bar{C}_{n_R} + \alpha_1 (1 + K'_B C_{y\delta_R}) \right] \quad (5.109)$$

$$K'_B = \frac{k_z C_{y\beta} \bar{C}_{n_R} + k_z k_R \bar{C}_{n\beta} - \alpha_0}{C_{y\delta_R} \left[\alpha_0 - k_R k_z C_{y\beta} \left(\frac{\bar{C}_{n\beta}}{C_{y\beta}} - \frac{\bar{C}_{n\delta_R}}{C_{y\delta_R}} \right) \right]} \quad (5.110)$$

given that the following constraints hold,

$$\left| \frac{K'_B}{K'_R} \right| \ll \left| \frac{1}{C_{y_R}} \frac{l'_F}{l'_D - l'_F} \right| \quad (5.111)$$

$$|K'_R| \ll \left| \frac{1}{k_R C_{y\delta_R}} \frac{l'_W}{l'_W - l'_F} \right| \quad (5.112)$$

These constraints are the NNDT equivalent of the constraints presented in equations (5.71) and (5.72). A special case of the above control law is obtained when the lateral specific acceleration feedback gain is manually set to zero. When this is done the feedback gains become,

$$K'_R = \frac{1}{k_z \bar{C}_{n\delta_R}} (C_{y\beta} + k_z \bar{C}_{n_R} + 2\zeta \omega'_n) \quad (5.113)$$

$$K'_B = 0 \quad (5.114)$$

and the closed loop natural frequency in the NNDT frequency plane remains,

$$\omega'_n = \sqrt{k_z (C_{y\beta} \bar{C}_{n_R} + k_R \bar{C}_{n\beta})} \quad (5.115)$$

Again note that this NNDT frequency will change only with large air density changes or large differences between the airspeed and ground speed. With the stability augmentation controller in place and the assumption that the closed loop directional dynamics poles are frequency separated from the desired closed loop bandwidth of the outer regulation control law, the transfer function from rudder through to lateral specific acceleration can be well approximated as follows,

$$B'_W \approx K'_{ss} \delta'_{R_R} \quad (5.116)$$

Here K'_{ss} is the steady state gain of the transfer function and is calculated in Appendix B to be,

$$K'_{ss} = k_R k_z C_{y\delta_R} C_{y\beta} \left(\frac{\bar{C}_{n\beta}}{C_{y\beta}} - \frac{\bar{C}_{n\delta_R}}{C_{y\delta_R}} \right) \frac{1}{\alpha_0} \left(1 + K'_B C_{y\delta_R} \right)^{-1} \quad (5.117)$$

given that the condition of equation (5.112) holds. Note that α_0 in equation (5.117) refers to the final term in the desired characteristic equation of equation (5.108). If the simplified stability augmentation controller with feedback gains of equations (5.113) and (5.114) is used then α_0 in the above equation should be replaced with $\omega_n'^2$ from equation (5.115).

An integral controller is designed to regulate the lateral specific acceleration. The frequency of the closed loop integrator pole is limited by the bound of equation (5.106). The pole will thus dominate the lateral specific acceleration response and ensure a practically feasible control system. Define the control law,

$$\delta'_{Rr} = -K'_E E'_B \quad (5.118)$$

$$\bar{E}'_B = B'_W - B'_{W_r} \quad (5.119)$$

where B'_{W_r} is the reference non-dimensional lateral specific acceleration. Then given the desired characteristic equation,

$$\alpha_c(s') = s' + \alpha_0 \quad (5.120)$$

it is straightforward to show that the integrator feedback gain must be,

$$K'_E = \frac{\alpha_0}{K'_{ss}} \quad (5.121)$$

to place the pole as desired.

5.4 Conclusion

This chapter covered the detailed design and associated analysis of the roll rate and lateral specific acceleration controllers (bottom two controllers on the right hand side of Figure 3.1). These controllers together with the analysis that lead up to their design form part of the primary contribution of this dissertation to the field of aircraft flight control. Showing that under mild, practically feasible conditions the MIMO lateral dynamics decouple into roll and directional dynamics, was the primary analysis contribution of this chapter. This decoupling in turn greatly simplified the resulting decoupled system analysis and control law design.

Pole placement was used for the roll control system with the rudder coupling analysed as a disturbance input. The directional control system was split into an inner stability augmentation part and outer acceleration regulation part. This split in the design was motivated by the far more harsh NMP zero frequency constraint that is typically found in the directional dynamics. NNNT variants of the roll rate and lateral specific acceleration controllers were also presented

as elegant solutions to the variable pole placement problem. All controllers were presented as closed form parameterised solutions to allow them to be readily applied to different aircraft.

Chapter 6

Outer Loop Guidance Controllers

With the inner loop controllers designed, the aircraft can now be viewed as a point mass under the influence of axial, lateral and normal specific accelerations and an inertially fixed gravitational acceleration. The attitude of the wind axis system determines the direction of application of the wind axes specific acceleration coordinates in inertial space. The roll rate inner loop controller provides the means with which to rotate this axis system about its axial unit vector i.e. the velocity vector.

This chapter focuses on developing a guidance level controller to steer the aircraft through inertial space. The guidance controller commands the inner loop specific acceleration and roll rate controllers (virtual actuators) and consequently is abstracted from the details of the specific aircraft being controlled. The chapter begins in section 6.1 with a rigorous investigation of the guidance level dynamics. The section introduces the concept of a feasible reference trajectory and develops the guidance error dynamics. In section 6.2, a number of possible guidance level control strategies are briefly discussed. The strategies typically trade computational complexity for accuracy of guidance control. In section 6.3, one particular guidance controller discussed in section 6.2 is developed in detail. This novel controller has the advantage that it provides an intuitive, closed form, computationally efficient guidance control solution that is practically applicable to a large class of aircraft.

6.1 Investigation of the guidance level dynamics

The guidance level dynamics are the point mass kinematics of equations (2.46) to (2.50) together with four possible first order lag abstraction models for the virtual actuator signals regulated by the inner loop controllers. These dynamics are summarised below for convenience,

Point mass kinematics:

$$\begin{bmatrix} \dot{e}_{11}^{WI} & \dot{e}_{12}^{WI} & \dot{e}_{13}^{WI} \\ \dot{e}_{21}^{WI} & \dot{e}_{22}^{WI} & \dot{e}_{23}^{WI} \\ \dot{e}_{31}^{WI} & \dot{e}_{32}^{WI} & \dot{e}_{33}^{WI} \end{bmatrix} = - \begin{bmatrix} 0 & -R_W & Q_W \\ R_W & 0 & -P_W \\ -Q_W & P_W & 0 \end{bmatrix} \begin{bmatrix} e_{11}^{WI} & e_{12}^{WI} & e_{13}^{WI} \\ e_{21}^{WI} & e_{22}^{WI} & e_{23}^{WI} \\ e_{31}^{WI} & e_{32}^{WI} & e_{33}^{WI} \end{bmatrix} \quad (6.1)$$

$$\begin{bmatrix} \dot{\bar{V}} \end{bmatrix} = \begin{bmatrix} g_w^x \end{bmatrix} + \begin{bmatrix} A_w \end{bmatrix} \quad (6.2)$$

$$\begin{bmatrix} \dot{P}_x \\ \dot{P}_y \\ \dot{P}_z \end{bmatrix} = \begin{bmatrix} e_{11}^{WI} \\ e_{12}^{WI} \\ e_{13}^{WI} \end{bmatrix} \bar{V} \quad (6.3)$$

with,

$$\begin{bmatrix} Q_w \\ R_w \end{bmatrix} = \frac{1}{\bar{V}} \begin{bmatrix} -g_w^z \\ g_w^y \end{bmatrix} + \frac{1}{\bar{V}} \begin{bmatrix} -C_w \\ B_w \end{bmatrix} \quad (6.4)$$

$$\begin{bmatrix} g_w^x \\ g_w^y \\ g_w^z \end{bmatrix} = \begin{bmatrix} e_{13}^{WI} \\ e_{23}^{WI} \\ e_{33}^{WI} \end{bmatrix} g \quad (6.5)$$

and potential virtual actuator lag models,

$$\dot{P}_w = -\frac{1}{\tau_p} P_w + \frac{1}{\tau_p} P_{w_c} \quad (6.6)$$

$$\dot{A}_w = -\frac{1}{\tau_A} A_w + \frac{1}{\tau_A} A_{w_c} \quad (6.7)$$

$$\dot{B}_w = -\frac{1}{\tau_B} B_w + \frac{1}{\tau_B} B_{w_c} \quad (6.8)$$

$$\dot{C}_w = -\frac{1}{\tau_C} C_w + \frac{1}{\tau_C} C_{w_c} \quad (6.9)$$

The objective of the guidance level controller is to regulate the motion of the wind axis system about a feasible reference trajectory. In order to fly coordinated turns, this should be done using only the axial and normal specific acceleration inputs together with the roll rate about the velocity vector. A feasible reference trajectory is one that satisfies the guidance level dynamics above as well as any actuator/state constraints. Note that when all virtual actuator lag dynamics can be ignored then the guidance dynamics are completely kinematic and the reference trajectory need only be *kinematically feasible*.

To incorporate the concept of a reference trajectory into the guidance dynamics, the total position, velocity and acceleration vectors of the aircraft's centre of mass are written as the sum of a reference and error to reference vector as follows,

$$P^{WI} = P^{WR} + P^{RI} \quad (6.10)$$

$$V^{WI} = V^{WR} + V^{RI} \quad (6.11)$$

$$A^{WI} = A^{WR} + A^{RI} \quad (6.12)$$

where the superscript R refers to a reference axis system. Substituting for \mathbf{P}^{WI} , \mathbf{V}^{WI} and \mathbf{A}^{WI} into the kinematic relationships of equations (2.1) and (2.2) gives,

$$\left. \frac{d}{dt} \mathbf{P}^{WR} + \mathbf{P}^{RI} \right|_I = \mathbf{V}^{WR} + \mathbf{V}^{RI} \quad (6.13)$$

$$\left. \frac{d}{dt} \mathbf{V}^{WR} + \mathbf{V}^{RI} \right|_I = \mathbf{A}^{WR} + \mathbf{A}^{RI} \quad (6.14)$$

For the reference trajectory to be feasible it must satisfy the kinematic relationships of equations (A.39) and (A.40), and thus,

$$\left. \frac{d}{dt} \mathbf{P}^{RI} \right|_I = \mathbf{V}^{RI} \quad (6.15)$$

$$\left. \frac{d}{dt} \mathbf{V}^{RI} \right|_I = \mathbf{A}^{RI} \quad (6.16)$$

Combing equations (6.13) to (6.16) gives the position and velocity error dynamics,

$$\left. \frac{d}{dt} \mathbf{P}^{WR} \right|_I = \mathbf{V}^{WR} \quad (6.17)$$

$$\left. \frac{d}{dt} \mathbf{V}^{WR} \right|_I = \mathbf{A}^{WR} \quad (6.18)$$

Further investigation of the total acceleration vector error in equation (6.12) yields the following relationship,

$$\begin{aligned} \mathbf{A}^{WR} &= \mathbf{A}^{WI} - \mathbf{A}^{RI} \\ &= \boldsymbol{\Sigma}^{WI} + \mathbf{G}^{WI} - \boldsymbol{\Sigma}^{RI} - \mathbf{G}^{RI} \\ &= \boldsymbol{\Sigma}^{WI} - \boldsymbol{\Sigma}^{RI} \\ &= \boldsymbol{\Sigma}^{WR} \end{aligned} \quad (6.19)$$

where use of equations (2.40) and (2.3) has been made as well as the fact that the gravitational acceleration vector is inertially fixed and invariant with position i.e. a uniform gravitational field. In words, equation (6.19) states that the total acceleration of the wind axis system with respect to the reference axis system is equal to the specific acceleration of the wind axis system with respect to the reference axis system. Thus, equation (6.18) can be rewritten as follows,

$$\left. \frac{d}{dt} \mathbf{V}^{WR} \right|_I = \boldsymbol{\Sigma}^{WR} \quad (6.20)$$

To express the attitude error between the wind and reference axis systems, a number of techniques can be employed. One method would be to continue in the same manner as above

and write the unit vectors of the wind axis system as the vector sum of the respective unit vectors of the reference axis system and error vectors as follows,

$$\mathbf{i}^W = \mathbf{i}^{WR} + \mathbf{i}^R \quad (6.21)$$

$$\mathbf{j}^W = \mathbf{j}^{WR} + \mathbf{j}^R \quad (6.22)$$

$$\mathbf{k}^W = \mathbf{k}^{WR} + \mathbf{k}^R \quad (6.23)$$

Then the wind axis system attitude dynamics become,

$$\left. \frac{d}{dt} \begin{bmatrix} \mathbf{i}^{WR} + \mathbf{i}^R & \mathbf{j}^{WR} + \mathbf{j}^R & \mathbf{k}^{WR} + \mathbf{k}^R \end{bmatrix} \right|_I = \boldsymbol{\omega}^{WI} \times \begin{bmatrix} \mathbf{i}^{WR} + \mathbf{i}^R & \mathbf{j}^{WR} + \mathbf{j}^R & \mathbf{k}^{WR} + \mathbf{k}^R \end{bmatrix} \quad (6.24)$$

The angular velocity of the wind axis system with respect to inertial space can be written as the sum of the angular velocity of the reference axis system with respect to inertial space and the angular velocity of the wind axis system with respect to the reference axis system as follows,

$$\boldsymbol{\omega}^{WI} = \boldsymbol{\omega}^{WR} + \boldsymbol{\omega}^{RI} \quad (6.25)$$

Substituting this into equation (6.24) and noting that for the reference trajectory to be feasible its unit vectors must also satisfy the attitude dynamics of equation (A.41) as follows,

$$\left. \frac{d}{dt} \begin{bmatrix} \mathbf{i}^R & \mathbf{j}^R & \mathbf{k}^R \end{bmatrix} \right|_I = \boldsymbol{\omega}^{RI} \times \begin{bmatrix} \mathbf{i}^R & \mathbf{j}^R & \mathbf{k}^R \end{bmatrix} \quad (6.26)$$

then the wind axis system attitude dynamics of equation (6.24) reduce to the attitude error vector dynamics below,

$$\left. \frac{d}{dt} \begin{bmatrix} \mathbf{i}^{WR} & \mathbf{j}^{WR} & \mathbf{k}^{WR} \end{bmatrix} \right|_I = \boldsymbol{\omega}^{WR} \times \begin{bmatrix} \mathbf{i}^{WR} + \mathbf{i}^R & \mathbf{j}^{WR} + \mathbf{j}^R & \mathbf{k}^{WR} + \mathbf{k}^R \end{bmatrix} + \boldsymbol{\omega}^{RI} \times \begin{bmatrix} \mathbf{i}^{WR} & \mathbf{j}^{WR} & \mathbf{k}^{WR} \end{bmatrix} \quad (6.27)$$

Rewriting the vector derivative in the above equation so that the error vector dynamics are taken with respect to the reference axis system yields the final error vector dynamics,

$$\begin{aligned} \left. \frac{d}{dt} \begin{bmatrix} \mathbf{i}^{WR} & \mathbf{j}^{WR} & \mathbf{k}^{WR} \end{bmatrix} \right|_R &= \boldsymbol{\omega}^{WR} \times \begin{bmatrix} \mathbf{i}^{WR} + \mathbf{i}^R & \mathbf{j}^{WR} + \mathbf{j}^R & \mathbf{k}^{WR} + \mathbf{k}^R \end{bmatrix} \\ &= \boldsymbol{\omega}^{WR} \times \begin{bmatrix} \mathbf{i}^{WR} & \mathbf{j}^{WR} & \mathbf{k}^{WR} \end{bmatrix} + \boldsymbol{\omega}^{WR} \times \begin{bmatrix} \mathbf{i}^R & \mathbf{j}^R & \mathbf{k}^R \end{bmatrix} \end{aligned} \quad (6.28)$$

A second method of describing the wind axis system attitude via the reference axis system is to maintain the attitude of the reference axis system with respect to inertial space and then to maintain the attitude of the wind axis system with respect to the reference axes. The attitude dynamics of the wind axis system with respect to the reference axis system are by definition,

$$\left. \frac{d}{dt} \begin{bmatrix} \mathbf{i}^w & \mathbf{j}^w & \mathbf{k}^w \end{bmatrix} \right|_R = \boldsymbol{\omega}^{wR} \times \begin{bmatrix} \mathbf{i}^w & \mathbf{j}^w & \mathbf{k}^w \end{bmatrix} \quad (6.29)$$

where the angular velocity of the wind axis system with respect to the reference axis system can be obtained from equation (6.25).

Although both attitude description methods described are equally valid, the *attitude difference* method described first displays a few complications and tends to provide a less intuitive solution compared to the *relative attitude* method described second. To see this, first consider that the attitude error vectors used in the attitude difference method can be orientated in any direction with respect to the reference axis system (even for very small attitude errors). Thus, more complicated non-singular attitude parameterisations would need to be used to maintain both the gross attitude (through the reference axis system) and the attitude error. On the other hand, when the guidance controllers are operating properly the relative attitude of the wind axis system with respect to the reference axis system will be small. Thus the relative attitude method allows for simple parameterisations with singularities to be used to describe the attitude of the wind axis system with respect to the reference axis system without penalty. A more complicated non-singular attitude parameterisation could instead be used for describing the reference axis system attitude which could potentially move through all attitudes with respect to inertial space.

A second motivation for the relative attitude description (that is linked to the first) arises when the perturbations between the wind and reference axis systems are assumed small and the error dynamics are linearised about the reference trajectory for control system design purposes. In this case, both attitude description techniques result in attitude error dynamics that break down at some attitudes when the attitude is parameterised by a set of parameters that involve a ‘background’ constraint e.g. quaternions with their normalisation constraint and generalised DCM parameters with their normalisation and orthogonality constraints. To see this for the DCM parameter case, consider that for small perturbations, the attitude difference and relative attitude dynamics of equations (6.28) and (6.29) would reduce to,

$$\left. \frac{d}{dt} \begin{bmatrix} \Delta \mathbf{i}^{wR} & \Delta \mathbf{j}^{wR} & \Delta \mathbf{k}^{wR} \end{bmatrix} \right|_R = \Delta \boldsymbol{\omega}^{wR} \times \begin{bmatrix} \mathbf{i}^R & \mathbf{j}^R & \mathbf{k}^R \end{bmatrix} \quad (6.30)$$

$$\left. \frac{d}{dt} \begin{bmatrix} \Delta \mathbf{i}^w & \Delta \mathbf{j}^w & \Delta \mathbf{k}^w \end{bmatrix} \right|_R = \Delta \boldsymbol{\omega}^{wR} \times \begin{bmatrix} \mathbf{i}^w & \mathbf{j}^w & \mathbf{k}^w \end{bmatrix} \quad (6.31)$$

respectively, where the symbol Δ has been used to denote a small perturbation in the vectors. Note that the first term of equation (6.28) has completely disappeared in the linearisation process since it was essentially a product of two sets of small perturbations. At certain reference attitudes, the cross products on the right hand side of equations (6.30) and (6.31) will yield zero. For example, when the wind, reference and inertial axis systems are all aligned,

then the three main diagonal elements on the right hand side of equations (6.30) and (6.31) will all be exactly zero. Thus, if general DCM parameters are used in each case, the three main diagonal attitude parameters will appear as uncontrollable open loop integrators in the linearised guidance dynamics. If a guidance controller architecture involving online pole placement or optimal control system synthesis was used then this problem would cause singularities in the online solution. Of course, these singularities are only as a result of the linearisation process and the attitude parameterisation used. The nonlinear system in actual fact remains completely controllable through the background constraint equations that the linear controllers ignore.

The arguments of the previous paragraph show that both attitude description methods can break down when linearised using constraint based attitude parameterisations. However, as discussed in the first point on motivating the relative attitude description, for small attitude errors, the attitude of the wind axis system with respect to the reference axis system can be parameterised using a simple singular parameterisation such as Euler 3-2-1 angles without penalty. The Euler parameterisations do not have background constraints and can be shown to linearise without resulting in seemingly uncontrollable states. Although interesting singularity switching methods could be used to allow different sets of Euler angles to parameterise the attitude difference dynamics, the relative attitude method provides a mathematically sound, intuitive approach with no extra logic required. For this reason it will be used in the remaining analysis of this section.

Finally, if virtual actuator lag dynamics are present then the reference trajectory will also include the lag states as part of the trajectory. With reference to equations (6.6) to (6.9), the lag states can be written as the sum of reference and perturbation states as follows,

$$P_W = P_{W_E} + P_{W_R} \quad (6.32)$$

$$A_W = A_{W_E} + A_{W_R} \quad (6.33)$$

$$B_W = B_{W_E} + B_{W_R} \quad (6.34)$$

$$C_W = C_{W_E} + C_{W_R} \quad (6.35)$$

where the subscript R denotes a reference variable and the subscript E denotes a perturbation variable. The full command inputs can also be written as the sum of reference and perturbation command inputs as follows,

$$P_{W_C} = P_{W_{C_E}} + P_{W_{C_R}} \quad (6.36)$$

$$A_{W_C} = A_{W_{C_E}} + A_{W_{C_R}} \quad (6.37)$$

$$B_{W_C} = B_{W_{C_E}} + B_{W_{C_R}} \quad (6.38)$$

$$C_{W_c} = C_{W_{cE}} + C_{W_{cR}} \quad (6.39)$$

where the subscripts used have the same meaning as described above. Then, substituting equations (6.32) to (6.39) into the actuator lag dynamics of equations (6.6) to (6.9) and noting that for the reference trajectory to be feasible,

$$\dot{P}_{W_R} = -\frac{1}{\tau_P} P_{W_R} + \frac{1}{\tau_P} P_{W_{cR}} \quad (6.40)$$

$$\dot{A}_{W_R} = -\frac{1}{\tau_A} A_{W_R} + \frac{1}{\tau_A} A_{W_{cR}} \quad (6.41)$$

$$\dot{B}_{W_R} = -\frac{1}{\tau_B} B_{W_R} + \frac{1}{\tau_B} B_{W_{cR}} \quad (6.42)$$

$$\dot{C}_{W_R} = -\frac{1}{\tau_C} C_{W_R} + \frac{1}{\tau_C} C_{W_{cR}} \quad (6.43)$$

then the error dynamics become,

$$\dot{P}_{W_E} = -\frac{1}{\tau_P} P_{W_E} + \frac{1}{\tau_P} P_{W_{cE}} \quad (6.44)$$

$$\dot{A}_{W_E} = -\frac{1}{\tau_A} A_{W_E} + \frac{1}{\tau_A} A_{W_{cE}} \quad (6.45)$$

$$\dot{B}_{W_E} = -\frac{1}{\tau_B} B_{W_E} + \frac{1}{\tau_B} B_{W_{cE}} \quad (6.46)$$

$$\dot{C}_{W_E} = -\frac{1}{\tau_C} C_{W_E} + \frac{1}{\tau_C} C_{W_{cE}} \quad (6.47)$$

With all of the error dynamics derived they can now be summarised concisely. Firstly, the vector derivatives of equations (6.17) and (6.20) are converted such that they are taken with respect to the reference axis system. The vectors in these two equations are then coordinated into reference axes to give the coordinate vector dynamics below,

$$\dot{\mathbf{P}}_R^{\text{WR}} = \mathbf{V}_R^{\text{WR}} - \mathbf{S}_{\omega_R^{\text{RI}}} \mathbf{P}_R^{\text{WR}} \quad (6.48)$$

$$\dot{\mathbf{V}}_R^{\text{WR}} = \mathbf{\Sigma}_R^{\text{WR}} - \mathbf{S}_{\omega_R^{\text{RI}}} \mathbf{V}_R^{\text{WR}} \quad (6.49)$$

with,

$$\mathbf{\Sigma}_R^{\text{WR}} = [\mathbf{DCM}^{\text{WR}}]^T \mathbf{\Sigma}_W^{\text{WI}} - \mathbf{\Sigma}_R^{\text{RI}} \quad (6.50)$$

With reference to Appendix A, coordinating all of the vectors of the relative attitude dynamics of equation (6.29) into reference axes gives,

$$\frac{d}{dt}[\mathbf{DCM}^{WR}] = -\mathbf{S}_{\omega_W^{WR}}[\mathbf{DCM}^{WR}] \quad (6.51)$$

with,

$$\omega_W^{WR} = \omega_W^{WI} - [\mathbf{DCM}^{WR}] \omega_R^{RI} \quad (6.52)$$

Expanding the coordinate vector guidance error dynamics of equations (6.48) to (6.52) and combining these with the optional actuator lag error dynamics of equations (6.44) to (6.47), the guidance error dynamics can be written as follows,

$$\begin{bmatrix} \dot{P}_x^{WR} \\ \dot{P}_y^{WR} \\ \dot{P}_z^{WR} \end{bmatrix} = \begin{bmatrix} V_x^{WR} \\ V_y^{WR} \\ V_z^{WR} \end{bmatrix} - \begin{bmatrix} 0 & -R_R & Q_R \\ R_R & 0 & -P_R \\ -Q_R & P_R & 0 \end{bmatrix} \begin{bmatrix} P_x^{WR} \\ P_y^{WR} \\ P_z^{WR} \end{bmatrix} \quad (6.53)$$

$$\begin{bmatrix} \dot{V}_x^{WR} \\ \dot{V}_y^{WR} \\ \dot{V}_z^{WR} \end{bmatrix} = \begin{bmatrix} A_x^{WR} \\ A_y^{WR} \\ A_z^{WR} \end{bmatrix} - \begin{bmatrix} 0 & -R_R & Q_R \\ R_R & 0 & -P_R \\ -Q_R & P_R & 0 \end{bmatrix} \begin{bmatrix} V_x^{WR} \\ V_y^{WR} \\ V_z^{WR} \end{bmatrix} \quad (6.54)$$

$$\begin{bmatrix} \dot{e}_{11}^{WR} & \dot{e}_{12}^{WR} & \dot{e}_{13}^{WR} \\ \dot{e}_{21}^{WR} & \dot{e}_{22}^{WR} & \dot{e}_{23}^{WR} \\ \dot{e}_{31}^{WR} & \dot{e}_{32}^{WR} & \dot{e}_{33}^{WR} \end{bmatrix} = - \begin{bmatrix} 0 & -R_W^{WR} & Q_W^{WR} \\ R_W^{WR} & 0 & -P_W^{WR} \\ -Q_W^{WR} & P_W^{WR} & 0 \end{bmatrix} \begin{bmatrix} e_{11}^{WR} & e_{12}^{WR} & e_{13}^{WR} \\ e_{21}^{WR} & e_{22}^{WR} & e_{23}^{WR} \\ e_{31}^{WR} & e_{32}^{WR} & e_{33}^{WR} \end{bmatrix} \quad (6.55)$$

with,

$$\begin{bmatrix} A_x^{WR} \\ A_y^{WR} \\ A_z^{WR} \end{bmatrix} = \begin{bmatrix} e_{11}^{WR} & e_{12}^{WR} & e_{13}^{WR} \\ e_{21}^{WR} & e_{22}^{WR} & e_{23}^{WR} \\ e_{31}^{WR} & e_{32}^{WR} & e_{33}^{WR} \end{bmatrix}^T \begin{bmatrix} A_W \\ B_W \\ C_W \end{bmatrix} - \begin{bmatrix} A_R \\ B_R \\ C_R \end{bmatrix} \quad (6.56)$$

$$\begin{bmatrix} P_W^{WR} \\ Q_W^{WR} \\ R_W^{WR} \end{bmatrix} = \begin{bmatrix} P_W \\ Q_W \\ R_W \end{bmatrix} - \begin{bmatrix} e_{11}^{WR} & e_{12}^{WR} & e_{13}^{WR} \\ e_{21}^{WR} & e_{22}^{WR} & e_{23}^{WR} \\ e_{31}^{WR} & e_{32}^{WR} & e_{33}^{WR} \end{bmatrix} \begin{bmatrix} P_R \\ Q_R \\ R_R \end{bmatrix} \quad (6.57)$$

$$\begin{bmatrix} Q_W \\ R_W \end{bmatrix} = \frac{\begin{bmatrix} -e_{31}^{WR} e_{13}^{RI} - e_{32}^{WR} e_{23}^{RI} - e_{33}^{WR} e_{33}^{RI} \\ e_{21}^{WR} e_{13}^{RI} + e_{22}^{WR} e_{23}^{RI} + e_{23}^{WR} e_{33}^{RI} \end{bmatrix} \mathbf{g} + \begin{bmatrix} -C_W \\ B_W \end{bmatrix}}{(\bar{V}_R + V_x^{WR}) e_{11}^{WR} + V_y^{WR} e_{12}^{WR} + V_z^{WR} e_{13}^{WR}} \quad (6.58)$$

and,

$$\dot{P}_{W_E} = -\frac{1}{\tau_P} P_{W_E} + \frac{1}{\tau_P} P_{W_{C_E}} \quad (6.59)$$

$$\dot{A}_{W_E} = -\frac{1}{\tau_A} A_{W_E} + \frac{1}{\tau_A} A_{W_{C_E}} \quad (6.60)$$

$$\dot{B}_{w_E} = -\frac{1}{\tau_B} B_{w_E} + \frac{1}{\tau_B} B_{w_{CE}} \quad (6.61)$$

$$\dot{C}_{w_E} = -\frac{1}{\tau_C} C_{w_E} + \frac{1}{\tau_C} C_{w_{CE}} \quad (6.62)$$

where the definition of the coordinates used is straightforward to obtain from the coordinate vector equations of (6.48) to (6.52). Finally, note that the guidance error dynamics together with the reference trajectory dynamics are equivalent to original guidance dynamics of equations (6.1) to (6.9).

6.2 Guidance controller design strategies

The previous section investigated the guidance level dynamics. The notion of a feasible reference trajectory was introduced and the guidance dynamics were adapted to become guidance error dynamics. The objective of the guidance control system can now be modified to that of driving the guidance error states to zero with the desired dynamic response. Before continuing note that due to the largely kinematic nature of the guidance dynamics they contain very little uncertainty. The only uncertainty that exists is that associated with the virtual control inputs and their lags and that of the gravitational model. The gravitational model typically has very little uncertainty. Furthermore, it is one of the primary purposes of the inner loop controllers to ensure robust, predictable closed loop responses of the virtual control inputs and in so doing encapsulate any uncertainty before it leaks into the guidance dynamics.

In this section three possible guidance control strategies are presented. Each strategy is discussed briefly in a purely qualitative fashion. The purpose of discussing a number of strategies is to sensitise the designer to the multitude of guidance level control strategies available within the manoeuvre autopilot architecture. Depending on the specific aircraft, mission profile and level of computational power available different guidance strategies can be adopted. In the following section, one of the guidance controllers discussed below is designed in detail.

6.2.1 Receding horizon predictive control

One possible strategy for regulating the guidance error dynamics is to employ RHPC [34-36]. This computationally intensive strategy allows the full nonlinear guidance error dynamics to be taken into account as well as any state and/or actuator constraints.

The RHPC strategy involves solving a finite horizon optimal control problem at each sample instance of the controller. At a specific sample instance, the controller would seek to find the control input signal over the finite horizon that would result in optimal convergence of the guidance error state vector to the origin. To mathematically quantify the optimal solution, a cost function involving the state and control signals would typically be used. The RHPC

strategy then uses only the initial portion of the optimal control solution before completely recalculating a new optimal convergence solution at some later stage. This new optimal solution would begin from the aircraft's measured/estimated state and so incorporate feedback into the control solution.

Although RHPC would arguably result in the most accurate guidance level controller, the computational burden of recalculating an optimal control solution to a nonlinear dynamics problem at each guidance control iteration would in most cases make its implementation impractical [13,36]. The control strategies presented in the following subsections will typically require far less computational power than that required by RHPC for a relatively small performance penalty.

6.2.2 Linearisation and successive linearisation control

When the guidance controller is functioning properly, the deviations of the wind axis system from the reference axis system should be small. Thus, for guidance controller design purposes, the nonlinear guidance error dynamics are well approximated by linearised guidance error dynamics about the reference trajectory. By constantly linearising about the reference trajectory, the Nonlinear Time Invariant (NTI) guidance control problem is converted to a Linear Time Varying (LTV) control problem. This is beneficial because far more formal methods exist for solving LTV problems than for NTI problems. Note it is here that it is important for the relative attitude description technique to be used in deriving the guidance attitude error dynamics of equation (6.51). This attitude description technique makes it feasible to use Euler angles, which linearise well, to parameterise the attitude of the wind axis system with respect to the reference axis system.

With the guidance control problem reduced to a LTV regulation problem any appropriate LTV control strategy can be applied. Linear RHPC is one such strategy [45]. Another strategy is to constantly update the guidance feedback gains such that the closed loop poles of the LTV system remain invariant over time (although stability still needs to be investigated explicitly in this case since fixed pole placement is not a sufficient condition for stability of a LTV system [26]). A further strategy similar in nature to the preceding one is to design a Linear Quadratic Regulator (LQR) at each controller iteration. Finally, depending on the type of reference trajectory, the LTV dynamics may become Linear Time Invariant (LTI) e.g. during straight and level flight or a constant turn. With LTI dynamics, a constant feedback gain controller can be designed offline to solve the guidance control problem for a specific type of reference trajectory. These reference trajectory 'building blocks' can then be strung together to allow for full 3D manoeuvre guidance.

Employing any of the above strategies is expected to result in a guidance controller that performs adequately. Successively linearising and designing an appropriate controller online at each guidance controller iteration can become computationally intensive. However, a fair

amount of the computational burden can be alleviated if as much as possible of the linearisation and controller design is done symbolically offline.

6.2.3 Specific acceleration matching

The design of all of the previously suggested guidance controllers is complicated by the fact that if turn coordination is desired then guidance accelerations can only be commanded in the plane instantaneously spanned by the i'' and k'' unit vectors. Thus, in order to reduce any lateral error between the wind and reference axis systems, the aircraft is required to roll the plane of acceleration via the roll rate command input. Consequently, the wind axis system attitude dynamics form an integral part of the guidance dynamics.

Most aircraft however can roll to a specific bank angle very quickly. This is due to their typically low roll moment of inertia (relative to the other axes) and the large moment arm to the ailerons. If it is assumed that the time taken to roll to a specific bank angle is negligible in comparison to the time constants involved in the guidance level dynamics then the aircraft can be thought of as being capable of directing its specific acceleration vector instantaneously in three dimensional space. If it is further assumed that the axial and normal specific acceleration magnitudes are regulated by the inner loop controllers at bandwidths much greater than those involved in the guidance dynamics, then both the magnitude and direction of the aircraft's specific acceleration vector in three dimensional space can be controlled instantaneously.

Being able to instantaneously command the total specific acceleration vector in three dimensional space provides great potential for simplifying the guidance controller. It allows the aircraft to simply be viewed as a point mass, moving in inertial space under the influence of an instantaneously commandable specific acceleration vector. The guidance controller can thus operate using inertially coordinated vectors to generate the commanded specific acceleration coordinate vector in inertial axes. The aircraft then matches the desired specific acceleration immediately (relative to the position and velocity guidance bandwidths) by rolling to the correct angle and setting the axial and normal specific acceleration magnitudes appropriately.

In the following section, a detailed design of the novel Specific Acceleration Matching (SAM) guidance controller is carried out. This guidance strategy yields a simple, closed form solution controller that is practically applicable to a large class of aircraft. Furthermore, it requires very little computing power and is capable of guiding an aircraft through the full kinematic flight envelope.

6.3 Specific acceleration matching controller design

The design of a guidance controller that orientates the aircraft to allow matching of the desired specific acceleration vector is carried out in this section. Critical to the design of this controller are the two assumptions listed below,

- The aircraft can direct its wind axis system normal unit vector in the plane perpendicular to the velocity vector at bandwidths much greater than those associated with the velocity and position dynamics.
- The inner loop axial and normal specific acceleration controllers can regulate their respective accelerations at bandwidths much greater than those associated with the velocity and position dynamics.

The first assumption essentially implies that the aircraft is capable of rolling to any ‘bank angle’ (although this is not strictly the correct term) in a negligibly small amount of time relative to the time constants involved with the point mass velocity and position dynamics. A frequency separation factor of approximately five between the respective controllers should be sufficient to ensure the timescale separation required. For a large class of aircraft, this assumption can be made to hold since aircraft roll dynamics are typically very fast.

The second assumption implies that a timescale separation must exist between the regulated axial and normal specific acceleration dynamics and the regulated point mass velocity and position dynamics. Again a frequency separation factor of approximately five is typically sufficient. For most aircraft, the required timescale separation between the normal specific acceleration dynamics and the velocity and position dynamics can be made to hold. The timescale separation between the axial specific acceleration dynamics and the velocity and position dynamics on the other hand can be problematic. This is because the thrust actuator is most often significantly band-limited which in turn limits the practically achievable upper bandwidth of the axial specific acceleration controller. Thus, in all likelihood it is this timescale separation that will start to clip the maximum allowable velocity and position dynamics bandwidth if the SAM guidance controller is to be used.

Methods of circumventing this problem do exist and will be the subject of future research as outlined in section 9.3. Briefly, the method of handling the problem involves using the axial specific acceleration to control only the velocity magnitude based on the dynamics of equation (2.47) and a combined dynamic inversion and pole placement control law. Two-dimensional cross track guidance is then achieved using specific acceleration matching with the remaining roll rate and normal specific acceleration actuators, where the timescale separation arguments hold well. This variation on the SAM control law also provides the opportunity for position based guidance (guidance errors determined as a function of the aircraft’s current position relative to the reference trajectory) as opposed to the time based guidance (guidance error determined by where the aircraft should be on the reference trajectory at a particular time) inherent in the control law to be introduced in this section. However, the control law in this section provides a good platform for the development of future guidance control laws and in a large number of cases will be practically feasible as seen in the examples of Chapter 8.

With the two assumptions listed above in place the aircraft can be seen as capable of

immediately directing its specific acceleration vector in any direction in inertial space. To see this, consider that with no assumptions, the aircraft's specific acceleration vector is constrained to lying in the wind axis system XZ-plane (for coordinated turns). With the second assumption in place, the specific acceleration vector can be commanded infinitely fast (relative to the velocity and position dynamics) but is still constrained to the wind axis system XZ-plane. However, when the first assumption is added it implies that the XZ-plane can rotate about the wind axis system axial unit vector to any angle immediately (again relative to the velocity and position dynamics). With immediate rotation of the XZ-plane, it is clear that the specific acceleration vector can instantaneously be directed in any direction in inertial space.

The above concept is critical to the simplicity of the SAM guidance controller. This is because it allows the controller to view the aircraft as a point mass moving in an inertial reference frame under the influence of an invariant gravity bias vector and the control of an instantaneously commandable three dimensional specific acceleration vector. The velocity and position controllers can thus be designed using inertially coordinated vectors which in turn results in linear, decoupled dynamics. Under the two assumptions stated at the beginning of this section, the commanded inertially coordinated specific acceleration vector is then simply transformed to axial and normal specific acceleration commands together with a normal specific acceleration direction command. An inner normal specific acceleration direction controller is then responsible for rolling the XZ-plane such that the desired specific acceleration can be realised. With this guidance controller architecture, the velocity and position controllers have no concern for the attitude of the aircraft (attitude of the wind axis system). The wind axis system attitude command results merely as a by-product of the commanded specific acceleration and velocity vector direction. This in turn greatly simplifies reference trajectory generation since no attitude dynamics need be satisfied by the reference trajectory. Reference trajectory generation will be the topic of Chapter 7.

Subsections 6.3.1 to 6.3.3 discuss the three parts of the SAM guidance controller. In subsection 6.3.1, a normal specific acceleration vector direction controller is designed. This controller is responsible for steering the wind axis system normal unit vector in the plane perpendicular to the velocity vector i.e. perpendicular to the wind axis system axial unit vector. Although the final control law for this part of the controller is nonlinear, it will be seen that the core of the controller is a proportional feedback control law operating on a purely linear plant. Once this controller has been designed, subsection 6.3.2 develops a specific acceleration transformation algorithm. This algorithm is used to transform the coordinates of a desired specific acceleration vector in inertial axes to axial and normal specific acceleration commands in wind axes together with a normal specific acceleration direction command. Finally in subsection 6.3.3, outer velocity and position controllers are designed using inertially coordinated vectors with the specific acceleration coordinate vector as a virtual control input.

6.3.1 Normal specific acceleration vector direction controller

The normal specific acceleration vector direction controller is responsible for steering the wind axis system normal unit vector \mathbf{k}^W in the plane perpendicular to the velocity vector i.e. normal to the wind axis system axial unit vector \mathbf{i}^W . To this end, define the commanded wind axis system normal unit vector \mathbf{k}^{Wc} . For this command vector to always remain in the plane perpendicular to \mathbf{i}^W the following constraint relationship must hold,

$$\mathbf{k}^{Wc} \cdot \mathbf{i}^W = 0 \quad (6.63)$$

There are a number of ways to quantify the error between the commanded and actual wind axis system normal unit vectors. One particularly simple way is to use the angle between the two vectors. Define the *error angle* ϕ as the angle between \mathbf{k}^W and \mathbf{k}^{Wc} when \mathbf{k}^W is rotated positively about \mathbf{i}^W . Note that the error angle is not in general equivalent to the commonly used bank/roll angle. The task is now reduced to designing a control system that drives the error angle to zero over time. As such, the normal specific acceleration vector direction controller will equivalently be referred to as the *error angle controller* in this document.

Investigating the error angle dynamics, a relationship between the error angle and the commanded and actual wind axis system normal unit vectors can be obtained through the dot product operator as follows,

$$\mathbf{k}^{Wc} \cdot \mathbf{k}^W = |\mathbf{k}^{Wc}| |\mathbf{k}^W| \cos \phi = \cos \phi \quad (6.64)$$

Taking the time derivative of the scalar quantities on both side of equation (6.64) gives,

$$\frac{d}{dt} \cos \phi = \frac{d}{dt} (\mathbf{k}^{Wc} \cdot \mathbf{k}^W) \quad (6.65)$$

Expanding the right hand side and noting that the derivative of a scalar quantity can be taken with respect to an axis system of choice yields,

$$\begin{aligned} \frac{d}{dt} \cos \phi &= \left. \frac{d}{dt} \mathbf{k}^{Wc} \right|_W \cdot \mathbf{k}^W + \mathbf{k}^{Wc} \cdot \left. \frac{d}{dt} \mathbf{k}^W \right|_W \\ &= \left(\left. \frac{d}{dt} \mathbf{k}^{Wc} \right|_{W_c} + \boldsymbol{\omega}^{W_c W} \times \mathbf{k}^{Wc} \right) \cdot \mathbf{k}^W \\ &= (\boldsymbol{\omega}^{W_c W} \times \mathbf{k}^{Wc}) \cdot \mathbf{k}^W \end{aligned} \quad (6.66)$$

where the derivatives have been taken with respect to wind axes to simplify the mathematics involved. The axis system W_c has been used in equation (6.66). This right handed orthogonal axis system is defined with its axial unit vector coinciding with \mathbf{i}^W and its normal unit vector coinciding with \mathbf{k}^{Wc} . Returning to the constraint of equation (6.63) and noting that for this constraint to hold for all time its first time derivative must also be zero. Thus,

$$\begin{aligned}
\frac{d}{dt}(\mathbf{i}^w \cdot \mathbf{k}^{w_c}) &= 0 \\
&= \left. \frac{d}{dt} \mathbf{i}^w \right|_w \cdot \mathbf{k}^{w_c} + \mathbf{i}^w \cdot \left. \frac{d}{dt} \mathbf{k}^{w_c} \right|_w \\
&= \mathbf{i}^w \cdot \left. \frac{d}{dt} \mathbf{k}^{w_c} \right|_w \\
&= \mathbf{i}^w \cdot (\boldsymbol{\omega}^{w_c w} \times \mathbf{k}^{w_c})
\end{aligned} \tag{6.67}$$

The above equation implies that the cross product in parenthesis must lie in the plane perpendicular to \mathbf{i}^w . Since \mathbf{k}^{w_c} already lies in this plane, the only way the result of the cross product can remain in the plane is if $\boldsymbol{\omega}^{w_c w}$ only has a component in the \mathbf{i}^w direction. This result makes intuitive sense. Writing $\boldsymbol{\omega}^{w_c w}$ as follows,

$$\begin{aligned}
\boldsymbol{\omega}^{w_c w} &= \boldsymbol{\omega}^{w_c I} - \boldsymbol{\omega}^{w I} \\
&= (P_{w_c} - P_w) \mathbf{i}^w
\end{aligned} \tag{6.68}$$

where P_{w_c} is the roll rate of the commanded normal specific acceleration unit vector. Substituting the result into equation (6.66) gives,

$$\begin{aligned}
\frac{d}{dt} \cos \phi &= ((P_{w_c} - P_w) \mathbf{i}^w \times \mathbf{k}^{w_c}) \cdot \mathbf{k}^w \\
&= -(P_{w_c} - P_w) \mathbf{j}^{w_c} \cdot \mathbf{k}^w \\
&= -(P_{w_c} - P_w) \cos(\pi/2 - \phi)
\end{aligned} \tag{6.69}$$

Simplifying the left and right hand sides of equation (6.69) yields,

$$-\dot{\phi} \sin \phi = -(P_{w_c} - P_w) \sin \phi \tag{6.70}$$

and so,

$$\dot{\phi} = (P_{w_c} - P_w) \frac{\sin \phi}{\sin \phi} \tag{6.71}$$

For those values of ϕ equal to $n\pi$ where $n \in \mathbb{Z}$, L'Hospital's rule can be used to show that the intuitive result below holds for all ϕ ,

$$\dot{\phi} = P_{w_c} - P_w \tag{6.72}$$

The linear dynamics of equation (6.72) are the error angle dynamics. These dynamics are applicable at all attitudes and require only that the constraint of equation (6.63) remains valid at all times. Assume now the following,

- The roll rate about the velocity vector is available to the error angle controller as a zero lag virtual control input.

Although as discussed later in this section this assumption is not required for the design of the error angle regulator, it does result in a simpler, pole placement type control law when valid. Furthermore, since most aircraft have very fast roll rate dynamics, it is a practically feasible assumption. For these reasons, development of an error angle control law valid under the assumption listed above is deemed worthwhile.

The assumption allows the virtual roll rate actuator lag dynamics of equation (6.6) to be ignored in the design of the error angle controller. With roll rate lag dynamics ignored, the closed loop error angle dynamics can be set arbitrarily through a proportional feedback control law. Defining the control law below,

$$P_w = P_{w_c} + K_\phi \phi \quad (6.73)$$

where P_{w_c} acts as a feed-forward term that will be determined by the specific reference trajectory being flown. With the feed-forward term in the control law, the feedback term is simply responsible for regulating the effects of any disturbances to the error angle. Substituting the control law of equation (6.73) into the dynamics of equation (6.72), the closed loop error angle dynamics become,

$$\dot{\phi} + K_\phi \phi = 0 \quad (6.74)$$

with a closed loop pole at,

$$s = -K_\phi \quad (6.75)$$

The feedback gain is determined by selecting an appropriate error angle pole location. The closed loop bandwidth is limited from above through the zero lag virtual actuator assumption. It is also limited from below through the timescale separation assumption to the velocity and position dynamics.

To complete the control law of equation (6.73), the error angle needs to be written in terms of the commanded and actual normal acceleration unit vectors. From equation (6.64) the error angle can be written as,

$$\phi = \cos^{-1}(\mathbf{k}^{w_c} \cdot \mathbf{k}^w) \quad (6.76)$$

However, due to the periodic nature of the cosine function, the arc cosine function is typically set to return an angle in the range $[0, \pi)$. Thus, in equation (6.76) the sign of the error angle is lost. There are a number of ways in which the sign can be regained. The dot product of the \mathbf{k}^{w_c} and \mathbf{j}^w returns,

$$\mathbf{k}^{w_c} \cdot \mathbf{j}^w = \cos(\pi/2 + \phi) = -\sin \phi \quad (6.77)$$

Thus,

$$\operatorname{sgn}(-\mathbf{k}^{w_c} \cdot \mathbf{j}^w) = \operatorname{sgn}(\sin \phi) = \begin{cases} +1 & \phi \in (0, \pi) \\ -1 & \phi \in (-\pi, 0) \\ 0 & \phi = \{-\pi, 0, \pi\} \end{cases} \quad (6.78)$$

Thus combining equations (6.76) and (6.78), a formula for the error angle valid in the range $(-\pi, \pi)$ is,

$$\phi = -\operatorname{sgn}(\mathbf{k}^{w_c} \cdot \mathbf{j}^w) \cos^{-1}(\mathbf{k}^{w_c} \cdot \mathbf{k}^w) \quad (6.79)$$

Another method is to note that,

$$\tan \phi = \frac{\sin \phi}{\cos \phi} = -\frac{\mathbf{k}^{w_c} \cdot \mathbf{j}^w}{\mathbf{k}^{w_c} \cdot \mathbf{k}^w} \quad (6.80)$$

and so,

$$\phi = \tan^{-1}\left(\frac{-\mathbf{k}^{w_c} \cdot \mathbf{j}^w}{\mathbf{k}^{w_c} \cdot \mathbf{k}^w}\right) \quad (6.81)$$

where a four quadrant arc tangent function can be used to yield a correctly signed error angle. Making use of the formula of equation (6.79) to avoid a divide operation, the control law of equation (6.73) becomes,

$$P_w = P_{w_c} - K_\phi \left[\operatorname{sgn}(\mathbf{k}^{w_c} \cdot \mathbf{j}^w) \cos^{-1}(\mathbf{k}^{w_c} \cdot \mathbf{k}^w) \right] \quad (6.82)$$

Note that with the control law above, the feedback signal will go to zero if the error angle is precisely $\pm\pi$. This situation corresponds to the case where the controller cannot decide which way to roll in order to reduce the error angle since either way is equally efficient. Practically this situation would never occur since a disturbance or measurement error would ensure that a particular direction was chosen. However, to mathematically handle the problem, a preferred direction algorithm could be employed to handle cases where the error angle approaches $\pm\pi$.

For implementation purposes, the vectors in the control law of equation (6.82) need to be coordinated into a specific axis system. Since the velocity and position controllers will command the specific acceleration coordinates in inertial axes, it is most useful for the normal acceleration unit vector \mathbf{k}^{w_c} to be coordinated in inertial axes too. This point will be further clarified in the following subsection when the specific acceleration transformation algorithm is developed.

Coordinating all vectors in equation (6.82) into inertial axes, the control law for regulating the error angle becomes,

$$P_w = P_{w_c} - K_\phi \left[\operatorname{sgn}(\mathbf{k}_1^{w_c^T} \mathbf{j}_1^w) \cos^{-1}(\mathbf{k}_1^{w_c^T} \mathbf{k}_1^w) \right] \quad (6.83)$$

The coordinate vectors required to implement the control law are $\mathbf{k}_1^{w_c}$, \mathbf{j}_1^w and \mathbf{k}_1^w together with the scalar feed-forward parameter P_{w_c} . The coordinate vectors \mathbf{j}_1^w and \mathbf{k}_1^w can be obtained from the parameters of the DCM matrix as illustrated in equation (2.10). These coordinate vectors are stated in terms of the wind-inertial DCM parameters below for convenience,

$$\mathbf{j}_1^w = \begin{bmatrix} e_{21}^{wI} & e_{22}^{wI} & e_{23}^{wI} \end{bmatrix}^T \quad (6.84)$$

$$\mathbf{k}_1^w = \begin{bmatrix} e_{31}^{wI} & e_{32}^{wI} & e_{33}^{wI} \end{bmatrix}^T \quad (6.85)$$

The commanded normal acceleration unit vector $\mathbf{k}_1^{w_c}$ will be obtained through the specific acceleration vector transformation algorithm developed in the following subsection. The feed-forward roll rate P_{w_c} is obtained from reference trajectory information and will be discussed further in Chapter 7.

Before continuing, a few points should be noted. Firstly, the control law of equation (6.83) is independent of the specific attitude parameterisation used. The appropriate DCM parameters are simply extracted and utilised directly in the control law. Secondly, although the control law of equation (6.83) appears nonlinear, the error angle dynamics have been shown to be linear. Consequently, the control law causes the error angle to converge in a well defined, stable manner as determined by the error angle closed loop pole.

6.3.1.1 Taking the inner loop roll rate dynamics into account

As previously stated, the zero lag roll rate actuator condition used above is not critical to the error angle controller design. Roll rate lag dynamics (whether the abstracted first order model of equation (6.6) or the actual inner loop closed loop dynamics are used) can easily be combined with the error angle dynamics of equation (6.72) to form the complete error angle dynamics. Of course, proportional feedback of the error angle alone provides only a single degree of feedback freedom in what would then be a second or third order system depending on the level of abstraction. Thus the closed loop error dynamics poles would be constrained to lying on a particular locus in the s-plane. However, combining the design of the roll rate and error angle controllers would allow the error angle dynamics to be set precisely. This combined design is the subject of this section.

Considering equations (5.24), (5.28), (5.29), (6.72) and (6.73), the roll rate dynamics are,

$$\dot{P} = \begin{bmatrix} \bar{I}_P \\ I_{xx} \end{bmatrix} P + \begin{bmatrix} \bar{I}_{\delta_A} \\ I_{xx} \end{bmatrix} \delta_A \quad (6.86)$$

with feedback control law,

$$\delta_A = -K_P P - K_E E_P + N_P P_R \quad (6.87)$$

$$\dot{E}_p = P - P_R \quad (6.88)$$

and the error angle dynamics are,

$$\dot{\phi} = P_{W_c} - P_W \quad (6.89)$$

with feedback control law,

$$P_R = P_{W_c} + K_\phi \phi \quad (6.90)$$

Note that in the control law of equation (6.90), P_W has been changed to P_R (the reference command to the roll rate controller) due to the removal of the timescale separation condition i.e. the roll rate command and actual roll rate are no longer considered equal. Also note with reference to equation (5.25) that under small incidence angle assumptions,

$$P_W = P \quad (6.91)$$

Combining the dynamics above and substituting the two control laws yields,

$$\begin{aligned} \begin{bmatrix} \dot{P} \\ \dot{E}_p \\ \dot{\phi} \end{bmatrix} &= \begin{bmatrix} \bar{L}_p/I_{xx} & 0 & 0 \\ 1 & 0 & 0 \\ -1 & 0 & 0 \end{bmatrix} \begin{bmatrix} P \\ E_p \\ \phi \end{bmatrix} + \begin{bmatrix} \bar{L}_{\delta_A}/I_{xx} \\ 0 \\ 0 \end{bmatrix} \delta_A + \begin{bmatrix} 0 \\ -1 \\ 0 \end{bmatrix} P_R + \begin{bmatrix} 0 \\ 0 \\ 1 \end{bmatrix} P_{W_c} \\ &= \begin{bmatrix} \bar{L}_p/I_{xx} - K_p \bar{L}_{\delta_A}/I_{xx} & -K_E \bar{L}_{\delta_A}/I_{xx} & K_\phi N_p \bar{L}_{\delta_A}/I_{xx} \\ 1 & 0 & -K_\phi \\ -1 & 0 & 0 \end{bmatrix} \begin{bmatrix} P \\ E_p \\ \phi \end{bmatrix} + \begin{bmatrix} N_p \bar{L}_{\delta_A}/I_{xx} \\ -1 \\ 1 \end{bmatrix} P_{W_c} \end{aligned} \quad (6.92)$$

Investigating the closed loop characteristic equation it is straightforward to show that,

$$\alpha_c(s) = s^3 + (K_p \bar{L}_{\delta_A}/I_{xx} - \bar{L}_p/I_{xx})s^2 + (K_E \bar{L}_{\delta_A}/I_{xx} + K_\phi N_p \bar{L}_{\delta_A}/I_{xx})s + (K_\phi K_E \bar{L}_{\delta_A}/I_{xx}) \quad (6.93)$$

Given the desired characteristic equation for the coupled system,

$$\alpha_c(s) = s^3 + \alpha_2 s^2 + \alpha_1 s + \alpha_0 \quad (6.94)$$

the feedback gains to realise the desired poles can be found by matching the coefficients as follows,

$$K_p = \frac{I_{xx}}{\bar{L}_{\delta_A}} \left(\alpha_2 + \frac{\bar{L}_p}{I_{xx}} \right) \quad (6.95)$$

$$K_E = \frac{I_{xx}}{\bar{L}_{\delta_A}} \left(\alpha_1 + \frac{\alpha_0}{z_{\text{int}}} \right) \quad (6.96)$$

$$K_\phi = \frac{\alpha_0}{\alpha_1 + \frac{\alpha_0}{z_{\text{int}}}} \quad (6.97)$$

with N_p set to cancel the inner loop roll rate controller integrator pole as follows,

$$N_p = -\frac{K_E}{z_{\text{int}}} \quad (6.98)$$

In the equations above z_{int} is the position of the zero used to cancel the inner loop integrator pole. Note that in the case where the feed-forward gain N_p is set to zero, z_{int} correspondingly moves to infinity and the gains of equations (6.96) and (6.97) simplify accordingly.

With the feedback gains calculated in this manner, the error angle dynamics can be set precisely. Note that because the control architecture has been kept the same, the feedback gains acquired in this manner can be used in the decoupled designs to determine where the decoupled poles would need to have been placed to result in the exact error angle dynamics. It is in fact important to carry out this investigation for the roll rate controller since designing for fast error angle dynamics poles may result in unacceptably fast internal roll rate dynamics.

In conclusion, the designer should weigh up the increased design accuracy of the coupled design approach with its added design complexity and the need to investigate the resulting inner loop roll dynamics. However, regardless of the design approach the fundamental consideration with the error angle controller is to ensure a well regulated closed loop response with a timescale separation to the outer velocity and position dynamics.

6.3.2 Specific acceleration transformation algorithm

The two assumptions stated at the beginning of section 6.3 imply that from a guidance point of view, the aircraft is capable of immediately directing and commanding the magnitude of its specific acceleration vector in three dimensional space. Thus, given the commanded specific acceleration vector Σ^{w_c} and the current wind axis system axial unit vector i^w , it is always possible to write the commanded specific acceleration vector as follows,

$$\Sigma^{w_c} = A_{w_c} i^w + C_{w_c} k^{w_c} \quad (6.99)$$

where A_{w_c} is the commanded axial specific acceleration, C_{w_c} is the commanded normal specific acceleration and k^{w_c} is the commanded normal unit vector direction. These three commands can be determined as follows,

$$A_{w_c} = \Sigma^{w_c} \cdot i^w \quad (6.100)$$

$$C_{w_c} = s |N^{w_c}| \quad (6.101)$$

$$\mathbf{k}^{w_c} = \frac{1}{C_{w_c}} \mathbf{N}^{w_c} \quad C_{w_c} \neq 0 \quad (6.102)$$

where,

$$s \in \{+1 \ -1\} \quad (6.103)$$

is a sign constant and \mathbf{N}^{w_c} is the component of the specific acceleration vector normal to the axial unit vector and can be determined as follows,

$$\mathbf{N}^{w_c} = \boldsymbol{\Sigma}^{w_c} - A_{w_c} \mathbf{i}^w \quad (6.104)$$

Note that with \mathbf{k}^{w_c} calculated using equation (6.102), it always satisfies the constraint of equation (6.63) as shown below,

$$\begin{aligned} \mathbf{k}^{w_c} \cdot \mathbf{i}^w &= \frac{1}{C_{w_c}} \mathbf{N}^{w_c} \cdot \mathbf{i}^w \\ &= \frac{1}{C_{w_c}} (\boldsymbol{\Sigma}^{w_c} - A_{w_c} \mathbf{i}^w) \cdot \mathbf{i}^w \\ &= \frac{1}{C_{w_c}} (\boldsymbol{\Sigma}^{w_c} \cdot \mathbf{i}^w - (\boldsymbol{\Sigma}^{w_c} \cdot \mathbf{i}^w) \mathbf{i}^w \cdot \mathbf{i}^w) \\ &= 0 \end{aligned} \quad (6.105)$$

The parameter s in equation (6.101) dictates the sign of C_{w_c} and in turn determines whether the vector \mathbf{N}^{w_c} is realised through a positive normal specific acceleration magnitude and an appropriately directed wind axis system normal unit vector or a negative normal specific acceleration magnitude and a wind axis system normal unit vector in the opposite direction. The parameter s can thus be used to command the aircraft to fly a particular reference trajectory in a non-inverted or inverted fashion. It is important to note that inverted and non-inverted flight is typically defined as a function of the trajectory being flown. For example, when flying a loop in the non-inverted fashion then at the top of the loop the aircraft would be in an orientation that would be considered inverted if it were flying straight and level. Assuming that the reference trajectory to be flown is always set up such that the reference axis system is orientated in a non-inverted fashion then \mathbf{k}^{w_c} should be selected such that the following constraint holds,

$$\text{sgn}(\mathbf{k}^{w_c} \cdot \mathbf{k}^R) = i \quad (6.106)$$

where,

$$i = \begin{cases} +1 & \text{for non-inverted flight} \\ -1 & \text{for inverted flight} \end{cases} \quad (6.107)$$

Substituting for \mathbf{k}^{w_c} from equation (6.102) and making use of equation (6.101) yields,

$$\operatorname{sgn}\left(s \frac{N^{w_c}}{|N^{w_c}|} \cdot \mathbf{k}^R\right) = \operatorname{sgn}(s N^{w_c} \cdot \mathbf{k}^R) = i \quad (6.108)$$

It is straightforward to show that s should be selected as follows,

$$s = i \operatorname{sgn}(N^{w_c} \cdot \mathbf{k}^R) \quad (6.109)$$

for the constraint of equation (6.106) to hold.

With reference to equation (6.102), when the normal specific acceleration magnitude command becomes zero i.e. Σ^{w_c} is aligned with i^w , then the direction of the normal specific acceleration unit vector command is free in the plane perpendicular to the axial unit vector. This situation corresponds to a vertical climb/fall or simply a free fall, where the aircraft is free to roll about its velocity vector without influencing the resulting trajectory. The transformation algorithm of equations (6.100) to (6.104) thus results in an undefined commanded normal unit vector at this point.

To practically handle this scenario, a default command direction or command signal could be given to the normal specific acceleration direction controller. For example, the aircraft could be commanded to hold its previous normal unit vector direction (a useful strategy when passing through the zero normal specific acceleration point) or to perform a specific manoeuvre such as roll slowly about the velocity vector. The major practical concern however is that if the aircraft was disturbed in a plane perpendicular to the reference trajectory when operating about the zero normal specific acceleration command condition, then very large jumps in the commanded normal unit vector direction would result. To see this, consider that with the specific acceleration vector constrained to lying in the wind axis system XZ-plane, the aircraft would have to roll the normal unit vector through 90 degrees in order to obtain specific acceleration lateral to its original orientation.

One solution to this problem is to disengage the outer velocity and position controllers when operating about a zero normal specific acceleration condition. The aircraft will then continue to fly the reference trajectory in an open loop fashion until the magnitude of the normal specific acceleration increases past a certain threshold again. While the velocity and position controllers are disengaged, C_{w_c} could be manually constrained to zero while \mathbf{k}^{w_c} could be set arbitrarily in the plane perpendicular to i^w . The value of C_{w_c} that would have been requested from the velocity and position controllers can constantly be monitored and compared to a threshold value to determine when to re-engage the outer loop controllers. Although this strategy will stop any potential jumps in \mathbf{k}^{w_c} , it will almost certainly result in some form of divergence from the reference trajectory if applied for any length of time.

A second solution to the problem is to violate the coordinated turn constraint in these situations and allow lateral specific accelerations to be commanded. This would allow the

reference trajectory to still be tracked through closed loop control and at the same time render \mathbf{k}^{wc} completely free in the plane perpendicular to \mathbf{i}^w . Given the commanded specific acceleration vector $\boldsymbol{\Sigma}^{wc}$, the current wind axis system axial unit vector \mathbf{i}^w and the desired normal specific acceleration direction vector \mathbf{k}^{wc} (in the plane perpendicular to \mathbf{i}^w), it is always possible to write the commanded specific acceleration vector as follows,

$$\boldsymbol{\Sigma}^{wc} = A_{w_c} \mathbf{i}^w + C_{w_c} \mathbf{k}^{wc} + B_{w_c} (\mathbf{k}^{wc} \times \mathbf{i}^w) \quad (6.110)$$

where B_{w_c} is the commanded lateral specific acceleration and given that \mathbf{k}^{wc} satisfies the constraint of equation (6.63). The three specific acceleration coordinates in wind axes could be determined from the given vectors as follows,

$$A_{w_c} = \boldsymbol{\Sigma}^{wc} \cdot \mathbf{i}^w \quad (6.111)$$

$$C_{w_c} = \mathbf{N}^{wc} \cdot \mathbf{k}^{wc} \quad (6.112)$$

$$B_{w_c} = \mathbf{N}^{wc} \cdot (\mathbf{k}^{wc} \times \mathbf{i}^w) \quad (6.113)$$

where \mathbf{N}^{wc} is defined in equation (6.104). The above specific acceleration vector transformation could be used during certain applicable phases of the reference trajectory while the magnitude of the commanded normal specific acceleration in equation (6.104) is below a certain threshold. This threshold could be determined by the maximum allowable lateral specific acceleration. Note that the bandwidth of the lateral specific acceleration controller may also limit the feasibility of employing the above transformation algorithm.

For practical implementation purposes, the vectors in the transformations of equations (6.100) to (6.104) and (6.111) to (6.113) are all coordinated into inertial axes to yield the final specific acceleration transformation algorithms:

When $|C_{w_c}| \geq \varepsilon$ and $\boldsymbol{\Sigma}_1^{wc}$ and \mathbf{i}_1^w are given then the *roll-to-turn* guidance control law is,

$$A_{w_c} = \boldsymbol{\Sigma}_1^{wc} \cdot \mathbf{i}_1^w \quad (6.114)$$

$$C_{w_c} = s |\mathbf{N}_1^{wc}| \quad (6.115)$$

$$\mathbf{k}_1^{wc} = \frac{1}{C_{w_c}} \mathbf{N}_1^{wc} \quad C_{w_c} \neq 0 \quad (6.116)$$

where,

$$\mathbf{N}_1^{wc} = \boldsymbol{\Sigma}_1^{wc} - A_{w_c} \mathbf{i}_1^w \quad (6.117)$$

When $|C_{w_c}| < \varepsilon$ and $\boldsymbol{\Sigma}_1^{wc}$, \mathbf{k}_1^{wc} and \mathbf{i}_1^w are given then the *skid-to-turn* guidance control law is,

$$A_{w_c} = \Sigma_1^{wI} \mathbf{i}_1^w \quad (6.118)$$

$$C_{w_c} = N_1^{wC} \mathbf{k}_1^{w_c} \quad (6.119)$$

$$B_{w_c} = N_1^{wC} S_{k_1^{w_c}} \mathbf{i}_1^w \quad (6.120)$$

where,

$$N_1^{w_c} = \Sigma_1^{wI} - A_{w_c} \mathbf{i}_1^w \quad (6.121)$$

In the algorithms above ε is the positive parameter used to determine when to switch between the roll-to-turn (aircraft rolls to track back to the trajectory) and skid-to-turn (aircraft makes use of direct lateral specific acceleration to track back to the trajectory) algorithms. In both algorithms, the specific acceleration vector coordinated in inertial axes (Σ_1^{wI}) will be obtained from the outer velocity and position controllers. The coordinates of the wind axis system axial unit vector in inertial axes (\mathbf{i}_1^w) can be obtained by inspecting the DCM of equation (2.10) and are provided below in terms of the wind-inertial DCM parameters for convenience,

$$\mathbf{i}_1^w = [e_{11}^{wI} \quad e_{12}^{wI} \quad e_{13}^{wI}]^T \quad (6.122)$$

Note that similarly to the error angle controller, the specific acceleration transformation control law is independent of the attitude parameterisation used.

6.3.3 Velocity and position controllers

At this point, the guidance problem is reduced to that of regulating the point mass velocity and position states in inertial space about a predefined reference trajectory. The virtual control input to the system is the axial specific acceleration vector while the inertially fixed, invariant gravity vector simply acts as a bias to the system.

The position and velocity error dynamics were derived in section 6.1 and are restated below for convenience,

$$\left. \frac{d}{dt} \mathbf{P}^{wR} \right|_I = \mathbf{V}^{wR} \quad (6.123)$$

$$\left. \frac{d}{dt} \mathbf{V}^{wR} \right|_I = \Sigma^{wR} \quad (6.124)$$

where,

$$\Sigma^{wR} = \Sigma^{wI} - \Sigma^{RI} \quad (6.125)$$

Note, with the velocity and position controllers independent of the wind axis system attitude, the reference trajectory need only satisfy the position and velocity dynamics of equations

(6.123) and (6.124). This simplification greatly reduces the complexity of reference trajectory generation as will be discussed in Chapter 7.

To design the velocity and position controllers all vectors in the above equations are coordinated into inertial axes to yield,

$$\dot{\mathbf{p}}_1^{\text{WR}} = \mathbf{v}_1^{\text{WR}} \quad (6.126)$$

$$\dot{\mathbf{v}}_1^{\text{WR}} = \boldsymbol{\Sigma}_1^{\text{WR}} \quad (6.127)$$

where,

$$\boldsymbol{\Sigma}_1^{\text{WR}} = \boldsymbol{\Sigma}_1^{\text{WI}} - \boldsymbol{\Sigma}_1^{\text{RI}} \quad (6.128)$$

A successive loop closure architecture is adopted for the velocity and position controllers. Only proportional feedback will be used due to the natural integrators in the position and velocity dynamics. However, this strategy will still render the closed loop system susceptible to factors such as biases on the regulated normal and axial specific accelerations which could result from specific acceleration estimate/measurement biases. However, these problems are better dealt with through bias estimation and are left as the subject of future estimation research as discussed in section 9.3.

Beginning with the design of the velocity control system. Define the control law,

$$\boldsymbol{\Sigma}_1^{\text{WI}} = K_v (\mathbf{v}_1^{\text{WRc}} - \mathbf{v}_1^{\text{WR}}) + \boldsymbol{\Sigma}_1^{\text{RI}} \quad (6.129)$$

where $\mathbf{v}_1^{\text{WRc}}$ is the commanded velocity error coordinate vector and K_v is the velocity vector feedback gain. Note that by only working with a scalar feedback gain, the closed loop velocity regulation dynamics will be the same in all three axes. If desired it is possible, through the use of three separate feedback gains, to independently set the closed loop dynamics in each of the three inertial axis system unit vector directions. In equation (6.129), the commanded velocity error coordinate vector $\mathbf{v}_1^{\text{WRc}}$ will be used by the outer position control system to regulate the position error. The feed-forward term $\boldsymbol{\Sigma}_1^{\text{RI}}$ is the reference trajectory specific acceleration i.e. the specific acceleration command required to perfectly fly the reference trajectory. Generating reference trajectories will be the topic of Chapter 7.

With the control law of equation (6.129), the closed loop velocity dynamics become,

$$\begin{aligned} \dot{\mathbf{v}}_1^{\text{WR}} &= K_v (\mathbf{v}_1^{\text{WRc}} - \mathbf{v}_1^{\text{WR}}) + \boldsymbol{\Sigma}_1^{\text{RI}} - \boldsymbol{\Sigma}_1^{\text{RI}} \\ &= K_v (\mathbf{v}_1^{\text{WRc}} - \mathbf{v}_1^{\text{WR}}) \end{aligned} \quad (6.130)$$

or otherwise stated,

$$\dot{\mathbf{v}}_1^{\text{WR}} + K_v \mathbf{v}_1^{\text{WR}} = K_v \mathbf{v}_1^{\text{WRc}} \quad (6.131)$$

If it is desired to regulate the velocity vector error only, then the feedback gain K_V can be chosen to place the poles of each decoupled, first order closed loop system by noting that,

$$s = -K_V \quad (6.132)$$

To regulate the position error define the proportional control law,

$$\mathbf{V}_1^{\text{WRc}} = K_p (\mathbf{P}_1^{\text{WRc}} - \mathbf{P}_1^{\text{WR}}) \quad (6.133)$$

where, $\mathbf{P}_1^{\text{WRc}}$ is set to zero to fly on the reference trajectory. Note that again a scalar position feedback gain has been used implying that the position error convergence dynamics will be identical in all three axes. Substituting the control law into equation (6.131), the closed loop position error dynamics become,

$$\dot{\mathbf{V}}_1^{\text{WR}} + K_V \mathbf{V}_1^{\text{WR}} = K_V K_p (\mathbf{P}_1^{\text{WRc}} - \mathbf{P}_1^{\text{WR}}) \quad (6.134)$$

Rearranging the above equation and making use of equation (6.126), the position error dynamics can be written as follows,

$$\ddot{\mathbf{P}}_1^{\text{WR}} + K_V \dot{\mathbf{P}}_1^{\text{WR}} + K_V K_p \mathbf{P}_1^{\text{WR}} = K_V K_p \mathbf{P}_1^{\text{WRc}} \quad (6.135)$$

Given the desired position error dynamics characteristic equation that should be applied to all three axes,

$$\alpha_c(s) = s^2 + \alpha_1 s + \alpha_0 \quad (6.136)$$

the feedback gains K_V and K_p can be calculated as follows,

$$K_V = \alpha_1 \quad (6.137)$$

$$K_p = \frac{\alpha_0}{\alpha_1} \quad (6.138)$$

The upper bandwidth of the closed loop guidance dynamics is constrained from above through the timescale separation assumption that allows for instantaneous commanding of the specific acceleration vector in three dimensional space. Thus, when selecting the guidance dynamics poles it is important to ensure that this constraint is adhered to for proper functionality of the controller.

6.3.4 Summary

A schematic overview of the specific acceleration matching guidance controller is shown in Figure 6.1. On the left hand side of the diagram is the velocity and position controller. This linear controller operates purely with inertially coordinated vectors and uses the specific acceleration coordinates as virtual actuators. The specific acceleration transformation

algorithm then takes the inertially coordinated specific acceleration command vector and transforms it to wind axes. The algorithm also calculates the desired wind axis system normal unit vector and passed this to the error angle controller. The extra signals required by the specific acceleration transformation algorithm are shown as entering the block from above, with ε used to determine which variant of the algorithm to use. Finally, the error angle controller compares the desired wind axis system normal unit vector with the actual wind axis system normal unit vector and commands a roll rate to drive this error to zero over time. The four signals on the right hand side of the diagram are then sent as commands to the respective inner loop controllers.

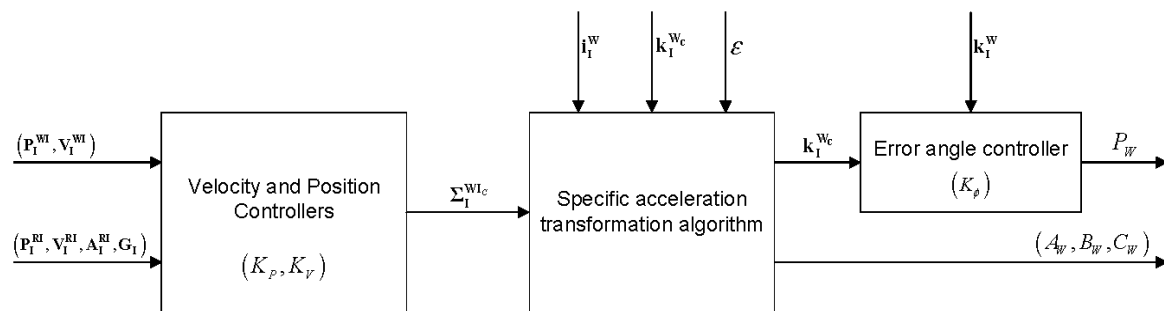


Figure 6.1 – Block diagram overview of the SAM guidance controller

It should be noted that if the inner loop controllers used are the NNDT variants then it may be necessary to schedule the guidance dynamics bandwidth in order for the timescale separation argument between the inner and outer loop controllers to hold. Given the non-dimensional natural frequency of the limiting NNDT controller (ω'_n), the corresponding dimensional natural frequency can be calculated using the equation below,

$$\omega_n = \frac{gS}{mV} \omega'_n \quad (6.139)$$

This equation was obtained by making use of equation (4.66). The dimensional frequency of equation (6.139) can be used to appropriately schedule the bandwidth of the guidance dynamics such that the inner and outer loop bandwidth ratios remain invariant.

6.4 Conclusion

This chapter focused on the design of guidance level controllers capable of guiding the aircraft through the entire 3D flight envelope (middle block of Figure 3.1). A number of guidance control strategies were presented and analysed qualitatively. One particular guidance strategy, specific acceleration matching, was developed in detail and forms an important part of this dissertation's contribution to the field of aircraft guidance and control. The strategy provides a particularly elegant, intuitive, computationally efficient guidance control solution that is well suited for use with the inner specific acceleration and roll rate controllers presented. The

controller architecture will be seen to also greatly simplify reference trajectory generation.

Chapter 7

Reference Trajectories

In the previous chapter, control strategies were investigated for regulation of the aircraft as a point mass about a feasible reference trajectory. In this chapter, the generation of feasible reference trajectories is considered. The chapter begins by setting up the general reference trajectory problem applicable to all of the guidance strategies discussed in section 6.2. It then moves on to adapt the dynamics that need to be satisfied by the reference trajectory given that the SAM guidance control law of section 6.3 is to be implemented. It shall be seen that generation of feasible reference trajectories for the SAM guidance controller is far simpler than generation of reference trajectories for the general guidance case. In section 7.2 a few simple reference trajectories suitable for the SAM guidance controller are derived. These simple trajectories serve as building blocks for navigation through inertial space and are used in the simulations of Chapter 8.

7.1 Reference trajectory dynamics

With reference to equations (6.15), (6.16), (6.26) and (6.40) to (6.43), a feasible reference trajectory for the general guidance dynamics developed in section 6.1 must satisfy the following constraints,

$$\left. \frac{d}{dt} \mathbf{p}^{RI} \right|_I = \mathbf{V}^{RI} \quad (7.1)$$

$$\left. \frac{d}{dt} \mathbf{V}^{RI} \right|_I = \mathbf{A}^{RI} \quad (7.2)$$

$$\left. \frac{d}{dt} \begin{bmatrix} \mathbf{i}^R & \mathbf{j}^R & \mathbf{k}^R \end{bmatrix} \right|_I = \boldsymbol{\omega}^{RI} \times \begin{bmatrix} \mathbf{i}^R & \mathbf{j}^R & \mathbf{k}^R \end{bmatrix} \quad (7.3)$$

with the algebraic relationship,

$$\mathbf{A}^{RI} = \boldsymbol{\Sigma}^{RI} + \mathbf{G}^{RI} \quad (7.4)$$

together with the four possible actuator lag (low pass filter) constraints,

$$\dot{P}_{W_R} = -\frac{1}{\tau_P} P_{W_R} + \frac{1}{\tau_P} P_{W_{CR}} \quad (7.5)$$

$$\dot{A}_{W_R} = -\frac{1}{\tau_A} A_{W_R} + \frac{1}{\tau_A} A_{W_{CR}} \quad (7.6)$$

$$\dot{B}_{W_R} = -\frac{1}{\tau_B} B_{W_R} + \frac{1}{\tau_B} B_{W_{CR}} \quad (7.7)$$

$$\dot{C}_{W_R} = -\frac{1}{\tau_C} C_{W_R} + \frac{1}{\tau_C} C_{W_{CR}} \quad (7.8)$$

as well as any constraints imposed on the virtual control inputs and the reference state vector e.g. saturation or slew rate limits. Equations (7.1) and (7.2) imply that a feasible reference trajectory must satisfy the point mass position and velocity kinematics while equation (7.3) imposes attitude kinematics constraints on the reference axis system. Equations (7.5) to (7.8) only constrain the reference trajectory if the virtual actuator lags are significant. The reference trajectory generation problem is that of determining feasible reference state and control trajectories that most closely match the desired motion of the aircraft through space.

7.1.1 Reference trajectories for the SAM guidance controller

When the assumptions associated with the SAM guidance controller hold, then a feasible reference trajectory need only satisfy the following dynamics,

$$\left. \frac{d}{dt} \mathbf{P}^{RI} \right|_I = \mathbf{V}^{RI} \quad (7.9)$$

$$\left. \frac{d}{dt} \mathbf{V}^{RI} \right|_I = \mathbf{A}^{RI} \quad (7.10)$$

with,

$$\mathbf{A}^{RI} = \boldsymbol{\Sigma}^{RI} + \mathbf{G}^{RI} \quad (7.11)$$

together with any reference trajectory state and control constraints. Note that in this case, the reference trajectory is no longer constrained by the attitude kinematics of equation (7.3) due to the assumption that the aircraft can roll to any ‘bank angle’ (not strictly the correct term) infinitely fast relative to the position and velocity dynamics. Furthermore, due to the assumption that the virtual actuator lags are negligible, the constraints of equations (7.5) to (7.8) also disappear.

With the reference trajectories only required to satisfy equations (7.9) and (7.10) as well as any state/actuator constraints, generation of feasible reference trajectories is greatly simplified. To see this consider that if all vectors in the reference trajectory dynamics are coordinated into inertial axes then the dynamics are linear. The only nonlinearities that enter the reference

trajectory dynamics are those of the state and actuator constraints since they are typically expressed in terms of wind axis system coordinates.

Once a kinematically feasible reference trajectory has been found, the fact that the specific acceleration vector is constrained to lying in the plane spanned by \mathbf{i}^R and \mathbf{k}^R can be used to calculate the roll rate P_R associated with the reference trajectory. This roll rate should then be assigned to the roll rate reference command P_{w_c} in the normal specific acceleration vector direction controller of section 6.3.1. This feed-forward term will ensure that the feedback control in the normal acceleration vector direction controller is responsible only for regulating perturbations in the error angle due to disturbances or jumps in the reference axis system roll attitude.

To determine the roll rate associated with the reference trajectory, begin with the angular velocity of the reference axis system with respect to inertial space,

$$\boldsymbol{\omega}^{RI} = P_R \mathbf{i}^R + Q_R \mathbf{j}^R + R_R \mathbf{k}^R \quad (7.12)$$

Taking the cross product of this vector with the \mathbf{k}^R vector yields,

$$\boldsymbol{\omega}^{RI} \times \mathbf{k}^R = -P_R \mathbf{j}^R + Q_R \mathbf{i}^R \quad (7.13)$$

Finally, taking the negative of the dot product of equation (7.13) with \mathbf{j}^R yields the result,

$$\begin{aligned} P_R &= -\mathbf{j}^R \cdot (\boldsymbol{\omega}^{RI} \times \mathbf{k}^R) \\ &= -\mathbf{j}^R \cdot \left(\left. \frac{d}{dt} \mathbf{k}^R \right|_I \right) \end{aligned} \quad (7.14)$$

Intuitively, equation (7.14) implies that the reference axis system experiences a roll rate whenever the normal unit vector changes with respect to inertial space as long as the change does not occur in the reference axis system's XZ-plane. In order to calculate P_R , the unit vectors in equation (7.14) need to be expressed as a function of the reference trajectory vectors. The reference axes normal unit vector can be written as follows,

$$\mathbf{k}^R = \frac{1}{C_R} N^{RI} \quad (7.15)$$

where,

$$N^{RI} = \boldsymbol{\Sigma}^{RI} - A_R \mathbf{i}^R \quad (7.16)$$

$$A_R = \boldsymbol{\Sigma}^{RI} \cdot \mathbf{i}^R \quad (7.17)$$

$$\mathbf{i}^R = \frac{1}{V_R} V^{RI} \quad (7.18)$$

$$\bar{V}_R = |V^{RI}| \quad (7.19)$$

$$C_R = s_{ref} |N^{RI}| \quad (7.20)$$

and,

$$s_{ref} = \text{sgn}(N^R \cdot k^{R_{ref}}) \quad (7.21)$$

Note that $k^{R_{ref}}$ is an appropriately selected reference vector that it used through equation (7.21) to set the direction of k^R for a non-inverted reference trajectory. Note that equation (7.21) originates from the relationship,

$$\text{sgn}(k^R \cdot k^{R_{ref}}) = 1 \quad (7.22)$$

implying that k^R will be made to point in the direction of $k^{R_{ref}}$ for non-inverted flight. Returning to the task of determining the reference axis system roll rate, substituting equation (7.15) into equation (7.14) gives,

$$\begin{aligned} P_R &= -j^R \cdot \left(\frac{d}{dt} \frac{1}{C_R} N^{RI} \Big|_I \right) \\ &= -j^R \cdot \left(\frac{d}{dt} \frac{1}{C_R} \Big|_I N^{RI} + \frac{1}{C_R} \frac{d}{dt} N^{RI} \Big|_I \right) \\ &= -\frac{1}{C_R} j^R \cdot \left(\frac{d}{dt} N^{RI} \Big|_I \right) \end{aligned} \quad (7.23)$$

where use has been made of the relationship,

$$j^R \cdot N^R = 0 \quad (7.24)$$

Substituting for N^{RI} from equation (7.16) yields,

$$\begin{aligned} P_R &= -\frac{1}{C_R} j^R \cdot \left(\frac{d}{dt} \Sigma^{RI} - A_R i^R \Big|_I \right) \\ &= -\frac{1}{C_R} j^R \cdot \left(\frac{d}{dt} \Sigma^{RI} \Big|_I - \frac{d}{dt} \frac{A_R}{V_R} \Big|_I V^{RI} - \frac{A_R}{V_R} \frac{d}{dt} V^{RI} \Big|_I \right) \\ &= -\frac{1}{C_R} j^R \cdot \left(\frac{d}{dt} \Sigma^{RI} \Big|_I - \frac{A_R}{V_R} A^{RI} \right) \\ &= -\frac{1}{C_R} j^R \cdot \left(\frac{d}{dt} A^{RI} \Big|_I - \frac{A_R}{V_R} G^{RI} \right) \end{aligned} \quad (7.25)$$

where use of equation (7.18) has been made and where it has been noticed that,

$$j^R \cdot V^{RI} = 0 \quad (7.26)$$

$$\mathbf{j}^R \cdot \boldsymbol{\Sigma}^{RI} = 0 \quad (7.27)$$

$$\left. \frac{d}{dt} \mathbf{G}^{RI} \right|_I = 0 \quad (7.28)$$

Finally, to remove the lateral unit vector from the equation note that,

$$\begin{aligned} \mathbf{j}^R &= \mathbf{k}^R \times \mathbf{i}^R \\ &= \frac{\mathbf{N}^{RI}}{C_R} \times \frac{\mathbf{V}^{RI}}{\bar{V}_R} \\ &= \frac{(\boldsymbol{\Sigma}^{RI} - A_R \mathbf{i}^R) \times \mathbf{V}^{RI}}{C_R \bar{V}_R} \\ &= \frac{\boldsymbol{\Sigma}^{RI} \times \mathbf{V}^{RI}}{C_R \bar{V}_R} \end{aligned} \quad (7.29)$$

where use has been made of the relationship,

$$\mathbf{i}^R \times \mathbf{V}^{RI} = 0 \quad (7.30)$$

Substituting equation (7.29) into equation (7.25) yields the final result,

$$P_R = -\frac{\boldsymbol{\Sigma}^{RI} \times \mathbf{V}^{RI}}{C_R^2 \bar{V}_R} \cdot \left(\mathbf{J}^{RI} - \frac{A_R}{\bar{V}_R} \mathbf{G}^{RI} \right) \quad (7.31)$$

where the jerk vector is defined as follows,

$$\mathbf{J}^{RI} \equiv \left. \frac{d}{dt} \mathbf{A}^{RI} \right|_I \quad (7.32)$$

Thus, with a feasible reference trajectory calculated, the corresponding velocity, acceleration and jerk vectors can be used to determine the roll rate associated with the reference trajectory. Typically, all vectors will be coordinated into inertial axes with the coordinate vector equations following naturally from the vector equations provided.

7.2 Building block reference trajectories

The SAM guidance controller of the previous chapter is capable of regulating the aircraft about any kinematically feasible reference trajectory. In practice, these reference trajectories could be generated either offline, as predefined manoeuvres for example, or online i.e. the trajectory could be generated based on obstacles to avoid, targets to track etc. To ease the process of both online and offline trajectory generation, defining base manoeuvre types is very useful. Definition of ‘building block’ trajectories serves to reduce the parameter space for higher level mission planning type algorithms. This section derives three fundamental building block reference trajectories for the SAM guidance controller. These are the straight line, vertical arc and horizontal spiral arc. All trajectories assume that no explicit actuator or state

constraints exist. The mathematics of the trajectories is developed in such a way that the trajectories can be easily strung together to form complex three dimensional manoeuvres. Such manoeuvres will be illustrated in the simulations of Chapter 8.

7.2.1 Straight line flight

For a straight line trajectory, the position vector is constrained as follows,

$$\mathbf{P}^{RI}(t) = \mathbf{P}^{SI} + p(t)\hat{\mathbf{r}} \quad (7.33)$$

where \mathbf{P}^{SI} is the starting position of the straight line, $\hat{\mathbf{r}}$ is the inertially fixed heading unit vector and p is the position coordinate along this vector. Investigating the corresponding velocity vector,

$$\begin{aligned} \mathbf{V}^{RI}(t) &= \left. \frac{d}{dt} p(t)\hat{\mathbf{r}} \right|_I \\ &= v(t)\hat{\mathbf{r}} \end{aligned} \quad (7.34)$$

where,

$$v(t) \equiv \dot{p}(t) \quad (7.35)$$

The corresponding acceleration vector is then,

$$\begin{aligned} \mathbf{A}^{RI}(t) &= \left. \frac{d}{dt} \dot{p}(t)\hat{\mathbf{r}} \right|_I \\ &= a(t)\hat{\mathbf{r}} \end{aligned} \quad (7.36)$$

where,

$$a(t) \equiv \dot{v}(t) \quad (7.37)$$

Limiting the acceleration to be a constant along the path (a_0) it is straightforward to show that the jerk vector is zero at all times,

$$\mathbf{J}^{RI}(t) = \mathbf{0} \quad (7.38)$$

Equations (7.35) and (7.37) can be used to solve for the position and velocity along the unit vector $\hat{\mathbf{r}}$ over time. Integrating equations (7.35) and (7.37) gives,

$$v(t) = v(t_s) + a_0(t - t_s) \quad (7.39)$$

$$p(t) = p(t_s) + v(t_s)(t - t_s) + \frac{1}{2}a_0(t - t_s)^2 \quad (7.40)$$

The above equations can be rewritten as follows,

$$v(t) = v(t_s) + \Delta v(t) \quad (7.41)$$

$$p(t) = p(t_s) + \Delta p(t) \quad (7.42)$$

where,

$$\Delta v(t) = a_0 \Delta t(t) \quad (7.43)$$

$$\Delta p(t) = v(t_s) \Delta t(t) + \frac{1}{2} a_0 \Delta t^2(t) \quad (7.44)$$

and,

$$\Delta t(t) = t - t_s \quad (7.45)$$

Given the starting position of the straight line \mathbf{P}^{SI} , the straight line heading unit vector \hat{r} , the initial position and velocity states $p(t_s)$ and $v(t_s)$ respectively and the constant linear acceleration a_0 , the position, velocity and acceleration vectors can be solved for as a function of time up until the chosen final time t_f . These vectors can be substituted into equation (7.31) to determine the reference roll rate associated with the trajectory. However, it is straightforward to show that the reference roll rate is zero at all times,

$$P_r(t) = 0 \quad (7.46)$$

7.2.1.1 Linking the trajectory

The initial position and velocity vectors for the trajectory ($\mathbf{P}^{RI}(t_s)$ and $\mathbf{V}^{RI}(t_s)$ respectively) will be available from the previous section of the reference trajectory. These two vectors place the following continuity constraints on the parameters involved in the straight line trajectory,

$$\mathbf{P}^{RI}(t_s) = \mathbf{P}^{SI} + p(t_s) \hat{r} \quad (7.47)$$

$$\mathbf{V}^{RI}(t_s) = v(t_s) \hat{r} \quad (7.48)$$

These constraints allow the parameters involved in the trajectory to be determined. From equation (7.47),

$$p(t_s) = (\mathbf{P}^{RI}(t_s) - \mathbf{P}^{SI}) \cdot \hat{r} \quad (7.49)$$

However, since \mathbf{P}^{SI} is still free to be chosen, then without loss of generality it can be set as follows,

$$\mathbf{P}^{SI} = \mathbf{P}^{RI}(t_s) \quad (7.50)$$

to yield,

$$p(t_s) = 0 \quad (7.51)$$

independently of the bearing unit vector \hat{r} . From equation (7.48), the initial velocity magnitude can be calculated as follows,

$$|v(t_s)| = |V^{RI}(t_s)| \quad (7.52)$$

If it is assumed that the bearing unit vector is further constrained such that the initial velocity along the straight line is positive (this is the obvious choice) then the following relationship holds,

$$v(t_s) = |v(t_s)| \quad (7.53)$$

From this, the bearing unit vector can be determined from equation (7.48) as follows,

$$\begin{aligned} \hat{r} &= \frac{V^{RI}(t_s)}{v(t_s)} \\ &= \frac{V^{RI}(t_s)}{|v(t_s)|} \end{aligned} \quad (7.54)$$

The only parameters still to be provided are the constant acceleration along the straight line a_0 and the final time t_f . Although these parameters can be provided directly, it is often more convenient to specify the desired velocity magnitude at the end time $|v(t_f)|$ together with the length of the straight line $|\Delta p(t_f)|$. Only the absolute values are required if it is further assumed that the velocity along the straight line never changes sign. This will in general be the case otherwise it would require the velocity magnitude to go through zero. Noting this, the relationship of equation (7.53) can be extended to all time to give,

$$v(t) = |v(t)| \quad t_s \leq t \leq t_f \quad (7.55)$$

Thus,

$$v(t_f) = |v(t_f)| \quad (7.56)$$

and providing the absolute value is equivalent to providing the signed value. Furthermore, through integration of equation (7.35) and substitution of equation (7.55) it can be shown that,

$$\Delta p(t) = \int_{t_s}^t v(t) dt = \int_{t_s}^t |v(t)| dt \quad (7.57)$$

Taking the absolute value yields the result,

$$|\Delta p(t)| = \left| \int_{t_s}^t |v(t)| dt \right| = \int_{t_s}^t |v(t)| dt \quad (7.58)$$

Combining equations (7.57) and (7.58) shows that,

$$\Delta p(t) = |\Delta p(t)| \quad (7.59)$$

and thus,

$$\Delta p(t_f) = |\Delta p(t_f)| \quad (7.60)$$

which again shows that the absolute value is equivalent to the signed value. With $v(t_f)$ and $\Delta p(t_f)$ available, the constant acceleration and final time can be calculated using equations (7.43) to (7.45), to yield,

$$t_f = t_s + \Delta t(t_f) \quad (7.61)$$

$$a_0 = \frac{\Delta v(t_f)}{\Delta p(t_f)} \left(v(t_s) + \frac{\Delta v(t_f)}{2} \right) \quad (7.62)$$

where,

$$\Delta t(t_f) = \frac{\Delta p(t_f)}{v(t_s) + \frac{\Delta v(t_f)}{2}} \quad (7.63)$$

Coordination of the vectors in the above developments into inertial axes follows very simply and is thus omitted.

7.2.1.2 Flight orientation reference vector

By convention, non-inverted straight line flight corresponds to when the reference axis system's normal unit vector has a component in the direction of the inertial down vector. Thus, with reference to equation (7.22), the flight orientation reference vector for the straight line is,

$$\mathbf{k}^{R_{ref}} = \mathbf{k}^I \quad (7.64)$$

7.2.2 Vertical arc

For vertical arc motion the position vector is constrained as follows,

$$\mathbf{P}^{RI}(t) = \mathbf{P}^{CI} + R\hat{\mathbf{r}}(t) \quad (7.65)$$

where \mathbf{P}^{CI} is the centre of the arc, R is the radius of the arc and $\hat{\mathbf{r}}$ is the radial unit vector and is parameterised using the arc angle θ as follows,

$$\hat{\mathbf{r}}(t) = \sin \theta(t) \hat{\boldsymbol{\psi}} + \cos \theta(t) \mathbf{k}^I \quad (7.66)$$

In equation (7.66), use has been made of the inertially fixed arc plane heading vector $\hat{\boldsymbol{\psi}}$, a second unit vector orthogonal to \mathbf{k}^I that together with \mathbf{k}^I uniquely defines the vertical arc plane. The arc plane heading vector can be parameterised using the heading angle ψ as follows,

$$\hat{\boldsymbol{\psi}} = \cos \psi \mathbf{i}^I + \sin \psi \mathbf{j}^I \quad (7.67)$$

Investigating the corresponding velocity while on the vertical arc locus,

$$\begin{aligned} \mathbf{V}^{RI}(t) &= \left. \frac{d}{dt} \mathbf{P}^{RI} \right|_I \\ &= \left. \frac{d}{dt} \mathbf{P}^{CI} + R \hat{\mathbf{r}}(t) \right|_I \\ &= R \left. \frac{d}{dt} \sin \theta(t) \hat{\boldsymbol{\psi}} + \cos \theta(t) \mathbf{k}^I \right|_I \\ &= R \omega(t) \hat{\boldsymbol{\theta}}(t) \end{aligned} \quad (7.68)$$

where,

$$\omega(t) \equiv \dot{\theta}(t) \quad (7.69)$$

and,

$$\hat{\boldsymbol{\theta}}(t) \equiv \cos \theta(t) \hat{\boldsymbol{\psi}} - \sin \theta(t) \mathbf{k}^I \quad (7.70)$$

Investigating the associated acceleration on the trajectory,

$$\begin{aligned} \mathbf{A}^{RI}(t) &= \left. \frac{d}{dt} R \omega(t) \hat{\boldsymbol{\theta}}(t) \right|_I \\ &= R \left(\alpha(t) \hat{\boldsymbol{\theta}}(t) + \omega(t) \left. \frac{d}{dt} \hat{\boldsymbol{\theta}}(t) \right|_I \right) \\ &= R \left(\alpha(t) \hat{\boldsymbol{\theta}}(t) - \omega^2(t) \hat{\mathbf{r}}(t) \right) \end{aligned} \quad (7.71)$$

where α is the angular acceleration defined below,

$$\alpha(t) \equiv \dot{\omega}(t) \quad (7.72)$$

Limiting the angular acceleration to be a constant (α_0), the jerk vector can be calculated as follows,

$$\begin{aligned}
\mathbf{J}^{RI}(t) &= \frac{d}{dt} R(\alpha(t)\hat{\boldsymbol{\theta}}(t) - \omega(t)^2 \hat{\mathbf{r}}(t)) \Big|_I \\
&= R(-\alpha(t)\omega(t)\hat{\mathbf{r}}(t) - 2\omega(t)\alpha(t)\hat{\mathbf{r}}(t) - \omega(t)^3 \hat{\boldsymbol{\theta}}(t)) \\
&= -R(3\alpha_0\omega(t)\hat{\mathbf{r}}(t) + \omega^3(t)\hat{\boldsymbol{\theta}}(t))
\end{aligned} \tag{7.73}$$

Integrating equations (7.69) and (7.72) to solve for the angular velocity and heading angle over time yields,

$$\omega(t) = \omega(t_s) + \alpha_0(t - t_s) \tag{7.74}$$

$$\theta(t) = \theta(t_s) + \omega(t_s)(t - t_s) + \frac{1}{2}\alpha_0(t - t_s)^2 \tag{7.75}$$

The above equations can be rewritten as follows,

$$\omega(t) = \omega(t_s) + \Delta\omega(t) \tag{7.76}$$

$$\theta(t) = \theta(t_s) + \Delta\theta(t) \tag{7.77}$$

where,

$$\Delta\omega(t) = \alpha_0\Delta t(t) \tag{7.78}$$

$$\Delta\theta(t) = \omega(t_s)\Delta t(t) + \frac{1}{2}\alpha_0\Delta t(t)^2 \tag{7.79}$$

and,

$$\Delta t(t) = t - t_s \tag{7.80}$$

Given the centre of the arc \mathbf{P}^{CI} , the radius of the arc R , the heading angle ψ , the initial arc angle and angular velocity states $\theta(t_s)$ and $\omega(t_s)$ respectively and the constant angular acceleration α_0 , the position, velocity and acceleration vectors can be solved for as a function of time up until the chosen final time t_f . These vectors can be substituted into equation (7.31) to determine the reference roll rate associated with the trajectory. However, due to the vertical nature of the arc it is straightforward to show that the reference roll rate is zero at all times,

$$P_r(t) = 0 \tag{7.81}$$

7.2.2.1 Linking the trajectory

The initial position and velocity vectors for the trajectory ($\mathbf{P}^{RI}(t_s)$ and $\mathbf{V}^{RI}(t_s)$ respectively) will be available from the previous section of the reference trajectory. These two vectors place the following continuity constraints on the parameters involved in the vertical arc,

$$\mathbf{P}^{RI}(t_s) = \mathbf{P}^{CI} + R\hat{\mathbf{r}}(t_s) \quad (7.82)$$

$$\mathbf{V}^{RI}(t_s) = R\omega(t_s)\hat{\boldsymbol{\theta}}(t_s) \quad (7.83)$$

These constraints allow a number of the parameters involved in the trajectory to be determined. Firstly, equations (7.82) and (7.83) constrain the centre position of the arc. Thus, although the centre position could be provided explicitly subject to the constraints of equations (7.82) and (7.83), it is more convenient to simply provide the arc radius and the desired direction of rotation about the unit vector normal to the arc plane, with the normal unit vector defined as follows,

$$\hat{\mathbf{n}} = \mathbf{k}^I \times \hat{\boldsymbol{\psi}} \quad (7.84)$$

Given the arc radius and direction of rotation about $\hat{\mathbf{n}}$, together with the initial position and velocity vectors, the centre position of the arc can be calculated. To see this, make the centre position of the arc the subject of the formula in equation (7.82),

$$\mathbf{P}^{CI} = \mathbf{P}^{RI}(t_s) - R\hat{\mathbf{r}}(t_s) \quad (7.85)$$

In the above equation only the initial radial unit vector is unknown. Taking the cross product of equation (7.83) with the arc plane normal unit vector $\hat{\mathbf{n}}$ yields,

$$\begin{aligned} \mathbf{V}^{RI}(t_s) \times \hat{\mathbf{n}} &= R\omega(t_s)\hat{\boldsymbol{\theta}}(t_s) \times \hat{\mathbf{n}} \\ &= R\omega(t_s)\hat{\mathbf{r}}(t_s) \end{aligned} \quad (7.86)$$

Investigating the magnitude relationship of the above equation,

$$\begin{aligned} |\mathbf{V}^{RI}(t_s) \times \hat{\mathbf{n}}| &= |R\omega(t_s)\hat{\boldsymbol{\theta}}(t_s) \times \hat{\mathbf{n}}| \\ &= R|\omega(t_s)| \end{aligned} \quad (7.87)$$

where it has been noted that,

$$R > 0 \quad (7.88)$$

Dividing equation (7.86) by equation (7.87) yields,

$$\frac{\mathbf{V}^{RI}(t_s) \times \hat{\mathbf{n}}}{|\mathbf{V}^{RI}(t_s) \times \hat{\mathbf{n}}|} = \frac{R\omega(t_s)\hat{\mathbf{r}}(t_s)}{R|\omega(t_s)|} \quad (7.89)$$

which can be rewritten as follows,

$$\begin{aligned}\hat{\mathbf{r}}(t_s) &= \frac{|\omega(t_s)|}{\omega(t_s)} \frac{\mathbf{V}^{RI}(t_s) \times \hat{\mathbf{n}}}{|\mathbf{V}^{RI}(t_s) \times \hat{\mathbf{n}}|} \\ &= a \frac{\mathbf{V}^{RI}(t_s) \times \hat{\mathbf{n}}}{|\mathbf{V}^{RI}(t_s) \times \hat{\mathbf{n}}|}\end{aligned}\quad (7.90)$$

where,

$$a = \frac{|\omega(t_s)|}{\omega(t_s)} = \begin{cases} +1 & \text{for a positive rotation about } \hat{\mathbf{n}} \\ -1 & \text{for a negative rotation about } \hat{\mathbf{n}} \end{cases}\quad (7.91)$$

With R and a given, the radial unit vector at the starting time can be calculated using equation (7.90) and the centre position of the arc can be calculated using equation (7.85). Use of equation (7.66) and the initial radial unit vector allows the initial arc angle to be calculated as follows,

$$\theta(t_s) = \tan^{-1} \left(\frac{\hat{\mathbf{r}}(t_s) \cdot \hat{\boldsymbol{\psi}}}{\hat{\mathbf{r}}(t_s) \cdot \mathbf{k}^I} \right)\quad (7.92)$$

where a four quadrant arc tangent should be used. This in turn allows the initial arc angle unit vector to be calculated from equation (7.70),

$$\hat{\boldsymbol{\theta}}(t_s) = \cos \theta(t_s) \hat{\boldsymbol{\psi}} - \sin \theta(t_s) \mathbf{k}^I\quad (7.93)$$

Taking the dot product of equation (7.83) with the initial arc angle unit vector yields the initial angular velocity,

$$\omega(t_s) = \frac{\mathbf{V}^{RI}(t_s) \cdot \hat{\boldsymbol{\theta}}(t_s)}{R}\quad (7.94)$$

The only parameters still missing in the vertical arc trajectory are the constant angular acceleration α_0 and the final time t_f . Although these parameters can be provided directly, it is often more convenient to specify the magnitude of the angle of the vertical arc to be subtended $|\Delta\theta(t_f)|$ as well as the velocity vector magnitude at the final time $|\mathbf{V}^{RI}(t_f)|$. To see why only the magnitude of these two quantities is required consider that the sign of the angular velocity does not change over the trajectory section. This must be true otherwise it would involve the magnitude of the velocity vector going to zero at some point along the trajectory. With this constraint, the relationship of equation (7.91) holds for all time as follows,

$$\omega(t) = a |\omega(t)| \quad t_s \leq t \leq t_f\quad (7.95)$$

where it has been noted that,

$$a = a^{-1}\quad (7.96)$$

Taking the magnitude of equation (7.68) and substituting for the angular velocity magnitude into equation (7.95) gives,

$$\omega(t) = a \frac{|V^{RI}(t)|}{R} \quad (7.97)$$

Thus, providing only the magnitude of the velocity vector at the final time is sufficient to determine the final angular velocity including its sign,

$$\omega(t_f) = a \frac{|V^{RI}(t_f)|}{R} \quad (7.98)$$

Furthermore, through integration of equation (7.69) and substitution of equation (7.95) the following result is obtained,

$$\begin{aligned} \Delta\theta(t) &= \int_{t_s}^t \omega(t) dt \\ &= a \int_{t_s}^t |\omega(t)| dt \end{aligned} \quad (7.99)$$

Taking the absolute value of both sides,

$$\begin{aligned} |\Delta\theta(t)| &= \left| a \int_{t_s}^t \omega(t) dt \right| \\ &= \int_{t_s}^t |\omega(t)| dt \end{aligned} \quad (7.100)$$

Dividing equation (7.99) by equation (7.100) gives,

$$\frac{\Delta\theta(t)}{|\Delta\theta(t)|} = a \quad (7.101)$$

Thus, providing only the magnitude of the change in the arc angle at the final time is enough to determine the signed change in arc angle at the final time,

$$\Delta\theta(t_f) = a |\Delta\theta(t_f)| \quad (7.102)$$

With the angular velocity at the final time and the change in arc angle at the final time available, the angular acceleration and final time can be determined using equations (7.78) to (7.80),

$$t_f = t_s + \Delta t(t_f) \quad (7.103)$$

$$\alpha_0 = \frac{\Delta\omega(t_f)}{\Delta\theta(t_f)} \left[\omega(t_s) + \frac{\Delta\omega(t_f)}{2} \right] \quad (7.104)$$

where,

$$\Delta t(t_f) = \frac{\Delta\theta(t_f)}{\omega(t_s) + \frac{\Delta\omega(t_f)}{2}} \quad (7.105)$$

Coordination of the vectors in the above developments into inertial axes follows very simply and is thus omitted.

7.2.2.2 Flight orientation reference vector

By convention, a non-inverted vertical arc is when the reference axis system's normal unit vector points towards the outside of the arc i.e. away from the arc centre. Thus, with reference to equation (7.22), the flight orientation reference vector for the vertical arc is,

$$\mathbf{k}^{Ref} = \hat{\mathbf{r}} \quad (7.106)$$

7.2.3 Horizontal spiral arc

For a horizontal spiral arc trajectory the position vector is constrained as follows,

$$\mathbf{P}^{RI}(t) = \mathbf{P}^{CI} + R\hat{\mathbf{r}}(t) + p(t)\mathbf{k}^I \quad (7.107)$$

where \mathbf{P}^{CI} is the centre point of the horizontal arc, R is the radius of the arc, p is the position coordinate along the \mathbf{k}^I unit vector and $\hat{\mathbf{r}}$ is the radial unit vector, parameterised by the heading angle ψ as follows,

$$\hat{\mathbf{r}}(t) = \cos\psi(t)\mathbf{i}^I + \sin\psi(t)\mathbf{j}^I \quad (7.108)$$

Investigating the associated velocity vector,

$$\begin{aligned} \mathbf{V}^{RI}(t) &= \left. \frac{d}{dt} \mathbf{P}^{CI} + R\hat{\mathbf{r}}(t) + p(t)\mathbf{k}^I \right|_I \\ &= R \left. \frac{d}{dt} \hat{\mathbf{r}}(t) \right|_I + \dot{p}(t)\mathbf{k}^I \\ &= R\dot{\psi}(t) [-\sin\psi(t)\mathbf{i}^I + \cos\psi(t)\mathbf{j}^I] + \dot{p}(t)\mathbf{k}^I \\ &= R\omega(t)\hat{\boldsymbol{\psi}}(t) + v(t)\mathbf{k}^I \end{aligned} \quad (7.109)$$

where,

$$v(t) \equiv \dot{p}(t) \quad (7.110)$$

$$\omega(t) \equiv \dot{\psi}(t) \quad (7.111)$$

and,

$$\hat{\psi}(t) = -\sin\psi(t)\mathbf{i}' + \cos\psi(t)\mathbf{j}' \quad (7.112)$$

Limiting the vertical velocity to be constant, the acceleration on the locus is then,

$$\begin{aligned} \mathbf{A}^{RI}(t) &= \left. \frac{d}{dt} R\omega(t)\hat{\psi}(t) + v(t)\mathbf{k}' \right|_I \\ &= \left. \frac{d}{dt} R\omega(t)\hat{\psi}(t) \right|_I \\ &= R(\alpha(t)\hat{\psi}(t) - \omega(t)^2 \hat{\mathbf{r}}(t)) \end{aligned} \quad (7.113)$$

where,

$$\alpha(t) \equiv \dot{\omega}(t) \quad (7.114)$$

Limiting the angular acceleration to be a constant (α_0), the jerk vector can be calculated as follows,

$$\begin{aligned} \mathbf{J}^{RI}(t) &= \left. \frac{d}{dt} R(\alpha(t)\hat{\psi}(t) - \omega(t)^2 \hat{\mathbf{r}}(t)) \right|_I \\ &= R(-\alpha(t)\omega(t)\hat{\mathbf{r}}(t) - 2\omega(t)\alpha(t)\hat{\mathbf{r}}(t) - \omega(t)^3 \hat{\psi}(t)) \\ &= -R(3\alpha_0\omega(t)\hat{\mathbf{r}}(t) + \omega^3(t)\hat{\psi}(t)) \end{aligned} \quad (7.115)$$

The vertical position, angular velocity and heading angles can be solved for through integration of equations (7.110), (7.111) and (7.114) to yield,

$$p(t) = p(t_s) + v_0(t - t_s) \quad (7.116)$$

$$\omega(t) = \omega(t_s) + \alpha_0(t - t_s) \quad (7.117)$$

$$\psi(t) = \psi(t_s) + \omega(t_s)(t - t_s) + \frac{1}{2}\alpha_0(t - t_s)^2 \quad (7.118)$$

where v_0 and α_0 are the constant vertical velocity and angular accelerations respectively and t_s is the starting time of the horizontal spiral arc trajectory. The above equations can be rewritten as follows,

$$p(t) = p(t_s) + \Delta p(t) \quad (7.119)$$

$$\omega(t) = \omega(t_s) + \Delta\omega(t) \quad (7.120)$$

$$\psi(t) = \psi(t_s) + \Delta\psi(t) \quad (7.121)$$

where,

$$\Delta p(t) = v_0 \Delta t(t) \quad (7.122)$$

$$\Delta \omega(t) = \alpha_0 \Delta t(t) \quad (7.123)$$

$$\Delta \psi(t) = \omega(t_s) \Delta t(t) + \frac{1}{2} \alpha_0 \Delta t(t)^2 \quad (7.124)$$

and,

$$\Delta t(t) = t - t_s \quad (7.125)$$

Given the centre of the arc \mathbf{P}^{CI} , the radius of the arc R , the initial position, heading angle and angular velocity states $p(t_s)$, $\psi(t_s)$ and $\omega(t_s)$ respectively and the constant vertical velocity v_0 and angular acceleration α_0 , the position, velocity and acceleration vectors can be solved for as a function of time up until the chosen final time t_f . These vectors can be substituted into equation (7.31) to determine the reference roll rate associated with the trajectory. In the case where both the vertical velocity is zero and the angular acceleration is zero, the reference roll rate can be shown to be zero.

7.2.3.1 Linking the trajectory

The initial position and velocity vectors for the trajectory ($\mathbf{P}^{RI}(t_s)$ and $\mathbf{V}^{RI}(t_s)$ respectively) will be available from the previous section of the reference trajectory. These two vectors place the following continuity constraints on the parameters involved in the horizontal spiral arc trajectory,

$$\mathbf{P}^{RI}(t_s) = \mathbf{P}^{CI} + R\hat{r}(t_s) + p(t_s)\mathbf{k}^I \quad (7.126)$$

$$\mathbf{V}^{RI}(t_s) = R\omega(t_s)\hat{\psi}(t_s) + v_0\mathbf{k}^I \quad (7.127)$$

These constraints allow a number of the parameters involved in the trajectory to be determined. To obtain the initial position state, take the dot product of equation (7.126) with the \mathbf{k}^I unit vector,

$$p(t_s) = (\mathbf{P}^{RI}(t_s) - \mathbf{P}^{CI}) \cdot \mathbf{k}^I \quad (7.128)$$

If the vertical position of the centre of the arc is chosen equal to that of the initial reference position then,

$$\mathbf{P}^{CI} \cdot \mathbf{k}^I = \mathbf{P}^{RI}(t_s) \cdot \mathbf{k}^I \quad (7.129)$$

and equation (7.128) reduces to,

$$p(t_s) = 0 \quad (7.130)$$

Taking the dot product of equation (7.127) with the \mathbf{k}^I unit vector yields the vertical velocity parameter,

$$v_0 = \mathbf{V}^{RI}(t_s) \cdot \mathbf{k}^I \quad (7.131)$$

Equations (7.126) and (7.127) constrain the centre position of the arc. Thus, although the centre position could be provided explicitly subject to the constraints of equations (7.126) and (7.127), it is more convenient to simply provide the arc radius and the desired direction of rotation about the \mathbf{k}^I unit vector. These two pieces of information, together with the initial position and velocity vectors, allow the centre position of the arc to be calculated. To see this, make the centre position of the arc the subject of the formula in equation (7.126),

$$\mathbf{P}^{CI} = \mathbf{P}^{RI}(t_s) - R\hat{\mathbf{r}}(t_s) \quad (7.132)$$

where it has been assumed that equation (7.130) holds. In the above equation only the initial radial unit vector is unknown. Taking the cross product of equation (7.127) with the \mathbf{k}^I unit vector yields,

$$\begin{aligned} \mathbf{V}^{RI}(t_s) \times \mathbf{k}^I &= R\omega(t_s)\hat{\boldsymbol{\mu}}(t_s) \times \mathbf{k}^I + v_0\mathbf{k}^I \times \mathbf{k}^I \\ &= R\omega(t_s)\hat{\mathbf{r}}(t_s) \end{aligned} \quad (7.133)$$

Investigating the magnitude relationship of the above equation yields,

$$\begin{aligned} |\mathbf{V}^{RI}(t_s) \times \mathbf{k}^I| &= |R\omega(t_s)\hat{\mathbf{r}}(t_s)| \\ &= R|\omega(t_s)| \end{aligned} \quad (7.134)$$

where it has been noted that,

$$R > 0 \quad (7.135)$$

Dividing equation (7.133) by equation (7.134) yields,

$$\frac{\mathbf{V}^{RI}(t_s) \times \mathbf{k}^I}{|\mathbf{V}^{RI}(t_s) \times \mathbf{k}^I|} = \frac{R\omega(t_s)\hat{\mathbf{r}}(t_s)}{R|\omega(t_s)|} \quad (7.136)$$

which can be rewritten as follows,

$$\begin{aligned} \hat{\mathbf{r}}(t_s) &= \frac{|\omega(t_s)|}{\omega(t_s)} \frac{\mathbf{V}^{RI}(t_s) \times \mathbf{k}^I}{|\mathbf{V}^{RI}(t_s) \times \mathbf{k}^I|} \\ &= a \frac{\mathbf{V}^{RI}(t_s) \times \mathbf{k}^I}{|\mathbf{V}^{RI}(t_s) \times \mathbf{k}^I|} \end{aligned} \quad (7.137)$$

where,

$$a = \frac{|\omega(t_s)|}{\omega(t_s)} = \begin{cases} +1 & \text{for a positive rotation about } \mathbf{k}' \\ -1 & \text{for a negative rotation about } \mathbf{k}' \end{cases} \quad (7.138)$$

With R and a given, the radial unit vector at the starting time can be calculated using equation (7.137) and the centre position of the arc can be calculated using equation (7.132). Use of equation (7.108) and the initial radial unit vector allows the initial heading angle to be calculated as follows,

$$\psi(t_s) = \tan^{-1} \left(\frac{\hat{\mathbf{r}}(t_s) \cdot \mathbf{j}'}{\hat{\mathbf{r}}(t_s) \cdot \mathbf{i}'} \right) \quad (7.139)$$

where a four quadrant arc tangent should be used. This in turn allows the initial heading unit vector to be calculated from equation (7.112),

$$\hat{\boldsymbol{\psi}}(t_s) = -\sin \psi(t_s) \mathbf{i}' + \cos \psi(t_s) \mathbf{j}' \quad (7.140)$$

Taking the dot product of equation (7.127) with the initial heading unit vector yields the initial angular velocity,

$$\omega(t_s) = \frac{\mathbf{V}^{RI}(t_s) \cdot \hat{\boldsymbol{\psi}}(t_s)}{R} \quad (7.141)$$

The only parameters still missing in the horizontal spiral arc trajectory are the constant angular acceleration α_0 and the final time t_f . Although these parameters can be provided directly, it is often more convenient to specify the magnitude of the angle of the horizontal arc to be subtended $|\Delta\psi(t_f)|$ as well as the magnitude of the velocity vector at the final time $|\mathbf{V}^{RI}(t_f)|$. A similar analysis to that carried out in section 7.2.2.1 can be used to show that,

$$\omega(t_f) = a |\omega(t_s)| \quad (7.142)$$

$$\Delta\psi(t_f) = a |\Delta\psi(t_s)| \quad (7.143)$$

where through taking the magnitude of equation (7.109) at the final time it can be shown that,

$$|\omega(t_f)| = \frac{\sqrt{|\mathbf{V}^{RI}(t_f)|^2 - v_0^2}}{R} \quad (7.144)$$

Thus providing only the magnitudes of the velocity vector and change in heading angle at the final time is sufficient information, together with a , to determine the signed values of the angular velocity and heading angle at the final time. From the information above, the angular acceleration and final time can be determined using equations (7.123) to (7.125),

$$t_f = t_s + \Delta t(t_f) \quad (7.145)$$

$$\alpha_0 = \frac{\Delta\omega(t_f)}{\Delta\psi(t_f)} \left[\omega(t_s) + \frac{\Delta\omega(t_f)}{2} \right] \quad (7.146)$$

where,

$$\Delta t(t_f) = \frac{\Delta\psi(t_f)}{\omega(t_s) + \frac{\Delta\omega(t_f)}{2}} \quad (7.147)$$

Coordination of the vectors in the above developments into inertial axes follows very simply and is thus omitted.

7.2.3.2 Flight orientation reference vector

By convention, a non-inverted horizontal spiral arc is described when the reference axis system's normal unit vector has a component in the direction of the inertial down vector. Thus, with reference to equation (7.22), the flight orientation reference vector for the horizontal spiral arc is,

$$\mathbf{k}^{R_{ref}} = \mathbf{k}^I \quad (7.148)$$

7.3 Conclusion

This chapter has addressed the problem of reference trajectory generation (left most block of Figure 3.1). The general reference trajectory problem was established in section 7.1 and simplified to the case applicable to the SAM guidance controller in section 7.1.1. There it was noted that reference trajectories for the SAM guidance controller need only satisfy linear second order position and velocity dynamics along all three inertial axes. The ease of defining this type of trajectory was again highlighted in section 7.2 where a number of building block reference trajectories were mathematically formulated. These trajectories were created in such a way so as to be easily strung together to form complex three dimensional manoeuvres. By defining building block reference trajectories the parameter space is reduced for higher level mission/manoeuvre planning algorithms. These algorithms would simply work with the set of available reference trajectories, linking them together to create a trajectory to achieve a desired goal. The SAM guidance controller would then track the trajectory, making use of the inner loop roll rate and specific acceleration controllers to steer the aircraft.

Chapter 8

Simulation of Example Applications

To verify the manoeuvre autopilot design and highlight its functionality and versatility, it is applied to three example aircraft with varied physical characteristics and reference trajectories. These are an aerobatic aircraft, a variable static stability blended-wing-body and a vertical takeoff and landing capable tail-stand fixed wing aircraft. All aircraft have been used at Stellenbosch University for various UAV research projects.

The simulations conducted model all six degrees of aircraft freedom as well as all couplings and nonlinearities that were ignored in the autopilot design. The simulations do not however model sensor noise and it is instead assumed that the full state vector is known perfectly and is available for feedback. Estimation strategies are left for future research as outlined in section 9.3. Effects such as wind and parameter uncertainty have also been neglected in the simulations so as not to cloud the fundamental differences between the actual and predicted responses that arise due to the simplifying assumptions made in the controller design.

All simulations were run with continuous states propagated at 1 kHz using a fourth order Runge-Kutta numerical integration algorithm. The inner loop and normal specific acceleration direction controllers were run at 500 Hz while the outer velocity and position guidance controllers were run at 50 Hz. These controller sample rates were selected to ensure that the discrete implementation of the continuous controllers resulted in no visible deterioration in the closed loop system dynamic responses. With the effects of discretisation negligible in the dynamic responses, any remaining differences between the actual and expected dynamics could again be attributed to and correlated with the simplifying assumptions made in the controller designs. It should be noted however that in practice the respective controllers can safely be implemented discretely at sample rates up to an order of magnitude lower than those used in the simulations with only minor deterioration of the closed loop dynamic responses.

Finally, unless otherwise stated, all units used in the design, analysis and simulations to follow are SI units with angles and angular rates in radians and radians per second respectively.

8.1 Manoeuvre control of an aerobatic aircraft

The aerobatic aircraft used for simulation in this section is a CAP-232 0.90 size, methanol powered UAV shown in Figure 8.1. The aircraft model parameters were first obtained in [13] and are restated in Appendix C for convenience. The purpose of the aerobatic aircraft example is to verify the controller design and illustrate the full 3D flight potential of the manoeuvre autopilot. As such, a detailed application of the control system to the aircraft is documented in section 8.1.1. Here all of the conditions for application of the autopilot are investigated thoroughly together with pole placement regions, desired poles and actual closed loop poles. The simulated performance of the autopilot is then investigated in section 8.1.2. The dynamic responses of the individual controllers is investigated and compared to the expected design responses of section 8.1.1. Finally, a complex 3D reference trajectory is created and the tracking performance of the autopilot evaluated.



Figure 8.1 – Picture of the aerobatic aircraft

8.1.1 Application of the manoeuvre autopilot

In this section the generic manoeuvre autopilot presented in this thesis is applied to the aerobatic aircraft. Dimensional time fixed pole placement versions of the inner loop controllers are utilised given that the aircraft is to operate close to its nominal trim velocity and air density during flights. The nominal velocity magnitude and air density values are,

$$\bar{V}_{nom} = 30 \text{ m/s} \quad (8.1)$$

$$\rho_{nom} = 1.225 \text{ kg/m}^3 \quad (8.2)$$

The dimensional time fixed pole placement inner loop control strategy will ensure that from an outer loop guidance perspective the aircraft continues to operate with the same performance (dynamic response) for all variations about the nominal flight condition. This in turn provides

the simplest interface for the guidance level controllers.

8.1.1.1 Axial specific acceleration controller design

The lower bound on the bandwidth of the closed loop axial acceleration dynamics due to the sensitivity function constraint of equation (4.18) is calculated first. Given a minimum operating velocity magnitude of 25 m/s and a maximum normal specific acceleration magnitude of 5 g's, then for a desired return disturbance rejection of at least 20 dB, the minimum closed loop bandwidth relative to the open loop thrust actuator bandwidth can be calculated using equation (4.18) to be,

$$\frac{\omega_n}{\omega_T} \geq 0.99 \quad (8.3)$$

Here a conservative estimate of 10 has been used for the minimum lift to drag ratio. The constraint above implies that the closed loop bandwidth should be at least equal to the open loop thrust actuator bandwidth of 4 rad/s. Selecting the desired closed loop poles with a natural frequency of 5 rad/s (provides a small buffer for uncertainty without overstressing the thrust actuator) and a conservative damping of 0.8 yields the desired characteristic equation,

$$\alpha_c(s) = s^2 + 8s + 25 \quad (8.4)$$

Figure 8.2 provides a Bode plot of the actual and approximated return disturbance transfer functions i.e. from equation (3.34) the return disturbance transfer function is,

$$\Delta C_w(s) = \left(-2 \frac{C_w}{\bar{V} R_{LD}} \frac{1}{s} \right) S_D(s) \quad (8.5)$$

where substitution of the actual or approximated sensitivity function (equations (4.13) and (4.14)) yields the actual or approximated return disturbance respectively. Also plotted are the actual and approximated sensitivity functions themselves as well as the term in parenthesis in equation (8.5) i.e. the normalised drag to normalised velocity perturbation transfer function. Figure 8.2 clearly illustrates the greater than 20 dB's of return disturbance rejection obtained over the entire frequency band due to the appropriate selection of the closed loop poles. The figure also shows how the return disturbance rejection is contributed towards by the controller at low frequencies and the natural velocity magnitude dynamics at high frequencies. The plot thus verifies the sensitivity function and return disturbance analysis done in sections 3.2.3 and 4.1.

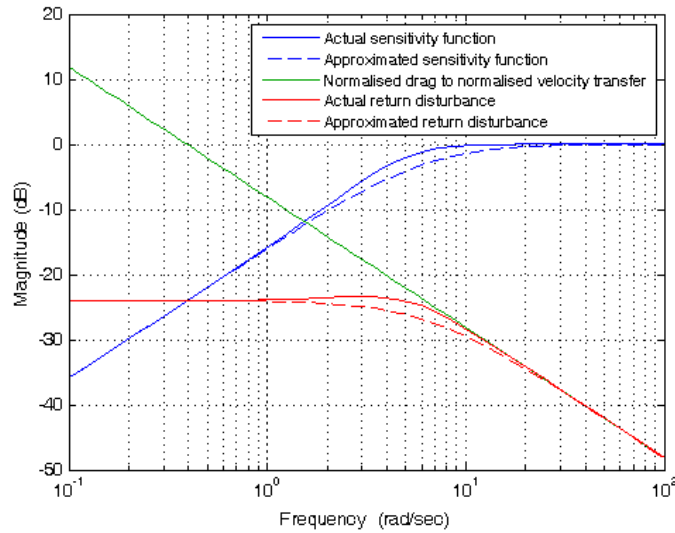


Figure 8.2 – Bode magnitude plot of the actual and approximated return disturbance transfer function and its constituents

8.1.1.2 Normal specific acceleration controller design

The aerobatic aircraft easily satisfies the standard aerodynamic assumption of equation (4.25) with,

$$\left| \frac{L_Q}{mV} \right| = 0.0710 \ll 1 \quad (14 \text{ times smaller}) \quad (8.6)$$

As a result, the pole and zero approximation equations of section 4.2.1 are expected to yield good results. This is verified by the actual and approximated open loop poles and elevator to normal specific acceleration zeros listed below,

$$\text{Actual:} \quad p_{1,2} = -10.62 \pm 7.85i \quad z_{1,2} = -46.72, 54.67 \quad (8.7)$$

$$\text{Approximated:} \quad p_{1,2} = -10.62 \pm 8.15i \quad z_{1,2} = -46.56, 54.51 \quad (8.8)$$

Equation (4.47) is then used to determine the NMP upper frequency bound constraint below,

$$\omega_n < 16.84 \quad (8.9)$$

To illustrate the validity of this constraint the controller of section 4.2.4 is applied to the aircraft with the desired complex poles selected to have a damping ratio of 0.7 while the natural frequency is varied between 5 and 24 rad/s. The desired real pole is selected equal to the real value of the complex poles. The desired and corresponding actual closed loop poles are illustrated in Figure 8.3. Also shown in the figure are the actual and approximated open loop poles (denoted by blue and green crosses respectively – note they are almost exactly on top of each other), the NMP frequency bound constraint and the lower timescale separation

frequency constraint given a desired velocity magnitude bandwidth of 1 rad/s (a feasible user selected value). Importantly the locus of actual closed loop poles is seen to remain similar to that of the desired poles while the upper NMP frequency bound is adhered to. Outside the bound the actual poles are seen to diverge quickly from the desired values. Also notice both the large feasible pole placement region and the fact that the open loop poles naturally satisfy the NMP frequency constraint.

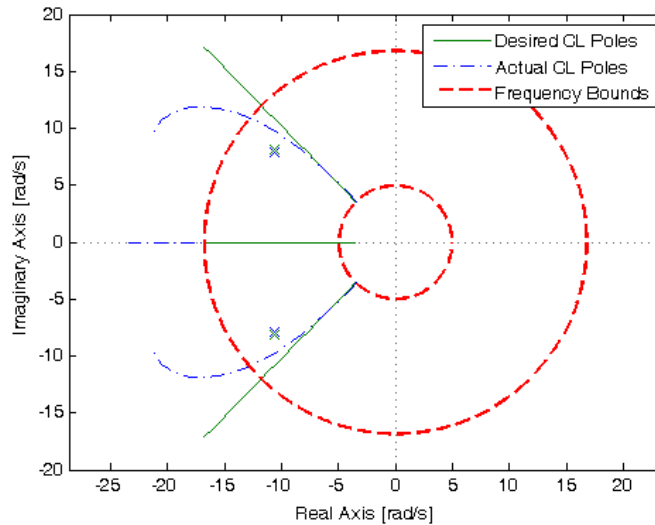


Figure 8.3 – Actual and approximated open loop poles, desired and actual closed loop poles and upper and lower normal specific acceleration frequency bounds

Figure 8.4 shows the corresponding feedback gains for the controller designs above. The gains are plotted as a function of the RHP zero position normalised to the desired natural frequency (r^{-1}). The feedback gains are normalised such that their maximum value shown is unity. It is clear from the plot that the feedback gains start to grow very quickly, and consequently start to become impractical, when the RHP zero is less than 3 times the desired natural frequency. The results of Figures 8.3 and 8.4 are all consistent with the arguments developed in sections 4.2.2 and 4.2.3.

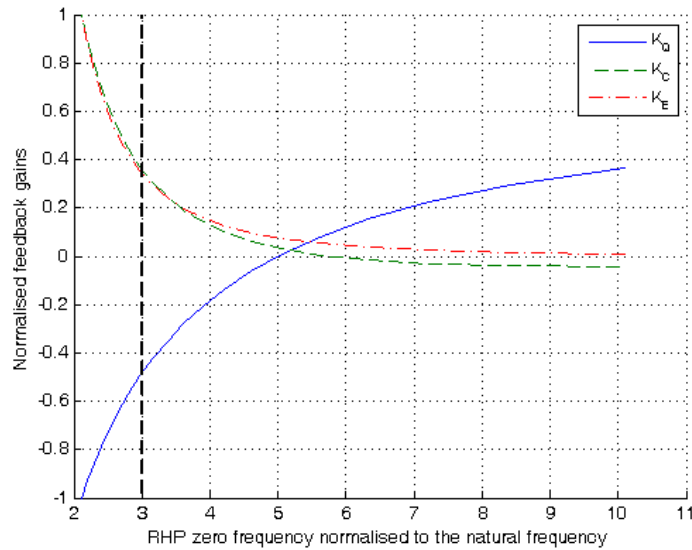


Figure 8.4 – Normalised normal specific acceleration controller gains as a function of the RHP zero position normalised to the desired natural frequency

Given the open loop pole positions and the frequency bound constraints illustrated in Figure 8.3, the desired closed loop normal dynamics poles are selected as follows,

$$\text{Desired CL: } p_{1,2,3} = -10 \pm 8i, -10 \quad (8.10)$$

In an attempt to avoid excessive control effort, the frequency of the desired poles has been chosen to be similar to the natural frequency of the open loop system. However, note that the poles are still chosen somewhat arbitrarily. Methods for intelligent pole placement are discussed in section 9.3 on future research. The above poles correspond to the desired characteristic equation below,

$$\alpha_c(s) = s^3 + 30s^2 + 364s + 1640 \quad (8.11)$$

Applying the control algorithm of section 4.2.4 yields the actual closed loop poles,

$$\text{Actual CL: } p_{1,2,3} = -10.34 \pm 7.48i, -10.21 \quad (8.12)$$

which are seen to be very similar to the desired poles.

8.1.1.3 Analysis of the lateral dynamics

Section 5.1 presented a number of conditions that should be satisfied by the lateral dynamics in order for them to decouple into roll and directional dynamics. The conditions of equations (5.4) to (5.7), (5.12) to (5.14) and (5.19) from section 5.1 are applied to the aerobatic aircraft below,

$$Y_p = 0.0811 \approx 0 \quad (8.13)$$

$$Y_{\delta_A} = -2.1223 \approx 0 \quad (8.14)$$

$$\left| \frac{Y_R}{m\bar{V}} \right| = 0.0112 \ll 1 \quad (89 \text{ times smaller}) \quad (8.15)$$

$$\left| \frac{\bar{C}_{n_p}}{\bar{C}_{l_p}} \right| = 0.0591 \ll 2.7778 = \left| \frac{\bar{C}_{n_R}}{\bar{C}_{l_R}} \right| \quad (47 \text{ times smaller}) \quad (8.16)$$

$$\left| \frac{\bar{C}_{n_p}}{\bar{C}_{l_p}} \right| = 0.0591 \ll 2.5982 = \left| \frac{\bar{C}_{n_\beta}}{\bar{C}_{l_\beta}} \right| \quad (44 \text{ times smaller}) \quad (8.17)$$

$$\left| \frac{\bar{C}_{n_p}}{\bar{C}_{l_p}} \right| = 0.0591 \ll 14.1125 = \left| \frac{\bar{C}_{n_{\delta_R}}}{\bar{C}_{l_{\delta_R}}} \right| \quad (239 \text{ times smaller}) \quad (8.18)$$

$$\left| \frac{\bar{C}_{n_{\delta_A}}}{\bar{C}_{l_{\delta_A}}} \right| = 0.0174 \ll 2.7778 = \left| \frac{\bar{C}_{n_R}}{\bar{C}_{l_R}} \right| \quad (159 \text{ times smaller}) \quad (8.19)$$

$$\left| \frac{\bar{C}_{n_{\delta_A}}}{\bar{C}_{l_{\delta_A}}} \right| = 0.0174 \ll 2.5982 = \left| \frac{\bar{C}_{n_\beta}}{\bar{C}_{l_\beta}} \right| \quad (149 \text{ times smaller}) \quad (8.20)$$

To quantify whether the numerical values in equations (8.13) and (8.14) are in fact negligible it is important to consider the units of the stability/control derivatives. For the stability derivative of equation (8.13), assuming a maximum roll rate of 180 deg/s, the corresponding lateral acceleration would be 0.05 m/s² which can be considered negligible. For the control derivative of equation (8.14), assuming a maximum aileron deflection of 20 deg, the corresponding lateral acceleration would be 0.15 m/s² which can again be considered negligible.

It is clear from the equations above that the aerobatic aircraft easily satisfies all of the lateral decoupling constraints and thus that the decoupled controller designs of sections 5.2 and 5.3 can be safely applied. To numerically verify an aspect of the lateral decoupling, the open loop lateral poles are listed together with the decoupled roll and directional dynamics poles below,

$$\text{Lateral:} \quad p_{1,2,3} = -1.90 \pm 8.78i, -29.19 \quad (8.21)$$

$$\text{Decoupled:} \quad p_{1,2,3} = -1.89 \pm 8.68i, -29.20 \quad (8.22)$$

It is clear that the decoupled dynamics poles are very similar to the coupled lateral dynamics poles.

8.1.1.4 Roll rate controller design

Based on the open loop roll rate dynamics the desired closed loop roll rate poles are selected to

be,

$$\text{Desired CL: } p_{1,2} = -25, -20 \quad (8.23)$$

which correspond to a desired characteristic equation,

$$\alpha_c(s) = s^2 + 45s + 500 \quad (8.24)$$

The open and closed loop rudder to roll rate coupling Bode diagrams are provided in Figure 8.5. The control system is seen to significantly reject the low frequency coupling. The maximum closed loop coupling from rudder to roll rate is seen to be -7.5 dB at approximately 25 rad/s. However, consider that the rudder will be used to control the directional dynamics whose closed loop bandwidth will be similar to its open loop bandwidth of approximately 9 rad/s. The disturbance coupling at this frequency is only -10.6 dB which implies that a worst case 9 rad/s sinusoidal rudder disturbance with an amplitude of 20 deg would cause a sinusoidal roll rate disturbance with an amplitude of about 6 deg/s. This coupling is arguably negligibly low.

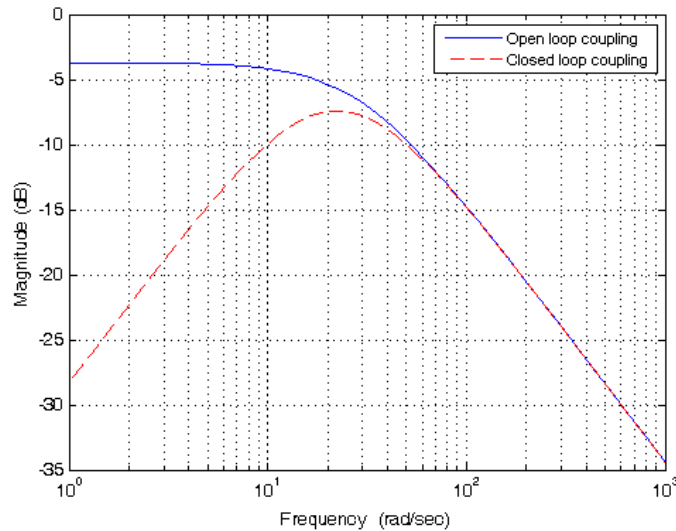


Figure 8.5 – Open and closed loop rudder coupling gain into roll rate over frequency

8.1.1.5 Lateral specific acceleration controller design

Considering how well the aerobatic aircraft satisfies equation (5.5) the pole and zero approximation equations of section 5.3.1 are expected to yield excellent results. This is verified by the actual and approximated open loop poles and rudder to lateral specific acceleration zeros listed below,

$$\text{Actual: } p_{1,2} = -1.89 \pm 8.68i \quad z_{1,2} = -7.03, 6.48 \quad (8.25)$$

$$\text{Approximated: } p_{1,2} = -1.89 \pm 8.73i \quad z_{1,2} = -7.02, 6.47 \quad (8.26)$$

The fixed natural frequency variation of the stability augmentation control law discussed in section 5.3.2.1 is implemented since the open loop natural frequency of the directional dynamics is deemed sufficient. A prudent closed loop damping ratio of 0.9 is selected in the knowledge that the outer regulation loop does not take the full directional dynamics into account and will consequently result in a loss of overall directional damping when implemented.

For the stability augmentation control law of section 5.3.2.1 to be implemented the gain relationships of equations (5.71) and (5.72) must be satisfied. Investigating these gain constraints for the nominal design yields the following results,

$$\left| \frac{K_B}{K_R} \right| = 0 \ll 14.71 = \left| \frac{m}{Y_R} \frac{l_F}{l_D - l_F} \right| \quad (\text{constraint always satisfied}) \quad (8.27)$$

$$\left| K_R \right| = 0.12 \ll 4.05 = \left| \frac{m \bar{V}}{Y_{\delta_R}} \frac{l_W}{l_W - l_F} \right| \quad (34 \text{ times smaller}) \quad (8.28)$$

Thus it is expected that the desired and actual closed loop poles will be very similar as is verified by the result below,

$$\text{Desired:} \quad p_{1,2} = -8.04 \pm 3.89i \quad (8.29)$$

$$\text{Actual:} \quad p_{1,2} = -8.04 \pm 4.07i \quad (8.30)$$

For the design of the outer regulation control law the NMP upper frequency constraint of equation (5.59) is first calculated with the result shown below,

$$\omega_n < 2.25 \quad (8.31)$$

The desired closed loop regulation pole is set to -1 rad/s, well within the NMP frequency bound above. Investigating now the desired and actual closed loop poles for the directional dynamics as a whole yields,

$$\text{Desired:} \quad p_{1,2,3} = -8.04 \pm 3.89i, -1 \quad (8.32)$$

$$\text{Actual:} \quad p_{1,2,3} = -6.54 \pm 4.60i, -1.25 \quad (8.33)$$

with the results depicted graphically in Figure 8.6. The desired poles are denoted by black dots while the actual poles are denoted with blue crosses. The NMP upper frequency bound is also shown in red.

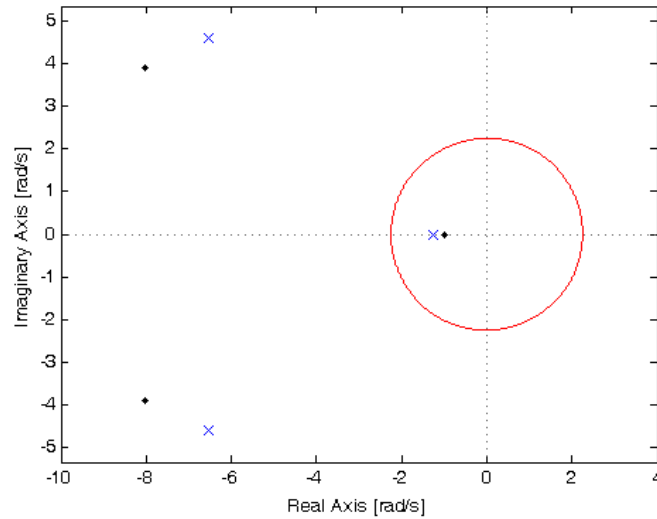


Figure 8.6 – Desired and actual closed loop directional dynamics

It is clear that approximating the stability augmented directional dynamics by its steady state gain introduces error into the regulation pole placement algorithm. To solve this problem however requires deriving a far more mathematically complex control law that involves designing the stability augmentation and regulation control laws simultaneously, taking into account effects such as the side force due to rudder deflection and yaw rate. In contrast the lateral specific acceleration control law of section 5.3.2 provides a simple decoupled design solution that can easily be tailored to yield the desired results e.g. over damp the inner loop poles in the knowledge that the damping will be reduced by the outer loop.

Considering the actual directional dynamics closed loop poles above, they are still deemed acceptable with the complex poles having a natural frequency of 8 rad/s and a damping 0.82 and the integrator pole still well within the NMP frequency bound of equation (5.59). Finally, the Bode magnitude plots of the transfer functions from aileron deflection through to lateral specific acceleration and attitude parameter through to lateral specific acceleration are shown in Figure 8.7.

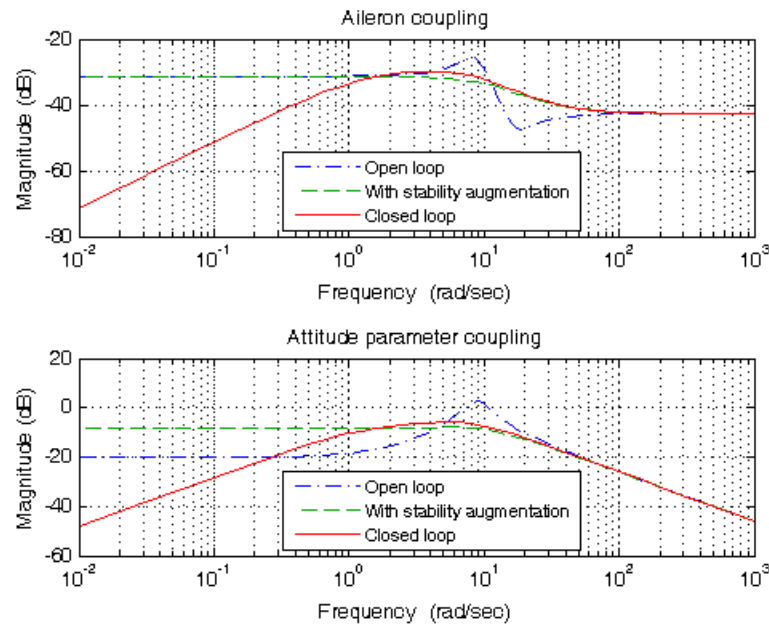


Figure 8.7 – Open and closed loop aileron and attitude parameter coupling gains into lateral specific acceleration over frequency

The maximum aileron coupling gain is -30 dB which implies that a worst case 20 deg amplitude aileron deflection sinusoid will result in a negligible lateral specific acceleration disturbance of 0.011 m/s^2 . The maximum attitude parameter coupling gain is -6 dB which implies that a worst case unity amplitude attitude parameter sinusoid will result in a lateral specific acceleration disturbance of 0.5 m/s^2 . This disturbance is acceptably small.

8.1.1.6 The actual closed loop lateral dynamics

Figure 8.8 provides a plot of the desired lateral dynamics poles (as black dots), as taken from equations (8.23) and (8.32), and the actual closed loop poles (as blue crosses) when all of the cross coupling in the lateral dynamics is present. The directional dynamics NMP upper frequency bound is also shown in red. The pole positions are also provided numerically below,

$$\text{Desired: } p_{1,2} = -25.00, -20.00, -8.04 \pm 3.89i, -1.00 \quad (8.34)$$

$$\text{Actual: } p_{1,2} = -24.42, -20.43, -6.63 \pm 4.55i, -1.22 \quad (8.35)$$

It is clear that for the aerobatic aircraft the lateral cross coupling is very weak and that most of the pole placement distortion takes place in the outer directional dynamics regulation control law as previously discussed.

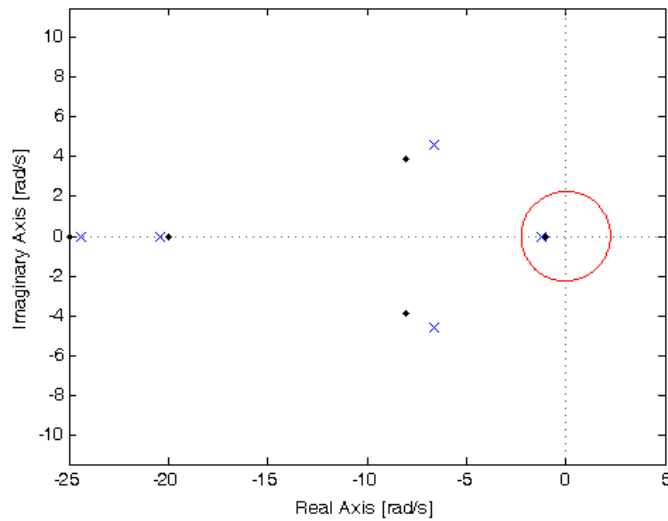


Figure 8.8 – Desired and actual closed loop lateral dynamics poles

8.1.1.7 Error angle controller design

The error angle controller must ensure that the error angle dynamics are timescale separated from the outer guidance dynamics. Thus, given that the velocity dynamics bandwidth will be 1 rad/s, the bandwidth of the error angle dynamics should be at least 5 rad/s. However, when considering the closed loop roll rate dynamics poles of equation (8.23), it is clear that in the case of the aerobatic aircraft, the roll rate dynamics will not be fully timescale separated from the error angle dynamics as required by the simplified, decoupled control law of section 6.3.1. To handle this problem, the coupled error angle control law of section 6.3.1.1 could be used instead to yield error angle dynamics that accurately match the desired dynamics. However, for the aerobatic aircraft example use of the simplified, decoupled controller will be illustrated, with candidate designs evaluated until satisfactory coupled closed loop poles are obtained.

After a small amount of iteration, setting the desired error angle dynamics pole to -3 rad/s yields the actual (with roll rate dynamics included) closed loop error angle dynamics shown in Figure 8.9. It is clear from the figure that the roll rate dynamics have resulted in some distortion of the error angle dynamics with the dominant error angle dynamics pole now being slightly faster at,

$$\text{Dominant: } p_1 = -5 \quad (8.36)$$

Thus the closed loop error angle dynamics will be sufficiently timescale separated from the guidance dynamics. Although the design method used was somewhat iterative, a satisfactory result was very quickly obtained.

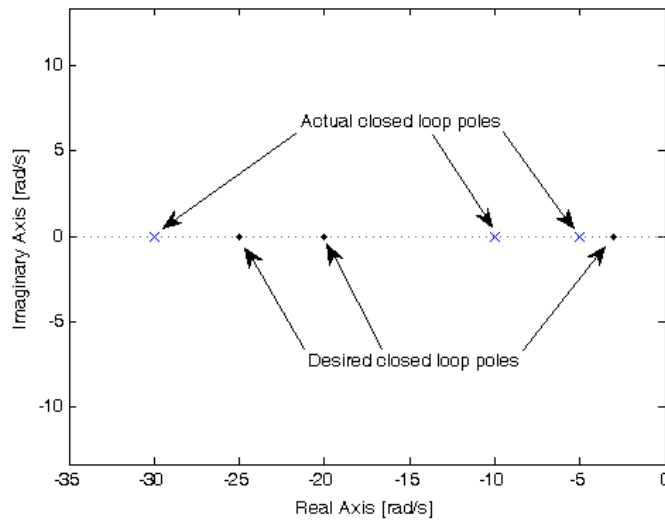


Figure 8.9 – Desired and actual closed loop error dynamics poles

8.1.1.8 Velocity and position controller designs

The guidance dynamics poles are selected at,

$$p_{1,2} = -0.5 \pm 0.2i \quad (8.37)$$

which translates into a desired characteristic equation of,

$$\alpha_c(s) = s^2 + s + 0.29 \quad (8.38)$$

With the poles selected as in equation (8.37) the velocity dynamics bandwidth will be 1 rad/s as specified in the design of the inner loop controllers.

8.1.2 Simulation

To verify the autopilot design of the previous subsection a full nonlinear simulation of the aerobatic aircraft in its six degree of freedom environment was set up. Section 8.1.2.1 investigates the actual and expected dynamic responses of the individual control loops and correlates any differences to the simplifying assumptions made during the specific controller design. Thereafter in section 8.1.2.2 the aircraft's tracking of a complex 3D reference trajectory is investigated and used to evaluate the performance of the autopilot as a whole.

8.1.2.1 Dynamic responses

Investigating the dynamic responses of the inner loop controllers within a complete six degree of freedom simulation environment is a challenging task. Due to the nature of the signals that these controller regulate (acceleration and angular velocity), kinematically dependent states such as velocity and position very quickly diverge from their trim values. Of course when the full autopilot is armed it is the responsibility of the outer loop guidance controllers to regulate

these states via the inner loop controllers. Of the outer kinematic states the most important to be aware of is the velocity magnitude since high rates of this variable would violate the timescale separation condition used in the design of the inner loop controllers.

Taking heed of the possible complication outlined above a simulation to test the inner loop dynamic responses was set up as follows. The simulation was begun with the aircraft trimmed for straight and level flight. With only the inner loop controllers armed a small step command was issued to one of the inner loop controllers. The simulation was concluded shortly after completion of the transient response before effects due to divergence of outer kinematic states could take effect. The simulation was then repeated until each inner loop controller had been stepped individually. The simulation results are presented in Figure 8.10 below. Note that the expected responses also plotted are the responses of the actual dynamics of the previous section and not the desired dynamics.

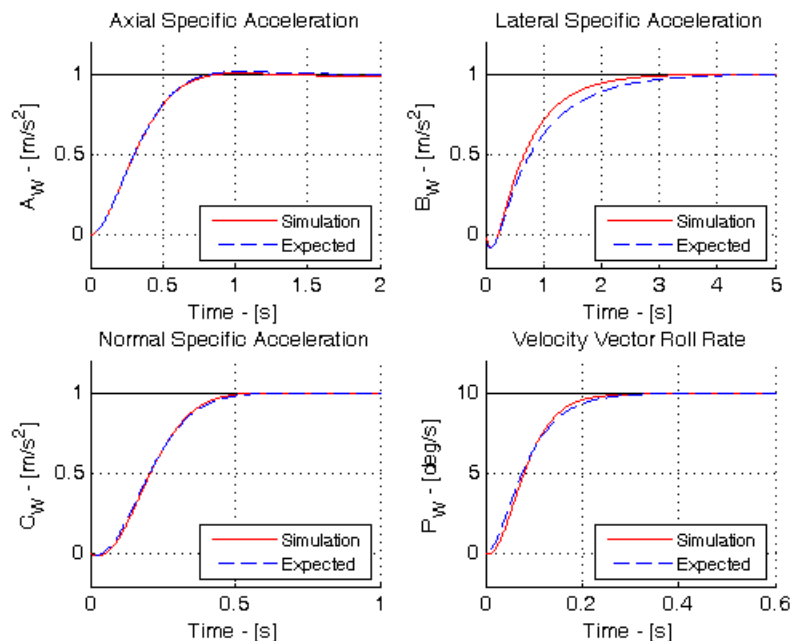


Figure 8.10 – Simulated and expected step responses of inner loop controllers

The results presented in Figure 8.10 verify the mathematics of the inner loop controllers. The axial specific acceleration, normal specific acceleration and velocity vector roll rate responses are almost identical to their expected responses. The actual lateral specific acceleration response shows a small reduction in damping when compared to the expected response. This damping reduction can most likely be attributed to finite roll-directional couplings and unaccounted for nonlinearities present in the six degree of freedom simulation.

To investigate the dynamic response of the error angle controller the aircraft was again set up to fly straight and level with all inner loop controllers armed. An artificial error angle offset was then injected directly into the controller thus causing it to respond in such a way so as to

reduce the error to zero. Introducing the error directly into the controller greatly simplified the dynamic response test since it avoided having to generate a series of valid normal specific acceleration unit vector commands. The simulation results are shown in Figure 8.11. It is clear from the results that the error angle controller is responding as designed.

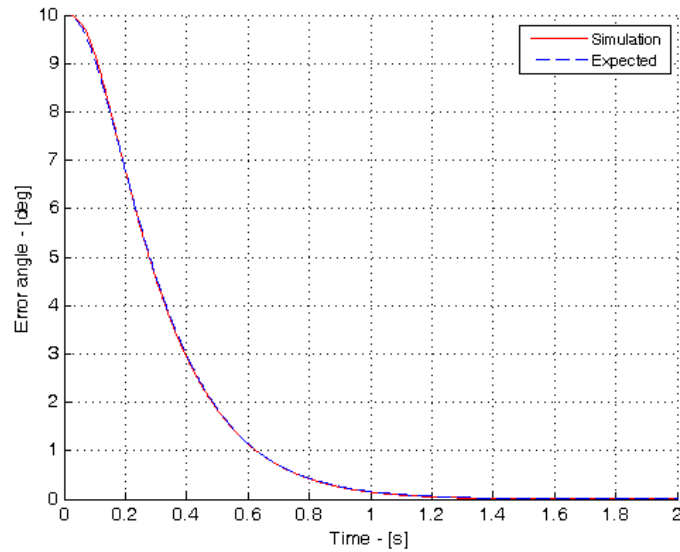


Figure 8.11 – Simulated and expected error angle response to a 10 degree error

To test the dynamic response of the inertially coordinated velocity controller, the simulation was again started with the aircraft flying straight and level north with all controllers except the position controllers armed. The velocity coordinates were then stepped individually to yield the results shown in Figure 8.12.

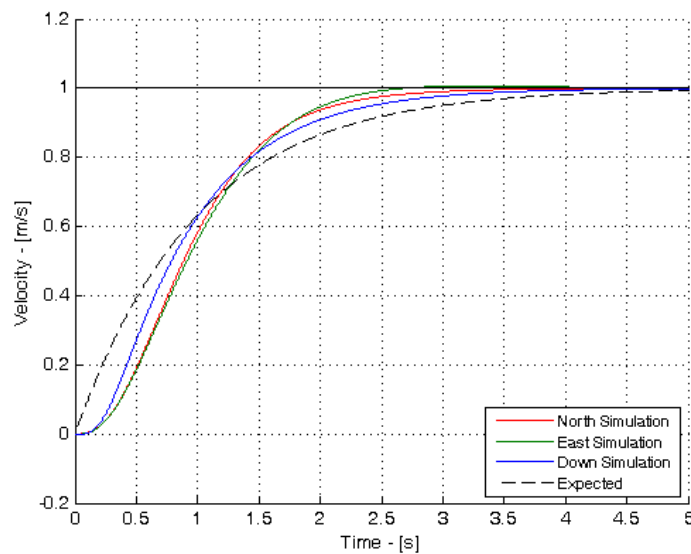


Figure 8.12 – Simulated and expected inertial velocity coordinate step responses

It is important to note that due to the architecture of the SAM guidance controller the dynamic

response of the velocity coordinates in inertial axes is dependent on the orientation of the aircraft relative to inertial space. This is clearly seen in the simulation results depicted in Figure 8.12. Considering the results, note firstly that all three responses closely match the desired dynamic response with the primary difference arising from the finite time responses of the inner loop controllers. Considering that the aircraft was set up to initially fly north, the north velocity response deterioration is due to the finite lag in the axial specific acceleration controller. The added lag in the east response arises primarily due to the finite bandwidth of the error angle and normal specific acceleration dynamics. The error angle dynamics are seen to be very similar to the closed loop axial specific acceleration dynamics thus explaining the similarity in the simulated north and east velocity responses. Finally, the added lag in the down velocity response is seen to be the smallest of the three. This is because with the initial aircraft orientation, the down velocity controller primarily makes use of the fast inner loop normal specific acceleration controller.

The position step responses were obtained in a similar manner to the velocity step responses above. Note that position steps are relative to where the aircraft should be on the reference trajectory at a particular point in time. In this case the reference trajectory was a straight line in the northerly direction with a reference velocity of 30 m/s. The simulation results are depicted in Figure 8.13. Note again the similarity between the expected and actual responses with the primary difference arising due to the finite bandwidth of the inner loop controllers. The difference between the north, east and down transient responses can be explained using the velocity step response arguments provided above.

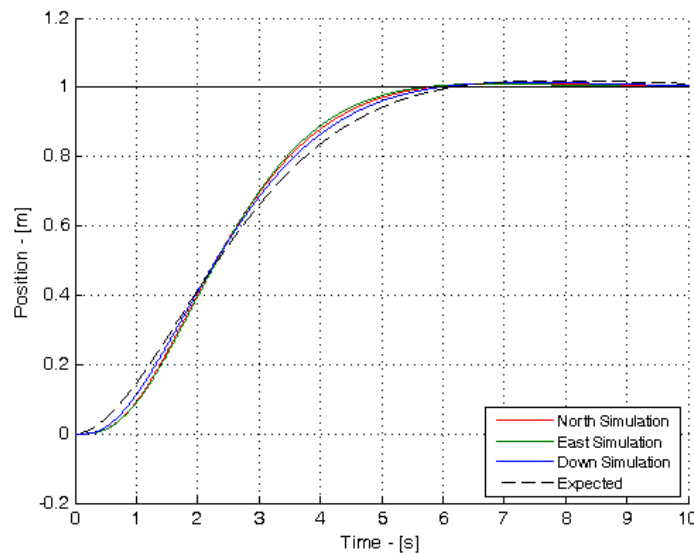


Figure 8.13 – Simulated and expected inertial position coordinate step responses

8.1.2.2 Reference trajectory flight

With the individual controller dynamic responses investigated and verified, this section

investigates the overall performance of the autopilot. To this end a full 3D flight reference trajectory was set up to demonstrate the manoeuvre flight capability of the autopilot. The reference trajectory is shown in Figure 8.14 and is described in point form below.

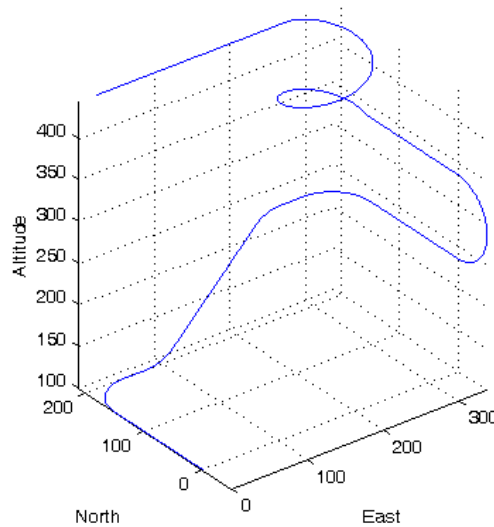


Figure 8.14 – Aerobatic aircraft reference trajectory

Reference trajectory description:

- The aircraft starts at 100 m altitude flying straight and level north with a velocity magnitude of 30 m/s.
- After 150 m the aircraft is commanded to turn east with a turn radius of 50 m. This turn radius corresponds to a steady state bank angle of just over 60 deg and consequently a normal specific acceleration of just over 2 g's.
- The aircraft then continues east for 30 m before it pulls up to a pitch angle of 45 deg with a pitching radius of 50 m. At the trim velocity this radius corresponds to a peak normal specific acceleration of 2.8 g's.
- The aircraft is then commanded to maintain the 45 deg climb at 30 m/s for 150 m before it is commanded to level out again with a downward pitching arc radius of 50 m.
- After flying a further 30 m straight and level the aircraft is commanded to fly south. The turn radius is again 50 m.
- The aircraft flies 150 m straight and level south before it is commanded to fly an Immelmann manoeuvre i.e. a 180 deg vertical arc with a barrel roll to revert back to non-inverted straight and level flight at the apex. The Immelmann arc radius is 50 m.
- The aircraft exits the Immelmann flying north and is commanded to maintain altitude and heading for a further 150 m.

- The aircraft is then commanded to pull up to a pitch angle of 15 deg and enter into a left handed horizontal spiral arc with a radius of 50 m. The pitch angle of 15 deg corresponds to a climb rate of just over 7.5 m/s during the arc.
- The aircraft is commanded to fly through one and a quarter horizontal spiral arc revolutions before levelling out again in a westerly direction.
- After flying 50 m straight and level west, the velocity magnitude is ramped up to 35 m/s over the next 75 m. This corresponds to an axial specific acceleration of a little over 2 m/s². The aircraft then holds this velocity for another 125 m before the simulation concludes.

Note that during the simulation the commanded thrust and commanded velocity vector roll rate were limited as follows,

$$T_c \in [0, 70] \text{ N} \quad (8.39)$$

$$P_w \in [-300, 300] \text{ deg/s} \quad (8.40)$$

The roll rate limit was imposed to avoid excessive roll rates during inversion manoeuvres. Furthermore, the normal specific acceleration lower limit used in section 6.3.2 to switch the guidance algorithm from roll-to-turn to skid-to-turn was set to,

$$\varepsilon = 2.5 \text{ m/s}^2 \quad (8.41)$$

In the case where direct lateral specific acceleration was used the autopilot was set to hold the current wind axis system normal unit vector direction.

The simulation results for the reference trajectory are displayed in Figures 8.15 to 8.18. Figure 8.15 plots the reference trajectory in 3D space together with the actual trajectory flown. The figure also includes time stamps to allow for easy comparison with the other figures. Figure 8.16 provides a plot of the difference between the actual and reference position and velocity coordinates in inertial axes over time. The commands issued to the inner loop controllers together with the actual inner loop signal responses are shown in Figure 8.17. Finally, the actuator command signals are shown in Figure 8.18.

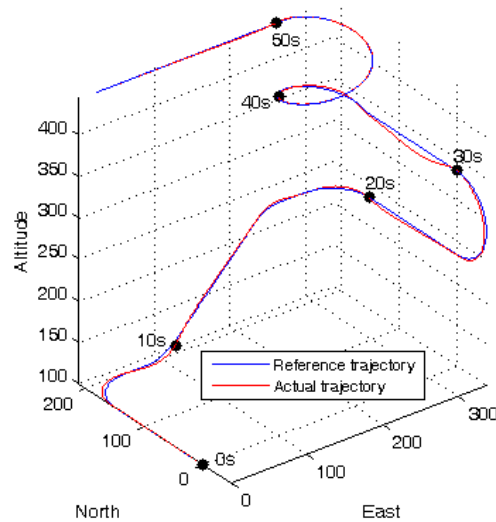


Figure 8.15 – Reference trajectory and actual trajectory flown

With reference to Figures 8.15 and 8.16, the aircraft is seen to track the reference trajectory well. The aircraft is never more than about 5 m in error of the trajectory along a particular inertial unit vector. Slight overshoots are visible at the start of each horizontal and vertical arc. This is due to the finite inner loop and error angle dynamics that are ignored by the SAM guidance controller. The slight divergence from the trajectory at the top of the Immelmann manoeuvre is due to the roll orientation inversion that takes place there. The aircraft is commanded to roll very quickly to a non-inverted flight state but due to bandwidth constraints the normal and lateral specific acceleration controllers are not able to respond quickly enough to result in a pure roll motion. As a result the aircraft loses altitude during the manoeuvre and is pulled to the left of the trajectory due to the clockwise roll rotation. Finally, note that the small finite roll rate offset produced by the feed-forward term in the error angle controller during the horizontal spiral arc allows the aircraft to perfectly track this section of the trajectory with only the proportional feedback error angle architecture. The small positive roll rate offset is visible in Figure 8.17.

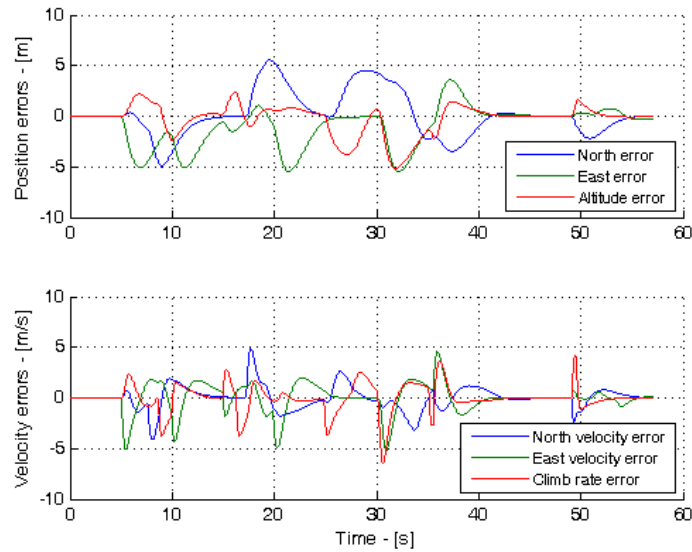


Figure 8.16 – Position and velocity errors relative to the reference trajectory

Considering Figure 8.17 further, it is clear that the inner loop signals track their commanded values as expected. The axial specific acceleration diverges from the commanded value slightly for significant negative specific acceleration commands. This is due to the lower thrust limit and the finite amount of drag in the system. For most of the reference trajectory the lateral specific acceleration command is set to zero to enforce coordinated flight. The actual lateral specific acceleration is seen to be constantly disturbed by coupling from the roll dynamics but is effectively driven back to zero by the controller. Note the small lateral specific acceleration command near the 10 s mark. This command is issued because the normal specific acceleration magnitude becomes less than ε in equation (8.41) thus placing the guidance controller into skid-to-turn mode. This situation again occurs very briefly close to the 50 s mark. The normal specific acceleration and roll rate are seen to track their commanded values very well. The roll rate command displays some sensitivity close to the 50 s mark where the normal specific acceleration is close to zero with the guidance controller just outside the zone where direct lateral specific accelerations are commanded. However, the roll command sensitivity is seen to be short lived and does not cause any appreciable deterioration to the aircraft's response.

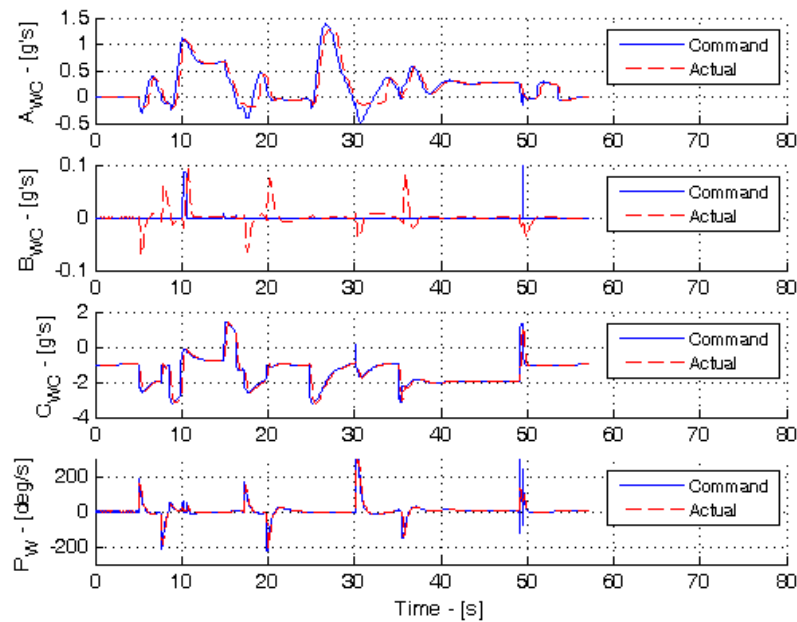


Figure 8.17 – Commanded and actual inner loop signals over the reference trajectory

Finally, Figure 8.18 illustrates the realistic nature of the actuator signals used over the reference trajectory. The thrust actuator does saturate against its upper and lower bounds a few times during the trajectory. However this situation is more a consequence of the highly aggressive reference trajectory than the underlying controller. The aerodynamic actuators are seen to be well within typical small angle limits. The aileron signal however can be reduced if desired by slowing the error angle controller and/or limiting the maximum roll rate commanded by the error angle controller.

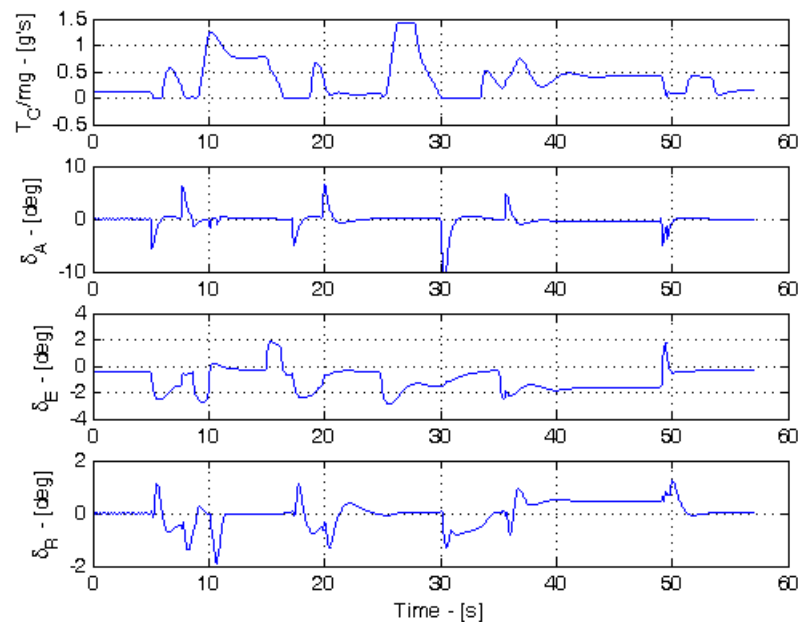


Figure 8.18 – Actuator signals over the reference trajectory

8.1.3 Comments

The results of the previous three subsections verify the design of the manoeuvre autopilot and illustrate clearly its potential for full 3D kinematic flight control. As intuitively expected, the aerobatic aircraft is seen to be well suited to the manoeuvre autopilot, having large feasible pole placement regions and satisfying all conditions required for implementation of the control laws.

8.2 Stabilisation and control of a variable stability aircraft

The variable stability aircraft is an electrically powered, blended-wing-body UAV. The aircraft, known as Sekwa and shown in Figure 8.19, was designed and built by the Council for Scientific and Industrial Research (CSIR) in South Africa and was optimised for minimum drag. As part of the design, the aircraft was equipped with the ability to slowly adjust its centre of mass in flight (the avionics and battery pack are shifted inside the aircraft using an electric motor), thereby providing an extra degree of longitudinal trim freedom. Consequently, the elevon control surfaces can be trimmed to their optimal aerodynamic efficiency positions for different flight conditions.

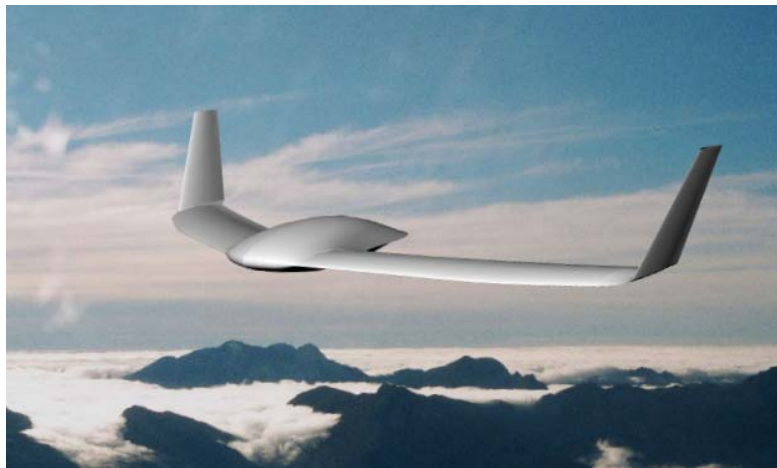


Figure 8.19 – Design diagram of Sekwa superimposed on a background

However, shifting the centre of mass also affects the static stability of the aircraft. The aerodynamically useful adjustable centre of mass range corresponds to varying the static stability of the aircraft from stable to significantly unstable. The task of the control system is thus first to restore the aircraft's static stability and then to regulate the aircraft's motion variables for autonomous flight. In this section it will be shown that the manoeuvre autopilot of this thesis provides a particularly elegant and effective solution to the variable stability stabilisation and flight control problem.

8.2.1 Application of the manoeuvre autopilot

This section applies the manoeuvre autopilot to the variable stability aircraft. Given that the

aircraft is to operate about the following trim velocity and air density,

$$\bar{V}_{nom} = 20 \text{ m/s} \quad (8.42)$$

$$\rho_{nom} = 1.0588 \text{ kg/m}^3 \quad (\text{Altitude of 1500m above sea level}) \quad (8.43)$$

the dimensional time variants of the inner loop controllers will be used. The focus of the application will be on the normal specific acceleration controller since the rest of the design is relatively standard. Feed-forward of the reference signal to cancel the closed loop integrator dynamics will also be illustrated in the normal specific acceleration controller design. Finally, note that the parameters for this aircraft were obtained from [48] and are summarised in Appendix C.

8.2.1.1 Axial specific acceleration controller design

Given the aircraft's minimum operating velocity magnitude of 15 m/s, its maximum normal specific acceleration magnitude of 3 g's and its minimum lift to drag ratio of 10, then for a desired return disturbance rejection of greater than 20 dB, the minimum closed loop axial specific acceleration bandwidth relative to the open loop thrust actuator bandwidth is,

$$\frac{\omega_n}{\omega_r} \geq 0.89 \quad (8.44)$$

The constraint above is easily satisfied by setting the closed loop axial specific acceleration bandwidth equal to the open loop thrust actuator bandwidth of 5 rad/s. With a conservative damping of 0.8 selected, the desired closed loop characteristic equation becomes,

$$\alpha_c(s) = s^2 + 8s + 25 \quad (8.45)$$

8.2.1.2 Normal specific acceleration controller design

The variable stability aircraft's normal dynamics will be a strong function of the centre of mass position. To provide initial insight into the normal dynamics, they are investigated with the centre of mass in its most forward position i.e. the aircraft in its most statically stable configuration. In this configuration, the standard aerodynamic assumption of equation (4.25) is easily satisfied with,

$$\left| \frac{L_Q}{m\bar{V}} \right| = 0.0323 \ll 1 \quad (31 \text{ times smaller}) \quad (8.46)$$

Since the lift due to pitch rate derivative will not be a strong function of the centre of mass position, and given how well the above constraint is satisfied, it will be assumed that it remains satisfied for all centre of mass positions. The actual and approximated open loop poles and zeros are listed below,

$$\text{Actual:} \quad p_{1,2} = -4.70 \pm 6.74i \quad z_{1,2} = -20.52, 19.20 \quad (8.47)$$

$$\text{Approximated:} \quad p_{1,2} = -4.70 \pm 6.86i \quad z_{1,2} = -20.51, 19.19 \quad (8.48)$$

with the associated NMP upper frequency bound,

$$\omega_n < 6.62 \quad (8.49)$$

Firstly, it is seen that the approximated poles and zeros very closely match the actual poles and zeros due to how strongly the constraint of equation (4.25) is satisfied. Secondly, note that the NMP upper frequency bound for this aircraft clamps the allowed normal specific acceleration bandwidth quite substantially. With a typical lower timescale separation frequency bound of 4 to 5 rad/s (depending on the desired velocity dynamics), the acceptable region for closed loop pole placement is somewhat limited. The low NMP frequency bound is due to the aircraft's exceptionally short effective length to the tail-plane as defined by equation (4.28). Finally, note that the open loop normal dynamics poles lie slightly outside the NMP upper frequency bound with a natural frequency of 8.22 rad/s. Thus it is expected that some distortion of the actual closed loop poles will occur during pole placement when the centre of mass is in its most forward position.

Consider now the effect on the open loop normal dynamics when the centre of mass is shifted rearward. As the static stability is reduced it is expected that the normal dynamics poles (the short period mode) will move towards the origin and break into a saddle point with the real, unstable pole describing the divergence dynamics of the aircraft. With reference to equation (4.32), the elevator to normal specific acceleration zeros are expected to move slightly further from the origin due to the shortening of the length to the neutral point as defined in equation (4.27). These results are verified in Figure 8.20. The figure illustrates the open loop elevator to normal specific acceleration poles and zeros (denoted by blue crosses and circles respectively) for nine different centre of mass positions. These nine centre of mass positions span the aircraft's entire allowable centre of mass range in increments of 2.5 mm. The centre of mass positions are measured relative to the stable flight configuration and thus 0 mm rearward corresponds to the most stable configuration and 20 mm rearward corresponds to the most unstable configuration.

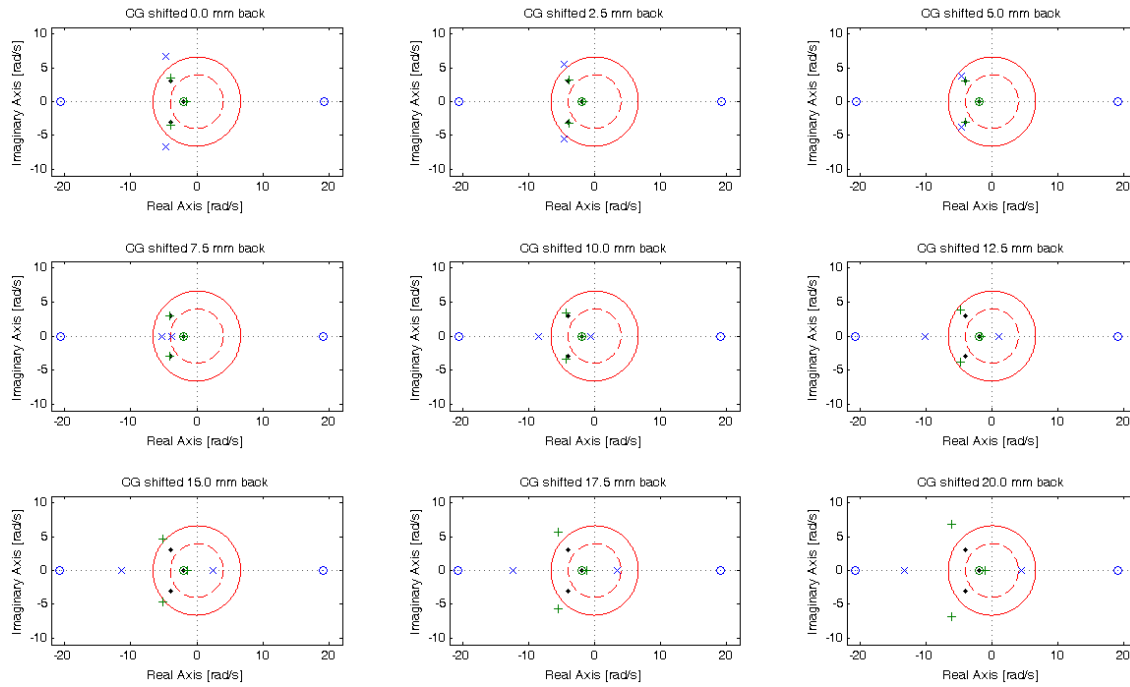


Figure 8.20 – Open loop poles and zeros, desired and actual closed loop poles, additional closed loop zero and upper and lower pole placement frequency bounds

Also shown in the figure is the NMP upper frequency bound (solid red line) and the lower timescale separation bound (dashed red line). The lower timescale separation bound has been set to 4 rad/s to allow for a velocity dynamics bandwidth of up to 0.8 rad/s. Finally, the figure also denotes the desired (black dot) and actual (green plus sign) closed loop poles and the additional closed loop integrator cancellation zero (green circle). The desired closed loop poles and additional zero have been set as follows,

$$\text{Desired CL: } p_{1,2,3} = -4 \pm 3i, -2 \quad z_1 = -2 \quad (8.50)$$

Note that the dominant closed loop poles have been set to lie within the frequency bounds with the dynamic effect of the slower integrator pole to be cancelled by the reference feed-forward induced zero.

Analysis of Figure 8.20 shows that for centre of mass position where the open loop poles lie within the NMP upper frequency bound constraint, there is little distortion in the placement of the closed loop poles. For centre of mass positions corresponding to very stable or very unstable flight, at least one of the open loop poles is seen to lie outside the NMP upper frequency bound and consequently there is significant distortion in the actual closed loop pole positions. The distortion in the two closed loop imaginary poles however is seen to have very little effect on their damping and thus the poles are still considered acceptable. Note however, that distortion to the slow closed loop integrator pole results in the feed-forward induced zero not perfectly cancelling the closed loop integrator dynamics. Thus, for very rearward centre of

mass positions it is expected that the effect of the slow integrator dynamics will start to become prominent in the closed loop normal specific acceleration response. Of course, the feed-forward gain could be appropriately adjusted to better cancel the closed loop integrator dynamics, but this level of fine adjustment is left for a more detailed application of the manoeuvre autopilot to the variable stability aircraft.

In conclusion, it is seen that the normal specific acceleration control law is capable of effectively stabilising the variable stability aircraft for all centre of mass positions. In its most unstable configuration the aircraft has an over 4 rad/s unstable divergence mode (time to double of less than 0.17 s) which is stabilised by the controller. It must be highlighted however that if the centre of mass position is to be changed in flight, then the bandwidth of this motion must be timescale separated from the normal specific acceleration dynamics for the control architecture to work. In the variable stability aircraft of this example this is most certainly the case. With the normal dynamics regulated by the normal specific acceleration controller, the aircraft will appear to outer loop guidance controllers as a stable, well regulated airframe and consequently will allow conventional outer loop controllers to be utilised. It is thus seen that the manoeuvre autopilot provides a particularly elegant solution to the variable stability stabilisation and flight control problem.

8.2.1.3 Analysis of the lateral dynamics

The lateral analysis and design for the variable stability aircraft will be handled very briefly. Note that it is assumed that the lateral dynamics remain invariant with centre of mass motion. Due to the very short distances that the centre of mass moves, this approximation is accurate as verified by [48]. The conditions of equations (5.4) to (5.7), (5.12) to (5.14) and (5.19) from section 5.1 are investigated below,

$$Y_p = -0.7396 \quad (8.51)$$

$$Y_{\delta_A} = -7.6993 \quad (8.52)$$

$$\left| \frac{Y_R}{m\bar{V}} \right| = 0.0130 \ll 1 \quad (77 \text{ times smaller}) \quad (8.53)$$

$$\left| \frac{\bar{C}_{n_p}}{\bar{C}_{l_p}} \right| = 0.0041 \ll 0.2066 = \left| \frac{\bar{C}_{n_R}}{\bar{C}_{l_R}} \right| \quad (50 \text{ times smaller}) \quad (8.54)$$

$$\left| \frac{\bar{C}_{n_p}}{\bar{C}_{l_p}} \right| = 0.0041 \ll 0.2747 = \left| \frac{\bar{C}_{n_\beta}}{\bar{C}_{l_\beta}} \right| \quad (67 \text{ times smaller}) \quad (8.55)$$

$$\left| \frac{\bar{C}_{n_p}}{\bar{C}_{l_p}} \right| = 0.0041 \ll 0.4509 = \left| \frac{\bar{C}_{n_{\delta_R}}}{\bar{C}_{l_{\delta_R}}} \right| \quad (109 \text{ times smaller}) \quad (8.56)$$

$$\left| \frac{\bar{C}_{n_{\delta_A}}}{\bar{C}_{l_{\delta_A}}} \right| = 0.0065 \ll 0.2066 = \left| \frac{\bar{C}_{n_R}}{\bar{C}_{l_R}} \right| \quad (32 \text{ times smaller}) \quad (8.57)$$

$$\left| \frac{\bar{C}_{n_{\delta_A}}}{\bar{C}_{l_{\delta_A}}} \right| = 0.0065 \ll 0.2747 = \left| \frac{\bar{C}_{n_{\beta}}}{\bar{C}_{l_{\beta}}} \right| \quad (42 \text{ times smaller}) \quad (8.58)$$

It should be noted that for the variable stability aircraft the side force due to roll rate and side force due to aileron deflection derivatives are in fact significant. This can largely be attributed to the aircraft's unconventional configuration. Although these larger than usual derivatives may suggest a coupled lateral controller design, the autopilot design will continue by neglecting these terms and any adverse effects will be noted in the simulation results. The actual open loop lateral dynamics poles are calculated to be,

$$\text{Actual OL: } p_{1,2,3} = -0.68 \pm 6.00i, -15.02 \quad (8.59)$$

8.2.1.4 Combined roll rate and error angle controller design

For the variable stability aircraft the error angle controller will be designed taking into account the roll rate dynamics. The combined design makes use of the feedback gains of equations (6.95) to (6.97). Given the approximated open loop roll rate dynamics,

$$\text{Approximated OL: } p_1 = -14.87 \quad (8.60)$$

and the lower timescale separation bound of 4 rad/s, the closed loop error angle poles are chosen as follows,

$$\text{Desired CL: } p_{1,2,3} = -4, -12 \pm 9i \quad (8.61)$$

The error angle dynamics will thus be dominated by the stable real pole at 4 rad/s. For controller feasibility reasons it is prudent to investigate the resultant inner loop roll rate dynamics given the desired error angle poles. Upon investigation it is found that the closed loop roll rate dynamics poles are at,

$$\text{Roll Rate CL: } p_{1,2} = -14.00 \pm 11.18i \quad (8.62)$$

Given the open loop roll rate bandwidth, these poles are practically feasible.

8.2.1.5 Lateral specific acceleration controller design

The actual and approximated open loop rudder to lateral specific acceleration poles and zeros lie at,

$$\text{Actual: } p_{1,2} = -0.75 \pm 5.97i \quad z_{1,2} = -1.64, 1.55 \quad (8.63)$$

$$\text{Approximated: } p_{1,2} = -0.75 \pm 6.01i \quad z_{1,2} = -1.64, 1.55 \quad (8.64)$$

The two degree of freedom pole placement variant of the directional stability augmentation controller is used for the variable stability aircraft. The stability augmented closed loop poles are selected at,

$$\text{Desired: } p_{1,2} = -6 \pm 2i \quad (8.65)$$

and result in the following actual closed loop poles,

$$\text{Actual: } p_{1,2} = -6.00 \pm 2.00i \quad (8.66)$$

To two decimal spaces the poles are seen to be exactly where desired. It is thus expected that the gain relationships of equations (5.71) and (5.72) will be well satisfied. Investigating these relationships yields the expected result,

$$\left| \frac{K_B}{K_R} \right| = 0.0231 \ll 30.5326 = \left| \frac{m}{Y_R} \frac{l_F}{l_D - l_F} \right| \quad (1320 \text{ times smaller}) \quad (8.67)$$

$$|K_R| = 0.36 \ll 30.28 = \left| \frac{m\bar{V}}{Y_{\delta_r}} \frac{l_w}{l_w - l_F} \right| \quad (83 \text{ times smaller}) \quad (8.68)$$

For the design of the outer regulation control law equation (5.59) is used to calculate the NMP upper frequency constraint below,

$$\omega_n < 0.53 \quad (8.69)$$

The strictness of this upper bound is due to the variable stability aircraft's unconventionally short effective length to the fin as defined in equation (5.57). Selecting the desired closed loop lateral specific acceleration regulation pole to be at -0.2 rad/s yields the final desired and actual closed loop directional dynamics poles,

$$\text{Desired: } p_{1,2,3} = -6 \pm 2i, -0.2 \quad (8.70)$$

$$\text{Actual: } p_{1,2,3} = -4.32 \pm 4.38i, -0.21 \quad (8.71)$$

Note again how the outer lateral specific acceleration regulation control law causes significant distortion to the stability augmented directional dynamics. This is due to the decoupled directional stability augmentation and regulation designs as discussed in section 5.3.2.

8.2.1.6 Velocity and position controller designs

Finally, the guidance dynamics poles are selected at,

$$p_{1,2} = -0.4 \pm 0.3i \quad (8.72)$$

These poles translate into velocity dynamics with a bandwidth of 0.8 rad/s, which in turn supports the 4 rad/s timescale separation bound used in the design of the inner loop controllers.

8.2.2 Simulation

To verify the autopilot design of the previous subsection and in particular the normal specific acceleration controller design, the dynamic responses of the various controllers are investigated in section 8.2.2.1. Then, in section 8.2.2.2, the variable stability autopilot is evaluated as a whole when the aircraft is made to fly a 3D reference trajectory while the centre of mass is slowly shifted from its most forward position to its most rearward position.

8.2.2.1 Dynamic responses

Figure 8.21 provides step response results of the four inner loop controllers when the aircraft has its centre of mass in its most forward position. It is clear from the figure that all controllers respond as expected with slight deviations due to ignored couplings and nonlinearities that are of course present in the six degree of freedom simulator. The small roll rate deviation from the expected response is most likely due to the greater than usual roll-directional coupling that exists in the variable stability aircraft due to its unconventional configuration.

It should be noted that in obtaining the step responses of Figure 8.21, the velocity magnitude was artificially held constant in the six degree of freedom simulator. This was done to avoid significant distortion of the lateral and normal specific acceleration responses. Due to the very long settle time of the lateral specific acceleration controller, the velocity magnitude can diverge significantly during its transient response and influence the step response dramatically. Similarly, the slow closed loop normal specific acceleration integrator dynamics that are not fully negated by the reference feed-forward term also begin to couple with the velocity dynamics when no guidance laws are in place and would consequently result in undue distortion of the step response.

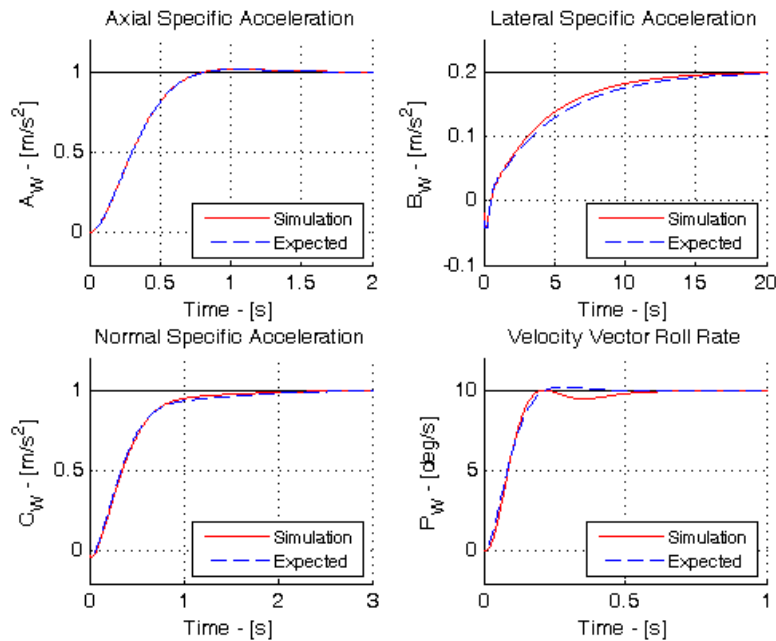


Figure 8.21 – Simulated and expected step responses of inner loop controllers with the centre of mass in its most forward position

Figure 8.22 investigates the normal specific acceleration response for different centre of mass positions. Analysing the results it is seen that as the centre of mass moves aft, the initial frequency of response increases slightly (i.e. the complex poles get slightly faster) but the slow integrator dynamics become more prominent. These results correlate well with the s-plane plots of Figure 8.20. The feed-forward controller gain could be adjusted to improve the dynamic responses, particularly when the centre of mass is 15 and 20 mm back from the nominal position. However, as previously argued this level of fine tuning will be omitted for this example application with the results of Figure 8.22 deemed acceptable.

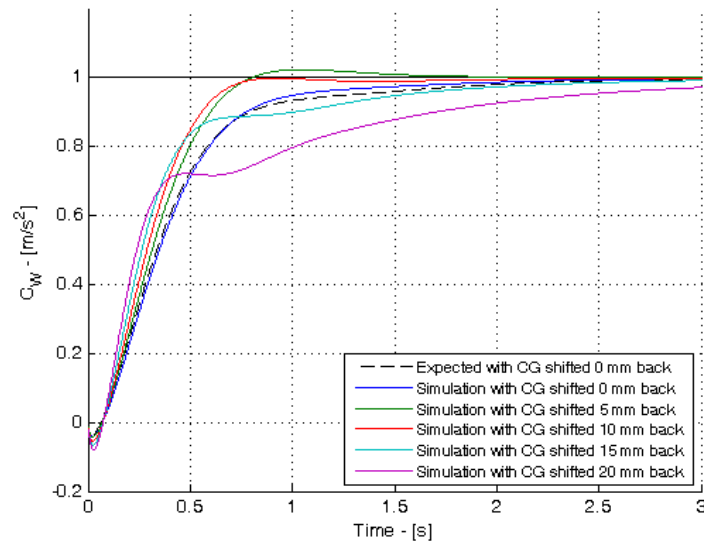


Figure 8.22 – Simulated step responses of the inner loop normal specific acceleration controller with the centre of mass in various positions

The error angle controller response is shown in Figure 8.23. The response is seen to match the expected response very well with slight differences arising due to the distortions in the roll rate response as seen in Figure 8.21.

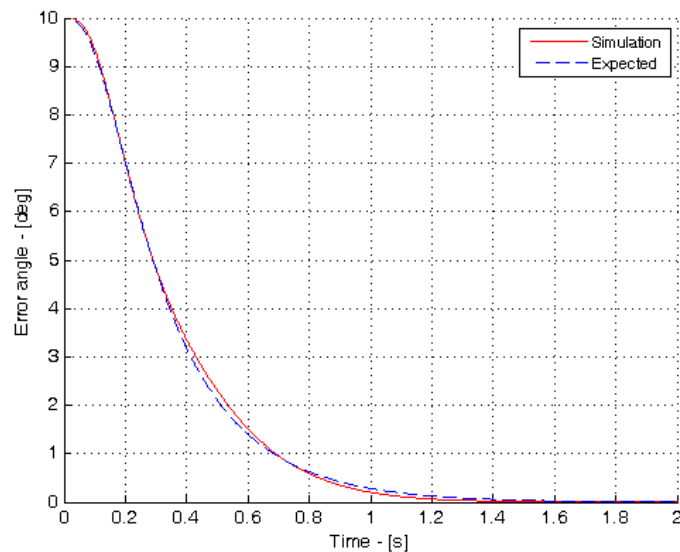


Figure 8.23 – Simulated and expected error angle response to a 10 degree error

The expected and actual north, east and down velocity and position step responses of the aircraft are shown in Figure 8.24. The simulation was set up with the aircraft flying straight and level north with the centre of mass in its most forward position. The responses match well with the general added lag and extra overshoot due to the finite bandwidths of the inner loop controllers. The slightly worse down response is most likely due to the ineffective cancellation

of the slow closed loop integrator dynamics present in the normal specific acceleration response. However, the result is still considered more than acceptable.

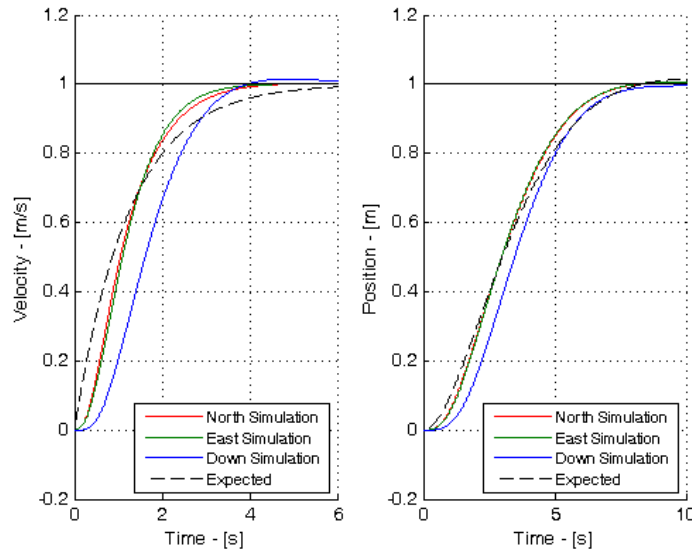


Figure 8.24 – Simulated and expected step responses of the velocity and position inertial coordinates

8.2.2.2 Reference trajectory flight

With the individual step responses investigated and verified, the aircraft is now commanded to fly the reference trajectory plotted in Figure 8.25 and described in point form below.

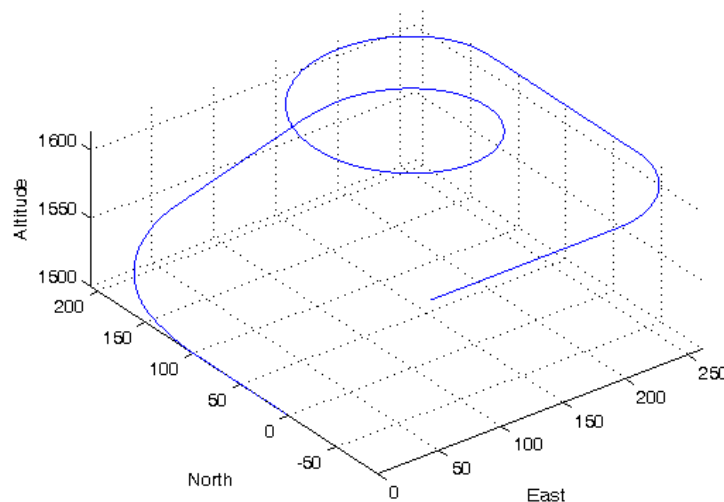


Figure 8.25 – Variable stability aircraft reference trajectory

Reference trajectory description:

- The aircraft starts at the origin of the north-east axis system, flying north with a velocity of 20 m/s and an altitude of 1500 m.

- After 100 m the aircraft is commanded to pull up to a pitch angle of 15 deg by flying an appropriate vertical arc with a radius of 150 m. The aircraft then enters into a horizontal spiral arc that turns it through 90 deg to leave it climbing at just over 5 m/s and flying east. The turn radius is 70 m which corresponds to a steady state straight and level flight bank angle of 30 deg.
- The aircraft then continues to climb and fly east for 100 m. It then reduces its pitch angle to 5 deg through an appropriate 150 m radius vertical arc and enters a 70 m radius horizontal spiral arc. The arc continues for one and a quarter revolutions before the aircraft levels out again by flying an appropriate 150 m radius vertical arc.
- With the aircraft now straight and level in a southerly direction, it is commanded to hold its course for a further 150 m. It is then commanded to turn right while maintaining speed and altitude until it is facing west. The turn radius is again 70 m. The trajectory is concluded with the aircraft flying west for a final 150 m.

Note that during the simulation the thrust command was limited as follows,

$$T_c \in [0, 20] \text{ N} \quad (8.73)$$

At the start of the simulation, the aircraft's centre of mass is in its most forward position. Over the course of the first minute of the simulation (the simulation is a little over one minute long), the centre of mass is shifted backwards to its most extreme point. The results of the simulation are shown in Figures 8.26 to 8.29.

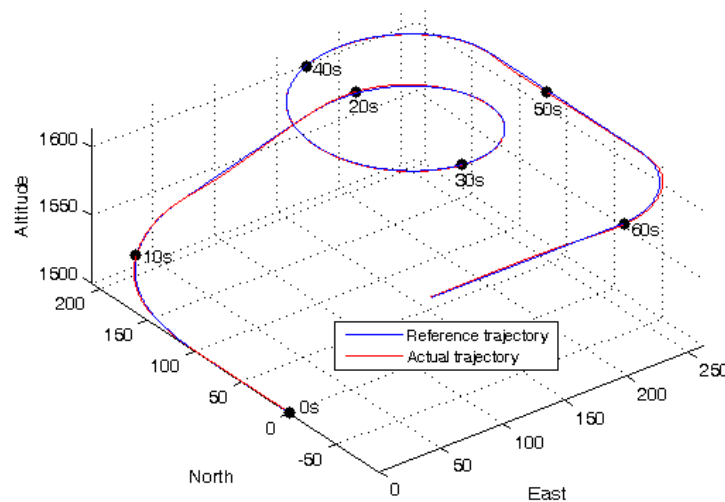


Figure 8.26 – Reference trajectory and actual trajectory flown

The 3D flight path of Figure 8.26 shows that the aircraft tracks the reference trajectory very well and shows no visible sign of the centre of mass even moving. The position and velocity tracking errors in Figure 8.27 verify this result with the position errors remaining within 3 m

along any inertial unit vector.

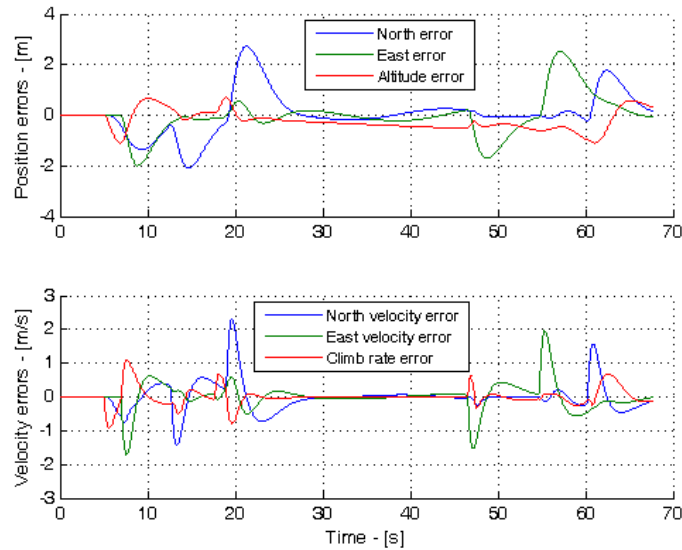


Figure 8.27 – Position and velocity errors relative to the reference trajectory

The commands to the inner loop controllers are seen to be well tracked in Figure 8.28. The small lateral specific accelerations induced by the roll rate controller are seen to be quickly damped by the inner loop directional stability augmentation controller with the slow lateral specific acceleration integrator dynamics only excited when a constant rudder command is required (such as during a steady turn).

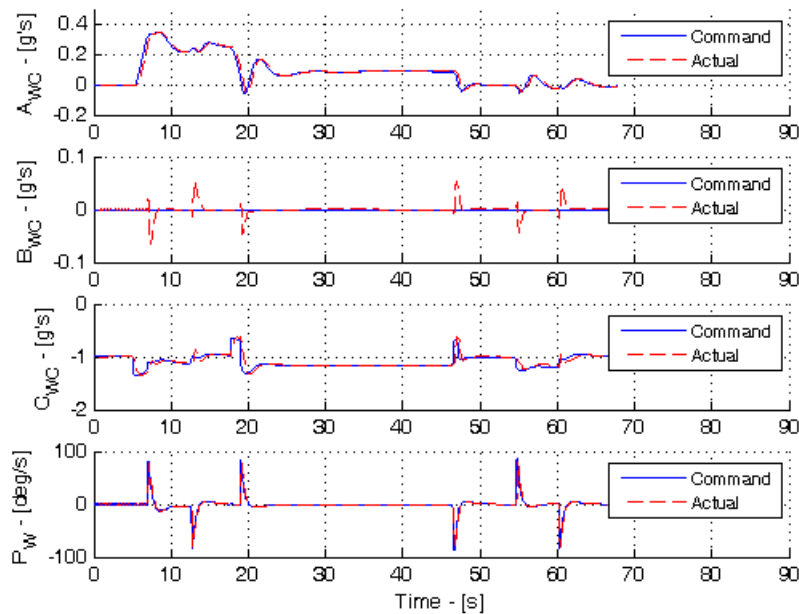


Figure 8.28 – Commanded and actual inner loop signals over the reference trajectory

The most telling of the simulation graphs is that of the elevator actuator signal in Figure 8.29.

The average elevator angle is seen to increase steadily (elevator moves downwards) over the first 60 s of the simulation while the centre of mass is shifted rearward. Also, in comparison to the elevator perturbation signals during the first 20 s of the simulation when the aircraft is still relatively stable, note the increased aggression in the elevator signal when the normal dynamics are excited with the aircraft in an unstable configuration (see just before the 50 s mark where the aircraft levels out after the horizontal spiral arc). The rest of the control signals are seen to behave normally and are well within typical bounds.

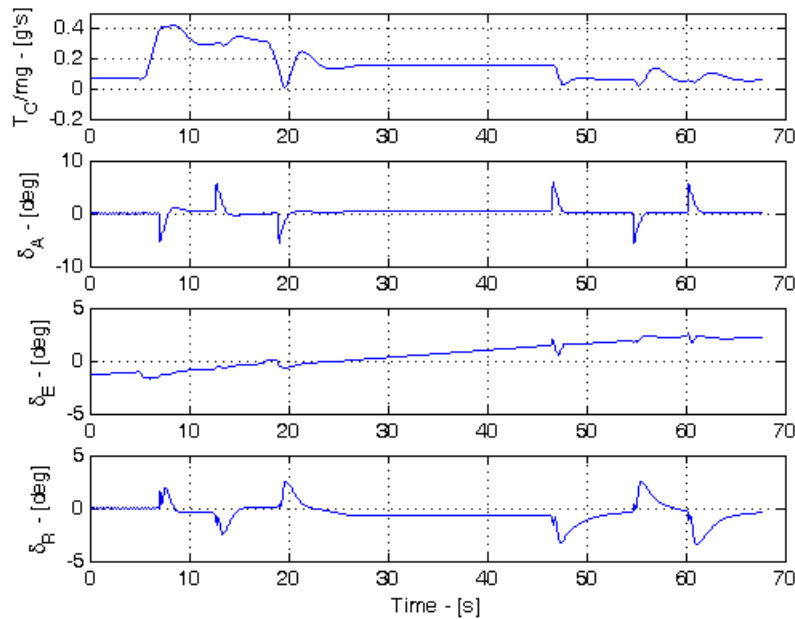


Figure 8.29 – Actuator signals over the reference trajectory

8.2.3 Comments

The simulation results of the previous section illustrate the ease and elegance with which the manoeuvre autopilot handles the variable stability stabilisation and flight control problem. The reference trajectory is seen to be flown without signs of the centre of mass even moving. In fact the only prominent visible sign that the centre of mass is actually moving to decrease the natural static stability of the aircraft is the elevator signal of Figure 8.29.

8.3 Transition control of a VTOL aircraft

As a final example the manoeuvre autopilot is applied to handle transition control of a Vertical Takeoff and Landing (VTOL) aircraft. The UAV, shown schematically in Figure 8.30, is a custom made tail-sitter aircraft with two electrically powered motors mounted on the wings and a number of aerodynamic control surfaces to allow for full control during both hover and forward flight. The aircraft model parameters were obtained from [16] and are restated in Appendix C for convenience.

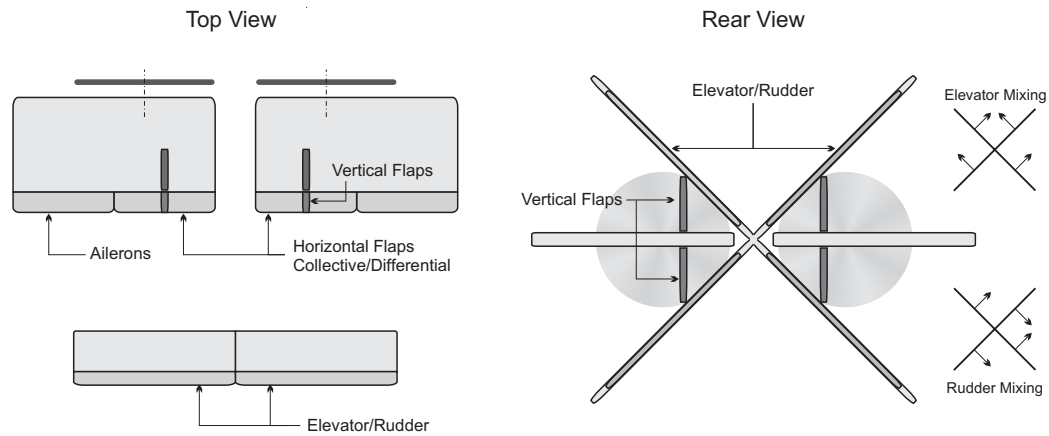


Figure 8.30 – Schematic diagram of the VTOL aircraft [16]

Broadly speaking, transition control involves guiding the aircraft from hover into forward flight and also from forward flight back to hover. Note that with the body axis system defined as for conventional aircraft, hover flight for the VTOL aircraft is equivalent to vertical flight. For the manoeuvre autopilot of this thesis to be applied to the transition control problem it is important that the transition trajectories satisfy the constraints of the autopilot. One of the constraints of importance to the transition trajectory is that the velocity magnitude should never become zero. At zero velocity magnitude the wind axis system becomes undefined, corresponding to a singularity in the control solution. Thus, to avoid this pitfall, it will be assumed that a hover and low speed flight controller is available to stabilise and guide the aircraft vertically up to speeds of 10 m/s. The transition controller thus need only guide the aircraft from this point forward and return it to this state for the transition system to be complete. A second point of concern during the transition trajectories is that of the incidence angles over the trajectories. To ensure that the incidence angles remain small as required by the autopilot (Chapter 3), vertical arc transition trajectories of sufficient radius will be used as in [16] to guide the aircraft from horizontal to vertical flight and back again.

8.3.1 Application of the manoeuvre autopilot

The example simulation will take place at sea level where the air density is,

$$\rho_{nom} = 1.225 \text{ kg/m}^3 \quad (8.74)$$

and the velocity magnitude range is limited to,

$$\bar{V} \in [10, 30] \text{ m/s} \quad (8.75)$$

Given that the forward flight trim velocity of the aircraft is 25 m/s, the transition control problem is one that involves considerable changes in velocity magnitude and consequently dynamic pressure. The VTOL aircraft transition control problem is thus well suited to the NNNT variants of the inner loop controllers. These controllers through their inherent

scheduling of the dimensional inner loop controller bandwidths will ensure the use of realistic actuator deflections throughout the transition manoeuvres. The sections that follow thus investigate the application of the NNDT variants of the inner loop controllers to the VTOL aircraft and show that these controllers can be used with the standard guidance controllers to effectively solve the transition control problem. It should be noted that for the purposes of simplifying the example application, propeller induced airflow effects over the aerodynamic surfaces will be ignored and instead it will be assumed that from 10 m/s onwards the airspeed over all of the actuators is equal to the velocity magnitude of the aircraft. Of course, a more detailed design could investigate adapting the inner loop dynamics slightly to cater for this effect and then use these new modified inner loop controllers to solve the transition control problem within the same manoeuvre autopilot architecture.

8.3.1.1 Axial specific acceleration controller design

Given the minimum operating velocity magnitude of 10 m/s, a maximum normal specific acceleration magnitude of 4 g's and a minimum lift to drag ratio of 10, then for a desired return disturbance rejection of at least 20 dB, the minimum axial specific acceleration closed loop bandwidth relative to the open loop thrust actuator bandwidth is calculated using equation (4.18) to be,

$$\frac{\omega_n}{\omega_r} \geq 1.40 \quad (8.76)$$

It can be seen that due to the very low minimum speed of the VTOL aircraft the constraint above is on the borderline of practical feasibility. However, the constraint is somewhat misleading for this application since at very low speeds the aircraft will be flying close to vertical. With close to vertical flight, the aircraft will have very small angles of attack and thus produce very small normal specific accelerations. The coupling of lift into drag with thus be small during this phase of flight simply because the amount of lift produced is small. Setting the desired bandwidth of the axial specific acceleration controller to 5 rad/s (1.2 times the open loop thrust actuator bandwidth) is thus expected to yield satisfactory, practically achievable results. The desired characteristic equation is thus made,

$$\alpha_c(s) = s^2 + 8s + 25 \quad (8.77)$$

8.3.1.2 NNDT normal specific acceleration controller design

The VTOL aircraft easily satisfies the standard aerodynamic assumption of equation (4.77) with,

$$\left| C_{L_q} \right| = 8.1626 \ll 139.3445 = \left| k_Q \right| \quad (17 \text{ times smaller}) \quad (8.78)$$

As a result, the NNDT pole and zero approximation equations of section 4.2.6 are expected to

yield good results. This is verified by the actual and approximated open loop poles and elevator to normal specific acceleration zeros listed below,

$$\text{Actual:} \quad p'_{1,2} = -7.68 \pm 17.26i \quad z'_{1,2} = -27.27, 33.47 \quad (8.79)$$

$$\text{Approximated:} \quad p'_{1,2} = -7.68 \pm 17.81i \quad z'_{1,2} = -27.11, 33.32 \quad (8.80)$$

with the NMP upper frequency bound constraint below,

$$\omega'_n < 10.07 \quad (8.81)$$

Note that the zeros and frequency bound above are for the case where only the elevator control surface is used (mixed using the four flaps on the tail structure as denoted in Figure 8.30). Considering the results it is noted that the open loop normal dynamics poles lie sufficiently far outside the NMP bound (at 18.32) to result in significant inaccuracies in the NNMT pole placement algorithm. This situation suggests that the aircraft's centre of mass is placed too far forward and that its natural flying qualities will be poor i.e. its actuation from the elevator will appear significantly lagged with visible undershoot effects. To solve this problem without changing the centre of mass position, the elevator control surface is combined with the horizontal flaps on the wing section to form a new virtual elevator actuator with more desirable control characteristics. The mixing is done such that the horizontal flaps, which produce very little pitching moment, deflect in the opposite direction to the primary elevator surface on the tail structure to increase the effective normalised length to the tail-plane as defined in equation (4.81). Increasing the effective normalised length to the tail-plane is shown in equation (4.83) to drive the zeros further from the origin and thereby increase the NMP upper frequency bound constraint. With this mixing strategy implemented with a mixing ratio magnitude of 1, the new normal dynamics zeros lie at,

$$\text{Actual:} \quad z'_{1,2} = -38.42, 68.85 \quad (8.82)$$

$$\text{Approximated:} \quad z'_{1,2} = -36.22, 66.65 \quad (8.83)$$

with the NMP upper frequency bound constraint,

$$\omega'_n < 17.14 \quad (8.84)$$

It can be seen that the open loop poles now lie only slightly outside the NMP frequency bound, but are deemed close enough to cause only a small amount of distortion to the closed loop poles. Selecting the desired poles in the NNMT frequency plane to be,

$$\text{Desired CL:} \quad p'_{1,2,3} = -10 \pm 10i, -14 \quad (8.85)$$

and applying the control algorithm of section 4.2.6 yields the actual closed loop poles,

$$\text{Actual CL: } p'_{1,2,3} = -11.56 \pm 10.28i, -10.49 \quad (8.86)$$

As expected, the actual closed loop poles have deviated somewhat from their desired positions but are still considered acceptable as a design.

With the closed loop poles fixed in the NNDT frequency plane, it is important for lower bound timescale separation reasons to investigate the equivalent dimensional poles for various dynamic pressures. Given that the altitude variations in this example are small, this amounts to investigating the corresponding dimensional dynamics for various velocity magnitudes. It is straightforward to convert the NNDT control law to its dimensional equivalent by substituting the definitions of the normalised state, output and control variables into the NNDT control law and matching the result with the dimensional control law. The dimensional control law can then be applied to the dimensional system to yield the corresponding dimensional poles for a particular velocity magnitude. Figure 8.31 provides a plot of the closed loop dimensional poles corresponding to a range of velocity magnitudes of interest. Also shown in each plot is the corresponding dimensional NMP upper frequency bound (red circle) and a lower timescale separation frequency bound of 4 rad/s (green dashed circle). The timescale separation bound corresponds to a maximum velocity magnitude bandwidth of 0.8 rad/s.

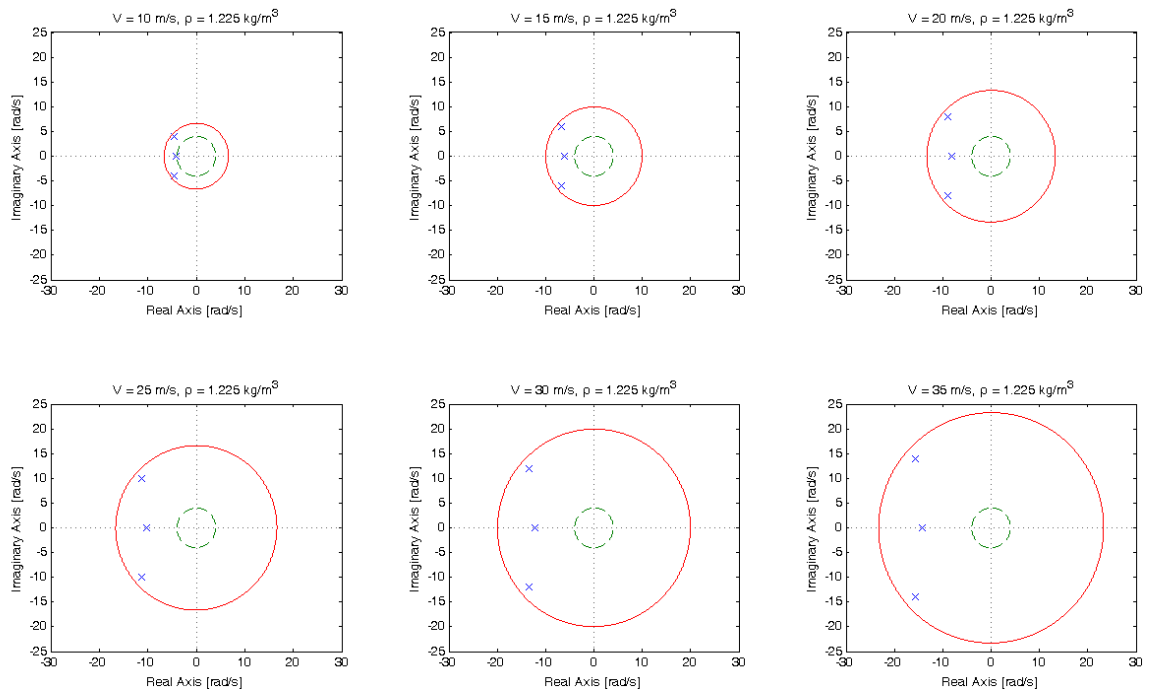


Figure 8.31 – Corresponding dimensional normal dynamics poles for various velocities

Note how with fixed NNDT poles, the bandwidth of the dimensional system is scheduled with velocity magnitude. At 10 m/s the closed loop poles only just satisfy the lower timescale separation bound while at the trim velocity of 25 m/s they satisfy it with ease. It is thus clear that the NNDT normal specific acceleration controller design will work effectively with

dynamically invariant guidance controllers of an appropriate bandwidth over the velocity magnitude range of interest.

8.3.1.3 Analysis of the lateral dynamics

To test whether the lateral dynamics will decouple into roll and directional dynamics, the conditions of equations (5.4) to (5.7), (5.12) to (5.14) and (5.19) from section 5.1 are applied to the VTOL aircraft below,

$$C_{Y_p} = 0.2557 \approx 0 \quad (8.87)$$

$$C_{Y_{\delta_A}} = 0.0009 \approx 0 \quad (8.88)$$

$$\left| C_{Y_r} \right| = 1.1875 \ll 32.8392 = \left| k_R \right| \quad (28 \text{ times smaller}) \quad (8.89)$$

$$\left| \frac{\bar{C}_{n_p}}{\bar{C}_{l_p}} \right| = 0.1049 \ll 3.2329 = \left| \frac{\bar{C}_{n_r}}{\bar{C}_{l_r}} \right| \quad (31 \text{ times smaller}) \quad (8.90)$$

$$\left| \frac{\bar{C}_{n_p}}{\bar{C}_{l_p}} \right| = 0.1049 \ll 110.3488 = \left| \frac{\bar{C}_{n_\beta}}{\bar{C}_{l_\beta}} \right| \quad (1052 \text{ times smaller}) \quad (8.91)$$

$$\left| \frac{\bar{C}_{n_p}}{\bar{C}_{l_p}} \right| = 0.1049 \ll 9.4756 = \left| \frac{\bar{C}_{n_{\delta_R}}}{\bar{C}_{l_{\delta_R}}} \right| \quad (90 \text{ times smaller}) \quad (8.92)$$

$$\left| \frac{\bar{C}_{n_{\delta_A}}}{\bar{C}_{l_{\delta_A}}} \right| = 0.0848 \ll 3.2329 = \left| \frac{\bar{C}_{n_r}}{\bar{C}_{l_r}} \right| \quad (38 \text{ times smaller}) \quad (8.93)$$

$$\left| \frac{\bar{C}_{n_{\delta_A}}}{\bar{C}_{l_{\delta_A}}} \right| = 0.0848 \ll 110.3488 = \left| \frac{\bar{C}_{n_\beta}}{\bar{C}_{l_\beta}} \right| \quad (1301 \text{ times smaller}) \quad (8.94)$$

In equation (8.88) it is clear that the side force due to aileron deflection is negligible for this aircraft. However similarly to the variable stability aircraft of section 8.2, the side force due to roll rate is unconventionally large. This is due to the abnormally large amount of vertical surface area present on the aircraft as a result of the cruciform tail and vertical flaps. At the trim velocity of 25 m/s, a roll rate of 90 deg/s would result in a lateral specific acceleration disturbance of 0.3 m/s². Although significant, this disturbance should quickly be damped by the lateral specific acceleration control system and as a result, its effect will be neglected for now and investigated in the simulations to follow.

8.3.1.4 NNDT roll rate controller design

With reference to section 5.2.3, when working with the decoupled roll rate system the actual and approximated dynamics are equivalent. The actual (and approximated) open loop NNDT roll rate dynamics are thus seen to be,

$$\text{Actual OL: } p'_1 = -8.20 \quad (8.95)$$

The desired closed loop roll rate dynamics poles are selected at,

$$\text{Desired CL: } p'_{1,2} = -10 \pm 5i \quad (8.96)$$

in the NNDT frequency plane. Figure 8.32 shows the results of an investigation of the corresponding dimensional time poles for various velocity magnitudes. Also plotted in the figure is the lower timescale separation frequency bound of 4 rad/s used in Figure 8.31. The results motivate the selection of the desired closed loop poles since it is seen that even at the lowest velocity of 10 m/s the dimensional time frequency bound to the guidance controllers is still satisfied.

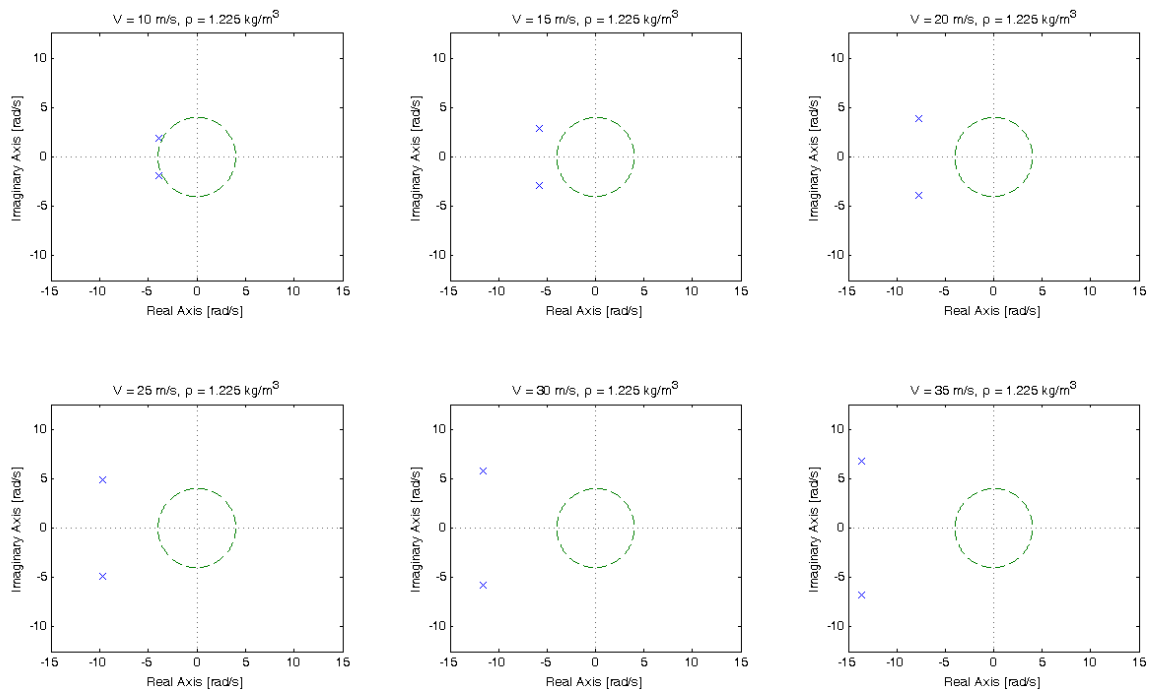


Figure 8.32 – Corresponding dimensional roll dynamics poles for various velocities

It should be noted however that with the architecture of the SAM guidance controller, a timescale separation also need exist between the roll rate and error angle dynamics which in turn need to be timescale separated from the guidance dynamics. It is thus clear that with the current selection of closed loop roll rate poles there will be significant coupling between the roll rate, error angle and guidance controllers when operating at low velocity magnitudes. One solution to this problem is to significantly increase the bandwidth of the NNDT roll rate controller. However, considering the open loop NNDT roll rate dynamics, the poles are already being moved a fair distance and it is expected that a further significant increase in the roll dynamics bandwidth will result in an impractical design with infeasible aileron commands. A second more practical solution is to keep the current roll rate controller design

and ensure that at low velocities the aircraft guides itself laterally using direct lateral specific acceleration. Intuitively this is how the aircraft should be controlled at low speeds with roll-to-turn control only being implemented at higher velocities when the aircraft is flying in a conventional manner. This concept will be further investigated in the sections to come.

8.3.1.5 NNDT lateral specific acceleration controller design

The actual and approximated directional dynamics poles and zeros are listed below,

$$\text{Actual:} \quad p'_{1,2} = -2.36 \pm 11.56i \quad z'_{1,2} = -6.90, 7.99 \quad (8.97)$$

$$\text{Approximated:} \quad p'_{1,2} = -2.36 \pm 11.77i \quad z'_{1,2} = -6.88, 7.97 \quad (8.98)$$

with the following NMP upper frequency bound,

$$\omega'_n < 2.48 \quad (8.99)$$

The zeros and the corresponding frequency bound listed above are for the case where only the rudder control surface is used (mixed using the four flaps on the tail structure as shown in Figure 8.30). Converting the frequency bound to its dimensional equivalent at a velocity magnitude of 10 m/s using equation (6.139) yields the result,

$$\omega_n = \frac{qS}{mV} \omega'_n < 0.96 \quad (8.100)$$

It is thus clear that if direct lateral specific acceleration is to be used for guidance at low velocities then the upper frequency bound constraint of equation (8.99) needs to be increased significantly through actuator mixing. This can be done by employing a similar actuation strategy to that employed in the normal specific acceleration controller design. Appropriately combining the rudder control surface with the vertical flaps on the wing section will result in a new virtual rudder actuator with more desirable characteristics. The mixing of the actuators is done such that the vertical flaps, which produce very little yaw moment, deflect in the opposite direction to the primary rudder surface on the tail structure to increase the effective normalised length to the fin as defined in equation (5.103). Increasing the effective normalised length to the fin is show by equation (5.105) to drive the zeros further from the origin and thereby increase the NMP upper frequency bound constraint. With this mixing strategy implemented with a mixing ratio magnitude of 2.5, the new directional dynamics zeros lie at,

$$\text{Actual:} \quad z'_{1,2} = -19.23, 32.17 \quad (8.101)$$

$$\text{Approximated:} \quad z'_{1,2} = -18.40, 31.34 \quad (8.102)$$

with NMP upper frequency bound constraint,

$$\omega'_n < 8.29 \quad (8.103)$$

Note that the lateral decoupling condition of equation (5.19) will be affected by the change in the effective length to the fin. However the change in the effective length to the fin will only strengthen how well the condition is satisfied.

With the mixed rudder actuation in place the two degree of freedom pole placement stability augmentation control law of equations (5.109) and (5.110) is used. The two degree of freedom pole placement strategy is chosen because it allows the natural frequency of the open loop directional dynamics poles to be increased. This is desirable since if the outer lateral specific acceleration regulation controller is to have a bandwidth close to that of the upper NMP frequency bound (for timescale separation reasons at low velocity magnitudes) then the augmented directional dynamics bandwidth should be somewhat higher than the NMP bound to limit the distortion to the closed loop poles. The desired stability augmented NNDT directional dynamics poles are chosen at,

$$\text{Desired: } p'_{1,2} = -15 \pm 10i \quad (8.104)$$

For the stability augmentation control law of section 5.3.4 to be implemented the gain relationships of equations (5.111) and (5.112) must be satisfied. Investigating these gain constraints with the feedback gains calculated using the desired poles of equation (8.104) yields,

$$\left| \frac{K'_B}{K'_R} \right| = 0.1326 \ll 1.0372 = \left| \frac{1}{C_{y_R}} \frac{l'_F}{l'_D - l'_F} \right| \quad (8 \text{ times smaller}) \quad (8.105)$$

$$\left| K'_R \right| = 6.3306 \ll 32.1572 = \left| \frac{1}{k_R C_{y_{\delta_R}}} \frac{l'_W}{l'_W - l'_F} \right| \quad (5 \text{ times smaller}) \quad (8.106)$$

Due to the significant change in frequency of the closed loop poles relative to the open loop poles, it is seen that the constraints are marginally satisfied. Thus, it is expected that the actual closed loop poles will display some distortion. Investigating the actual closed loop poles yields,

$$\text{Actual: } p'_{1,2} = -16.54 \pm 8.96i \quad (8.107)$$

Although there is some distortion to the poles, it is not considered significant enough to warrant a redesign. Continuing with the control system design, after some iteration the desired lateral specific acceleration regulation control law pole is selected at -5 which results in the following desired and actual closed loop directional dynamics poles,

$$\text{Desired: } p'_{1,2,3} = -15 \pm 10i, -5 \quad (8.108)$$

$$\text{Actual: } p'_{1,2,3} = -11.44 \pm 9.14i, -7.57 \quad (8.109)$$

It is clear that there has been some coupling between the closed loop stability augmentation poles and the lateral specific acceleration regulation pole. However, the actual closed loop poles are considered acceptable with the lateral specific acceleration regulation pole still within the NMP upper frequency bound.

Figure 8.33 shows the dimensional directional dynamics poles corresponding to the NNDT design. Also shown in each plot is the corresponding dimensional NMP upper frequency bound (red circle) and a lower timescale separation frequency bound of 4 rad/s (green dashed circle). It is seen that in all cases except the 10 m/s case, the dominant closed loop directional dynamics satisfy both the dimensional timescale separation and NMP frequency bounds. At 10 m/s, the design only just fails to meet the lower timescale separation frequency constraint. The effect of this will be to cause slightly more overshoot than expected in the guidance controllers. However, the overall influence is expected to be negligible and the design is considered satisfactory.

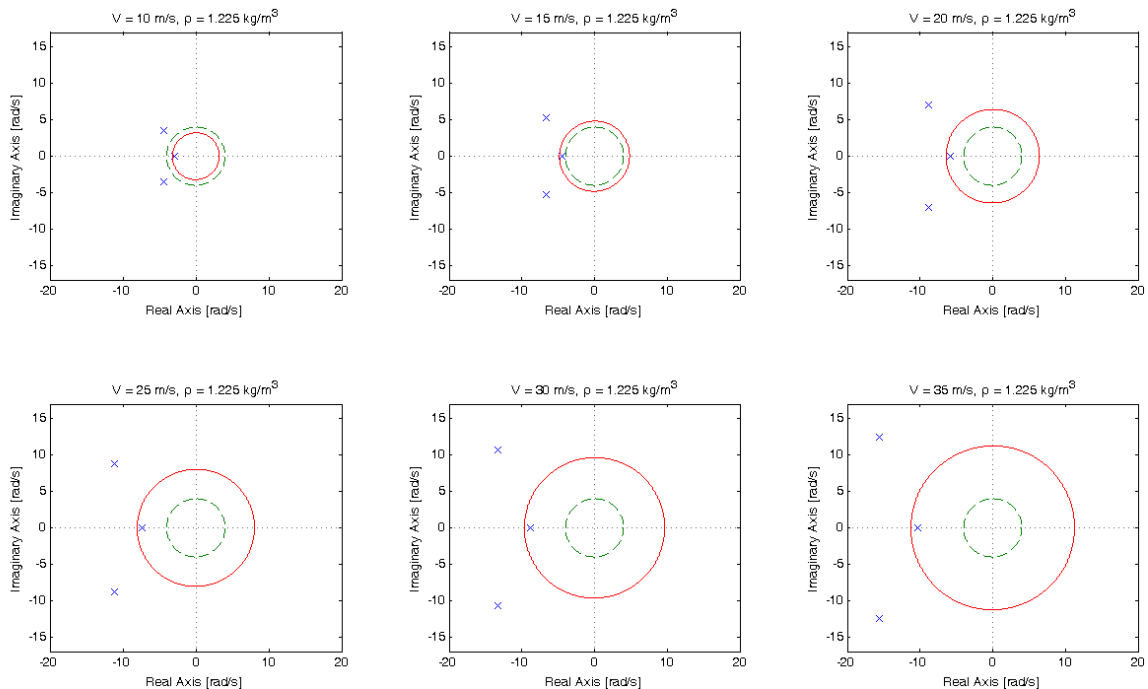


Figure 8.33 – Corresponding dimensional directional dynamics poles for various velocities

8.3.1.6 Error angle controller design

The simplified, decoupled error angle controller design of section 6.3.1 will be used for the VTOL aircraft. As previously mentioned, at low velocities there is expected to be very large amounts of coupling between the roll rate dynamics and the error angle dynamics. However, roll-to-turn control will only be used at higher velocities where the roll rate dynamics will be sufficiently decoupled from the desired error angle dynamics to allow for a decoupled design.

In the knowledge that the roll rate coupling will tend to increase the error angle dynamics bandwidth (as was seen in Figure 8.9), the desired error angle dynamics pole is selected at,

$$\text{Desired: } p_1 = -2 \quad (8.110)$$

8.3.1.7 Velocity and position controller designs

The guidance dynamics poles are selected at,

$$p_{1,2} = -0.4 \pm 0.4i \quad (8.111)$$

With the poles above, the velocity dynamics bandwidth will be 0.8 rad/s which justifies the 4 rad/s timescale separation frequency bound used in Figures 8.31 to 8.33.

8.3.2 Simulation

To verify the autopilot design of the previous subsection the dynamic responses of the inner loop NNDT controllers is investigated together with the dynamic response of the guidance controllers. Thereafter, a simulation involving flight transitions is set up to evaluate the overall performance of the autopilot.

8.3.2.1 Dynamic responses

Figure 8.34 provides step response plots of the NNDT inner loop normal specific acceleration, lateral specific acceleration and roll rate controllers for three largely different velocity magnitudes. The top row of the figure plots the step responses in dimensional time i.e. how they would be experienced by the outer guidance loops, while the bottom row of the figure plots the inherent NNDT response of the controller. Also plotted on the bottom row are the expected NNDT responses of each controller. Note that the amplitude of the NNDT plots has not been normalised to allow for easy comparison with the dimensional plots. Also note that in obtaining the step responses of Figure 8.34, the velocity magnitude was artificially held constant in the six degree of freedom simulator so as not to distort the dimensional time responses through attitude induced changes to the velocity magnitude.

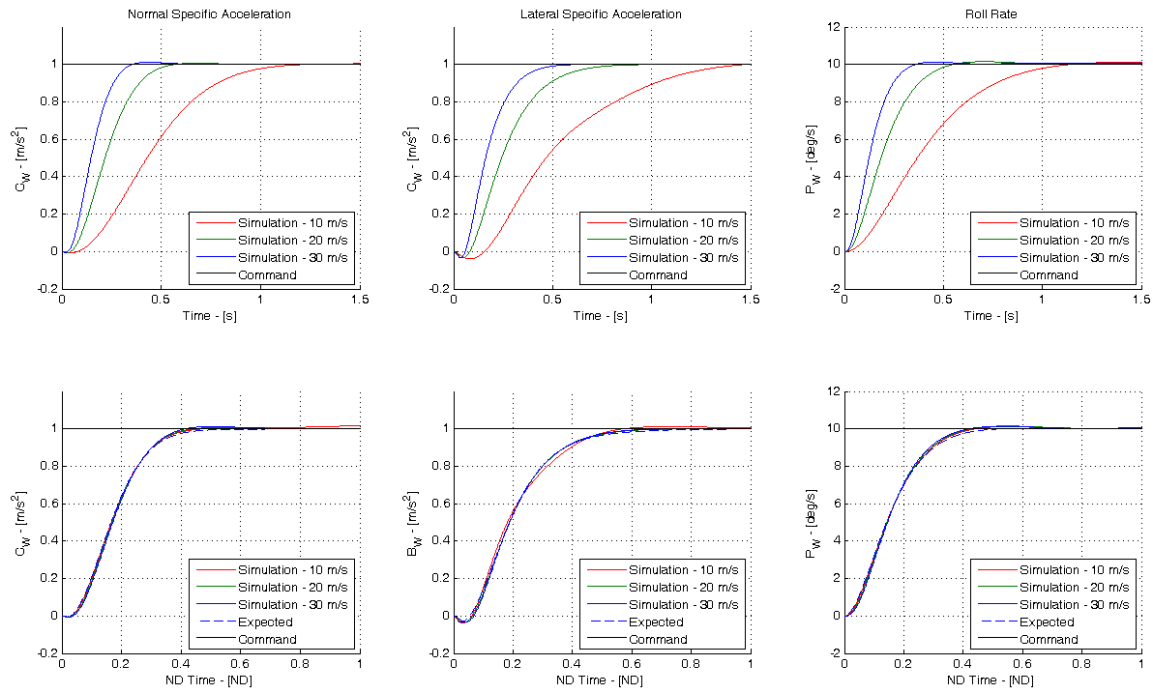


Figure 8.34 – Simulated and expected step responses of the NNDT inner loop controllers with corresponding dimensional time responses

The step response results of Figure 8.34 support the results of Figures 8.31 to 8.33 and again reveal how a fixed dynamic response in non-dimensional time corresponds to an appropriately varying dynamic response in dimensional time. When the velocity magnitude is low, the dimensional time responses are slow and will thus tend not to cause actuator saturation. When the velocity magnitude is high, the dimensional time responses increase accordingly and will tend to result in similar levels of actuator signals as they did at the low velocity. The corresponding non-dimensional time responses however remain invariant with velocity magnitude and are seen to match the expected responses very well, thus verifying the designs of the previous section.

Figures 8.35 and 8.36 show step response plots of the north, east and down inertial velocity and position coordinates at three largely different velocities. The difference between the two figures is that roll-to-turn was employed in the generation of Figure 8.35 while skid-to-turn (or direct lateral specific acceleration) was employed in generating Figure 8.36. The simulations were run with the aircraft initially flying straight and level north. Thus, north step responses will tend to use the axial specific acceleration controller, east step responses will tend to use the roll rate or lateral specific acceleration controllers and down step responses will tend to use the normal specific acceleration controller.

Firstly, considering the two figures it is clear that for velocities greater than 10 m/s the actual step responses match the desired step responses relatively well with the extra lag and slightly

reduced damping as a result of the finite bandwidths of the inner loop controllers. At 10 m/s, the reduced stability in the roll-to-turn east step responses of Figure 8.35 is evident as discussed in section 8.3.1.4. However, by employing skid-to-turn at low velocities the lateral guidance stability is restored as expected as seen in Figure 8.36.

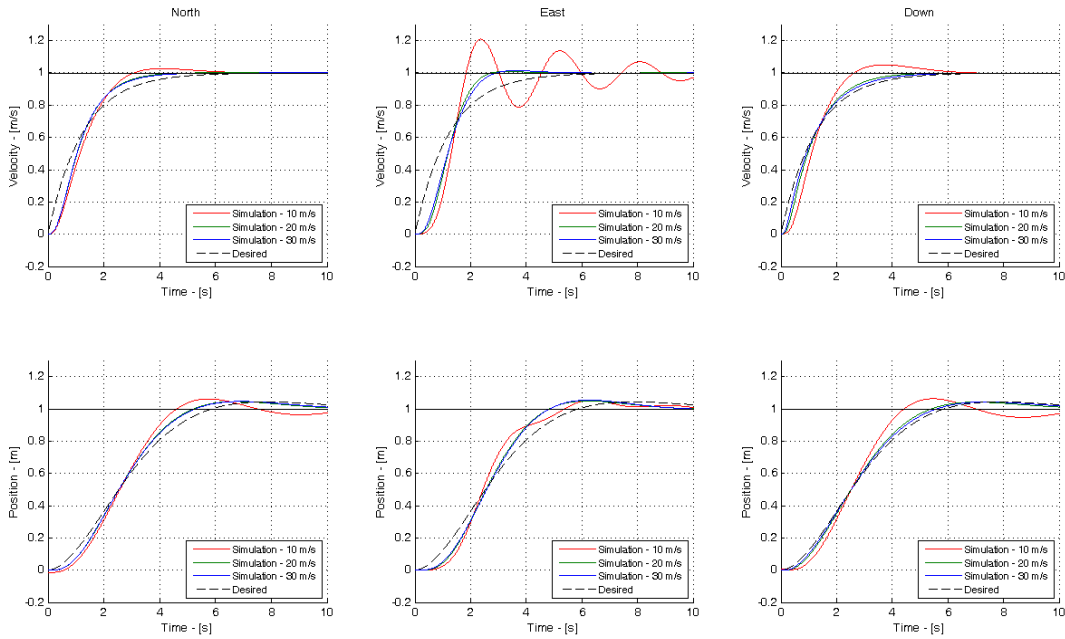


Figure 8.35 – Simulated and expected inertial velocity coordinate step responses with roll-to-turn implemented

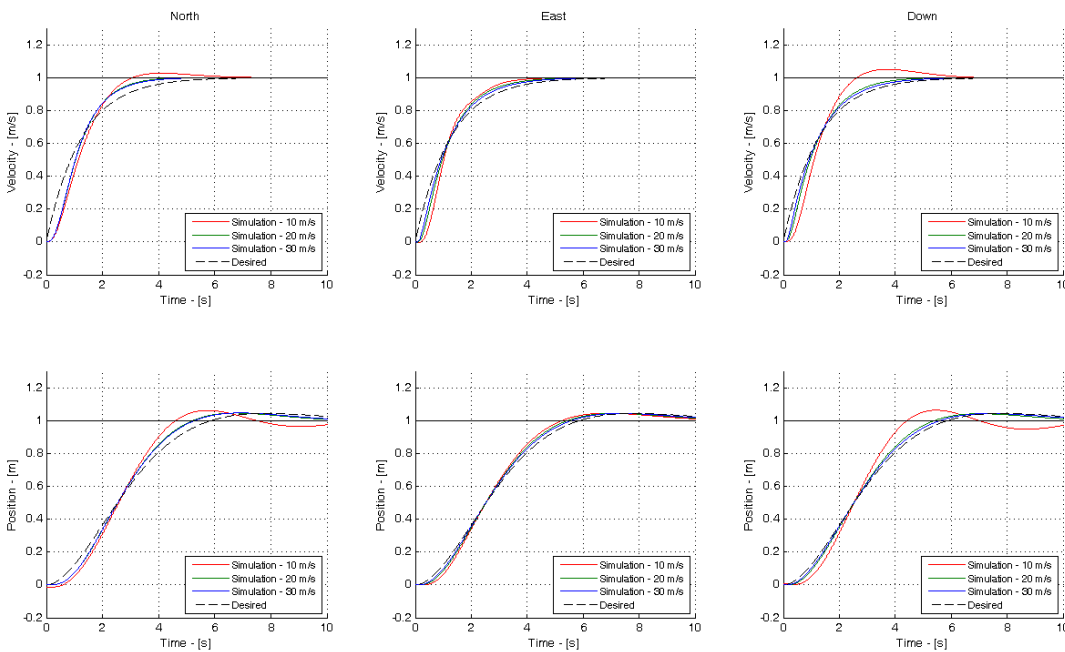


Figure 8.36 – Simulated and expected inertial velocity coordinate step responses with skid-to-turn implemented

8.3.2.2 Reference trajectory flight

With the step response results of the previous section verifying the functionality of the individual autopilot controllers, the aircraft is now made to fly a representative transition trajectory to allow its overall performance to be evaluated. The reference trajectory is shown in Figure 8.37 and described in point form below.

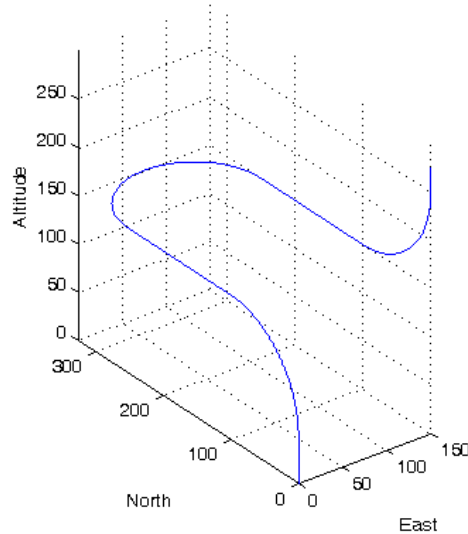


Figure 8.37 – VTOL aircraft reference trajectory

Reference trajectory description:

- The aircraft starts at the origin of the NED axis system flying vertically at 10 m/s.
- After 50 m the aircraft is commanded to fly a 90 deg vertical arc with a radius of 100 m that will leave it flying north at the end of the manoeuvre. Along the arc the velocity magnitude is commanded to linearly increase from 10 m/s to 25 m/s.
- The aircraft is then commanded to fly straight and level north for 150 m at 25 m/s before entering a constant speed and altitude right turn through 180 deg. The turn radius is 75 m which corresponds to an approximately 40 deg steady state bank angle during the turn.
- Upon exiting the turn the aircraft is commanded to fly straight and level south for a further 150 m before being commanded to fly a 90 deg vertical arc upwards with an arc radius of 100 m. During the arc the velocity magnitude is commanded to decrease linearly from 25 m/s to 10 m/s.
- Once the vertical arc is complete the aircraft is commanded to continue flying vertically at 10 m/s for a further 50 m before the simulation ends.

Note that during the simulation the commanded thrust was limited as follows,

$$T_c \in [0,120] \text{ N} \quad (8.112)$$

Furthermore, the normal specific acceleration lower limit used to switch the guidance algorithm from roll-to-turn to skid-to-turn in section 6.3.2 was set to,

$$\varepsilon = 5.0 \text{ m/s}^2 \quad (8.113)$$

In the case where direct lateral specific acceleration is used the autopilot was set to hold the current wind axis system normal unit vector direction. To illustrate the correct operation of the control system in skid-to-turn mode, the simulation was begun with the aircraft offset 10 m north and 5 m west from the reference trajectory. The initial orientation of the aircraft was vertical with the wind axis system normal unit vector facing north. The simulation results for the reference trajectory are shown in Figures 8.38 to 8.42.

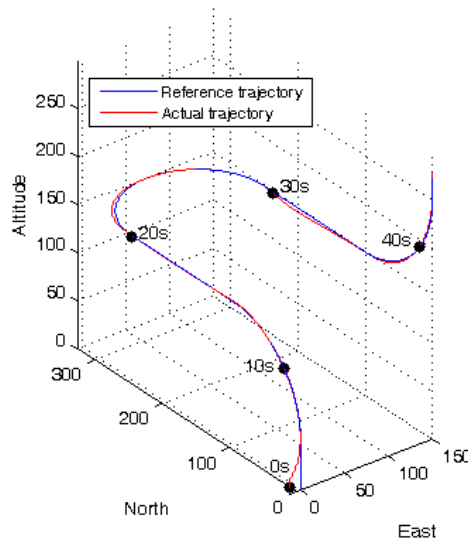


Figure 8.38 – Reference trajectory and actual trajectory flown

Figure 8.38 shows the reference trajectory and actual trajectory flown in 3D space. Again time stamps are provided on the trajectory to allow for easy comparison with the other figures. The 3D plot shows that the aircraft tracks the reference trajectory very well. Figure 8.39 plots the inertial coordinates of the position and velocity errors relative to the trajectory over time. The initial 10 m north and 5 m west position errors are seen to converge exponentially to zero. For the rest of the flight the trajectory is tracked to within 5 m with the position errors originating due to the finite bandwidths of the inner loop and error angle controllers.

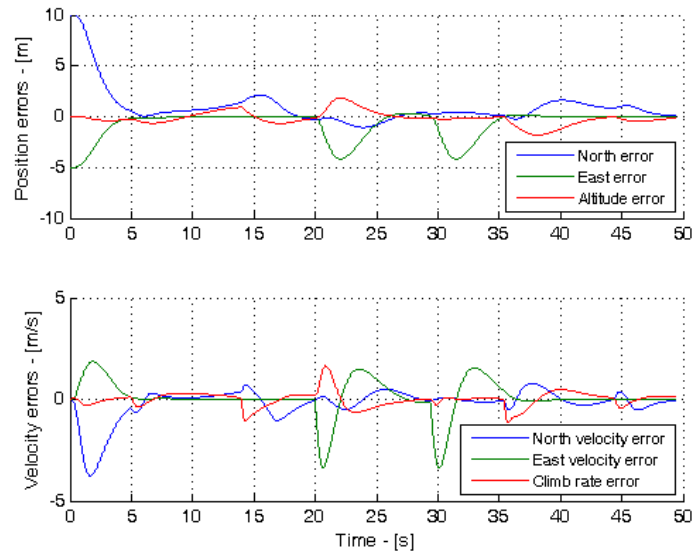


Figure 8.39 – Position and velocity errors relative to the reference trajectory

The polar coordinates of the simulated velocity vector are shown in Figure 8.40. It is clear that the aircraft tracks the desired velocity magnitude well. Note that since position is being regulated along the trajectory, the velocity magnitude deviations seen are also partly due to commands issued by the position controllers to drive their errors to zero. The large changes in the angle of attack and sideslip at the beginning of the simulation are due to the initial offset from the reference trajectory and the skid-to-turn control architecture. After the initial transient the angle of sideslip is seen to remain very close to zero throughout the flight. The angle of attack changes over a wide range during the trajectory but always has a magnitude of less than 12 deg. With angles of attack close to 12 deg, the aircraft will be at risk of stalling in practice. The primary reason for these high angles of attack is not the aggressive trajectory but the aircraft's very high level-flight wing loading of approximately 16. To solve this problem in practice the mass of the aircraft would need to be reduced significantly or the wingspan increased appropriately.

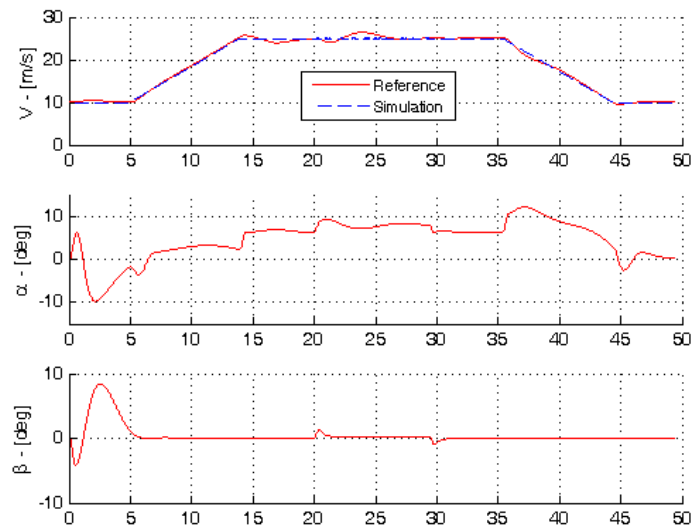


Figure 8.40 – Velocity magnitude, angle of attack and angle of sideslip over the reference trajectory

The inner loop commands generated by the guidance controllers over the trajectory as well as the actual inner loop regulated signals are plotted in Figure 8.41. In the normal specific acceleration plot the roll/skid-to-turn threshold of equation (8.113) is also indicated. It is clear that all signals follow the commanded values well. Note how direct lateral specific acceleration is automatically commanded at the beginning of the simulation to regulate the west error to zero. Once level flight has been reached after approximately 15 s, roll rate commands are seen to be used in conjunction with the then significant normal specific acceleration offset to regulate lateral cross track errors. The two roll rate peaks seen in the roll rate plot correspond to entering and exiting the 180 deg turn respectively. Note how disturbances to the lateral specific acceleration are regulated to zero during this phase of the flight.

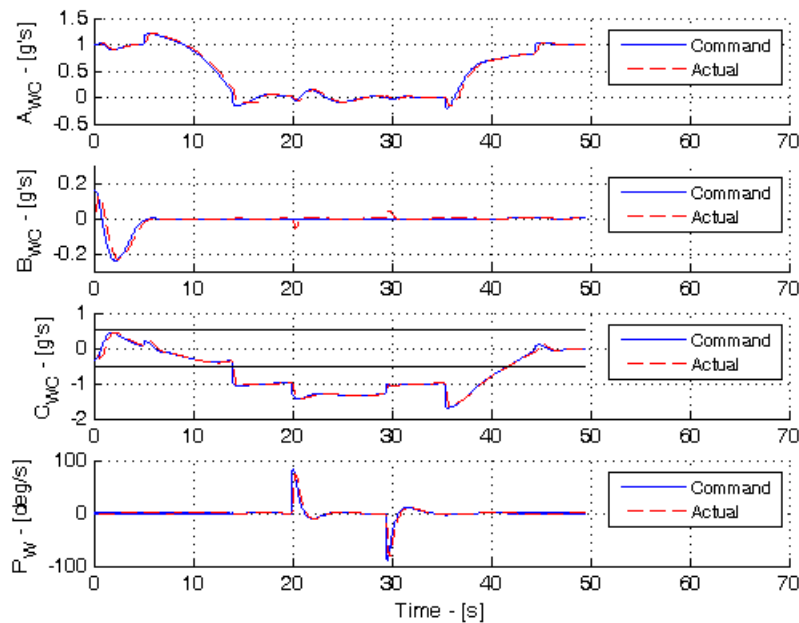


Figure 8.41 – Commanded and actual inner loop signals over the reference trajectory

The actuator commands during the reference trajectory are shown in Figure 8.42. The actuator signals commanded appear to be practically feasible and well balanced throughout the reference trajectory. However it should be noted that with the rudder to vertical flaps mixing ratio magnitude of 2.5, the vertical flap deflections would peak at approximately 30 deg when regulating the initial 5 m west offset. One method of handling this problem would be to reduce the rudder to flaps mixing. However, the consequence of this would be a reduction in the allowable bandwidth of the closed loop system. Of course the bandwidth of the guidance controllers could then simply be scheduled to handle the slower lateral specific acceleration response at low velocities. Other options include limiting the maximum allowable lateral specific acceleration command and modifying the aircraft itself to provide more effective control authority.

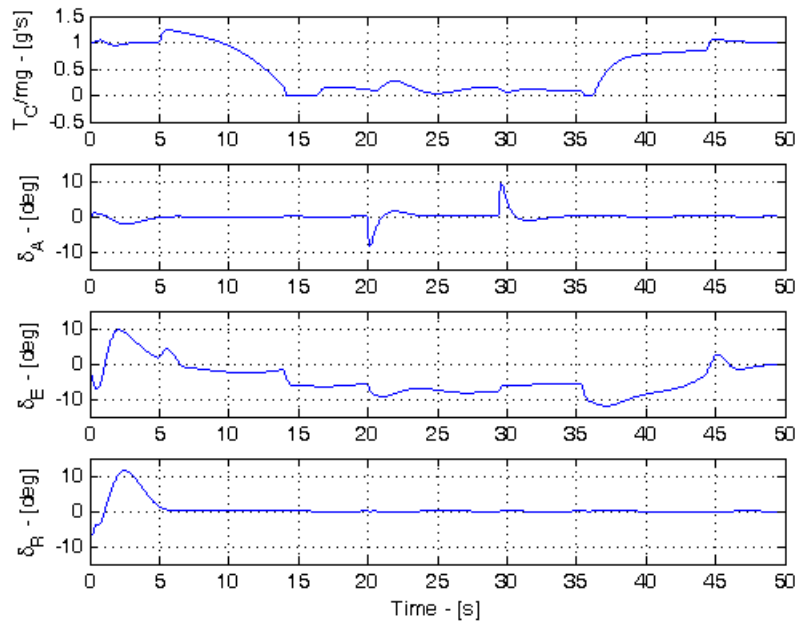


Figure 8.42 – Actuator signals over the reference trajectory

8.3.3 Comments

The VTOL aircraft example has effectively displayed the use of the NNDT inner loop controllers and illustrated the potential of the manoeuvre autopilot by elegantly solving the transition flight control problem. The autopilot was seen to naturally handle the transition from skid-to-turn to roll-to-turn lateral guidance and the NNDT inner loop controllers ensured realistic use of the actuators at all times.

8.4 Conclusion

This chapter illustrated the application of the acceleration based manoeuvre autopilot of this thesis to three vastly different aircraft. The aircraft and reference trajectories were chosen to allow the capability and versatility of the autopilot and its internal controller variants to be illustrated. The autopilot was seen in all three cases to solve the respective flight control problems elegantly and effectively. The example applications verify the mathematics of the autopilot and its associated application conditions. Where differences were seen between actual and desired/predicted responses, these could always be correlated to application conditions that were not fully satisfied by either the aircraft or a controller. The results of this chapter thus support the generic, practically feasible nature of the autopilot that has been motivated throughout this thesis.

Chapter 9

Conclusion

This chapter concludes the thesis with a summary of the work presented and highlights the fundamental results. Its original contributions to the field of aircraft dynamics, control and guidance are then noted in point form for convenience. Finally, further related research topics are discussed.

9.1 Summary

An acceleration based control strategy for the design of an autopilot capable of guiding an aircraft through the full 3D flight envelope has been presented. The core of the strategy involved the design of attitude independent specific acceleration controllers. Adoption of the control strategy was argued to provide a practically feasible, robust, effective and elegant solution to the manoeuvre flight control problem. Detailed analysis and design of the inner loop acceleration control system was carried out for the case where the incidence angles are small. A guidance algorithm well suited for use with the acceleration controllers was designed and the system verified through simulation with a number of different aircraft and reference trajectories. The closed form, non-iterative nature of the control laws developed also yield a computationally efficient solution to the 3D manoeuvre flight control problem, requiring only basic mathematical operations for implementation.

The details of the manoeuvre autopilot architecture were provided in Chapter 2. There the feasibility of the manoeuvre autopilot design strategy was illustrated mathematically. It was shown that the aircraft dynamics could be decoupled into rigid body rotational dynamics and point mass kinematics if a timescale separation and dynamic inversion condition could be met. It was argued that for a very large class of aircraft these conditions could indeed be met, thus practically enabling the split dynamics design. No force and moment structure was enforced during the analysis of Chapter 2 with typical dependencies only highlighted. The purpose thereof was to illustrate the full scope of the manoeuvre autopilot design strategy.

In Chapter 3, the force and moment models were structured for the case where the incidence angles are small. This model structure allowed for further detailed analysis and design of the

autopilot. It was shown that under certain practically feasible conditions the rigid body rotational dynamics become linear and decouple into axial, normal and lateral dynamics. The timescale separation condition required to dynamically decouple the point mass and rigid body rotational dynamics was shown not to apply to the axial dynamics, which, due to the band-limited nature of thrust actuators, greatly increased the practical feasibility of the control strategy. The normal and lateral dynamics were also seen to correspond with the classic Short Period and Roll/Dutch Roll mode approximations respectively.

The detailed design of the axial and normal specific acceleration controllers was handled in Chapter 4. During the axial specific acceleration controller design the decoupling sensitivity function constraint developed in Chapter 3 was investigated and found to be practically achievable. The natural elevator to normal specific acceleration dynamics were investigated in detail and found to be typically weakly NMP with the zero locations shown to be a function of the aircraft's characteristic lengths. Time and frequency domain analyses resulted in an upper bound frequency constraint on the system poles for the NMP nature of the system to be ignored. Ignoring the system's NMP nature was argued to be necessary for the dynamic inversion part of the pole placement control system and to avoid large closed loop sensitivity function peaks. A NNDT variant of the controller was then designed with the benefit of being able to handle large dynamic pressure changes much better than its dimensional counterpart. Integrator pole placement strategies were discussed for both variants of the controller and the mathematics to determine the feed-forward gain to cancel the closed loop integrator dynamics was presented.

The lateral dynamics were analysed at the start of Chapter 5 and shown under practically feasible conditions to decouple into roll and directional dynamics. Both dimensional and NNDT roll rate controllers were designed with integrator pole placement and feed-forward gain issues discussed. A transfer function for the analysis of the closed loop rudder to roll rate cross coupling was also derived. The rudder to lateral specific acceleration dynamics were analysed in a similar fashion to the elevator to normal specific acceleration dynamics. Although the structure of these two sets of dynamics was seen to be similar, the typical natural dynamics were argued to differ greatly due to the lack of a primary lateral lifting surface. This difference lead to a fundamentally different control system design strategy with an inner stability augmentation law and an outer acceleration regulation law. No dynamic inversion was used in the control system after the gravity coupling was argued to typically be negligible. The chapter was concluded with the design of a NNDT variant of the controller.

Aircraft guidance was handled in Chapter 6. With dynamically invariant inner loop acceleration controllers in place, the aircraft was shown to reduce to a point mass with a steerable acceleration vector from a guidance perspective. This in turn meant that control at a guidance level remained completely aircraft independent. After introducing a number of potential guidance strategies, the detailed design of a SAM strategy, well suited for use with

the inner acceleration controllers, was presented. A variant on the design for the case when the commanded normal specific acceleration magnitude tends to zero was also presented. Practical limitations of the strategy were discussed and methods to address the issues were provided.

The subject of reference trajectory generation was addressed in Chapter 7. Due to the autopilot architecture it was illustrated how reference trajectories need only be kinematically feasible instead of being dynamically feasible as with many other manoeuvre autopilot designs. Generation of kinematically feasible reference trajectories for the SAM guidance controller was shown to be a straightforward process and a number of building block reference trajectories were derived. These building block trajectories were created to allow more complex manoeuvres to be easily created and to reduce the parameter space for potential higher level mission planning algorithms.

Finally in Chapter 8 the complete autopilot was simulated using three different aircraft with very different dynamics and reference trajectories. The autopilot was found to perform well in all three cases and elegantly and effectively solved the respective flight control problems. All differences between actual and predicted/desired responses were well correlated with violations in the corresponding controller application conditions. The closed form, parameterised nature of the control system and the fact that controller design freedom is reduced to that of selecting appropriate closed loop poles, made its application to the different aircraft very straightforward. The example applications thus highlighted the autopilot's generic nature and motivated its practical applicability.

9.2 Contributions to the field

To the best of the author's knowledge, the unique contributions of this dissertation to the field of aircraft dynamics, control and guidance are summarised in point form below:

- Development of the manoeuvre autopilot control strategy i.e. the manoeuvre autopilot architecture presented in Chapter 2.
- Development of conditions/arguments to linearise and decouple the rigid body rotational dynamics, particularly the lift into drag decoupling condition (section 3.2).
- Analysis of when feedback linearisation of inertial cross coupling terms in typically weakly NMP aircraft starts to have adverse effects (section 3.3.2).
- Illustrating mathematically that under the linearising and decoupling conditions of Chapter 3, the classic Short Period, Roll and Dutch Roll modes of an aircraft are independent of gross attitude (sections 3.4.1 and 3.4.2).
- Derivation of the lower bound bandwidth constraint for the closed loop axial specific acceleration dynamics (section 4.1).

- Determining analytically accurate approximations for the following zeros: elevator to normal specific acceleration (section 4.2.1), aileron to roll rate (section 5.1.1), rudder to yaw rate (section 5.1.2) and rudder to lateral specific acceleration (section 5.1.3).
- Determination of a frequency bound constraint for the NMP nature of a system to be considered negligible (section 4.2.2). In turn this result, together with analytic knowledge of the zero positions (see point above), lead to the concept of a feasible pole placement region as a function of the aircraft parameters. This pole placement region was discussed in section 4.2.3 and applied to the normal and lateral specific acceleration controllers of sections 4.2.4 and 5.3.2 respectively.
- Derivation of conditions for decoupling the MIMO lateral dynamics into roll and directional dynamics for control system design purposes (section 5.1).
- Derivation of closed form, parameterised feedback control algorithms for arbitrary closed loop pole placement of the axial, normal, roll and directional dynamics (sections 4.1, 4.2.4, 5.2.1 and 5.3.2 respectively).
- Derivation of the NNDT variants of the normal specific acceleration, roll rate and lateral specific acceleration controllers above (sections 4.2.6, 5.2.3 and 5.3.4 respectively). Coupled to this was the identification of the associated benefits and tradeoffs of the NNDT controller variants (sections 4.2.5, 5.2.2 and 5.3.3 respectively).
- Development of a generic, computationally efficient, closed form specific acceleration matching guidance control law well suited for use with the inner acceleration based control system (section 6.3).

9.3 Further research

A number of future research topics arise directly from the results presented in this thesis. These topics are briefly discussed in the paragraphs that follow.

The specific acceleration and roll rate controllers of Chapters 4 and 5 reduce the design freedom to that of selecting appropriate closed loop poles. Intelligent selection of these closed loop poles could be the subject of further research. When selecting closed loop poles, a designer is typically not concerned with the exact placement of the poles. More, the concern is that the poles lie within some acceptable region. Thus, given this acceptable region, an optimisation algorithm could be developed to minimise some form of cost function. A LQR type cost function is one option where control effort and system performance would be weighed against each other. A second option for a cost function could be the cumulative effect of parameter variation on the system given the statistical properties of the individual parameters. In cases where more than one actuator drives into each of the linear decoupled systems (e.g. in the normal dynamics when both an elevator and a set of canards are present), then the design optimisation freedom is further increased and the results of such research

would play a significant role in increasing overall controller robustness and efficiency.

The incidence angles referred to in the inner loop dynamics are the incidence angles of the body axis system with respect to the body-inertial velocity vector (aircraft velocity vector with respect to inertial space). In the presence of wind, the aerodynamic forces and moments are of course a function of the incidence angles of the body axis system with respect to the body-air velocity vector (aircraft velocity vector with respect to the air mass). Future research should investigate expanding the manoeuvre autopilot controllers to explicitly take this difference into account. Wind could be modelled as having a constant (or slowly changing) component and a superimposed gust component. Only the constant component would need to be explicitly addressed in the context of the problem introduced above, with the gust component acting as a disturbance input to the system. With the air mass modelled as moving at a constant velocity relative to inertial space, it too could act as an inertial reference frame. Thus, it is expected that very few changes would be required to modify the controllers to function in the presence of constant wind. More care would however need to be taken at a guidance level where accelerations are mapped onto the aircraft, since the body-air and body-inertial velocity vectors could point in significantly different directions.

The linear, decoupled, NNDT inner loop dynamics presented in Chapters 4 and 5 provide an excellent platform for further system identification research. The dynamics in this form are seen to expose the core of the normal, roll and directional dynamics with the non-dimensional stability and control derivatives directly exposed in the system matrices. In cases where the aircraft's normalised mass and relative airspeed to ground speed remain close to constant, the NNDT dynamics become time invariant and are furthermore valid at any gross attitude. Thus, by recording appropriate normalised control inputs and normalised system outputs, system identification of the aircraft parameters could take place in NNDT state space with data recorded at any dynamic pressure and at any gross attitude. The normalisation of states and non-dimensionalising of time is thus seen to shape all recorded data for use in NNDT state space which can be viewed as the underlying, fundamental state space model for aircraft dynamics. Working with the NNDT dynamics not only provides an opportunity for simpler parameter identification but also makes self configuring and/or adaptive control possible since the control algorithms in this thesis allow poles to be placed as a function of the identified parameters.

The SAM guidance algorithm of Chapter 6 requires a timescale separation to exist between the outer position and velocity dynamics and the inner axial specific acceleration dynamics. However, in practice this timescale separation often does not exist due to the band-limited nature of thrust actuators. To handle this a variant of the SAM guidance controller could be designed where the axial specific acceleration is used only to control the velocity magnitude. The control law for this would be based on the velocity magnitude and axial specific acceleration dynamics of equations (2.47), (3.61) and (3.62), and could involve a combination

of dynamic inversion and pole placement to ensure that the flight path angle coupling in equation (2.47) is rejected. The timescale separation requirement imposed by the SAM controller of section 6.3 on the axial specific acceleration would then fall away, with its lag dynamics taken into account in the velocity magnitude controller. Two dimensional cross track guidance would then be achieved using specific acceleration matching with the remaining roll rate and normal specific acceleration actuators, where the timescale separation arguments hold well. This variation on the SAM control law also provides the opportunity for position based guidance as opposed to the time based guidance inherent in the SAM control law.

The building block reference trajectories developed in Chapter 7 reduce the parameter space for optimisation in higher level mission planning type algorithms. These mission planning algorithms will be the subject of future research. Given a global objective, the resources available and the system constraints, a mission planning algorithm would be responsible for generating appropriate reference trajectories for UAVs to complete a task. By limiting the set of available manoeuvres to a small fundamental set that can easily be strung together, the computational burden of mission planning algorithms is greatly decreased.

Estimation of the feedback signals required by the autopilot developed in this thesis remains a topic for future research. Although the task of estimating the required states is not deemed a particularly difficult one, of interest from a future research perspective is the use of the split between the rigid body rotational dynamics and the point mass kinematics to simplify the state estimation procedure. The split in dynamics would allow two separate estimators to be designed instead of one large estimator. An aircraft dependent rigid body rotational dynamics estimator would accept actuator inputs and make use of body fixed angular rate gyroscopes and accelerometers to estimate the inner loop states. Due to the coupling from the point mass kinematics, this estimator would also require knowledge of the attitude angles, velocity magnitude and air density for its propagation phase. These signals would be obtained from an outer aircraft independent point mass kinematics state estimator that accepts wind axes specific acceleration and roll rate coordinates and uses GPS receiver and magnetometer measurements to bound position, velocity magnitude and gross attitude state estimates. Having two separated estimators instead of one large estimator would allow for a significant reduction in the computational burden associated with full state estimation algorithms. Furthermore, in certain cases, the linear decoupled inner loop dynamics could be used to further simplify the rigid body rotational dynamics estimator e.g. the normal dynamics could be used to estimate angle of attack on its own.

Appendix A

Rigid Body Dynamics

A.1 Preliminaries

This section introduces the vector and matrix notation used in this thesis as well as the vector and matrix operators.

A.1.1 Axis systems, vectors and coordinate vectors

An axis system A is defined by an origin vector o^A and three basis unit vectors i^A , j^A and k^A that originate from o^A and span three dimensional space. Note that vectors are denoted by boldface, italic symbols. Most often the basis vectors are chosen orthogonal for simplifying purposes. Unless otherwise stated, all axis systems referred to in this document will be assumed to have orthogonal basis vectors.

For the developments that follow, consider axis systems A and B , and the vector R . Vector R can be written as a linear combination of the basis vectors of any axis system, as shown for axis system A below,

$$\mathbf{R} = X^A \mathbf{i}^A + Y^A \mathbf{j}^A + Z^A \mathbf{k}^A \quad (\text{A.1})$$

Writing vector R in this fashion is referred to as coordinating it into axis system A . Note, by convention the coordinate variables are denoted with the superscript of the respective axis system. The superscript notation is convenient when the same vector is coordinated into a number of different axis systems since the same coordinate symbols can be used.

The full vector notation of equation (A.1) can become cumbersome. As a result, when coordinating R into A , the basis vectors of A will often be dropped and only the coordinates written in the following matrix form,

$$\mathbf{R}_A = \begin{bmatrix} X^A \\ Y^A \\ Z^A \end{bmatrix} \quad (\text{A.2})$$

Here, a boldface, non-italic symbol is used to show that only the coordinates of the vector, in

the subscripted axis system, are being referred to and not the vector itself. Consequently, \mathbf{R}_A is referred to as a *coordinate vector*. The difference between vectors and coordinate vectors is a source of much confusion in vector mathematics. Coordinating a vector \mathbf{R} into an axis system does not change the vector thus making it perfectly legal to write,

$$\mathbf{R} = X^A \mathbf{i}^A + Y^A \mathbf{j}^A + Z^A \mathbf{k}^A = X^B \mathbf{i}^B + Y^B \mathbf{j}^B + Z^B \mathbf{k}^B \quad (\text{A.3})$$

However, if only the coordinates of the vector in equation (A.3) are referred to then the following is true,

$$\mathbf{R}_A \neq \mathbf{R}_B \quad (\text{A.4})$$

unless the two axis systems coincide. In order to provide a means with which to return from a coordinate vector to a vector, the square bracket operator is introduced,

$$\mathbf{R} = [\mathbf{R}_A]_A = X^A \mathbf{i}^A + Y^A \mathbf{j}^A + Z^A \mathbf{k}^A \quad (\text{A.5})$$

In words the operator appends, in order, each of the coordinates of the coordinate vector in square brackets to the basis vectors of the subscripted axis system.

A.1.2 The dot and cross product operators

This section defines two important vector operators. Consider axis system A and the vectors \mathbf{P} and \mathbf{R} . The dot or scalar product of \mathbf{P} and \mathbf{R} is defined as follows,

$$\mathbf{P} \cdot \mathbf{R} \equiv |\mathbf{P}| |\mathbf{R}| \cos \theta_{PR} \quad (\text{A.6})$$

where θ_{PR} is the angle between the vectors and $||$ is the vector magnitude or norm operator. If \mathbf{P} and \mathbf{R} are both coordinated in the same axis system, then the dot product can be written as a function of the respective coordinate vectors,

$$\mathbf{P} \cdot \mathbf{R} = \mathbf{P}_A^T \mathbf{R}_A \quad (\text{A.7})$$

This result is easily proved by making use of the fact that the dot product of orthogonal basis vectors is zero and the dot product of a basis vector with itself is unity. The cross or vector product of vectors \mathbf{P} and \mathbf{R} is defined as follows,

$$\mathbf{P} \times \mathbf{R} \equiv (|\mathbf{P}| |\mathbf{R}| \sin \theta_{PR}) \mathbf{i}_{PR} \quad (\text{A.8})$$

where θ_{PR} is the angle between the vectors and \mathbf{i}_{PR} is a vector perpendicular to the plane spanned by \mathbf{P} and \mathbf{R} . The positive sense of \mathbf{i}_{PR} is defined by the right hand rule when \mathbf{P} is rotated through θ_{PR} to \mathbf{R} . If \mathbf{P} and \mathbf{R} are both coordinated into the same axis system, then the cross product can be written as a function of the respective coordinate vectors,

$$\mathbf{P} \times \mathbf{R} = [\mathbf{S}_{\mathbf{P}_A} \mathbf{R}_A]_A \quad (\text{A.9})$$

where,

$$\mathbf{S}_{\mathbf{P}_A} = \begin{bmatrix} 0 & -Z^A & Y^A \\ Z^A & 0 & -X^A \\ -Y^A & X^A & 0 \end{bmatrix} \quad (\text{A.10})$$

and X^A , Y^A and Z^A are the components of \mathbf{P} when coordinated in A . This result is also easily proved by noting that the cross product of two orthogonal basis vectors yields a vector in the subspace spanned by the third basis vector and that the cross product of a basis vector with itself is zero. Note that due to the properties of cross products,

$$\mathbf{S}_{\mathbf{P}_A} \mathbf{R}_A = -\mathbf{S}_{\mathbf{R}_A} \mathbf{P}_A \quad (\text{A.11})$$

A.1.3 Time derivative of a vector

The time derivative of the vector \mathbf{R} with respect to axis system A is defined as follows,

$$\left. \frac{d}{dt} \mathbf{R} \right|_A \equiv \lim_{\Delta t \rightarrow 0} \frac{[\mathbf{R}(t + \Delta t) - \mathbf{R}(t)]_A}{\Delta t} = \lim_{\Delta t \rightarrow 0} \frac{\Delta \mathbf{R}(t)_A}{\Delta t} \quad (\text{A.12})$$

where the notation used in the numerator of the limits denotes that the change is relative to axis system A . The vector \mathbf{R} can change in both magnitude and direction with respect to A . To assist in the derivation of a more useful formula for the derivative, \mathbf{R} is written as the product of a vector magnitude and a unit direction vector as follows,

$$\mathbf{R} = \bar{R} \mathbf{i}^R \quad (\text{A.13})$$

The time derivative of \mathbf{R} can thus be written as,

$$\left. \frac{d}{dt} \mathbf{R} \right|_A = \lim_{\Delta t \rightarrow 0} \frac{[\bar{R}(t + \Delta t) \mathbf{i}^R(t + \Delta t) - \bar{R}(t) \mathbf{i}^R(t)]_A}{\Delta t} \quad (\text{A.14})$$

Expanding each of the terms in $t + \Delta t$ in a Taylor series about t gives,

$$\bar{R}(t + \Delta t) = \bar{R}(t) + \left. \frac{d}{dt} \bar{R}(t) \right|_A \Delta t + \frac{1}{2!} \left. \frac{d^2}{dt^2} \bar{R}(t) \right|_A \Delta t^2 + h.o.t.(\Delta t) \quad (\text{A.15})$$

$$\mathbf{i}^R(t + \Delta t) = \mathbf{i}^R(t) + \left. \frac{d}{dt} \mathbf{i}^R(t) \right|_A \Delta t + \frac{1}{2!} \left. \frac{d^2}{dt^2} \mathbf{i}^R(t) \right|_A \Delta t^2 + h.o.t.(\Delta t) \quad (\text{A.16})$$

where $h.o.t.(\Delta t)$ implies higher order terms in Δt . Multiplying these terms together and substituting into equation (A.14) gives,

$$\begin{aligned}
\left. \frac{d}{dt} \mathbf{R} \right|_A &= \lim_{\Delta t \rightarrow 0} \frac{\left[\left. \bar{\mathbf{R}}(t) \mathbf{i}^R(t) + \frac{d}{dt} \bar{\mathbf{R}}(t) \right|_A \mathbf{i}^R(t) \Delta t + \bar{\mathbf{R}}(t) \left. \frac{d}{dt} \mathbf{i}^R(t) \right|_A \Delta t + h.o.t. - \bar{\mathbf{R}}(t) \mathbf{i}^R(t) \right]}{\Delta t} \\
&= \lim_{\Delta t \rightarrow 0} \frac{\left[\left. \frac{d}{dt} \bar{\mathbf{R}}(t) \right|_A \mathbf{i}^R(t) \Delta t + \bar{\mathbf{R}}(t) \left. \frac{d}{dt} \mathbf{i}^R(t) \right|_A \Delta t + h.o.t. \right]}{\Delta t} \\
&= \left. \dot{\bar{\mathbf{R}}}(t) \mathbf{i}^R(t) + \bar{\mathbf{R}}(t) \frac{d}{dt} \mathbf{i}^R(t) \right|_A
\end{aligned} \tag{A.17}$$

where the time derivative of a scalar is denoted by a dot. The above equation is simply the product rule of differentiation. The final term of equation (A.17) denotes the change in \mathbf{R} due to its change in direction relative to A . This term can be simplified as follows,

$$\left. \frac{d}{dt} \mathbf{i}^R(t) \right|_A = \boldsymbol{\omega}^{RA} \times \mathbf{i}^R(t) \tag{A.18}$$

where $\boldsymbol{\omega}^{RA}$ is the angular velocity of the unit vector \mathbf{i}^R with respect to axis system A , and is defined such that the above equation holds. Considering equations (A.18), (A.17) and (A.13) the following result is obtained,

$$\left. \frac{d}{dt} \mathbf{R} \right|_A = \dot{\bar{\mathbf{R}}}(t) \mathbf{i}^R(t) + \boldsymbol{\omega}^{RA} \times \mathbf{R}(t) \tag{A.19}$$

In deriving the equations of motion of an aircraft, it is useful to be able to write the derivative of a vector with respect to one axis system in terms of the derivative of the same vector with respect to another axis system (typically one which rotates with the vector). Beginning with the derivative of \mathbf{R} with respect to A and making use of equation (A.19) the following result is obtained,

$$\begin{aligned}
\left. \frac{d}{dt} \mathbf{R} \right|_A &= \left. \frac{d}{dt} (X^B \mathbf{i}^B + Y^B \mathbf{j}^B + Z^B \mathbf{k}^B) \right|_A \\
&= \left(\left. \frac{d}{dt} X^B \right|_A \mathbf{i}^B + \left. \frac{d}{dt} Y^B \right|_A \mathbf{j}^B + \left. \frac{d}{dt} Z^B \right|_A \mathbf{k}^B \right) + \left(X^B \left. \frac{d}{dt} \mathbf{i}^B \right|_A + Y^B \left. \frac{d}{dt} \mathbf{j}^B \right|_A + Z^B \left. \frac{d}{dt} \mathbf{k}^B \right|_A \right) \\
&= (\dot{X}^B \mathbf{i}^B + \dot{Y}^B \mathbf{j}^B + \dot{Z}^B \mathbf{k}^B) + (X^B \boldsymbol{\omega}^{BA} \times \mathbf{i}^B + Y^B \boldsymbol{\omega}^{BA} \times \mathbf{j}^B + Z^B \boldsymbol{\omega}^{BA} \times \mathbf{k}^B) \\
&= (\dot{X}^B \mathbf{i}^B + \dot{Y}^B \mathbf{j}^B + \dot{Z}^B \mathbf{k}^B) + \boldsymbol{\omega}^{BA} \times (X^B \mathbf{i}^B + Y^B \mathbf{j}^B + Z^B \mathbf{k}^B) \\
&= \left. \frac{d}{dt} \mathbf{R} \right|_B + \boldsymbol{\omega}^{BA} \times \mathbf{R}
\end{aligned} \tag{A.20}$$

A.1.4 Coordinate vector transformations

Given a vector \mathbf{R} , it is often very useful to be able to relate the coordinates of \mathbf{R} in A to the coordinates of \mathbf{R} in B . This section derives a generalised transformation matrix that quantifies this relationship. Intuitively, it is expected that the transformation matrix would be a function of the basis vectors of the axis systems in question. This will be shown to be true in the

derivation below.

Consider coordinating an arbitrary vector \mathbf{R} into orthogonal axis system A . This can be done using the dot product operator as follows,

$$\mathbf{R} = (\mathbf{R} \cdot \mathbf{i}^A) \mathbf{i}^A + (\mathbf{R} \cdot \mathbf{j}^A) \mathbf{j}^A + (\mathbf{R} \cdot \mathbf{k}^A) \mathbf{k}^A = X^A \mathbf{i}^A + Y^A \mathbf{j}^A + Z^A \mathbf{k}^A \quad (\text{A.21})$$

Now, given the coordinates of \mathbf{R} in A , it is desired to find the transformation matrix that, through matrix multiplication, yields the coordinates of \mathbf{R} in B . Coordinating the basis vectors of A into axis system B using the dot product operator gives,

$$\begin{aligned} \mathbf{R} &= X^A \mathbf{i}^A + Y^A \mathbf{j}^A + Z^A \mathbf{k}^A \\ &= X^A \left[(\mathbf{i}^A \cdot \mathbf{i}^B) \mathbf{i}^B + (\mathbf{i}^A \cdot \mathbf{j}^B) \mathbf{j}^B + (\mathbf{i}^A \cdot \mathbf{k}^B) \mathbf{k}^B \right] + \\ &\quad Y^A \left[(\mathbf{j}^A \cdot \mathbf{i}^B) \mathbf{i}^B + (\mathbf{j}^A \cdot \mathbf{j}^B) \mathbf{j}^B + (\mathbf{j}^A \cdot \mathbf{k}^B) \mathbf{k}^B \right] + \\ &\quad Z^A \left[(\mathbf{k}^A \cdot \mathbf{i}^B) \mathbf{i}^B + (\mathbf{k}^A \cdot \mathbf{j}^B) \mathbf{j}^B + (\mathbf{k}^A \cdot \mathbf{k}^B) \mathbf{k}^B \right] \\ &= X^B \mathbf{i}^B + Y^B \mathbf{j}^B + Z^B \mathbf{k}^B \end{aligned} \quad (\text{A.22})$$

Writing equation (A.22) in a matrix form gives,

$$\begin{bmatrix} \mathbf{i}^B & \mathbf{j}^B & \mathbf{k}^B \end{bmatrix} \begin{bmatrix} X^B \\ Y^B \\ Z^B \end{bmatrix} = \begin{bmatrix} \mathbf{i}^B & \mathbf{j}^B & \mathbf{k}^B \end{bmatrix} \begin{bmatrix} \mathbf{i}^A \cdot \mathbf{i}^B & \mathbf{j}^A \cdot \mathbf{i}^B & \mathbf{k}^A \cdot \mathbf{i}^B \\ \mathbf{i}^A \cdot \mathbf{j}^B & \mathbf{j}^A \cdot \mathbf{j}^B & \mathbf{k}^A \cdot \mathbf{j}^B \\ \mathbf{i}^A \cdot \mathbf{k}^B & \mathbf{j}^A \cdot \mathbf{k}^B & \mathbf{k}^A \cdot \mathbf{k}^B \end{bmatrix} \begin{bmatrix} X^A \\ Y^A \\ Z^A \end{bmatrix} \quad (\text{A.23})$$

which yields the desired result,

$$\begin{aligned} \begin{bmatrix} X^B \\ Y^B \\ Z^B \end{bmatrix} &= \begin{bmatrix} \mathbf{i}^A \cdot \mathbf{i}^B & \mathbf{j}^A \cdot \mathbf{i}^B & \mathbf{k}^A \cdot \mathbf{i}^B \\ \mathbf{i}^A \cdot \mathbf{j}^B & \mathbf{j}^A \cdot \mathbf{j}^B & \mathbf{k}^A \cdot \mathbf{j}^B \\ \mathbf{i}^A \cdot \mathbf{k}^B & \mathbf{j}^A \cdot \mathbf{k}^B & \mathbf{k}^A \cdot \mathbf{k}^B \end{bmatrix} \begin{bmatrix} X^A \\ Y^A \\ Z^A \end{bmatrix} \\ &= \begin{bmatrix} \cos \theta_{\mathbf{i}^A \mathbf{i}^B} & \cos \theta_{\mathbf{j}^A \mathbf{i}^B} & \cos \theta_{\mathbf{k}^A \mathbf{i}^B} \\ \cos \theta_{\mathbf{i}^A \mathbf{j}^B} & \cos \theta_{\mathbf{j}^A \mathbf{j}^B} & \cos \theta_{\mathbf{k}^A \mathbf{j}^B} \\ \cos \theta_{\mathbf{i}^A \mathbf{k}^B} & \cos \theta_{\mathbf{j}^A \mathbf{k}^B} & \cos \theta_{\mathbf{k}^A \mathbf{k}^B} \end{bmatrix} \begin{bmatrix} X^A \\ Y^A \\ Z^A \end{bmatrix} \end{aligned} \quad (\text{A.24})$$

or,

$$\mathbf{R}_B = [\text{DCM}^{BA}] \mathbf{R}_A \quad (\text{A.25})$$

The transformation matrix of equation (A.24) is know as a Direction Cosine Matrix (DCM) since each element is the cosine of the angle between the respective axis system basis vectors. The DCM is an orthonormal matrix and this property can be used to simplify its inverse calculation. To prove the orthonormal property, the vector \mathbf{R} in equation (A.22) could initially have been coordinated into axis system B and the derivation continued as normal to yield,

$$\begin{bmatrix} X^A \\ Y^A \\ Z^A \end{bmatrix} = \begin{bmatrix} \mathbf{i}^B \cdot \mathbf{i}^A & \mathbf{j}^B \cdot \mathbf{i}^A & \mathbf{k}^B \cdot \mathbf{i}^A \\ \mathbf{i}^B \cdot \mathbf{j}^A & \mathbf{j}^B \cdot \mathbf{j}^A & \mathbf{k}^B \cdot \mathbf{j}^A \\ \mathbf{i}^B \cdot \mathbf{k}^A & \mathbf{j}^B \cdot \mathbf{k}^A & \mathbf{k}^B \cdot \mathbf{k}^A \end{bmatrix} \begin{bmatrix} X^B \\ Y^B \\ Z^B \end{bmatrix} \quad (\text{A.26})$$

or,

$$\mathbf{R}_A = [\mathbf{DCM}^{AB}] \mathbf{R}_B \quad (\text{A.27})$$

Noting that the DCMs of equations (A.24) and (A.26) are simply the transpose of each other, the following result is obtained,

$$\mathbf{R}_B = [\mathbf{DCM}^{BA}] \mathbf{R}_A = [\mathbf{DCM}^{BA}] [\mathbf{DCM}^{BA}]^T \mathbf{R}_B \quad (\text{A.28})$$

Thus,

$$[\mathbf{DCM}^{BA}] [\mathbf{DCM}^{BA}]^T = \mathbf{I} \quad (\text{A.29})$$

Equation (A.29) shows that the inverse of a DCM relating the coordinates of two orthogonal axis systems is merely its transpose. This is a sufficient condition for orthonormality of a matrix [49].

A.1.4.1 A useful special case of the transformation matrix

Often in aircraft modelling, the need arises to transform a coordinate vector from one axis system to another, where the only difference between the two axis systems is that one of them has been rotated through the angle θ about a common unit vector. To more clearly describe the scenario, consider axis systems A and B where initially B coincides with A . Let B be rotated positively through the angle θ about one of the common basis vectors of A and B i.e. after the rotation, only two of B 's basis vectors differ from A 's.

Transforming the coordinates of a vector in A to coordinates in B can be done by using the appropriate DCM as shown in equation (A.25). However, in the special case when the difference between the two axis systems is parameterised by a single angle θ , the transformation matrix (or DCM) can be simplified as follows,

$$\mathbf{T}_0^i = \begin{bmatrix} 1 & 0 & 0 \\ 0 & \cos \theta & \sin \theta \\ 0 & -\sin \theta & \cos \theta \end{bmatrix} \quad \mathbf{T}_0^j = \begin{bmatrix} \cos \theta & 0 & -\sin \theta \\ 0 & 1 & 0 \\ \sin \theta & 0 & \cos \theta \end{bmatrix} \quad \mathbf{T}_0^k = \begin{bmatrix} \cos \theta & \sin \theta & 0 \\ -\sin \theta & \cos \theta & 0 \\ 0 & 0 & 1 \end{bmatrix} \quad (\text{A.30})$$

Here, the transformation matrix is denoted with a \mathbf{T} and has been derived by substituting the appropriate angles into equation (A.24). The superscript indicates the common axis about which axis system B has been rotated relative to A . The subscript indicates the symbol used to parameterise the rotation angle. Thus for the three cases above the following transformations would be used,

$$\mathbf{R}_B = [\mathbf{T}_0^i] \mathbf{R}_A \quad \mathbf{R}_B = [\mathbf{T}_0^j] \mathbf{R}_A \quad \mathbf{R}_B = [\mathbf{T}_0^k] \mathbf{R}_A \quad (\text{A.31})$$

A.1.4.2 Transforming the elements of a cross product matrix

Consider the cross product,

$$\mathbf{P} = \boldsymbol{\omega}^{BA} \times \mathbf{R} \quad (\text{A.32})$$

Coordinating the above equation into axis systems A and B gives,

$$\mathbf{P}_A = \mathbf{S}_{\omega_A^{BA}} \mathbf{R}_A \quad (\text{A.33})$$

$$\mathbf{P}_B = \mathbf{S}_{\omega_B^{BA}} \mathbf{R}_B \quad (\text{A.34})$$

Note that the cross product matrix in equation (A.33) makes use of the coordinates of $\boldsymbol{\omega}^{BA}$ in A while the cross product matrix of equation (A.34) makes use of the coordinates of the same vector $\boldsymbol{\omega}^{BA}$ but in B . It is useful to be able to relate the two cross product matrices through the DCM describing the relative attitude of A and B . To this end, equating the two equations above through the appropriate DCM gives,

$$\mathbf{S}_{\omega_A^{BA}} \mathbf{R}_A = [\mathbf{DCM}^{AB}] \mathbf{S}_{\omega_B^{BA}} \mathbf{R}_B \quad (\text{A.35})$$

Relating the coordinates of \mathbf{R} in each axis system through the appropriate DCM gives,

$$\mathbf{S}_{\omega_A^{BA}} \mathbf{R}_A = [\mathbf{DCM}^{AB}] \mathbf{S}_{\omega_B^{BA}} [\mathbf{DCM}^{BA}] \mathbf{R}_A \quad (\text{A.36})$$

This equation must hold for all \mathbf{R}_A thus yielding the desired result,

$$\mathbf{S}_{\omega_A^{BA}} = [\mathbf{DCM}^{BA}]^T \mathbf{S}_{\omega_B^{BA}} [\mathbf{DCM}^{BA}] \quad (\text{A.37})$$

A.2 Kinematics

The mathematics of maintaining the position, velocity and acceleration of a point within a body is presented in this section. Various useful attitude parameterisations are introduced and discussed.

A.2.1 The motion of a point through space

Denote the position of a point P in space relative to axis system A with the position vector \mathbf{P}^{PA} . If P forms part of a rigid body, then it is often more useful to refer to its position relative to some axis system centred at a reference point in the body, and then to maintain the position and attitude of the reference axes in space. Denote the reference axis system as B . The position of P can then be written as the vector sum,

$$\mathbf{P}^{PA} = \mathbf{P}^{BA} + \mathbf{P}^{PB} \quad (\text{A.38})$$

With P fixed relative to B , maintaining the position of P over time involves maintaining the position and attitude of axis system B over time. Maintaining attitude is equivalent to maintaining the unit vectors of an axis system over time.

In terms of position kinematics, the first and second time derivatives of a position vector are by definition the velocity and acceleration vectors as shown below for \mathbf{P}^{PA} ,

$$\mathbf{V}^{PA} \equiv \left. \frac{d}{dt} \mathbf{P}^{PA} \right|_A \quad (\text{A.39})$$

$$\mathbf{A}^{PA} \equiv \left. \frac{d}{dt} \mathbf{V}^{PA} \right|_A \quad (\text{A.40})$$

In rigid body modelling, it is only necessary to take time derivatives up to an acceleration level since the kinetic equations to be discussed in section A.3 relate forces to acceleration.

In terms of attitude kinematics, equation (A.18) shows that the time derivatives of the basis vectors of B are by definition related to the angular velocity between axis systems B and A as follows,

$$\left. \frac{d}{dt} \begin{bmatrix} \mathbf{i}^B & \mathbf{j}^B & \mathbf{k}^B \end{bmatrix} \right|_A = \boldsymbol{\omega}^{BA} \times \begin{bmatrix} \mathbf{i}^B & \mathbf{j}^B & \mathbf{k}^B \end{bmatrix} \quad (\text{A.41})$$

Equations (A.39), (A.40) and (A.41) are the three fundamental kinematic vector equations used to describe the motion of an arbitrary point fixed relative to a translating, rotating axis system. To gain further insight and develop useful relationships for the body of this document, the vector equations (A.39) and (A.40) are expanded by substituting equation (A.38). The velocity of P relative to A is then,

$$\begin{aligned} \mathbf{V}^{PA} &= \left. \frac{d}{dt} \mathbf{P}^{BA} + \mathbf{P}^{PB} \right|_A \\ &= \left. \frac{d}{dt} \mathbf{P}^{BA} \right|_A + \left. \frac{d}{dt} \mathbf{P}^{PB} \right|_A \\ &= \left. \frac{d}{dt} \mathbf{P}^{BA} \right|_A + \left. \frac{d}{dt} \mathbf{P}^{PB} \right|_B + \boldsymbol{\omega}^{BA} \times \mathbf{P}^{PB} \\ &= \mathbf{V}^{BA} + \boldsymbol{\omega}^{BA} \times \mathbf{P}^{PB} \end{aligned} \quad (\text{A.42})$$

where the fact that P is fixed in position relative to B has been used to simplify the equation. The acceleration of P relative to A is then,

$$\begin{aligned}
\mathbf{A}^{PA} &= \left. \frac{d}{dt} \mathbf{V}^{BA} + \boldsymbol{\omega}^{BA} \times \mathbf{P}^{PB} \right|_A \\
&= \left. \frac{d}{dt} \mathbf{V}^{BA} \right|_A + \left. \frac{d}{dt} \boldsymbol{\omega}^{BA} \times \mathbf{P}^{PB} \right|_A \\
&= \mathbf{A}^{BA} + \left. \frac{d}{dt} \boldsymbol{\omega}^{BA} \right|_A \times \mathbf{P}^{PB} + \boldsymbol{\omega}^{BA} \times \left. \frac{d}{dt} \mathbf{P}^{PB} \right|_A \\
&= \mathbf{A}^{BA} + \boldsymbol{\alpha}^{BA} \times \mathbf{P}^{PB} + \boldsymbol{\omega}^{BA} \times (\boldsymbol{\omega}^{BA} \times \mathbf{P}^{PB})
\end{aligned} \tag{A.43}$$

where the angular acceleration vector $\boldsymbol{\alpha}^{BA}$ is defined as follows,

$$\boldsymbol{\alpha}^{BA} \equiv \left. \frac{d}{dt} \boldsymbol{\omega}^{BA} \right|_A \tag{A.44}$$

Note that the fact that P is fixed in position relative to B has again been used to simplify the equation. Equations (A.38), (A.42) and (A.43) describe the position, velocity and acceleration of point P over time given the position of P relative to B and the position, translational velocity, translational acceleration, rotational velocity and rotational acceleration of axis system B relative to A .

To practically work with equations (A.38), (A.42) and (A.43), they need to be coordinated into an axis system. Most often, in the case of aircraft modelling, the vectors are coordinated into axis system B . Carrying out the coordination gives,

$$\dot{\mathbf{V}}_A^{PA} = [\mathbf{DCM}^{AB}] (\mathbf{V}_B^{BA} + \mathbf{S}_{\omega_B^{BA}} \mathbf{P}_B^{PB}) \tag{A.45}$$

$$\dot{\mathbf{V}}_A^{PA} = [\mathbf{DCM}^{AB}] (\mathbf{A}_B^{BA} + \mathbf{S}_{a_B^{BA}} \mathbf{P}_B^{PB} + \mathbf{S}_{\omega_B^{BA}} \mathbf{S}_{\omega_B^{BA}} \mathbf{P}_B^{PB}) \tag{A.46}$$

Returning to equation (A.41) and coordinating all vectors into axis system A gives,

$$\frac{d}{dt} [\mathbf{i}_A^B \quad \mathbf{j}_A^B \quad \mathbf{k}_A^B] = \mathbf{S}_{\omega_A^{BA}} [\mathbf{i}_A^B \quad \mathbf{j}_A^B \quad \mathbf{k}_A^B] \tag{A.47}$$

Considering the DCM of equation (A.26), with the vectors used in the dot products coordinated into axis system A , the following relationship is obtained,

$$[\mathbf{DCM}^{AB}] = \begin{bmatrix} \mathbf{i}_A^{A^T} \mathbf{i}_A^B & \mathbf{i}_A^{A^T} \mathbf{j}_A^B & \mathbf{i}_A^{A^T} \mathbf{k}_A^B \\ \mathbf{j}_A^{A^T} \mathbf{i}_A^B & \mathbf{j}_A^{A^T} \mathbf{j}_A^B & \mathbf{j}_A^{A^T} \mathbf{k}_A^B \\ \mathbf{k}_A^{A^T} \mathbf{i}_A^B & \mathbf{k}_A^{A^T} \mathbf{j}_A^B & \mathbf{k}_A^{A^T} \mathbf{k}_A^B \end{bmatrix} = \begin{bmatrix} \mathbf{i}_A^{A^T} \\ \mathbf{j}_A^{A^T} \\ \mathbf{k}_A^{A^T} \end{bmatrix} [\mathbf{i}_A^B \quad \mathbf{j}_A^B \quad \mathbf{k}_A^B] = [\mathbf{i}_A^B \quad \mathbf{j}_A^B \quad \mathbf{k}_A^B] \tag{A.48}$$

The DCM is shown to concisely maintain the attitude of an axis system. Substituting this relationship into equation (A.47) gives,

$$\frac{d}{dt} [\mathbf{DCM}^{AB}] = \mathbf{S}_{\omega_A^{BA}} [\mathbf{DCM}^{AB}] \tag{A.49}$$

Transposing both sides and applying the relationship of equation (A.37) gives,

$$\frac{d}{dt}[\mathbf{DCM}^{BA}] = -\mathbf{S}_{\omega_B^{BA}}[\mathbf{DCM}^{BA}] \quad (\text{A.50})$$

Note that the six DCM constraints of equation (A.29) imply that only three of the nine differential equations need be integrated. Equations (A.45), (A.46) and (A.50) form a set of kinematic equations up to an acceleration level. Kinematics up to this level are all that is necessary since the kinetic equations developed in section A.3 relate forces to accelerations.

A.2.2 Attitude parameterisations

Maintaining the attitude of axis system A with respect to axis system B involves maintaining the basis vectors of A relative to B at all time. The DCM was shown in the previous section to do just this. However, equation (A.29) shows that the nine DCM parameters are related through six constraint equations describing the orthonormal nature of the basis vectors that the DCM parameters describe. Thus it is desirable to seek alternative attitude parameterisations that use a reduced number of parameters that inherently satisfy the orthonormal constraint equations. This section is devoted to describing two of the more commonly used attitude parameterisations.

A.2.2.1 Euler angles

The philosophy behind Euler angles is to use three angles and a predefined order of rotation to describe the attitude of axis system B with respect to axis system A . The Euler 3-2-1 sequence is most commonly used. To describe the attitude of B relative to A , begin with a temporary axis system B_0 coinciding with A and carry out the following sequence of rotations in order,

- Yaw B_0 through the angle Ψ positively about the vector \mathbf{k}^{B_0} . Denote this new axis system B_1 .
- Pitch B_1 through the angle Θ positively about the vector \mathbf{j}^{B_1} . Denote this new axis system B_2 .
- Roll B_2 through the angle Φ positively about the vector \mathbf{i}^{B_2} . Denote this new axis system B .

The Euler angles attitude parameters are thus concisely defined by the ordered set,

$$\mathbf{E}^{BA} = \{\Phi, \Theta, \Psi\} \quad (\text{A.51})$$

To relate the Euler angles to the nine generic DCM parameters begin with equation (A.48),

$$[\mathbf{DCM}^{AB}] = [\mathbf{i}_A^B \quad \mathbf{j}_A^B \quad \mathbf{k}_A^B] \quad (\text{A.52})$$

From the definition of Euler angles, each of the unit coordinate vectors of the DCM above can be written as follows,

$$\begin{aligned} [\mathbf{DCM}^{AB}] &= [\mathbf{T}_\Phi^1 \mathbf{T}_\Theta^2 \mathbf{T}_\Psi^3 \mathbf{i}_A^A \quad \mathbf{T}_\Phi^1 \mathbf{T}_\Theta^2 \mathbf{T}_\Psi^3 \mathbf{j}_A^A \quad \mathbf{T}_\Phi^1 \mathbf{T}_\Theta^2 \mathbf{T}_\Psi^3 \mathbf{k}_A^A] \\ &= [\mathbf{T}_\Phi^1 \mathbf{T}_\Theta^2 \mathbf{T}_\Psi^3] [\mathbf{i}_A^A \quad \mathbf{j}_A^A \quad \mathbf{k}_A^A] \\ &= [\mathbf{T}_\Phi^1 \mathbf{T}_\Theta^2 \mathbf{T}_\Psi^3] \end{aligned} \quad (\text{A.53})$$

Expanding this equation gives,

$$\begin{aligned} [\mathbf{DCM}^{BA}] &= \begin{bmatrix} 1 & 0 & 0 \\ 0 & \cos \Phi & \sin \Phi \\ 0 & -\sin \Phi & \cos \Phi \end{bmatrix} \begin{bmatrix} \cos \Theta & 0 & -\sin \Theta \\ 0 & 1 & 0 \\ \sin \Theta & 0 & \cos \Theta \end{bmatrix} \begin{bmatrix} \cos \Psi & \sin \Psi & 0 \\ -\sin \Psi & \cos \Psi & 0 \\ 0 & 0 & 1 \end{bmatrix} \\ &= \begin{bmatrix} C_\Psi C_\Theta & S_\Psi C_\Theta & -S_\Theta \\ C_\Psi S_\Theta S_\Phi - S_\Psi C_\Phi & S_\Psi S_\Theta S_\Phi + C_\Psi C_\Phi & C_\Theta S_\Phi \\ C_\Psi S_\Theta C_\Phi + S_\Psi S_\Phi & S_\Psi S_\Theta C_\Phi - C_\Psi S_\Phi & C_\Theta C_\Phi \end{bmatrix} \quad C_0 \equiv \cos(\) \quad S_0 \equiv \sin(\) \end{aligned} \quad (\text{A.54})$$

which inherently satisfies all six orthonormality constraints for any choice of Euler angles. This together with its intuitive nature is the major advantage of the Euler angle parameterisation. Equation (A.50) could be used to relate the time rate of change of the Euler angles to the coordinates of the angular velocity vector in axis system B . However, the relationship is more easily derived as follows,

$$\boldsymbol{\omega}^{BA} = \dot{\Phi} \hat{\boldsymbol{\phi}} + \dot{\Theta} \hat{\boldsymbol{\theta}} + \dot{\Psi} \hat{\boldsymbol{\psi}} \quad (\text{A.55})$$

where $\hat{\boldsymbol{\phi}}$, $\hat{\boldsymbol{\theta}}$ and $\hat{\boldsymbol{\psi}}$ are the unit vectors about which the respective Euler angle rotations occur. Considering the temporary axis systems used when defining the Euler angles, it is straightforward to see that,

$$\hat{\boldsymbol{\phi}} = \mathbf{i}^{B_2} \quad \hat{\boldsymbol{\theta}} = \mathbf{j}^{B_1} \quad \hat{\boldsymbol{\psi}} = \mathbf{k}^{B_0} \quad (\text{A.56})$$

Coordinating all of the vectors into axis system B gives,

$$\begin{aligned} \boldsymbol{\omega}_B^{BA} &= \dot{\Phi} \mathbf{i}_B^{B_2} + \dot{\Theta} \mathbf{j}_B^{B_1} + \dot{\Psi} \mathbf{k}_B^{B_0} \\ &= \dot{\Phi} [\mathbf{T}_\Phi^1] \mathbf{i}_{B_2}^{B_2} + \dot{\Theta} [\mathbf{T}_\Phi^1 \mathbf{T}_\Theta^2] \mathbf{j}_{B_1}^{B_1} + \dot{\Psi} [\mathbf{T}_\Phi^1 \mathbf{T}_\Theta^2 \mathbf{T}_\Psi^3] \mathbf{k}_{B_0}^{B_0} \end{aligned} \quad (\text{A.57})$$

which expanded gives the coordinate relationship,

$$\boldsymbol{\omega}_B^{BA} = \begin{bmatrix} 1 & 0 & -\sin \Theta \\ 0 & \cos \Phi & \cos \Theta \sin \Phi \\ 0 & -\sin \Phi & \cos \Theta \cos \Phi \end{bmatrix} \begin{bmatrix} \dot{\Phi} \\ \dot{\Theta} \\ \dot{\Psi} \end{bmatrix} \quad (\text{A.58})$$

Inverting the above equation provides the desired kinematic relationship,

$$\begin{bmatrix} \dot{\Phi} \\ \dot{\Theta} \\ \dot{\Psi} \end{bmatrix} = \begin{bmatrix} 1 & \sin \Phi \tan \Theta & \cos \Phi \tan \Theta \\ 0 & \cos \Phi & -\sin \Phi \\ 0 & \sin \Phi \sec \Theta & \cos \Phi \sec \Theta \end{bmatrix} \boldsymbol{\omega}_B^{\text{BA}} \quad |\Theta| \neq \frac{\pi}{2} \quad (\text{A.59})$$

The singularity in the above result highlights the main disadvantage of using Euler angles. For more information on Euler angles see [43,50].

A.2.2.2 Quaternions

The philosophy behind quaternions is based on Euler's theorem which states that the orientation of axis system B relative to A can be uniquely described by rotating B from A about a vector λ through a rotation angle μ . For mathematical singularity reasons, the quaternion parameters are defined to be,

$$\mathbf{q} = \begin{bmatrix} q_1 \\ q_2 \\ q_3 \\ q_4 \end{bmatrix} = \begin{bmatrix} \lambda_x \sin \mu/2 \\ \lambda_y \sin \mu/2 \\ \lambda_z \sin \mu/2 \\ \cos \mu/2 \end{bmatrix} \quad (\text{A.60})$$

where,

$$\lambda = \lambda_x \mathbf{i}^A + \lambda_y \mathbf{j}^A + \lambda_z \mathbf{k}^A \quad (\text{A.61})$$

and are further constrained by the relationship,

$$q_1^2 + q_2^2 + q_3^2 + q_4^2 = 1 \quad (\text{A.62})$$

In [50] it is shown that the DCM matrix can be written in terms of quaternions as follows,

$$[\mathbf{DCM}^{\text{BA}}] = \begin{bmatrix} q_4^2 + q_1^2 - q_2^2 - q_3^2 & 2(q_1q_2 + q_3q_4) & 2(q_1q_3 - q_2q_4) \\ 2(q_1q_2 - q_3q_4) & q_4^2 - q_1^2 + q_2^2 - q_3^2 & 2(q_2q_3 + q_1q_4) \\ 2(q_1q_3 + q_2q_4) & 2(q_2q_3 - q_1q_4) & q_4^2 - q_1^2 - q_2^2 + q_3^2 \end{bmatrix} \quad (\text{A.63})$$

Note that the nine DCM parameters and the six constraints have been reduced to four parameters with a single constraint. The other five constraints are inherently satisfied for any choice of quaternions.

For details on relating the coordinates of the angular velocity vector to the quaternion parameters see [50]. The result however is simply stated below,

$$\dot{\mathbf{q}}^{\text{BA}} = \frac{1}{2} \boldsymbol{\Omega}^{\text{BA}} \boldsymbol{\omega}_B^{\text{BA}} \quad (\text{A.64})$$

and in expanded form yields,

$$\begin{bmatrix} \dot{q}_1 \\ \dot{q}_2 \\ \dot{q}_3 \\ \dot{q}_4 \end{bmatrix} = \frac{1}{2} \begin{bmatrix} q_4 & -q_3 & q_2 \\ q_3 & q_4 & -q_1 \\ -q_2 & q_1 & q_4 \\ -q_1 & -q_2 & -q_3 \end{bmatrix} \boldsymbol{\omega}_B^{\text{BA}} \quad (\text{A.65})$$

The advantage of parameterising attitude with quaternions over Euler angles is that there are no singularities in the resulting attitude kinematics. However, Quaternions do require the use of an extra parameter and have an associated constraint equation. Furthermore, unlike Euler angles, the physical meaning of the quaternion parameters is difficult to readily interpret. Thus, for most applications that do not involve large pitch angles, the Euler 3-2-1 attitude parameterisation is used. For further details regarding quaternions, see [50].

A.3 Kinetics

The previous section investigated the kinematic equations describing the motion of a point through space. The topic of kinetics is now considered. This topic involves how forces acting upon a body translate into accelerations. Once the accelerations have been determined the kinematic equations describe how they propagate into attitude, velocity and position over time. With the scope limited to rigid bodies, Newton's equations of motion for a point mass particle are used to develop the kinetic equations relating resultant forces and moments acting upon a rigid body to the acceleration of the body.

A.3.1 Newton's laws of motion for mass particles

Newton provides three laws that govern the motion of infinitely small mass elements or particles. Denote a mass particle by dm . The three laws are stated below,

- A mass particle dm will continue with rectilinear motion at a constant velocity V with respect to inertial space unless acted upon by a force vector dF . This law provides a test to determine whether a space is in fact an inertial space.
- A mass particle dm acted on by a force dF moves such that the time rate change with respect to inertial space of the particle's momentum ($V^{dmI} dm$) is equal to the force vector (where V^{dmI} is the particle's velocity with respect to inertial space).
- If mass particle A exerts a force on mass particle B then mass particle B exerts an equal and opposite force on mass particle A. Because the focus is limited to infinitely small mass elements, the forces are collinear.

A.3.2 Modelling a rigid body

Consider a body made up of a number of infinitely small mass particles dm . Describing the motion of the body requires being able to describe the motion of each mass element within the body. Due to the infinitely small nature of the mass elements, it would be impossible to

maintain each of their position trajectories over time. However, if the scope is limited to rigid bodies then to determine the position trajectory of any mass element it is only necessary to maintain the position trajectory of one mass element together with the attitude of the body over time.

To obtain a mathematical hold on the problem two axis systems are introduced. They are,

- The Inertial Axis System (I): Newton's laws of motion can be applied in this axis system. It is typically chosen in some convenient manner appropriate to the specific application.
- The Body Axis System (B): This right handed axis system has its origin coinciding with the aircraft's centre of mass. The i^B unit vector runs along a selected reference line in the plane of symmetry of the aircraft (typically parallel to the chord of the wing, facing forwards). The j^B unit vector lies normal to the aircraft's plane of symmetry in the direction of the starboard wing. The k^B unit vector completes the right handed axis system.

A third axis system that will not be used in this section but will be used significantly throughout this thesis is,

- The Wind Axis System (W): This right handed axis system has its origin coinciding with the aircraft's centre of mass. The i^W unit vector is parallel to the aircraft's velocity vector. The k^W unit vector is orthogonal to i^W and lies in the aircraft's plane of symmetry. The j^W unit vector completes the right handed axis system and for typical angles of attack and sideslip points in the direction of the starboard wing.

With these axis systems in place, and with reference to equation (A.38) the position of an arbitrary particle in the body with respect to inertial space can be written as follows,

$$\mathbf{P}^{dmI} = \mathbf{P}^{BI} + \mathbf{P}^{dmB} \quad (\text{A.66})$$

Taking the time derivative of the above equation with respect to inertial space provides the velocity of that particle with respect to inertial space,

$$\begin{aligned} \mathbf{V}^{dmI} &= \left. \frac{d}{dt} \mathbf{P}^{dmI} \right|_I \\ &= \left. \frac{d}{dt} \mathbf{P}^{BI} \right|_I + \left. \frac{d}{dt} \mathbf{P}^{dmB} \right|_I \\ &= \mathbf{V}^{BI} + \left. \frac{d}{dt} \mathbf{P}^{dmB} \right|_B + \boldsymbol{\omega}^{BI} \times \mathbf{P}^{dmB} \\ &= \mathbf{V}^{BI} + \mathbf{V}^{dmB} + \boldsymbol{\omega}^{BI} \times \mathbf{P}^{dmB} \\ &= \mathbf{V}^{BI} + \boldsymbol{\omega}^{BI} \times \mathbf{P}^{dmB} \end{aligned} \quad (\text{A.67})$$

since,

$$\mathbf{V}^{dmB} = \mathbf{0} \quad (\text{A.68})$$

for a rigid body. From equation (A.67) it is clear that for a rigid body, where \mathbf{P}^{dmB} for each mass element is fixed, the velocity of every mass element is uniquely described by the translational velocity of the origin of the body axis system with respect to inertial space (i.e. the mass element that coincides with the origin), and the angular velocity of the body axis system with respect to inertial space. The motion of each mass element can thus be considered the superposition of the translational and rotational motions of the body axis system.

With the above ideas fixed, define now for a single mass element the incremental linear momentum vector and the incremental angular momentum vector about the origin of B .

$$\text{Linear:} \quad d\mathbf{L} \equiv \mathbf{V}^{dmI} dm \quad (\text{A.69})$$

$$\text{Angular:} \quad d\mathbf{H}^B \equiv \mathbf{P}^{dmB} \times d\mathbf{L} = \mathbf{P}^{dmB} \times \mathbf{V}^{dmI} dm \quad (\text{A.70})$$

Although both types of momentum use the absolute velocity of a mass element (\mathbf{V}^{dmI}), when the momentum is integrated over the volume of the body (V), the following is found,

$$\begin{aligned} \text{Linear:} \quad \mathbf{L} &= \int_V \mathbf{V}^{dmI} dm \\ &= \int_V \mathbf{V}^{BI} + \boldsymbol{\omega}^{BI} \times \mathbf{P}^{dmB} dm \\ &= \mathbf{V}^{BI} \int_V dm + \boldsymbol{\omega}^{BI} \times \int_V \mathbf{P}^{dmB} dm \end{aligned} \quad (\text{A.71})$$

$$\begin{aligned} \text{Angular:} \quad \mathbf{H}^B &= \int_V \mathbf{P}^{dmB} \times \mathbf{V}^{dmI} dm \\ &= \int_V \mathbf{P}^{dmB} \times (\mathbf{V}^{BI} + \boldsymbol{\omega}^{BI} \times \mathbf{P}^{dmB}) dm \\ &= \int_V \mathbf{P}^{dmB} dm \times \mathbf{V}^{BI} + \int_V \mathbf{P}^{dmB} \times (\boldsymbol{\omega}^{BI} \times \mathbf{P}^{dmB}) dm \end{aligned} \quad (\text{A.72})$$

If the origin of the body axis system B is selected such that,

$$\int_V \mathbf{P}^{dmB} dm = \mathbf{0} \quad (\text{A.73})$$

then the expressions for the linear and angular momentums of the entire body reduce to,

$$\text{Linear:} \quad \mathbf{L} = \mathbf{V}^{BI} \int_V dm \quad (\text{A.74})$$

$$\text{Angular:} \quad \mathbf{H}^B = \int_V \mathbf{P}^{dmB} \times (\boldsymbol{\omega}^{BI} \times \mathbf{P}^{dmB}) dm \quad (\text{A.75})$$

When the origin of B is chosen to satisfy equation (A.73), it is referred to as coinciding with the body's centre of mass i.e. the mass weighted average position of the body. With this choice, equations (A.74) and (A.75) show that the linear momentum quantifies only the

translational momentum of the body i.e. consider the body non-rotating with all particles moving at the same velocity V^{BI} , while the angular momentum about B quantifies the momentum due to rotational motion only i.e. consider the centre of mass stationary while the body rotates at ω^{BI} . It will now be shown that the linear and angular momentums of a body are useful quantities because of their relationships to the external forces and moments acting on the body. Taking the time derivative of the respective total momentums with respect to inertial space and making use of Newton's laws yields the following results,

$$\begin{aligned}
 \frac{d}{dt} \mathbf{L} \Big|_I &= \frac{d}{dt} \int_V \mathbf{V}^{dmI} dm \Big|_I \\
 \text{Linear:} \quad &= \int_V \frac{d}{dt} \mathbf{V}^{dmI} \Big|_I dm \\
 &= \int_V \mathbf{A}^{dmI} dm
 \end{aligned} \tag{A.76}$$

$$\begin{aligned}
 \frac{d}{dt} \mathbf{H}^B \Big|_I &= \frac{d}{dt} \int_V \mathbf{P}^{dmB} \times \mathbf{V}^{dmI} dm \Big|_I \\
 &= \int_V \frac{d}{dt} \mathbf{P}^{dmB} \times \mathbf{V}^{dmI} \Big|_I dm \\
 &= \int_V \frac{d}{dt} \mathbf{P}^{dmB} \Big|_I \times \mathbf{V}^{dmI} dm + \int_V \mathbf{P}^{dmB} \times \frac{d}{dt} \mathbf{V}^{dmI} \Big|_I dm \\
 &= \int_V \left(\frac{d}{dt} \mathbf{P}^{dmB} \Big|_B + \boldsymbol{\omega}^{BI} \times \mathbf{P}^{dmB} \right) \times \mathbf{V}^{dmI} dm + \int_V \mathbf{P}^{dmB} \times \frac{d}{dt} \mathbf{V}^{dmI} \Big|_I dm \\
 \text{Angular:} \quad &= \int_V \left(\mathbf{V}^{dmB} + \boldsymbol{\omega}^{BI} \times \mathbf{P}^{dmB} \right) \times \mathbf{V}^{dmI} dm + \int_V \mathbf{P}^{dmB} \times \mathbf{A}^{dmI} dm \\
 &= \int_V \left(\boldsymbol{\omega}^{BI} \times \mathbf{P}^{dmB} \right) \times \left(\mathbf{V}^{BI} + \boldsymbol{\omega}^{BI} \times \mathbf{P}^{dmB} \right) dm + \int_V \mathbf{P}^{dmB} \times \mathbf{A}^{dmI} dm \\
 &= \int_V \left(\boldsymbol{\omega}^{BI} \times \mathbf{P}^{dmB} \right) dm \times \mathbf{V}^{BI} + \int_V \mathbf{P}^{dmB} \times \mathbf{A}^{dmI} dm \\
 &= \left(\boldsymbol{\omega}^{BI} \times \int_V \mathbf{P}^{dmB} dm \right) \times \mathbf{V}^{BI} + \int_V \mathbf{P}^{dmB} \times \mathbf{A}^{dmI} dm \\
 &= \int_V \mathbf{P}^{dmB} \times \mathbf{A}^{dmI} dm
 \end{aligned} \tag{A.77}$$

Note that to get to the simple expression of equation (A.77), use has been made of equations (A.68) and (A.73). Newton's second law is now applied to each mass element in the integrals of equations (A.76) and (A.77) to give,

$$\text{Linear:} \quad \frac{d}{dt} \mathbf{L} \Big|_I = \int_V d\mathbf{F} \tag{A.78}$$

$$\text{Angular:} \quad \frac{d}{dt} \mathbf{H}^B \Big|_I = \int_V \mathbf{P}^{dmB} \times d\mathbf{F} \tag{A.79}$$

To proceed, the forces acting on each mass element are now considered. In any body, both internal and external forces act on the mass particles. Thus, the forces acting on a particle can

be written as follows,

$$d\mathbf{F} = d\mathbf{F}^E + d\mathbf{F}^I \quad (\text{A.80})$$

where the superscript E stands for external and the superscript I stands for internal. Newton's third law states that for every internal force exerted by mass particle A on mass particle B, there will be an equal and opposite internal force exerted by particle B on particle A. These forces are also collinear. Thus, integrating the incremental force vector over the volume of the body yields the following result,

$$\begin{aligned} \mathbf{F} &= \int_V d\mathbf{F} \\ &= \int_V d\mathbf{F}^E + \int_V d\mathbf{F}^I \\ &= \int_V d\mathbf{F}^E \\ &= \mathbf{F}^E \end{aligned} \quad (\text{A.81})$$

Furthermore, define the incremental moment that the incremental force element $d\mathbf{F}$ produces about B to be,

$$d\mathbf{M}^B \equiv \mathbf{P}^{dmB} \times d\mathbf{F} \quad (\text{A.82})$$

Integrating the incremental moment vector over the volume of the body yields,

$$\begin{aligned} \mathbf{M}^B &= \int_V \mathbf{P}^{dmB} \times d\mathbf{F} \\ &= \int_V \mathbf{P}^{dmB} \times d\mathbf{F}^E + \int_V \mathbf{P}^{dmB} \times d\mathbf{F}^I \\ &= \int_V \mathbf{P}^{dmB} \times d\mathbf{F}^E \\ &= \mathbf{M}^{BE} \end{aligned} \quad (\text{A.83})$$

Combining equations (A.81) and (A.83) with equations (A.78) and (A.79) gives the kinetic equations for a rigid body where the origin of B is the centre of mass and the force and moment vectors are due to the external forces only,

$$\text{Linear:} \quad \mathbf{F} = \left. \frac{d}{dt} \mathbf{L} \right|_I \quad \text{with} \quad \mathbf{L} = V^{BI} \int_V dm \quad (\text{A.84})$$

$$\text{Angular:} \quad \mathbf{M}^B = \left. \frac{d}{dt} \mathbf{H}^B \right|_I \quad \text{with} \quad \mathbf{H}^B = \int_V \mathbf{P}^{dmB} \times (\boldsymbol{\omega}^{BI} \times \mathbf{P}^{dmB}) dm \quad (\text{A.85})$$

A.3.2.1 Insight into the linear and angular momentum integrals

To gain insight into the linear and angular momentum integrals they are further simplified. First define the total mass of the body as follows,

$$m \equiv \int_V dm \quad (\text{A.86})$$

Thus,

$$\mathbf{L} = m\mathbf{V}^{BI} \quad (\text{A.87})$$

To further simplify the angular momentum it is required to coordinate the vectors involved into an axis system. It is usually most convenient to coordinate the angular momentum about B into axis system B . Thus,

$$\begin{aligned} \mathbf{H}_B^B &= \int_V \mathbf{S}_{P_B^B} \left(\mathbf{S}_{\omega_B^{BI}} \mathbf{P}_B^{dmB} \right) dm \\ &= \int_V \mathbf{S}_{P_B^{dmB}} \left(-\mathbf{S}_{P_B^{dmB}} \omega_B^{BI} \right) dm \\ &= \left[-\int_V \mathbf{S}_{P_B^{dmB}} \mathbf{S}_{P_B^{dmB}} dm \right] \omega_B^{BI} \\ &= \mathbf{I}_B^B \omega_B^{BI} \end{aligned} \quad (\text{A.88})$$

where,

$$\mathbf{I}_B^B \equiv -\int_V \mathbf{S}_{P_B^{dmB}} \mathbf{S}_{P_B^{dmB}} dm \quad (\text{A.89})$$

\mathbf{I}_B^B is known as the moment of inertia matrix about B , coordinated into B . Due to the fact that in aircraft modelling, unless otherwise stated the moments and moments of inertia are always taken about the centre of mass (origin of the body axis system), the superscript indicating this will be omitted to avoid clutter. To gain insight into the form of \mathbf{I}_B (note the superscript has been omitted), denote the coordinates of the position of an incremental mass element in B as follows,

$$\mathbf{P}^{dmB} = x\mathbf{i}^B + y\mathbf{j}^B + z\mathbf{k}^B \quad (\text{A.90})$$

Then,

$$\begin{aligned}
\mathbf{I}_B &= -\int_V \mathbf{S}_{p_B^{cmB}} \mathbf{S}_{p_B^{cmB}} dm \\
&= -\int_V \begin{bmatrix} 0 & -z & y \\ z & 0 & -x \\ -y & x & 0 \end{bmatrix} \begin{bmatrix} 0 & -z & y \\ z & 0 & -x \\ -y & x & 0 \end{bmatrix} dm \\
&= \int_V \begin{bmatrix} y^2 + z^2 & -xy & -xz \\ -xy & x^2 + z^2 & -yz \\ -xz & -yz & x^2 + y^2 \end{bmatrix} dm \\
&= \begin{bmatrix} \int_V y^2 + z^2 dm & -\int_V xy dm & -\int_V xz dm \\ -\int_V xy dm & \int_V x^2 + z^2 dm & -\int_V yz dm \\ -\int_V xz dm & -\int_V yz dm & \int_V x^2 + y^2 dm \end{bmatrix} \\
&= \begin{bmatrix} I_{xx} & -I_{xy} & -I_{xz} \\ -I_{xy} & I_{yy} & -I_{yz} \\ -I_{xz} & -I_{yz} & I_{zz} \end{bmatrix}
\end{aligned} \tag{A.91}$$

The inertia properties of the body are thus concisely summarised by the mass m and the moment of inertia matrix \mathbf{I}_B .

Appendix B

Detailed Derivations

B.1 Non-minimum phase system analysis

The maximum undershoot of a stable second order system with a single right half plane zero is determined in this section as a function of the system parameters. Consider the second order NMP system below,

$$\begin{aligned} G(s) &= k \frac{\omega_n^2}{s^2 + 2\zeta\omega_n + \omega_n^2} \frac{z_0 - s}{z_0} \\ &= G_n(s) - \frac{s}{z_0} G_n(s) \end{aligned} \tag{B.1}$$

where,

$$G_n(s) = k \frac{\omega_n^2}{s^2 + 2\zeta\omega_n + \omega_n^2} \tag{B.2}$$

is a classical second order system with no zeros. For simplicity, the analysis continues with $k = 1$. The exact value of the DC gain makes no difference to the result. The Laplace transform of the NMP system's step response is,

$$Y(s) = Y_1(s) - Y_2(s) \tag{B.3}$$

where,

$$Y_1(s) = G_1(s) \frac{1}{s} \tag{B.4}$$

$$Y_2(s) = \frac{1}{z_0} G_1(s) \tag{B.5}$$

Inverse Laplace transforming through partial fraction expansion the step response equations (B.4) and (B.5) above yields the intermediate results,

$$Y_1(s) = \frac{A}{s + \sigma - j\omega_d} + \frac{A^*}{s + \sigma + j\omega_d} + \frac{B}{s} \quad (\text{B.6})$$

$$Y_2(s) = \frac{C}{s + \sigma - j\omega_d} + \frac{C^*}{s + \sigma + j\omega_d} \quad (\text{B.7})$$

with,

$$A = \frac{\omega_n^2}{\omega_d} \frac{1}{-\sigma + j\omega_d} \frac{1}{2j} \quad (\text{B.8})$$

$$B = 1 \quad (\text{B.9})$$

$$C = \frac{1}{z_0} \frac{\omega_n^2}{\omega_d} \frac{1}{2j} \quad (\text{B.10})$$

Continuing to inverse Laplace transform equations (B.6) and (B.7) yields the time signals,

$$\begin{aligned} y_1(t) &= \frac{\omega_n^2}{\omega_d} \frac{1}{2j} \left(\frac{1}{-\sigma + j\omega_d} e^{-\sigma + j\omega_d t} - \frac{1}{-\sigma - j\omega_d} e^{-\sigma - j\omega_d t} \right) + 1 \\ &= 1 - \frac{e^{-\sigma t}}{\omega_d} [\sigma \sin(\omega_d t) + \omega_d \cos(\omega_d t)] \end{aligned} \quad (\text{B.11})$$

$$\begin{aligned} y_2(t) &= \frac{\omega_n^2}{z_0 \omega_d} \frac{(e^{-\sigma + j\omega_d t} - e^{-\sigma - j\omega_d t})}{2j} \\ &= \frac{\omega_n^2}{z_0 \omega_d} e^{-\sigma t} \sin(\omega_d t) \end{aligned} \quad (\text{B.12})$$

The complete step response time domain signal is thus,

$$\begin{aligned} y(t) &= y_1(t) - y_2(t) \\ &= 1 - \frac{e^{-\sigma t}}{\omega_d} [\sigma \sin(\omega_d t) + \omega_d \cos(\omega_d t)] - \frac{\omega_n^2}{z_0 \omega_d} e^{-\sigma t} \sin(\omega_d t) \\ &= 1 - \frac{e^{-\sigma t}}{\omega_d} \left[\left(\sigma + \frac{\omega_n^2}{z_0} \right) \sin(\omega_d t) + \omega_d \cos(\omega_d t) \right] \\ &= 1 - \frac{1}{\sin \phi} e^{-\sigma t} \sin(\omega_d t + \phi) \end{aligned} \quad (\text{B.13})$$

where,

$$r = \frac{\omega_d}{z_0} \quad (\text{B.14})$$

$$\phi = \tan^{-1} \left(\frac{\sqrt{1 - \zeta^2}}{\zeta + r} \right) \quad (\text{B.15})$$

To solve for the minimum undershoot point, equation (B.13) is differentiated with respect to

time,

$$\begin{aligned}\dot{y}(t) &= \sigma \frac{1}{\sin \phi} e^{-\sigma t} \sin(\omega_d t + \phi) - \frac{\omega_d}{\sin \phi} e^{-\sigma t} \cos(\omega_d t + \phi) \\ &= \frac{1}{\sin \phi} e^{-\sigma t} (\sigma \sin(\omega_d t + \phi) - \omega_d \cos(\omega_d t + \phi))\end{aligned}\quad (\text{B.16})$$

Setting the derivative to zero and solving allows the peak undershoot time to be solved for,

$$\begin{aligned}t_{\min} &= \frac{1}{\omega_d} \left[\tan^{-1} \left(\frac{\omega_d}{\sigma} \right) - \phi \right] \\ &= \frac{\theta - \phi}{\omega_d}\end{aligned}\quad (\text{B.17})$$

where,

$$\begin{aligned}\theta &= \tan^{-1} \left(\frac{\sqrt{1 - \zeta^2}}{\zeta} \right) \\ &= \cos^{-1}(\zeta)\end{aligned}\quad (\text{B.18})$$

Substituting the peak undershoot time into equation (B.13) allows the peak undershoot to be calculated,

$$\begin{aligned}y_{\min} &= y(t_{\min}) \\ &= 1 - \frac{1}{\sin \phi} e^{-\frac{\sigma}{\omega_d}(\theta - \phi)} \sin \theta \\ &= 1 - \frac{\sin \theta}{\sin \phi} e^{-\left(\frac{\theta - \phi}{\tan \theta}\right)}\end{aligned}\quad (\text{B.19})$$

B.2 Normal dynamics

The normal dynamics can be written as follows,

$$\dot{\mathbf{x}} = \mathbf{A}\mathbf{x} + \mathbf{B}\delta_E + \mathbf{B}_1 + \mathbf{B}_2 e_{33}^{WI} \quad (\text{B.20})$$

$$C_W = \mathbf{C}\mathbf{x} + D\delta_E \quad (\text{B.21})$$

where,

$$\mathbf{x} = \begin{bmatrix} \alpha \\ Q \end{bmatrix} \quad (\text{B.22})$$

and,

$$\mathbf{A} = \begin{bmatrix} -\frac{L_\alpha}{m\bar{V}} & 1 \\ \frac{M_\alpha}{I_{yy}} & \frac{M_Q}{I_{yy}} \end{bmatrix} \quad \mathbf{B} = \begin{bmatrix} -\frac{L_{\delta_E}}{m\bar{V}} \\ \frac{M_{\delta_E}}{I_{yy}} \end{bmatrix} \quad \mathbf{B}_1 = \begin{bmatrix} -\frac{L_0}{m\bar{V}} \\ \frac{M_0}{I_{yy}} \end{bmatrix} \quad \mathbf{B}_2 = \begin{bmatrix} \frac{g}{\bar{V}} \\ 0 \end{bmatrix} \quad (\text{B.23})$$

$$\mathbf{C} = \begin{bmatrix} -\frac{L_\alpha}{m} & -\frac{L_Q}{m} \end{bmatrix} \quad \mathbf{D} = \begin{bmatrix} -\frac{L_{\delta_E}}{m} \end{bmatrix} \quad (\text{B.24})$$

The following standard aircraft assumption has been used to simplify the dynamics [43],

$$\left| \frac{L_Q}{m\bar{V}} \right| \ll 1 \quad (\text{B.25})$$

B.2.1 Characteristic equation for the poles

The poles of the system in equation (B.20) are the roots of the characteristic equation,

$$p(s) = \det(s\mathbf{I} - \mathbf{A}) \quad (\text{B.26})$$

Expanding this equation yields,

$$\begin{aligned} p(s) &= \det \begin{bmatrix} s + \frac{L_\alpha}{m\bar{V}} & -1 \\ -\frac{M_\alpha}{I_{yy}} & s - \frac{M_Q}{I_{yy}} \end{bmatrix} \\ &= s^2 + \left(\frac{L_\alpha}{m\bar{V}} - \frac{M_Q}{I_{yy}} \right) s - \left(\frac{L_\alpha}{m\bar{V}} \frac{M_Q}{I_{yy}} + \frac{M_\alpha}{I_{yy}} \right) \end{aligned} \quad (\text{B.27})$$

B.2.2 Characteristic equation for the zeros

The zeros from elevator through to normal specific acceleration are the roots of the characteristic equation,

$$z(s) = \text{Cadj}(s\mathbf{I} - \mathbf{A})\mathbf{B} + \mathbf{D} \det(s\mathbf{I} - \mathbf{A}) \quad (\text{B.28})$$

Expanding the first term of equation (B.28) gives,

$$\begin{aligned} \text{Cadj}(s\mathbf{I} - \mathbf{A})\mathbf{B} &= \begin{bmatrix} -\frac{L_\alpha}{m} & -\frac{L_Q}{m} \end{bmatrix} \begin{bmatrix} s - \frac{M_Q}{I_{yy}} & 1 \\ \frac{M_\alpha}{I_{yy}} & s + \frac{L_\alpha}{m\bar{V}} \end{bmatrix} \begin{bmatrix} -\frac{L_{\delta_E}}{m\bar{V}} \\ \frac{M_{\delta_E}}{I_{yy}} \end{bmatrix} \\ &= \frac{L_{\delta_E}}{m\bar{V}} \frac{L_\alpha}{m} s - \frac{L_{\delta_E}}{m\bar{V}} \frac{L_\alpha}{m} \frac{M_Q}{I_{yy}} + \frac{L_{\delta_E}}{m\bar{V}} \frac{L_Q}{m} \frac{M_\alpha}{I_{yy}} - \frac{M_{\delta_E}}{I_{yy}} \frac{L_\alpha}{m} - \frac{M_{\delta_E}}{I_{yy}} \frac{L_Q}{m} s - \frac{M_{\delta_E}}{I_{yy}} \frac{L_Q}{m} \frac{L_\alpha}{m\bar{V}} \\ &= \frac{L_{\delta_E}}{m} \left[\left(\frac{L_\alpha}{m\bar{V}} - \frac{M_{\delta_E}}{I_{yy}} \frac{L_Q}{I_{yy}} \right) s + \left(-\frac{L_\alpha}{m\bar{V}} \frac{M_Q}{I_{yy}} + \frac{L_Q}{m\bar{V}} \frac{M_\alpha}{I_{yy}} - \frac{M_{\delta_E}}{I_{yy}} \frac{L_\alpha}{m} - \frac{M_{\delta_E}}{I_{yy}} \frac{L_Q}{m} \frac{L_\alpha}{m\bar{V}} \right) \right] \end{aligned} \quad (\text{B.29})$$

The determinant of the second term in equation (B.28) has already been evaluated in equation (B.27). Thus, the characteristic equation for the zeros becomes,

$$\begin{aligned}
 z(s) &= \frac{L_{\delta_E}}{m} \left[\left(\frac{L_\alpha}{m\bar{V}} - \frac{M_{\delta_E} L_Q}{L_{\delta_E} I_{yy}} \right) s + \left(-\frac{L_\alpha M_Q}{m\bar{V} I_{yy}} + \frac{L_Q M_\alpha}{m\bar{V} I_{yy}} - \frac{M_{\delta_E} L_\alpha}{L_{\delta_E} I_{yy}} - \frac{M_{\delta_E} L_Q L_\alpha}{L_{\delta_E} I_{yy} m\bar{V}} \right) \right. \\
 &\quad \left. -s^2 - \left(\frac{L_\alpha}{m\bar{V}} - \frac{M_Q}{I_{yy}} \right) s + \left(\frac{L_\alpha M_Q}{m\bar{V} I_{yy}} + \frac{M_\alpha}{I_{yy}} \right) \right] \\
 &= \frac{L_{\delta_E}}{m} \left[-s^2 + \frac{L_Q}{I_{yy}} \left(\frac{M_Q}{L_Q} - \frac{M_{\delta_E}}{L_{\delta_E}} \right) s + \frac{L_\alpha}{I_{yy}} \left(\frac{M_\alpha}{L_\alpha} - \frac{M_{\delta_E}}{L_{\delta_E}} \right) \left(1 + \frac{L_Q}{m\bar{V}} \right) \right] \\
 &\approx \frac{L_{\delta_E}}{m} \left[-s^2 + \frac{L_Q}{I_{yy}} \left(\frac{M_Q}{L_Q} - \frac{M_{\delta_E}}{L_{\delta_E}} \right) s + \frac{L_\alpha}{I_{yy}} \left(\frac{M_\alpha}{L_\alpha} - \frac{M_{\delta_E}}{L_{\delta_E}} \right) \right]
 \end{aligned} \tag{B.30}$$

where the simplifying assumption of equation (B.25) has again been used. Since only the roots of equation (B.30) are desired, the characteristic equation for the zeros becomes,

$$z(s) = s^2 - \frac{L_Q}{I_{yy}} \left(\frac{M_Q}{L_Q} - \frac{M_{\delta_E}}{L_{\delta_E}} \right) s - \frac{L_\alpha}{I_{yy}} \left(\frac{M_\alpha}{L_\alpha} - \frac{M_{\delta_E}}{L_{\delta_E}} \right) \tag{B.31}$$

B.2.3 Normal specific acceleration controller design

As argued in section 4.2.4 the normal dynamics reduce to,

$$\begin{bmatrix} \dot{\alpha} \\ \dot{Q} \end{bmatrix} = \begin{bmatrix} -\frac{L_\alpha}{m\bar{V}} & 1 \\ \frac{M_\alpha}{I_{yy}} & \frac{M_Q}{I_{yy}} \end{bmatrix} \begin{bmatrix} \alpha \\ Q \end{bmatrix} + \begin{bmatrix} 0 \\ \frac{M_{\delta_E}}{I_{yy}} \end{bmatrix} \delta_E + \begin{bmatrix} -\frac{L_0}{m\bar{V}} \\ \frac{M_0}{I_{yy}} \end{bmatrix} + \begin{bmatrix} \frac{g}{\bar{V}} \\ 0 \end{bmatrix} e_{33}^{WT} \tag{B.32}$$

$$C_w = \begin{bmatrix} -\frac{L_\alpha}{m} & 0 \end{bmatrix} \begin{bmatrix} \alpha \\ Q \end{bmatrix} + [0] \delta_E + \begin{bmatrix} -\frac{L_0}{m} \end{bmatrix} \tag{B.33}$$

when the effect of the zeros of section B.2.2 can be neglected. To dynamically invert the effect of the gravity coupling on the normal specific acceleration dynamics requires differentiating the output of interest until the control input appears in the same equation. The control can then be used to directly cancel the undesirable terms. Beginning with the normal specific acceleration output equation,

$$C_w = \begin{bmatrix} -\frac{L_\alpha}{m} \\ \frac{L_0}{m} \end{bmatrix} \alpha + \begin{bmatrix} -\frac{L_0}{m} \end{bmatrix} \tag{B.34}$$

Differentiating this equation once with respect to time, remembering that all quantities inside the matrices of equations (B.32) and (B.33) are considered parameters due to either their static nature or the timescale separation condition yields,

$$\begin{aligned}\dot{C}_w &= \begin{bmatrix} -\frac{L_\alpha}{m} \end{bmatrix} \dot{\alpha} \\ &= \begin{bmatrix} -\frac{L_\alpha}{m\bar{V}} \end{bmatrix} C_w + \begin{bmatrix} -\frac{L_\alpha}{m} \end{bmatrix} Q + \begin{bmatrix} -\frac{L_\alpha g}{m\bar{V}} \end{bmatrix} e_{33}^{wI} \end{aligned} \quad (\text{B.35})$$

where the fact that,

$$\dot{\alpha} = Q + \frac{1}{\bar{V}} (C_w + g e_{33}^{wI}) \quad (\text{B.36})$$

has been used. Differentiating the normal specific acceleration a second time gives,

$$\begin{aligned}\ddot{C}_w &= \begin{bmatrix} -\frac{L_\alpha}{m\bar{V}} \end{bmatrix} \dot{C}_w + \begin{bmatrix} -\frac{L_\alpha}{m} \end{bmatrix} \dot{Q} + \begin{bmatrix} -\frac{L_\alpha g}{m\bar{V}} \end{bmatrix} \dot{e}_{33}^{wI} \\ &= \begin{bmatrix} -\frac{L_\alpha}{m\bar{V}} \end{bmatrix} \dot{C}_w + \begin{bmatrix} -\frac{L_\alpha M_\alpha}{mI_{yy}} \end{bmatrix} \alpha + \begin{bmatrix} -\frac{L_\alpha M_Q}{mI_{yy}} \end{bmatrix} Q + \begin{bmatrix} -\frac{L_\alpha M_{\delta_E}}{mI_{yy}} \end{bmatrix} \delta_E + \begin{bmatrix} -\frac{L_\alpha M_0}{mI_{yy}} \end{bmatrix} + \begin{bmatrix} -\frac{L_\alpha g}{m\bar{V}} \end{bmatrix} \dot{e}_{33}^{wI} \\ &= \begin{bmatrix} -\frac{L_\alpha}{m\bar{V}} \end{bmatrix} \dot{C}_w + \begin{bmatrix} \frac{M_\alpha}{I_{yy}} \end{bmatrix} C_w + \begin{bmatrix} -\frac{L_\alpha M_Q}{mI_{yy}} \end{bmatrix} Q + \begin{bmatrix} -\frac{L_\alpha M_{\delta_E}}{mI_{yy}} \end{bmatrix} \delta_E + \begin{bmatrix} \frac{L_0 M_\alpha}{mI_{yy}} - \frac{L_\alpha M_0}{mI_{yy}} \end{bmatrix} + \begin{bmatrix} -\frac{L_\alpha g}{m\bar{V}} \end{bmatrix} \dot{e}_{33}^{wI} \end{aligned} \quad (\text{B.37})$$

To eliminate the Q term equation (B.36) is rewritten with Q as the subject of the formula and $\dot{\alpha}$ is substituted from equation (B.35) to give,

$$Q = \begin{bmatrix} -\frac{L_\alpha}{m} \end{bmatrix}^{-1} \left(\dot{C}_w + \begin{bmatrix} \frac{L_\alpha}{m\bar{V}} \end{bmatrix} C_w + \begin{bmatrix} \frac{L_\alpha g}{m\bar{V}} \end{bmatrix} e_{33}^{wI} \right) \quad (\text{B.38})$$

Thus,

$$\ddot{C}_w = \begin{bmatrix} \frac{M_Q}{I_{yy}} - \frac{L_\alpha}{m\bar{V}} \end{bmatrix} \dot{C}_w + \begin{bmatrix} \frac{M_\alpha}{I_{yy}} + \frac{L_\alpha M_Q}{m\bar{V}I_{yy}} \end{bmatrix} C_w + \begin{bmatrix} -\frac{L_\alpha M_{\delta_E}}{mI_{yy}} \end{bmatrix} \delta_E + \begin{bmatrix} \frac{L_0 M_\alpha}{mI_{yy}} - \frac{L_\alpha M_0}{mI_{yy}} \end{bmatrix} + \begin{bmatrix} \frac{L_\alpha M_Q g}{m\bar{V}I_{yy}} \end{bmatrix} e_{33}^{wI} + \begin{bmatrix} -\frac{L_\alpha g}{m\bar{V}} \end{bmatrix} \dot{e}_{33}^{wI} \quad (\text{B.39})$$

The elevator control input could now be used to cancel the effect of the gravity coupling terms on the normal specific acceleration dynamics. However, the output feedback control law to be implemented will make use of pitch rate feedback. Upon analysis of equation (B.38), it is clear that pitch rate feedback will reintroduce gravity coupling terms into the normal specific acceleration dynamics. Thus, the feedback control law is first defined and substituted into the dynamics, and then the dynamic inversion is carried out.

The feedback control law is defined below,

$$\delta_E = -K_Q Q - K_C C_w - K_E \int_{t_0}^t C_w - C_{w_r} dt + \delta_{E_G} \quad (\text{B.40})$$

The control law is of a PI form with enough degrees of freedom to allow for arbitrary pole placement. The integral action of the control law is introduced to ensure that the normal specific acceleration is tracked with zero error in the steady state. Provision is also made in the

control law for dynamic inversion of the gravity coupling terms through the introduction of δ_{E_G} . The control law can be rewritten as follows,

$$\delta_E = -K_Q Q - K_C C_W - K_E E_C + \delta_{E_G} \quad (\text{B.41})$$

where,

$$\dot{E}_C = C_W - C_{W_R} \quad (\text{B.42})$$

Substituting the control law into the normal specific acceleration dynamics of equation (B.39) and ignoring the static offset terms gives,

$$\begin{aligned} \ddot{C}_W &= \left[\frac{M_Q}{I_{yy}} - \frac{L_\alpha}{m\bar{V}} \right] \dot{C}_W + \left[\frac{M_\alpha}{I_{yy}} + \frac{L_\alpha M_Q}{m\bar{V}I_{yy}} + \frac{L_\alpha M_{\delta_E}}{mI_{yy}} K_C \right] C_W + \left[\frac{L_\alpha M_{\delta_E}}{mI_{yy}} K_Q \right] Q + \left[\frac{L_\alpha M_{\delta_E}}{mI_{yy}} K_E \right] E_C + \\ &\quad \left[-\frac{L_\alpha M_{\delta_E}}{mI_{yy}} \right] \delta_{E_G} + \left[\frac{L_\alpha M_Q \mathbf{g}}{m\bar{V}I_{yy}} \right] e_{33}^{wI} + \left[-\frac{L_\alpha \mathbf{g}}{m\bar{V}} \right] \dot{e}_{33}^{wI} \\ &= \left[\frac{M_Q}{I_{yy}} - \frac{L_\alpha}{m\bar{V}} - \frac{M_{\delta_E}}{I_{yy}} K_Q \right] \dot{C}_W + \left[\frac{M_\alpha}{I_{yy}} + \frac{L_\alpha M_Q}{m\bar{V}I_{yy}} + \frac{L_\alpha M_{\delta_E}}{mI_{yy}} K_C - \frac{L_\alpha M_{\delta_E}}{m\bar{V}I_{yy}} K_Q \right] C_W + \left[\frac{L_\alpha M_{\delta_E}}{mI_{yy}} K_E \right] E_C + \\ &\quad \left[-\frac{L_\alpha M_{\delta_E}}{mI_{yy}} \right] \delta_{E_G} + \left[\frac{L_\alpha M_Q \mathbf{g}}{m\bar{V}I_{yy}} - \frac{L_\alpha M_{\delta_E} \mathbf{g}}{m\bar{V}I_{yy}} K_Q \right] e_{33}^{wI} + \left[-\frac{L_\alpha \mathbf{g}}{m\bar{V}} \right] \dot{e}_{33}^{wI} \end{aligned} \quad (\text{B.43})$$

The normal specific acceleration dynamics become,

$$\ddot{C}_W = \left[\frac{M_Q}{I_{yy}} - \frac{L_\alpha}{m\bar{V}} - \frac{M_{\delta_E}}{I_{yy}} K_Q \right] \dot{C}_W + \left[\frac{M_\alpha}{I_{yy}} + \frac{L_\alpha M_Q}{m\bar{V}I_{yy}} + \frac{L_\alpha M_{\delta_E}}{mI_{yy}} K_C - \frac{L_\alpha M_{\delta_E}}{m\bar{V}I_{yy}} K_Q \right] C_W + \left[\frac{L_\alpha M_{\delta_E}}{mI_{yy}} K_E \right] E_C \quad (\text{B.44})$$

$$\dot{E}_C = C_W - C_{W_R} \quad (\text{B.45})$$

when,

$$\left[-\frac{L_\alpha M_{\delta_E}}{mI_{yy}} \right] \delta_{E_G} + \left[\frac{L_\alpha M_Q \mathbf{g}}{m\bar{V}I_{yy}} - \frac{L_\alpha M_{\delta_E} \mathbf{g}}{m\bar{V}I_{yy}} K_Q \right] e_{33}^{wI} + \left[-\frac{L_\alpha \mathbf{g}}{m\bar{V}} \right] \dot{e}_{33}^{wI} = 0 \quad (\text{B.46})$$

Thus, the dynamic inversion part of the control law is,

$$\begin{aligned} \delta_{E_G} &= \frac{\mathbf{g}}{\bar{V}} \left(\left[\frac{M_Q}{M_{\delta_E}} - K_Q \right] e_{33}^{wI} - \left[\frac{I_{yy}}{M_{\delta_E}} \right] \dot{e}_{33}^{wI} \right) \\ &= \frac{\mathbf{g}}{\bar{V}} \left(\left[\frac{M_Q}{M_{\delta_E}} - K_Q \right] e_{33}^{wI} + \left[\frac{I_{yy}}{M_{\delta_E}} \right] \left[\left(\frac{C_W + e_{33}^{wI} \mathbf{g}}{\bar{V}} \right) e_{13}^{wI} + P_w e_{23}^{wI} \right] \right) \end{aligned} \quad (\text{B.47})$$

where use of equations (2.46) and (2.49) has been made to eliminate the attitude parameter derivative. Note that the control law is a function of the still to be determined pitch rate feedback gain. The closed loop system with the dynamic inversion control law in place can be written in spate space form as follows,

$$\begin{bmatrix} \ddot{C}_w \\ \dot{C}_w \\ \dot{E}_C \end{bmatrix} = \begin{bmatrix} \left(\frac{M_Q}{I_{yy}} - \frac{L_\alpha}{m\bar{V}} - \frac{M_{\delta_E}}{I_{yy}} K_Q \right) & \left(\frac{M_\alpha}{I_{yy}} + \frac{L_\alpha M_Q}{m\bar{V}I_{yy}} + \frac{L_\alpha M_{\delta_E}}{mI_{yy}} K_C - \frac{L_\alpha M_{\delta_E}}{m\bar{V}I_{yy}} K_Q \right) & \left(\frac{L_\alpha M_{\delta_E}}{mI_{yy}} K_E \right) \\ 1 & 0 & 0 \\ 0 & 1 & 0 \end{bmatrix} \begin{bmatrix} \dot{C}_w \\ C_w \\ E_C \end{bmatrix} + \begin{bmatrix} 0 \\ 0 \\ -1 \end{bmatrix} C_{w_r} \quad (\text{B.48})$$

Noting that because the system is in control canonical form, the characteristic equation is,

$$s^3 - s^2 \left(\frac{M_Q}{I_{yy}} - \frac{L_\alpha}{m\bar{V}} - \frac{M_{\delta_E}}{I_{yy}} K_Q \right) - s \left(\frac{M_\alpha}{I_{yy}} + \frac{L_\alpha M_Q}{m\bar{V}I_{yy}} + \frac{L_\alpha M_{\delta_E}}{mI_{yy}} K_C - \frac{L_\alpha M_{\delta_E}}{m\bar{V}I_{yy}} K_Q \right) - \left(\frac{L_\alpha M_{\delta_E}}{mI_{yy}} K_E \right) = 0 \quad (\text{B.49})$$

Given the desired closed loop characteristic equation,

$$\alpha_c(s) = s^3 + \alpha_2 s^2 + \alpha_1 s + \alpha_0 \quad (\text{B.50})$$

the feedback gains can be calculated by matching coefficients,

$$\alpha_2 = - \left(\frac{M_Q}{I_{yy}} - \frac{L_\alpha}{m\bar{V}} - \frac{M_{\delta_E}}{I_{yy}} K_Q \right) \quad (\text{B.51})$$

$$\alpha_1 = - \left(\frac{M_\alpha}{I_{yy}} + \frac{L_\alpha M_Q}{m\bar{V}I_{yy}} + \frac{L_\alpha M_{\delta_E}}{mI_{yy}} K_C - \frac{L_\alpha M_{\delta_E}}{m\bar{V}I_{yy}} K_Q \right) \quad (\text{B.52})$$

$$\alpha_0 = - \left(\frac{L_\alpha M_{\delta_E}}{mI_{yy}} K_E \right) \quad (\text{B.53})$$

Thus,

$$K_Q = \frac{I_{yy}}{M_{\delta_E}} \left(\alpha_2 + \frac{M_Q}{I_{yy}} - \frac{L_\alpha}{m\bar{V}} \right) \quad (\text{B.54})$$

$$K_C = - \frac{mI_{yy}}{L_\alpha M_{\delta_E}} \left(\alpha_1 + \frac{M_\alpha}{I_{yy}} - \frac{L_\alpha}{m\bar{V}} \left(\alpha_2 - \frac{L_\alpha}{m\bar{V}} \right) \right) \quad (\text{B.55})$$

$$K_E = - \frac{mI_{yy}}{L_\alpha M_{\delta_E}} \alpha_0 \quad (\text{B.56})$$

Substituting the pitch rate feedback gain into the dynamic inversion control law gives,

$$\delta_{E_g} = \frac{I_{yy} \mathbf{g}}{M_{\delta_E} \bar{V}} \left(\left[\frac{L_\alpha}{m\bar{V}} - \alpha_2 \right] e_{33}^{WI} + \left[\left(\frac{C_w + e_{33}^{WI} \mathbf{g}}{\bar{V}} \right) e_{13}^{WI} + P_w e_{23}^{WI} \right] \right) \quad (\text{B.57})$$

With the controller above, the design freedom is reduced to that of placing the three poles that govern the closed loop normal dynamics.

B.2.4 Deriving the NNDT normal dynamics

The normalising definitions of equations (4.62) to (4.68) can be written as follows,

$$\mathbf{x}' = \mathbf{T}_x \mathbf{x} \quad (\text{B.58})$$

$$\delta'_E = T_u \delta_E \quad (\text{B.59})$$

$$C'_W = T_y C_W \quad (\text{B.60})$$

$$\bar{\mathbf{x}} = T_d \dot{\mathbf{x}} \quad (\text{B.61})$$

with,

$$\mathbf{x}' = \begin{bmatrix} \alpha' \\ \mathcal{Q}' \end{bmatrix} \quad (\text{B.62})$$

and \mathbf{x} from equation (B.22), with transformation matrices,

$$\mathbf{T}_x = \begin{bmatrix} 1 & 0 \\ 0 & \frac{\bar{c}}{2\bar{V}_a} \end{bmatrix} \quad T_u = 1 \quad T_y = \frac{m}{qS} \quad T_d = \frac{m\bar{V}}{qS} \quad (\text{B.63})$$

Substituting the above relationships into the normal dynamics of equations (B.20) and (B.21) yields,

$$\mathbf{T}_x^{-1} T_d^{-1} \bar{\mathbf{x}}' = \mathbf{A} \mathbf{T}_x^{-1} \mathbf{x}' + \mathbf{B} T_u^{-1} \delta'_E + \mathbf{B}_1 + \mathbf{B}_2 e^{WI} \quad (\text{B.64})$$

$$T_y^{-1} C'_W = \mathbf{C} \mathbf{T}_x^{-1} \mathbf{x}' + D T_u^{-1} \delta'_E \quad (\text{B.65})$$

where it has been noted that all transformation matrices are static relative to the normal dynamics. Rearranging above gives,

$$\bar{\mathbf{x}}' = \mathbf{A}' \mathbf{x}' + \mathbf{B}' \delta'_E + \mathbf{B}'_1 + \mathbf{B}'_2 e^{WI} \quad (\text{B.66})$$

$$C'_W = \mathbf{C}' \mathbf{x}' + D' \delta'_E \quad (\text{B.67})$$

with,

$$\mathbf{A}' = T_d \mathbf{T}_x \mathbf{A} \mathbf{T}_x^{-1} \quad \mathbf{B}' = T_d \mathbf{T}_x \mathbf{B} T_u^{-1} \quad \mathbf{B}'_1 = T_d \mathbf{T}_x \mathbf{B}_1 \quad \mathbf{B}'_2 = T_d \mathbf{T}_x \mathbf{B}_2 \quad (\text{B.68})$$

$$\mathbf{C}' = T_y \mathbf{C} \mathbf{T}_x^{-1} \quad D' = T_y D T_u^{-1} \quad (\text{B.69})$$

Multiplying the above matrices out gives,

$$\mathbf{A}' = \begin{bmatrix} -C_{L\alpha} & k_Q \\ k_y C_{m\alpha} & k_y C_{m_Q} \end{bmatrix} \quad \mathbf{B}' = \begin{bmatrix} -C_{L\delta_E} \\ k_y C_{m\delta_E} \end{bmatrix} \quad \mathbf{B}'_1 = \begin{bmatrix} -C_{L_0} \\ k_y C_{m_0} \end{bmatrix} \quad \mathbf{B}'_2 = \begin{bmatrix} g' \\ 0 \end{bmatrix} \quad (\text{B.70})$$

$$\mathbf{C}' = \begin{bmatrix} -C_{L\alpha} & -C_{L\dot{\alpha}} \end{bmatrix} \quad D' = -C_{L\delta_e} \quad (\text{B.71})$$

where,

$$k_Q = 4m'_Q \bar{V}' \quad (\text{B.72})$$

$$k_y = \frac{1}{2} \frac{\bar{V}'}{r_y'^2} \quad (\text{B.73})$$

$$g' = \frac{mg}{qS} \quad (\text{B.74})$$

and,

$$m'_Q = \frac{m}{\rho S \bar{c}} \quad (\text{B.75})$$

$$\bar{V}' = \frac{\bar{V}}{\bar{V}_a} \quad (\text{B.76})$$

$$r_y' = \frac{r_y}{\bar{c}} \quad (\text{B.77})$$

with,

$$r_y = \sqrt{\frac{I_{yy}}{m}} \quad (\text{B.78})$$

In equations (B.72) and (B.73), m'_Q is the aircraft's mass normalised to a longitudinal reference air mass, \bar{V}' is the relative ground to airspeed magnitude and r_y' is the normalised pitch radius of gyration. Note that it has been assumed that,

$$|C_{L\dot{\alpha}}| \ll |k_Q| \quad (\text{B.79})$$

which is equivalent to the standard aircraft assumption of equation (B.25).

B.2.5 Characteristic equation for the NNDT poles

The poles of the system in equation (B.66) are the roots of the characteristic equation,

$$p(s') = \det(s'\mathbf{I} - \mathbf{A}') \quad (\text{B.80})$$

Expanding this equation,

$$\begin{aligned}
p(s') &= \det \left(\begin{bmatrix} s' + C_{L_\alpha} & -k_Q \\ -k_y C_{m_\alpha} & s' - k_y C_{m_Q} \end{bmatrix} \right) \\
&= (s')^2 + (C_{L_\alpha} - k_y C_{m_Q}) s' - (k_y C_{m_Q} C_{L_\alpha} + k_Q k_y C_{m_\alpha})
\end{aligned} \tag{B.81}$$

B.2.6 Characteristic equation for the NNDT zeros

The NNDT zeros from the elevator through to normal specific acceleration are the roots of the characteristic equation,

$$z(s') = C' \text{adj}(s' \mathbf{I} - \mathbf{A}') \mathbf{B}' + D' \det(s' \mathbf{I} - \mathbf{A}') \tag{B.82}$$

Expanding the first term in the above equation yields,

$$\begin{aligned}
T_1 &= \begin{bmatrix} -C_{L_\alpha} & -C_{L_Q} \end{bmatrix} \begin{bmatrix} s' - k_y C_{m_Q} & k_Q \\ k_y C_{m_\alpha} & s' + C_{L_\alpha} \end{bmatrix} \begin{bmatrix} -C_{L_{\delta E}} \\ k_y C_{m_{\delta E}} \end{bmatrix} \\
&= -C_{L_\alpha} \left[-C_{L_{\delta E}} (s' - k_y C_{m_Q}) + k_Q k_y C_{m_{\delta E}} \right] - C_{L_Q} \left[-k_y C_{L_{\delta E}} C_{m_\alpha} + k_y C_{m_{\delta E}} (s' + C_{L_\alpha}) \right] \\
&= C_{L_{\delta E}} \left[\left(C_{L_\alpha} - C_{L_Q} k_y \frac{C_{m_{\delta E}}}{C_{L_{\delta E}}} \right) s' + k_y \left(-C_{L_\alpha} C_{m_Q} + C_{L_Q} C_{m_\alpha} - k_Q C_{L_\alpha} \frac{C_{m_{\delta E}}}{C_{L_{\delta E}}} - C_{L_\alpha} C_{L_Q} \frac{C_{m_{\delta E}}}{C_{L_{\delta E}}} \right) \right]
\end{aligned} \tag{B.83}$$

where T_1 has been used to denote the first term. The determinant of the second term of equation (B.82) has already been calculated in equation (B.81) and so the characteristic equation for the zeros becomes,

$$\begin{aligned}
z(s') &= C_{L_{\delta E}} \left[\left(C_{L_\alpha} - C_{L_Q} k_y \frac{C_{m_{\delta E}}}{C_{L_{\delta E}}} \right) s' + k_y \left(-C_{L_\alpha} C_{m_Q} + C_{L_Q} C_{m_\alpha} - k_Q C_{L_\alpha} \frac{C_{m_{\delta E}}}{C_{L_{\delta E}}} - C_{L_\alpha} C_{L_Q} \frac{C_{m_{\delta E}}}{C_{L_{\delta E}}} \right) \right] \\
&\quad - (s')^2 - (C_{L_\alpha} - k_y C_{m_Q}) s' + k_y (C_{m_Q} C_{L_\alpha} + k_Q C_{m_\alpha}) \\
&= C_{L_{\delta E}} \left[- (s')^2 + k_y C_{L_Q} \left(\frac{C_{m_Q}}{C_{L_Q}} - \frac{C_{m_{\delta E}}}{C_{L_{\delta E}}} \right) s' + k_y C_{L_\alpha} \left(\frac{C_{m_\alpha}}{C_{L_\alpha}} - \frac{C_{m_{\delta E}}}{C_{L_{\delta E}}} \right) (k_Q + C_{L_Q}) \right] \\
&\approx C_{L_{\delta E}} \left[- (s')^2 + k_y C_{L_Q} \left(\frac{C_{m_Q}}{C_{L_Q}} - \frac{C_{m_{\delta E}}}{C_{L_{\delta E}}} \right) s' + k_Q k_y C_{L_\alpha} \left(\frac{C_{m_\alpha}}{C_{L_\alpha}} - \frac{C_{m_{\delta E}}}{C_{L_{\delta E}}} \right) \right]
\end{aligned} \tag{B.84}$$

where equation (B.79) has been used to simplify the result. Since only the roots of equation (B.84) are desired the characteristic equation can be simplified to,

$$z(s') = (s')^2 - k_y C_{L_Q} \left(\frac{C_{m_Q}}{C_{L_Q}} - \frac{C_{m_{\delta E}}}{C_{L_{\delta E}}} \right) s' - k_Q k_y C_{L_\alpha} \left(\frac{C_{m_\alpha}}{C_{L_\alpha}} - \frac{C_{m_{\delta E}}}{C_{L_{\delta E}}} \right) \tag{B.85}$$

B.2.7 NNDT normal specific acceleration controller design

Following similar arguments to those provided in section 4.2.4, the NNDT normal dynamics reduce to,

$$\begin{bmatrix} \bar{\alpha}' \\ \bar{Q}' \end{bmatrix} = \begin{bmatrix} -C_{L_\alpha} & k_Q \\ k_y C_{m_\alpha} & k_y C_{m_Q} \end{bmatrix} \begin{bmatrix} \alpha' \\ Q' \end{bmatrix} + \begin{bmatrix} 0 \\ k_y C_{m_{s_E}} \end{bmatrix} \delta'_E + \begin{bmatrix} -C_{L_0} \\ k_y C_{m_0} \end{bmatrix} + \begin{bmatrix} g' \\ 0 \end{bmatrix} e_{33}^{WI} \quad (\text{B.86})$$

$$C'_W = \begin{bmatrix} -C_{L_\alpha} & 0 \end{bmatrix} \begin{bmatrix} \alpha' \\ Q' \end{bmatrix} + [0] \delta'_E + [-C_{L_0}] \quad (\text{B.87})$$

when the effect of the zeros of section B.2.6 are neglected. It is desired to dynamically invert the effect of the gravity coupling on normal specific acceleration. This is achieved by differentiating the normal specific acceleration until the control input appears in the dynamics. The control is then used to directly cancel the undesired terms. Beginning with the NNDT normal specific acceleration output equation,

$$C'_W = -C_{L_\alpha} \alpha' - C_{L_0} \quad (\text{B.88})$$

Differentiating this equation once with respect to non-dimensional time, remembering that all quantities inside the matrices of equations (B.66) and (B.67) are considered parameters due to either their static nature or the timescale separation condition,

$$\begin{aligned} \bar{C}'_W &= -C_{L_\alpha} \bar{\alpha}' \\ &= [-C_{L_\alpha}] C'_W + [-C_{L_\alpha} k_Q] Q' + [-C_{L_\alpha} g'] e_{33}^{WI} \end{aligned} \quad (\text{B.89})$$

Differentiating the normal specific acceleration a second time gives,

$$\begin{aligned} \bar{\bar{C}}'_W &= [-C_{L_\alpha}] \bar{C}'_W + [-C_{L_\alpha} k_Q] \bar{Q}' + [-C_{L_\alpha} g'] \bar{e}_{33}^{WI} \\ &= [-C_{L_\alpha}] \bar{C}'_W + [-k_y C_{m_\alpha} C_{L_\alpha} k_Q] \alpha' + [-k_y C_{m_Q} C_{L_\alpha} k_Q] Q' + \\ &\quad [-k_y C_{m_{s_E}} C_{L_\alpha} k_Q] \delta'_E + [-k_y C_{m_0} C_{L_\alpha} k_Q] + [-C_{L_\alpha} g'] \bar{e}_{33}^{WI} \\ &= [-C_{L_\alpha}] \bar{C}'_W + [k_y C_{m_\alpha} k_Q] C'_W + [-k_y C_{m_Q} C_{L_\alpha} k_Q] Q' + \\ &\quad [-k_y C_{m_{s_E}} C_{L_\alpha} k_Q] \delta'_E + [k_y (C_{L_0} C_{m_\alpha} - C_{m_0} C_{L_\alpha}) k_Q] + [-C_{L_\alpha} g'] \bar{e}_{33}^{WI} \end{aligned} \quad (\text{B.90})$$

To eliminate the Q' term equation (B.89) is rewritten with Q' as the subject of the formula,

$$Q' = [-C_{L_\alpha} k_Q]^{-1} \left(\bar{C}'_W + [C_{L_\alpha}] C'_W + [C_{L_\alpha} g'] e_{33}^{WI} \right) \quad (\text{B.91})$$

Substituting into equation (B.90) gives,

$$\begin{aligned} \bar{\bar{C}}'_W &= [k_y C_{m_Q} - C_{L_\alpha}] \bar{C}'_W + [k_y C_{m_\alpha} k_Q + k_y C_{m_Q} C_{L_\alpha}] C'_W + [-k_y C_{m_{s_E}} C_{L_\alpha} k_Q] \delta'_E + \\ &\quad [k_y (C_{L_0} C_{m_\alpha} - C_{m_0} C_{L_\alpha}) k_Q] + [k_y C_{m_Q} C_{L_\alpha} g'] e_{33}^{WI} + [-C_{L_\alpha} g'] \bar{e}_{33}^{WI} \end{aligned} \quad (\text{B.92})$$

Define the PI control law with freedom for dynamic inversion,

$$\delta'_E = -K'_Q Q' - K'_C C'_W - K'_E E'_C + \delta'_{E_G} \quad (\text{B.93})$$

$$\bar{E}'_C = C'_W - C'_{W_R} \quad (\text{B.94})$$

Substituting the control law into the NNDT normal specific acceleration dynamics of equation (B.92) and ignoring the static offset terms (due to the integrator in the control law) gives,

$$\begin{aligned} \bar{C}'_W &= \left[k_y C_{m_Q} - C_{L_\alpha} \right] \bar{C}'_W + \left[k_y C_{m_\alpha} k_Q + k_y C_{m_Q} C_{L_\alpha} + k_y C_{m_{\delta_E}} C_{L_\alpha} k_Q K'_C \right] C'_W + \left[k_y C_{m_{\delta_E}} C_{L_\alpha} k_Q K'_Q \right] Q' + \\ &\quad \left[k_y C_{m_{\delta_E}} C_{L_\alpha} k_Q K'_E \right] E'_C + \left[-k_y C_{m_{\delta_E}} C_{L_\alpha} k_Q \right] \delta'_{E_G} + \left[k_y C_{m_Q} C_{L_\alpha} g' \right] e_{33}^{WI} + \left[-C_{L_\alpha} g' \right] \bar{e}_{33}^{WI} \\ &= \left[k_y C_{m_Q} - C_{L_\alpha} - k_y C_{m_{\delta_E}} K'_Q \right] \bar{C}'_W + \left[k_y C_{m_\alpha} k_Q + k_y C_{m_Q} C_{L_\alpha} + k_y C_{m_{\delta_E}} C_{L_\alpha} k_Q K'_C - k_y C_{m_{\delta_E}} C_{L_\alpha} K'_Q \right] C'_W + \\ &\quad \left[k_y C_{m_{\delta_E}} C_{L_\alpha} k_Q K'_E \right] E'_C + \left[-k_y C_{m_{\delta_E}} C_{L_\alpha} k_Q \right] \delta'_{E_G} + \left[k_y C_{m_Q} C_{L_\alpha} g' - k_y C_{m_{\delta_E}} C_{L_\alpha} g' K'_Q \right] e_{33}^{WI} + \left[-C_{L_\alpha} g' \right] \bar{e}_{33}^{WI} \end{aligned} \quad (\text{B.95})$$

The normal specific acceleration dynamics become,

$$\begin{aligned} \bar{C}'_W &= \left[k_y C_{m_Q} - C_{L_\alpha} - k_y C_{m_{\delta_E}} K'_Q \right] \bar{C}'_W + \left[k_y C_{m_\alpha} k_Q + k_y C_{m_Q} C_{L_\alpha} + k_y C_{m_{\delta_E}} C_{L_\alpha} k_Q K'_C - k_y C_{m_{\delta_E}} C_{L_\alpha} K'_Q \right] C'_W + \\ &\quad \left[k_y C_{m_{\delta_E}} C_{L_\alpha} k_Q K'_E \right] E'_C \end{aligned} \quad (\text{B.96})$$

$$\bar{E}'_C = C'_W - C'_{W_R} \quad (\text{B.97})$$

when,

$$\left[-k_y C_{m_{\delta_E}} C_{L_\alpha} k_Q \right] \delta'_{E_G} + \left[k_y C_{m_Q} C_{L_\alpha} g' - k_y C_{m_{\delta_E}} C_{L_\alpha} g' K'_Q \right] e_{33}^{WI} + \left[-C_{L_\alpha} g' \right] \bar{e}_{33}^{WI} = 0 \quad (\text{B.98})$$

Thus, the dynamic inversion control law is,

$$\begin{aligned} \delta'_{E_G} &= \frac{g'}{k_Q} \left(\left[\frac{C_{m_Q}}{C_{m_{\delta_E}}} - K'_Q \right] e_{33}^{WI} - \left[\frac{1}{k_y C_{m_{\delta_E}}} \right] \bar{e}_{33}^{WI} \right) \\ &= \frac{g'}{k_Q} \left(\left[\frac{C_{m_Q}}{C_{m_{\delta_E}}} - K'_Q \right] e_{33}^{WI} + \left[\frac{1}{k_y C_{m_{\delta_E}}} \right] \left[\left(\frac{C_W + e_{33}^{WI} g'}{\bar{V}} \right) e_{13}^{WI} + P_W e_{23}^{WI} \right] \frac{m \bar{V}}{qS} \right) \\ &= \frac{g'}{k_Q} \left(\left[\frac{C_{m_Q}}{C_{m_{\delta_E}}} - K'_Q \right] e_{33}^{WI} + \left[\frac{1}{k_y C_{m_{\delta_E}}} \right] \left[\left(C'_W + e_{33}^{WI} g' \right) e_{13}^{WI} + P'_W e_{23}^{WI} \right] \right) \end{aligned} \quad (\text{B.99})$$

where use of equations (B.61), (2.46) and (2.49) has been made and the non-dimensional roll rate about the axial wind axis system unit vector is defined as,

$$P'_W = \frac{m \bar{V}}{qS} P_W \quad (\text{B.100})$$

Note that the dynamic inversion control law is a function of the still to be determined pitch rate feedback gain. The closed loop system with the dynamic inversion control law in place can be written in state space form as follows,

$$\begin{bmatrix} \bar{C}'_W \\ \bar{C}'_W \\ \bar{E}'_C \end{bmatrix} = \begin{bmatrix} a_{11} & a_{12} & a_{13} \\ 1 & 0 & 0 \\ 0 & 1 & 0 \end{bmatrix} \begin{bmatrix} \bar{C}'_W \\ C'_W \\ E'_C \end{bmatrix} + \begin{bmatrix} 0 \\ 0 \\ -1 \end{bmatrix} C'_{W_r} \quad (\text{B.101})$$

where,

$$a_{11} = k_y C_{m_Q} - C_{L_\alpha} - k_y C_{m_{\delta_E}} K'_Q \quad (\text{B.102})$$

$$a_{12} = k_y C_{m_\alpha} k_Q + k_y C_{m_Q} C_{L_\alpha} + k_y C_{m_{\delta_E}} C_{L_\alpha} k_Q K'_C - k_y C_{m_{\delta_E}} C_{L_\alpha} K'_Q \quad (\text{B.103})$$

$$a_{13} = k_y C_{m_{\delta_E}} C_{L_\alpha} k_Q K'_E \quad (\text{B.104})$$

Noting that the system is in control canonical form the characteristic equation is,

$$(s')^3 - a_{11}(s')^2 - a_{12}s' - a_{13} = 0 \quad (\text{B.105})$$

Given the desired closed loop characteristic equation,

$$\alpha_c(s') = (s')^3 + \alpha_2(s')^2 + \alpha_1(s') + \alpha_0 \quad (\text{B.106})$$

the feedback gains can be calculated by matching the coefficients,

$$\alpha_2 = -(k_y C_{m_Q} - C_{L_\alpha} - k_y C_{m_{\delta_E}} K'_Q) \quad (\text{B.107})$$

$$\alpha_1 = -(k_y C_{m_\alpha} k_Q + k_y C_{m_Q} C_{L_\alpha} + k_y C_{m_{\delta_E}} C_{L_\alpha} k_Q K'_C - k_y C_{m_{\delta_E}} C_{L_\alpha} K'_Q) \quad (\text{B.108})$$

$$\alpha_0 = -(k_y C_{m_{\delta_E}} C_{L_\alpha} k_Q K'_E) \quad (\text{B.109})$$

Thus,

$$K'_Q = \frac{\alpha_2 + k_y C_{m_Q} - C_{L_\alpha}}{k_y C_{m_{\delta_E}}} \quad (\text{B.110})$$

$$K'_C = -\frac{\alpha_1 + k_Q k_y C_{m_\alpha} - C_{L_\alpha} (\alpha_2 - C_{L_\alpha})}{k_Q k_y C_{L_\alpha} C_{m_{\delta_E}}} \quad (\text{B.111})$$

$$K'_E = -\frac{\alpha_0}{k_Q k_y C_{L_\alpha} C_{m_{\delta_E}}} \quad (\text{B.112})$$

Substituting the pitch rate feedback gain into the dynamic inversion part of the control law gives,

$$\delta'_{E_g} = \frac{g'}{k_Q k_y C_{m_{\delta_E}}} \left[(C_{L_\alpha} - \alpha_2) e_{33}^{Wl} + \left[(C'_W + e_{33}^{Wl} g') e_{13}^{Wl} + P'_W e_{23}^{Wl} \right] \right] \quad (\text{B.113})$$

With the controller above, the design freedom is reduced to that of placing the three poles in the NNDT frequency plane.

B.3 Lateral dynamics

With reference to equations (5.1) and (5.2) the lateral dynamics can be written as,

$$\dot{\mathbf{x}} = \mathbf{A}\mathbf{x} + \mathbf{B}\mathbf{u} + \mathbf{B}_1 e_{23}^{WT} \quad (\text{B.114})$$

$$\mathbf{y} = \mathbf{C}\mathbf{x} + \mathbf{D}\mathbf{u} \quad (\text{B.115})$$

where,

$$\mathbf{x} = \begin{bmatrix} \beta \\ P \\ R \end{bmatrix} \quad (\text{B.116})$$

$$\mathbf{u} = \begin{bmatrix} \delta_A \\ \delta_R \end{bmatrix} \quad (\text{B.117})$$

$$\mathbf{y} = \begin{bmatrix} B_W \\ P_W \end{bmatrix} \quad (\text{B.118})$$

and,

$$\mathbf{A} = \begin{bmatrix} \frac{Y_\beta}{m\bar{V}} & 0 & -1 \\ \bar{L}_\beta & \bar{L}_P & \bar{L}_R \\ I_{xx} & I_{xx} & I_{xx} \\ \bar{N}_\beta & \bar{N}_P & \bar{N}_R \\ I_{zz} & I_{zz} & I_{zz} \end{bmatrix} \quad \mathbf{B} = [\mathbf{B}_A \quad \mathbf{B}_R] = \begin{bmatrix} 0 & \frac{Y_{\delta_R}}{m\bar{V}} \\ \bar{L}_{\delta_A} & \bar{L}_{\delta_R} \\ I_{xx} & I_{xx} \\ \bar{N}_{\delta_A} & \bar{N}_{\delta_R} \\ I_{zz} & I_{zz} \end{bmatrix} \quad \mathbf{B}_1 = \begin{bmatrix} \frac{g}{\bar{V}} \\ 0 \\ 0 \end{bmatrix} \quad (\text{B.119})$$

$$\mathbf{C} = \begin{bmatrix} \mathbf{C}_B \\ \mathbf{C}_P \end{bmatrix} = \begin{bmatrix} \frac{Y_\beta}{m} & 0 & \frac{Y_R}{m} \\ 0 & 1 & 0 \end{bmatrix} \quad \mathbf{D} = \begin{bmatrix} D_{BA} & D_{BR} \\ D_{PA} & D_{PR} \end{bmatrix} = \begin{bmatrix} 0 & \frac{Y_{\delta_R}}{m} \\ 0 & 0 \end{bmatrix} \quad (\text{B.120})$$

and the following standard aircraft assumptions have been used to simplify the dynamics [43],

$$Y_p \approx 0 \quad (\text{B.121})$$

$$Y_{\delta_A} \approx 0 \quad (\text{B.122})$$

$$\left| \frac{Y_R}{m\bar{V}} \right| \ll 1 \quad (\text{B.123})$$

B.3.1 Characteristic equation for the poles

The characteristic equation for the lateral dynamics poles is,

$$p(s) = \det(s\mathbf{I} - \mathbf{A}) \quad (\text{B.124})$$

Expanding this equation yields,

$$\begin{aligned} p(s) &= \left(s - \frac{Y_\beta}{m\bar{V}}\right) \left(s - \frac{\bar{L}_P}{I_{xx}}\right) \left(s - \frac{\bar{N}_R}{I_{zz}}\right) + \left(\frac{\bar{L}_\beta \bar{N}_P}{I_{xx} I_{zz}}\right) - \left(-\frac{\bar{N}_\beta}{I_{zz}}\right) \left(s - \frac{\bar{L}_P}{I_{xx}}\right) - \left(s - \frac{Y_\beta}{m\bar{V}}\right) \left(\frac{\bar{N}_P}{I_{zz}}\right) \left(\frac{\bar{L}_R}{I_{xx}}\right) \\ &= \left[s^2 - \left(\frac{\bar{L}_P}{I_{xx}} + \frac{\bar{N}_R}{I_{zz}}\right)s + \frac{\bar{L}_P \bar{L}_R}{I_{xx} I_{zz}} \left(\frac{\bar{N}_R}{\bar{L}_R} - \frac{\bar{N}_P}{\bar{L}_P}\right)\right] \left(s - \frac{Y_\beta}{m\bar{V}}\right) + \left[\frac{\bar{N}_\beta}{I_{zz}}s - \frac{\bar{L}_P \bar{L}_\beta}{I_{xx} I_{zz}} \left(\frac{\bar{N}_\beta}{\bar{L}_\beta} - \frac{\bar{N}_P}{\bar{L}_P}\right)\right] \\ &\approx \left[s^2 - \left(\frac{\bar{L}_P}{I_{xx}} + \frac{\bar{N}_R}{I_{zz}}\right)s + \frac{\bar{L}_P \bar{N}_R}{I_{xx} I_{zz}}\right] \left(s - \frac{Y_\beta}{m\bar{V}}\right) + \left(\frac{\bar{N}_\beta}{I_{zz}}s - \frac{\bar{L}_P \bar{N}_\beta}{I_{xx} I_{zz}}\right) \\ &= \left(s - \frac{\bar{L}_P}{I_{xx}}\right) \left(s - \frac{\bar{N}_R}{I_{zz}}\right) \left(s - \frac{Y_\beta}{m\bar{V}}\right) + \frac{\bar{N}_\beta}{I_{zz}} \left(s - \frac{\bar{L}_P}{I_{xx}}\right) \\ &= \left[s^2 - \left(\frac{Y_\beta}{m\bar{V}} + \frac{\bar{N}_R}{I_{zz}}\right)s + \left(\frac{Y_\beta \bar{N}_R}{m\bar{V} I_{zz}} + \frac{\bar{N}_\beta}{I_{zz}}\right)\right] \left(s - \frac{\bar{L}_P}{I_{xx}}\right) \end{aligned} \quad (\text{B.125})$$

under the following conditions,

$$\left| \frac{\bar{C}_{n_p}}{\bar{C}_{l_p}} \right| \ll \left| \frac{\bar{C}_{n_R}}{\bar{C}_{l_R}} \right| \quad (\text{B.126})$$

$$\left| \frac{\bar{C}_{n_p}}{\bar{C}_{l_p}} \right| \ll \left| \frac{\bar{C}_{n_\beta}}{\bar{C}_{l_\beta}} \right| \quad (\text{B.127})$$

B.3.2 Aileron to roll rate zeros characteristic equation

The characteristic equation for the zeros from ailerons to roll rate is,

$$\begin{aligned} z(s) &= \mathbf{C}_p \text{adj}(s\mathbf{I} - \mathbf{A}) \mathbf{B}_A + D_{pA} \det(s\mathbf{I} - \mathbf{A}) \\ &= [0 \quad 1 \quad 0] \text{adj}(s\mathbf{I} - \mathbf{A}) \begin{bmatrix} 0 & \bar{L}_{\delta_A} & \bar{N}_{\delta_A} \\ I_{xx} & & I_{zz} \end{bmatrix} \end{aligned} \quad (\text{B.128})$$

where the adjoint matrix above is,

$$\text{adj}(s\mathbf{I} - \mathbf{A}) = \begin{bmatrix} \left(s - \frac{\bar{L}_P}{I_{xx}}\right) \left(s - \frac{\bar{N}_R}{I_{zz}}\right) - \frac{\bar{N}_P \bar{L}_R}{I_{zz} I_{xx}} & -\frac{\bar{N}_P}{I_{zz}} & -\left(s - \frac{\bar{L}_P}{I_{xx}}\right) \\ \frac{\bar{L}_\beta}{I_{xx}} \left(s - \frac{\bar{N}_R}{I_{zz}}\right) + \frac{\bar{N}_\beta \bar{L}_R}{I_{zz} I_{xx}} & \left(s - \frac{Y_\beta}{m\bar{V}}\right) \left(s - \frac{\bar{N}_R}{I_{zz}}\right) + \frac{\bar{N}_\beta}{I_{zz}} & \frac{\bar{L}_R}{I_{xx}} \left(s - \frac{Y_\beta}{m\bar{V}}\right) - \frac{\bar{L}_\beta}{I_{xx}} \\ \frac{\bar{N}_\beta}{I_{zz}} \left(s - \frac{\bar{L}_P}{I_{xx}}\right) + \frac{\bar{L}_\beta \bar{N}_P}{I_{xx} I_{zz}} & \frac{\bar{N}_P}{I_{zz}} \left(s - \frac{Y_\beta}{m\bar{V}}\right) & \left(s - \frac{Y_\beta}{m\bar{V}}\right) \left(s - \frac{\bar{L}_P}{I_{xx}}\right) \end{bmatrix} \quad (\text{B.129})$$

Using this result in equation (B.128) yields the following characteristic equation,

$$\begin{aligned}
z(s) &= \left[\left(s - \frac{Y_\beta}{m\bar{V}} \right) \left(s - \frac{\bar{N}_R}{I_{zz}} \right) + \frac{\bar{N}_\beta}{I_{zz}} \right] \frac{\bar{L}_{\delta_A}}{I_{xx}} + \left[\frac{\bar{L}_R}{I_{xx}} \left(s - \frac{Y_\beta}{m\bar{V}} \right) + \frac{\bar{L}_\beta}{I_{xx}} \right] \frac{\bar{N}_{\delta_A}}{I_{zz}} \\
&= \left[\frac{\bar{L}_{\delta_A}}{I_{xx}} s - \frac{\bar{L}_{\delta_A} \bar{L}_R}{I_{xx} I_{zz}} \left(\frac{\bar{N}_R}{\bar{L}_R} + \frac{\bar{N}_{\delta_A}}{\bar{L}_{\delta_A}} \right) \right] \left(s - \frac{Y_\beta}{m\bar{V}} \right) + \frac{\bar{L}_{\delta_A} \bar{L}_\beta}{I_{xx} I_{zz}} \left(\frac{\bar{N}_\beta}{\bar{L}_\beta} - \frac{\bar{N}_{\delta_A}}{\bar{L}_{\delta_A}} \right) \\
&\approx \frac{\bar{L}_{\delta_A}}{I_{xx}} \left(s - \frac{\bar{N}_R}{I_{zz}} \right) \left(s - \frac{Y_\beta}{m\bar{V}} \right) + \frac{\bar{L}_{\delta_A} \bar{N}_\beta}{I_{xx} I_{zz}} \\
&= \frac{\bar{L}_{\delta_A}}{I_{xx}} \left[s^2 - \left(\frac{Y_\beta}{m\bar{V}} + \frac{\bar{N}_R}{I_{zz}} \right) s + \left(\frac{Y_\beta}{m\bar{V}} \frac{\bar{N}_R}{I_{zz}} + \frac{\bar{N}_\beta}{I_{zz}} \right) \right]
\end{aligned} \tag{B.130}$$

under the conditions below,

$$\left| \frac{\bar{C}_{n_{\delta_A}}}{\bar{C}_{l_{\delta_A}}} \right| \ll \left| \frac{\bar{C}_{n_R}}{\bar{C}_{l_R}} \right| \tag{B.131}$$

$$\left| \frac{\bar{C}_{n_{\delta_A}}}{\bar{C}_{l_{\delta_A}}} \right| \ll \left| \frac{\bar{C}_{n_\beta}}{\bar{C}_{l_\beta}} \right| \tag{B.132}$$

B.3.3 Rudder to yaw rate zeros characteristic equation

The characteristic equation for the zeros from the rudder to the yaw rate is,

$$\begin{aligned}
z(s) &= \mathbf{C}_Y \text{adj}(s\mathbf{I} - \mathbf{A}) \mathbf{B}_R + D_{YR} \det(s\mathbf{I} - \mathbf{A}) \\
&= [0 \quad 0 \quad 1] \text{adj}(s\mathbf{I} - \mathbf{A}) \begin{bmatrix} Y_{\delta_R} & \bar{L}_{\delta_R} & \bar{N}_{\delta_R} \\ m\bar{V} & I_{xx} & I_{zz} \end{bmatrix}^T
\end{aligned} \tag{B.133}$$

where the adjoint matrix is provided by equation (B.129). Expanding equation (B.133) yields,

$$\begin{aligned}
z(s) &= \frac{Y_{\delta_R}}{m\bar{V}} \left[\frac{\bar{N}_\beta}{I_{zz}} \left(s - \frac{\bar{L}_P}{I_{xx}} \right) + \frac{\bar{L}_\beta}{I_{xx}} \frac{\bar{N}_P}{I_{zz}} \right] + \frac{\bar{L}_{\delta_R}}{I_{xx}} \frac{\bar{N}_P}{I_{zz}} \left(s - \frac{Y_\beta}{m\bar{V}} \right) + \frac{\bar{N}_{\delta_R}}{I_{zz}} \left(s - \frac{Y_\beta}{m\bar{V}} \right) \left(s - \frac{\bar{L}_P}{I_{xx}} \right) \\
&= \frac{Y_{\delta_R}}{m\bar{V}} \left[\frac{\bar{N}_\beta}{I_{zz}} s - \frac{\bar{L}_P \bar{L}_\beta}{I_{xx} I_{zz}} \left(\frac{\bar{N}_\beta}{\bar{L}_\beta} - \frac{\bar{N}_P}{\bar{L}_P} \right) \right] + \left[\frac{\bar{N}_{\delta_R}}{I_{zz}} s - \frac{\bar{L}_P \bar{L}_{\delta_R}}{I_{xx} I_{zz}} \left(\frac{\bar{N}_{\delta_R}}{\bar{L}_{\delta_R}} - \frac{\bar{N}_P}{\bar{L}_P} \right) \right] \left(s - \frac{Y_\beta}{m\bar{V}} \right) \\
&\approx \frac{Y_{\delta_R}}{m\bar{V}} \frac{\bar{N}_\beta}{I_{zz}} \left(s - \frac{\bar{L}_P}{I_{xx}} \right) + \frac{\bar{N}_{\delta_R}}{I_{zz}} \left(s - \frac{\bar{L}_P}{I_{xx}} \right) \left(s - \frac{Y_\beta}{m\bar{V}} \right) \\
&= \frac{\bar{N}_{\delta_R}}{I_{zz}} \left[s - \frac{Y_\beta}{m\bar{V}} \frac{Y_{\delta_R}}{\bar{N}_{\delta_R}} \left(\frac{\bar{N}_{\delta_R}}{Y_{\delta_R}} - \frac{\bar{N}_\beta}{Y_\beta} \right) \right] \left(s - \frac{\bar{L}_P}{I_{xx}} \right)
\end{aligned} \tag{B.134}$$

under the condition of equation (B.127) and the condition below,

$$\left| \frac{\bar{C}_{n_P}}{\bar{C}_{l_P}} \right| \ll \left| \frac{\bar{C}_{n_{\delta_R}}}{\bar{C}_{l_{\delta_R}}} \right| \tag{B.135}$$

B.3.4 Rudder to lateral specific acceleration zeros characteristic equation

The characteristic equation for the zeros from rudder to lateral specific acceleration is,

$$\begin{aligned} z(s) &= \mathbf{C}_B \text{adj}(s\mathbf{I} - \mathbf{A}) \mathbf{B}_R + D_{BR} \det(s\mathbf{I} - \mathbf{A}) \\ &= \begin{bmatrix} Y_\beta & 0 \\ m & m \end{bmatrix} \text{adj}(s\mathbf{I} - \mathbf{A}) \begin{bmatrix} Y_{\delta_r} & \bar{L}_{\delta_r} & \bar{N}_{\delta_r} \\ m\bar{V} & I_{xx} & I_{zz} \end{bmatrix}^T + \frac{Y_{\delta_r}}{m} \det(s\mathbf{I} - \mathbf{A}) \end{aligned} \quad (\text{B.136})$$

where the adjoint matrix is provided by equation (B.129) and the determinant by equation (B.125). Denoting the first term in the above equation as T_1 and expanding it yields,

$$\begin{aligned} T_1 &= \frac{Y_{\delta_r}}{m\bar{V}} \left[\frac{Y_\beta}{m} \left[\left(s - \frac{\bar{L}_P}{I_{xx}} \right) \left(s - \frac{\bar{N}_R}{I_{zz}} \right) - \frac{\bar{N}_P \bar{L}_R}{I_{zz} I_{xx}} \right] + \frac{Y_R}{m} \left[\frac{\bar{N}_\beta}{I_{zz}} \left(s - \frac{\bar{L}_P}{I_{xx}} \right) + \frac{\bar{L}_\beta \bar{N}_P}{I_{xx} I_{zz}} \right] \right] + \\ &\quad \frac{\bar{L}_{\delta_r}}{I_{xx}} \left[-\frac{Y_\beta \bar{N}_P}{m I_{zz}} + \frac{Y_R \bar{N}_P}{m I_{zz}} \left(s - \frac{Y_\beta}{m\bar{V}} \right) \right] + \frac{\bar{N}_{\delta_r}}{I_{zz}} \left[-\frac{Y_\beta}{m} \left(s - \frac{\bar{L}_P}{I_{xx}} \right) + \frac{Y_R}{m} \left(s - \frac{Y_\beta}{m\bar{V}} \right) \right] \left(s - \frac{\bar{L}_P}{I_{xx}} \right) \\ &= \frac{Y_{\delta_r}}{m\bar{V}} \left[\frac{Y_\beta}{m} \left[s^2 - \left(\frac{\bar{L}_P}{I_{xx}} + \frac{\bar{N}_R}{I_{zz}} \right) s + \frac{\bar{L}_P \bar{L}_R}{I_{xx} I_{zz}} \left(\frac{\bar{N}_R}{\bar{L}_R} - \frac{\bar{N}_P}{\bar{L}_P} \right) \right] + \frac{Y_R}{m} \left[\frac{\bar{N}_\beta}{I_{zz}} s - \frac{\bar{L}_P \bar{L}_\beta}{I_{xx} I_{zz}} \left(\frac{\bar{N}_\beta}{\bar{L}_\beta} - \frac{\bar{N}_P}{\bar{L}_P} \right) \right] \right] + \\ &\quad \left[\frac{Y_R}{m} \left(s - \frac{Y_\beta}{m\bar{V}} \right) - \frac{Y_\beta}{m} \right] \left[\frac{\bar{N}_{\delta_r}}{I_{zz}} s - \frac{\bar{L}_P \bar{L}_{\delta_r}}{I_{xx} I_{zz}} \left(\frac{\bar{N}_{\delta_r}}{\bar{L}_{\delta_r}} - \frac{\bar{N}_P}{\bar{L}_P} \right) \right] \\ &\approx \frac{Y_{\delta_r}}{m\bar{V}} \left[\frac{Y_\beta}{m} \left(s - \frac{\bar{L}_P}{I_{xx}} \right) \left(s - \frac{\bar{N}_R}{I_{zz}} \right) + \frac{Y_R \bar{N}_\beta}{m I_{zz}} \left(s - \frac{\bar{L}_P}{I_{xx}} \right) \right] + \frac{\bar{N}_{\delta_r}}{I_{zz}} \left[\frac{Y_R}{m} \left(s - \frac{Y_\beta}{m\bar{V}} \right) - \frac{Y_\beta}{m} \right] \left(s - \frac{\bar{L}_P}{I_{xx}} \right) \\ &= \frac{Y_{\delta_r}}{m} \left[\left(\frac{Y_\beta}{m\bar{V}} + \frac{\bar{N}_{\delta_r} Y_R}{Y_{\delta_r} I_{zz}} \right) s + \left(-\frac{Y_\beta \bar{N}_R}{m\bar{V} I_{zz}} + \frac{Y_R \bar{N}_\beta}{m\bar{V} I_{zz}} - \frac{\bar{N}_{\delta_r} Y_\beta}{Y_{\delta_r} I_{zz}} - \frac{\bar{N}_{\delta_r} Y_R Y_\beta}{Y_{\delta_r} I_{zz} m\bar{V}} \right) \right] \left(s - \frac{\bar{L}_P}{I_{xx}} \right) \end{aligned} \quad (\text{B.137})$$

subject to the conditions of equations (B.126), (B.127) and (B.135). The characteristic equation for the zeros then becomes,

$$\begin{aligned} z(s) &= \frac{Y_{\delta_r}}{m} \left[\left(\frac{Y_\beta}{m\bar{V}} + \frac{\bar{N}_{\delta_r} Y_R}{Y_{\delta_r} I_{zz}} \right) s + \left(-\frac{Y_\beta \bar{N}_R}{m\bar{V} I_{zz}} + \frac{Y_R \bar{N}_\beta}{m\bar{V} I_{zz}} - \frac{\bar{N}_{\delta_r} Y_\beta}{Y_{\delta_r} I_{zz}} - \frac{\bar{N}_{\delta_r} Y_R Y_\beta}{Y_{\delta_r} I_{zz} m\bar{V}} \right) \right] \left(s - \frac{\bar{L}_P}{I_{xx}} \right) + \\ &\quad \frac{Y_{\delta_r}}{m} \left[s^2 - \left(\frac{Y_\beta}{m\bar{V}} + \frac{\bar{N}_R}{I_{zz}} \right) s + \left(\frac{Y_\beta \bar{N}_R}{m\bar{V} I_{zz}} + \frac{\bar{N}_\beta}{I_{zz}} \right) \right] \left(s - \frac{\bar{L}_P}{I_{xx}} \right) \\ &= \frac{Y_{\delta_r}}{m} \left[s^2 - \frac{Y_R}{I_{zz}} \left(\frac{\bar{N}_R}{Y_R} - \frac{\bar{N}_{\delta_r}}{Y_{\delta_r}} \right) s + \frac{Y_\beta}{I_{zz}} \left(\frac{\bar{N}_\beta}{Y_\beta} - \frac{\bar{N}_{\delta_r}}{Y_{\delta_r}} \right) \left(1 + \frac{Y_R}{m\bar{V}} \right) \right] \left(s - \frac{\bar{L}_P}{I_{xx}} \right) \\ &\approx \frac{Y_{\delta_r}}{m} \left[s^2 - \frac{Y_R}{I_{zz}} \left(\frac{\bar{N}_R}{Y_R} - \frac{\bar{N}_{\delta_r}}{Y_{\delta_r}} \right) s + \frac{Y_\beta}{I_{zz}} \left(\frac{\bar{N}_\beta}{Y_\beta} - \frac{\bar{N}_{\delta_r}}{Y_{\delta_r}} \right) \right] \left(s - \frac{\bar{L}_P}{I_{xx}} \right) \end{aligned} \quad (\text{B.138})$$

where the assumption of equation (B.123) has been used to simplify the result.

B.4 Roll dynamics

With reference to section 5.1.4, the roll dynamics are,

$$\dot{P} = \begin{bmatrix} \bar{L}_P \\ I_{xx} \end{bmatrix} P + \begin{bmatrix} \bar{L}_{\delta_A} \\ I_{xx} \end{bmatrix} \delta_A + \begin{bmatrix} \bar{L}_{\delta_R} \\ I_{xx} \end{bmatrix} \delta_R \quad (\text{B.139})$$

$$P_W = P \quad (\text{B.140})$$

The details of the roll rate controller design and the derivation of the closed loop disturbance transfer function from rudder through to roll rate are provided in this section.

B.4.1 Roll rate controller design

Define a PI control law to provide the desired dynamic response and counter any steady state disturbances due to asymmetry in the aircraft,

$$\delta_A = -K_P P - K_E E_P \quad (\text{B.141})$$

$$\dot{E}_P = P - P_R \quad (\text{B.142})$$

Then the closed loop dynamics become,

$$\dot{P} = \begin{bmatrix} \bar{L}_P - \frac{\bar{L}_{\delta_A}}{I_{xx}} K_P \\ I_{xx} \end{bmatrix} P + \begin{bmatrix} -\frac{\bar{L}_{\delta_A}}{I_{xx}} K_E \\ I_{xx} \end{bmatrix} E_P + \begin{bmatrix} \bar{L}_{\delta_R} \\ I_{xx} \end{bmatrix} \delta_R \quad (\text{B.143})$$

The closed loop dynamics in state space form are,

$$\begin{bmatrix} \dot{P} \\ \dot{E}_P \end{bmatrix} = \begin{bmatrix} \bar{L}_P - \frac{\bar{L}_{\delta_A}}{I_{xx}} K_P & -\frac{\bar{L}_{\delta_A}}{I_{xx}} K_E \\ 1 & 0 \end{bmatrix} \begin{bmatrix} P \\ E_P \end{bmatrix} + \begin{bmatrix} 0 \\ -1 \end{bmatrix} P_R + \begin{bmatrix} \bar{L}_{\delta_R} \\ I_{xx} \\ 0 \end{bmatrix} \delta_R \quad (\text{B.144})$$

with characteristic equation,

$$s^2 - \left(\frac{\bar{L}_P}{I_{xx}} - \frac{\bar{L}_{\delta_A}}{I_{xx}} K_P \right) s - \left(-\frac{\bar{L}_{\delta_A}}{I_{xx}} K_E \right) = 0 \quad (\text{B.145})$$

Given the desired closed loop characteristic equation,

$$\alpha_c(s) = s^2 + \alpha_1 s + \alpha_0 \quad (\text{B.146})$$

The feedback gains can be calculated by matching the coefficients,

$$\alpha_1 = - \left(\frac{\bar{L}_P}{I_{xx}} - \frac{\bar{L}_{\delta_A}}{I_{xx}} K_P \right) \quad (\text{B.147})$$

$$\alpha_0 = - \left(-\frac{\bar{L}_{\delta_A}}{I_{xx}} K_E \right) \quad (\text{B.148})$$

Thus,

$$K_P = \frac{1}{L_{\delta_A}} (\bar{L}_P + I_{xx} \alpha_1) \quad (\text{B.149})$$

$$K_E = \frac{I_{xx}}{L_{\delta_A}} \alpha_0 \quad (\text{B.150})$$

and the design freedom is reduced to that of selecting appropriate closed loop poles.

B.4.2 Rudder to roll rate disturbance transfer function

To investigate the disturbance to the closed loop system due to rudder inputs begin with the closed loop state space model of equation (B.144),

$$\begin{bmatrix} \dot{P} \\ \dot{E}_P \end{bmatrix} = \begin{bmatrix} -\alpha_1 & -\alpha_0 \\ 1 & 0 \end{bmatrix} \begin{bmatrix} P \\ E_P \end{bmatrix} + \begin{bmatrix} 0 \\ -1 \end{bmatrix} P_R + \begin{bmatrix} \bar{L}_{\delta_R} \\ I_{xx} \\ 0 \end{bmatrix} \delta_R \quad (\text{B.151})$$

The transfer function from the rudder input through to roll rate is then,

$$\begin{aligned} \frac{P(s)}{\delta_R(s)} &= \frac{[1 \ 0] \text{adj} \left(\begin{bmatrix} s + \alpha_1 & \alpha_0 \\ -1 & s \end{bmatrix} \right) \begin{bmatrix} \bar{L}_{\delta_R} \\ I_{xx} \\ 0 \end{bmatrix}}{s^2 + \alpha_1 s + \alpha_0} \\ &= \frac{\bar{L}_{\delta_R}}{I_{xx}} \frac{s}{s^2 + \alpha_1 s + \alpha_0} \end{aligned} \quad (\text{B.152})$$

B.5 Directional dynamics

The directional dynamics are,

$$\dot{\mathbf{x}} = \mathbf{A}\mathbf{x} + \mathbf{B}\delta_R + \mathbf{B}_1\delta_A + \mathbf{B}_2 e^{Wt} \quad (\text{B.153})$$

$$B_W = \mathbf{C}\mathbf{x} + D\delta_R \quad (\text{B.154})$$

where,

$$\mathbf{x} = \begin{bmatrix} \beta \\ R \end{bmatrix} \quad (\text{B.155})$$

and,

$$\mathbf{A} = \begin{bmatrix} \frac{Y_\beta}{m\bar{V}} & -1 \\ \frac{\bar{N}_\beta}{I_{zz}} & \frac{\bar{N}_R}{I_{zz}} \end{bmatrix} \quad \mathbf{B} = \begin{bmatrix} \frac{Y_{\delta_R}}{m\bar{V}} \\ \frac{\bar{N}_{\delta_R}}{I_{zz}} \end{bmatrix} \quad \mathbf{B}_1 = \begin{bmatrix} 0 \\ \frac{\bar{N}_{\delta_A}}{I_{zz}} \end{bmatrix} \quad \mathbf{B}_2 = \begin{bmatrix} \frac{g}{\bar{V}} \\ 0 \end{bmatrix} \quad (\text{B.156})$$

$$\mathbf{C} = \begin{bmatrix} \frac{Y_\beta}{m} & \frac{Y_R}{m} \end{bmatrix} \quad D = \frac{Y_{\delta_R}}{m} \quad (\text{B.157})$$

B.5.1 Directional dynamics gravity coupling transfer function

The transfer function from the attitude angle coupling through to the lateral specific acceleration is,

$$\frac{B_w(s)}{e_{23}^{wl}(s)} = \frac{\mathbf{C} \text{adj}(s\mathbf{I} - \mathbf{A}) \mathbf{B}_2}{\det(s\mathbf{I} - \mathbf{A})} \quad (\text{B.158})$$

The adjoint matrix is easily shown to be,

$$\text{adj}(s\mathbf{I} - \mathbf{A}) = \begin{bmatrix} s - \frac{\bar{N}_R}{I_{zz}} & -1 \\ \frac{\bar{N}_\beta}{I_{zz}} & s - \frac{Y_\beta}{m\bar{V}} \end{bmatrix} \quad (\text{B.159})$$

Expanding the numerator of equation (B.158) gives,

$$\begin{aligned} \mathbf{C} \text{adj}(s\mathbf{I} - \mathbf{A}) \mathbf{B}_2 &= \begin{bmatrix} \frac{Y_\beta}{m} & \frac{Y_R}{m} \end{bmatrix} \begin{bmatrix} s - \frac{\bar{N}_R}{I_{zz}} & -1 \\ \frac{\bar{N}_\beta}{I_{zz}} & s - \frac{Y_\beta}{m\bar{V}} \end{bmatrix} \begin{bmatrix} \frac{g}{\bar{V}} \\ 0 \end{bmatrix} \\ &= \frac{g}{\bar{V}} \left[\frac{Y_\beta}{m} \left(s - \frac{\bar{N}_R}{I_{zz}} \right) + \frac{Y_R}{m} \frac{\bar{N}_\beta}{I_{zz}} \right] \\ &= \frac{g}{\bar{V}} \frac{Y_\beta}{m} \left[s + \frac{Y_R}{I_{zz}} \left(\frac{\bar{N}_\beta}{Y_\beta} - \frac{\bar{N}_R}{Y_R} \right) \right] \\ &= \frac{g}{\bar{V}} \frac{Y_\beta}{m} \left[s + \frac{Y_R}{I_{zz}} (I_D - I_W) \right] \end{aligned} \quad (\text{B.160})$$

where use of equations (5.55) and (5.56) has been made. The denominator of equation (B.158) is easily shown to be,

$$\det(s\mathbf{I} - \mathbf{A}) = s^2 - \left(\frac{Y_\beta}{m\bar{V}} + \frac{\bar{N}_R}{I_{zz}} \right) s + \left(\frac{Y_\beta}{m\bar{V}} \frac{\bar{N}_R}{I_{zz}} + \frac{\bar{N}_\beta}{I_{zz}} \right) \quad (\text{B.161})$$

Thus the transfer function becomes,

$$\frac{B_w(s)}{e_{23}^{wl}(s)} = \frac{g}{\bar{V}} \frac{Y_\beta}{m} \frac{s + \frac{Y_R}{I_{zz}} (I_D - I_W)}{s^2 - \left(\frac{Y_\beta}{m\bar{V}} + \frac{\bar{N}_R}{I_{zz}} \right) s + \left(\frac{Y_\beta}{m\bar{V}} \frac{\bar{N}_R}{I_{zz}} + \frac{\bar{N}_\beta}{I_{zz}} \right)} \quad (\text{B.162})$$

B.5.2 Analysis of adverse yaw static inversion

To analyse the effect of implementing the static inversion control law for adverse yaw, the aileron to lateral specific acceleration transfer function is investigated for both the case when the control law is implemented and when it is not. The ratio of these two transfer functions will then provide insight into the usefulness of implementing the control law at all. Beginning with the nominal transfer function i.e. no static inversion control law,

$$\frac{B_W(s)}{\delta_A(s)} = \frac{\text{Cadj}(s\mathbf{I} - \mathbf{A})\mathbf{B}_1}{\det(s\mathbf{I} - \mathbf{A})} \quad (\text{B.163})$$

Expanding the numerator first using the adjoint matrix of equation (B.159) gives,

$$\begin{aligned} \text{Cadj}(s\mathbf{I} - \mathbf{A})\mathbf{B}_1 &= \begin{bmatrix} Y_\beta & Y_R \\ m & m \end{bmatrix} \begin{bmatrix} s - \frac{\bar{N}_R}{I_{zz}} & -1 \\ \frac{\bar{N}_\beta}{I_{zz}} & s - \frac{Y_\beta}{m\bar{V}} \end{bmatrix} \begin{bmatrix} 0 \\ \frac{\bar{N}_{\delta_A}}{I_{zz}} \end{bmatrix} \\ &= \frac{\bar{N}_{\delta_A}}{I_{zz}} \begin{bmatrix} -\frac{Y_\beta}{m} + \frac{Y_R}{m} \left(s - \frac{Y_\beta}{m\bar{V}} \right) \end{bmatrix} \\ &= \frac{\bar{N}_{\delta_A}}{I_{zz}} \frac{Y_R}{m} \begin{bmatrix} s - \frac{Y_\beta}{Y_R} \left(\frac{Y_R}{m\bar{V}} + 1 \right) \end{bmatrix} \\ &\approx \frac{\bar{N}_{\delta_A}}{I_{zz}} \frac{Y_R}{m} \begin{bmatrix} s - \frac{Y_\beta}{Y_R} \end{bmatrix} \end{aligned} \quad (\text{B.164})$$

where the simplifying approximation of equation (B.123) has been used. With reference to equation (B.161), the transfer function becomes,

$$\frac{B_W(s)}{\delta_A(s)} = \frac{\bar{N}_{\delta_A} Y_R}{I_{zz} m} \frac{s - \frac{Y_\beta}{Y_R}}{s^2 - \left(\frac{Y_\beta}{m\bar{V}} + \frac{\bar{N}_R}{I_{zz}} \right) s + \left(\frac{Y_\beta \bar{N}_R}{m\bar{V} I_{zz}} + \frac{\bar{N}_\beta}{I_{zz}} \right)} \quad (\text{B.165})$$

Now, with the static inversion control law of equation (5.61) enforced,

$$\delta_R = \delta'_R - \frac{\bar{N}_{\delta_A}}{\bar{N}_{\delta_R}} \delta_A \quad (\text{B.166})$$

the closed loop system becomes,

$$\dot{\mathbf{x}} = \mathbf{A}\mathbf{x} + \mathbf{B}\delta'_R + \mathbf{B}'_1\delta_A + \mathbf{B}_2 e^{Wt} \quad (\text{B.167})$$

$$B_W = \mathbf{C}\mathbf{x} + D\delta'_R + D'_1\delta_A \quad (\text{B.168})$$

with,

$$\mathbf{B}'_1 = \begin{bmatrix} -\frac{Y_{\delta_r} \bar{N}_{\delta_A}}{m \bar{V} \bar{N}_{\delta_r}} \\ 0 \end{bmatrix} \quad (\text{B.169})$$

$$D'_1 = -\frac{Y_{\delta_r} \bar{N}_{\delta_A}}{m \bar{N}_{\delta_r}} \quad (\text{B.170})$$

The transfer function from aileron deflection through to lateral specific acceleration then becomes,

$$\frac{B_w(s)}{\delta_A(s)} = \frac{\text{Cadj}(s\mathbf{I} - \mathbf{A})\mathbf{B}'_1 + D'_1 \det(s\mathbf{I} - \mathbf{A})}{\det(s\mathbf{I} - \mathbf{A})} \quad (\text{B.171})$$

Expanding the first term of the numerator making use of the adjoint matrix of equation (B.159) gives,

$$\begin{aligned} \text{Cadj}(s\mathbf{I} - \mathbf{A})\mathbf{B}'_1 &= \begin{bmatrix} \frac{Y_\beta}{m} & \frac{Y_R}{m} \\ \frac{\bar{N}_\beta}{I_{zz}} & s - \frac{Y_\beta}{m \bar{V}} \end{bmatrix} \begin{bmatrix} s - \frac{\bar{N}_R}{I_{zz}} & -1 \\ \frac{\bar{N}_\beta}{I_{zz}} & s - \frac{Y_\beta}{m \bar{V}} \end{bmatrix} \begin{bmatrix} -\frac{Y_{\delta_r} \bar{N}_{\delta_A}}{m \bar{V} \bar{N}_{\delta_r}} \\ 0 \end{bmatrix} \\ &= -\frac{Y_{\delta_r} \bar{N}_{\delta_A}}{m \bar{V} \bar{N}_{\delta_r}} \left[\frac{Y_\beta}{m} \left(s - \frac{\bar{N}_R}{I_{zz}} \right) + \frac{Y_R \bar{N}_\beta}{m I_{zz}} \right] \\ &= -\frac{Y_{\delta_r} \bar{N}_{\delta_A} Y_\beta}{m \bar{V} \bar{N}_{\delta_r} m} \left[s + \frac{Y_R}{I_{zz}} \left(\frac{\bar{N}_\beta}{Y_\beta} - \frac{\bar{N}_R}{Y_R} \right) \right] \end{aligned} \quad (\text{B.172})$$

Making use of equations (B.172), (B.170) and (B.161), the numerator of equation (B.171) becomes,

$$\begin{aligned} z(s) &= -\frac{Y_{\delta_r} \bar{N}_{\delta_A} Y_\beta}{m \bar{V} \bar{N}_{\delta_r} m} \left[s + \frac{Y_R}{I_{zz}} \left(\frac{\bar{N}_\beta}{Y_\beta} - \frac{\bar{N}_R}{Y_R} \right) \right] - \frac{Y_{\delta_r} \bar{N}_{\delta_A}}{m \bar{N}_{\delta_r}} \left[s^2 - \left(\frac{Y_\beta}{m \bar{V}} + \frac{\bar{N}_R}{I_{zz}} \right) s + \left(\frac{Y_\beta \bar{N}_R}{m \bar{V} I_{zz}} + \frac{\bar{N}_\beta}{I_{zz}} \right) \right] \\ &= -\frac{Y_{\delta_r} \bar{N}_{\delta_A}}{m \bar{N}_{\delta_r}} \left[s^2 - \left(\frac{Y_\beta}{m \bar{V}} + \frac{\bar{N}_R}{I_{zz}} - \frac{Y_\beta}{m \bar{V}} \right) s + \left(\frac{Y_\beta \bar{N}_R}{m \bar{V} I_{zz}} + \frac{\bar{N}_\beta}{I_{zz}} + \frac{Y_R \bar{N}_\beta}{m \bar{V} I_{zz}} - \frac{Y_\beta \bar{N}_R}{m \bar{V} I_{zz}} \right) \right] \\ &= -\frac{Y_{\delta_r} \bar{N}_{\delta_A}}{m \bar{N}_{\delta_r}} \left[s^2 - \frac{\bar{N}_R}{I_{zz}} s + \frac{\bar{N}_\beta}{I_{zz}} \left(1 + \frac{Y_R}{m \bar{V}} \right) \right] \\ &\approx -\frac{Y_{\delta_r} \bar{N}_{\delta_A}}{m \bar{N}_{\delta_r}} \left(s^2 - \frac{\bar{N}_R}{I_{zz}} s + \frac{\bar{N}_\beta}{I_{zz}} \right) \end{aligned} \quad (\text{B.173})$$

where the approximation of equation (B.123) has been used. Substituting equation (B.173) and (B.161) into equation (B.171) yields the result,

$$\frac{B_W(s)}{\delta_A(s)} = -\frac{Y_{\delta_R} \bar{N}_{\delta_A}}{m \bar{N}_{\delta_R}} \frac{s^2 - \frac{\bar{N}_R}{I_{zz}} s + \frac{\bar{N}_\beta}{I_{zz}}}{s^2 - \left(\frac{Y_\beta}{m\bar{V}} + \frac{\bar{N}_R}{I_{zz}}\right) s + \left(\frac{Y_\beta}{m\bar{V}} \frac{\bar{N}_R}{I_{zz}} + \frac{\bar{N}_\beta}{I_{zz}}\right)} \quad (\text{B.174})$$

Now divide the transfer function of equation (B.174) by the transfer function of equation (B.165) to provide a transfer function that describes the ratio of aileron to lateral specific acceleration gains with frequency,

$$\begin{aligned} \Delta(s) &= -\frac{\frac{Y_{\delta_R} \bar{N}_{\delta_A}}{m \bar{N}_{\delta_R}} s^2 - \frac{\bar{N}_R}{I_{zz}} s + \frac{\bar{N}_\beta}{I_{zz}}}{\frac{\bar{N}_{\delta_A} Y_R}{I_{zz} m} s - \frac{Y_\beta}{Y_R}} \\ &= -\frac{Y_{\delta_R} \bar{N}_{\delta_A} I_{zz}}{\bar{N}_{\delta_R} Y_R} \frac{s^2 - \frac{\bar{N}_R}{I_{zz}} s + \frac{\bar{N}_\beta}{I_{zz}}}{s - \frac{Y_\beta}{Y_R}} \end{aligned} \quad (\text{B.175})$$

Investigating only the steady state gain of this transfer function yields the result,

$$\Delta(0) = \frac{Y_{\delta_R} \bar{N}_\beta}{\bar{N}_{\delta_R} Y_\beta} = \frac{l_W}{l_F} \quad (\text{B.176})$$

where use of equations (5.55) and (5.57) has been made.

B.5.3 Directional stability augmentation

Define the stability augmentation control law,

$$\delta_R = -K_R R - K_B B_W + \delta_{R_0} \quad (\text{B.177})$$

Substituting for the lateral specific acceleration from equation (B.154) gives,

$$\begin{aligned} \delta_R &= \left(1 + K_B \frac{Y_{\delta_R}}{m}\right)^{-1} \left(\left[\begin{array}{c} -K_B \frac{Y_\beta}{m} \\ -\left(K_R + K_B \frac{Y_R}{m}\right) \end{array} \right] \left[\begin{array}{c} \beta \\ R \end{array} \right] + \delta_{R_0} \right) \\ &= X \left(\left[\begin{array}{c} -K_B \frac{Y_\beta}{m} \\ -K'_R \end{array} \right] \left[\begin{array}{c} \beta \\ R \end{array} \right] + \delta_{R_0} \right) \end{aligned} \quad (\text{B.178})$$

with,

$$X = \left(1 + K_B \frac{Y_{\delta_R}}{m}\right)^{-1} \quad (\text{B.179})$$

$$K'_R = K_R + K_B \frac{Y_R}{m} \quad (\text{B.180})$$

Substituting the control law into the directional dynamics of equation (B.153) gives,

$$\begin{bmatrix} \dot{\beta} \\ \dot{R} \end{bmatrix} = \begin{bmatrix} \frac{Y_\beta}{m\bar{V}} - K_B \frac{Y_\beta}{m} \frac{Y_{\delta_r}}{m\bar{V}} X & -1 - K'_R \frac{Y_{\delta_r}}{m\bar{V}} X \\ \frac{\bar{N}_\beta}{I_{zz}} - K_B \frac{Y_\beta}{m} \frac{\bar{N}_{\delta_r}}{I_{zz}} X & \frac{\bar{N}_R}{I_{zz}} - K'_R \frac{\bar{N}_{\delta_r}}{I_{zz}} X \end{bmatrix} \begin{bmatrix} \beta \\ R \end{bmatrix} + \begin{bmatrix} \frac{Y_{\delta_r}}{m\bar{V}} X \\ \frac{\bar{N}_{\delta_r}}{I_{zz}} X \end{bmatrix} \delta_{R_r} \quad (\text{B.181})$$

The closed loop poles are the roots of the characteristic equation,

$$\alpha_c(s) = \det \left(\begin{bmatrix} s - \frac{Y_\beta}{m\bar{V}} + K_B \frac{Y_\beta}{m} \frac{Y_{\delta_r}}{m\bar{V}} X & 1 + K'_R \frac{Y_{\delta_r}}{m\bar{V}} X \\ -\frac{\bar{N}_\beta}{I_{zz}} + K_B \frac{Y_\beta}{m} \frac{\bar{N}_{\delta_r}}{I_{zz}} X & s - \frac{\bar{N}_R}{I_{zz}} + K'_R \frac{\bar{N}_{\delta_r}}{I_{zz}} X \end{bmatrix} \right) = 0 \quad (\text{B.182})$$

Expanding the determinant above yields,

$$\alpha_c(s) = s^2 + a_1 s + a_0 \quad (\text{B.183})$$

where,

$$a_1 = -\left(\frac{Y_\beta}{m\bar{V}} + \frac{\bar{N}_R}{I_{zz}} \right) + \left(\frac{\bar{N}_{\delta_r}}{I_{zz}} K'_R + \frac{Y_\beta}{m} \frac{Y_{\delta_r}}{m\bar{V}} K_B \right) X \quad (\text{B.184})$$

$$a_0 = \left(\frac{Y_\beta}{m\bar{V}} \frac{\bar{N}_R}{I_{zz}} + \frac{\bar{N}_\beta}{I_{zz}} \right) + \left(\left(\frac{\bar{N}_\beta}{I_{zz}} \frac{Y_{\delta_r}}{m\bar{V}} - \frac{\bar{N}_{\delta_r}}{I_{zz}} \frac{Y_\beta}{m\bar{V}} \right) K'_R - \left(\frac{\bar{N}_R}{I_{zz}} \frac{Y_\beta}{m} \frac{Y_{\delta_r}}{m\bar{V}} + \frac{Y_\beta}{m} \frac{\bar{N}_{\delta_r}}{I_{zz}} \right) K_B \right) X \quad (\text{B.185})$$

Expanding the above coefficients yields,

$$\begin{aligned} a_1 &= -\left(\frac{Y_\beta}{m\bar{V}} + \frac{\bar{N}_R}{I_{zz}} + \frac{\bar{N}_R}{I_{zz}} \frac{Y_{\delta_r}}{m} K_B - \frac{\bar{N}_{\delta_r}}{I_{zz}} K'_R \right) X \\ &= -\left(\frac{Y_\beta}{m\bar{V}} + \frac{\bar{N}_R}{I_{zz}} - \frac{\bar{N}_{\delta_r}}{I_{zz}} K_R \left(1 - \frac{Y_\beta}{m} \frac{Y_{\delta_r}}{\bar{N}_{\delta_r}} \left(\frac{\bar{N}_R}{Y_\beta} - \frac{\bar{N}_{\delta_r}}{Y_{\delta_r}} \right) \frac{K_B}{K_R} \right) \right) X \\ &\approx -\left(\frac{Y_\beta}{m\bar{V}} + \frac{\bar{N}_R}{I_{zz}} - \frac{\bar{N}_{\delta_r}}{I_{zz}} K_R \right) X \end{aligned} \quad (\text{B.186})$$

$$\begin{aligned} a_0 &= \left[\frac{Y_\beta}{m\bar{V}} \frac{\bar{N}_R}{I_{zz}} + \frac{\bar{N}_\beta}{I_{zz}} + \left(\frac{\bar{N}_\beta}{I_{zz}} \frac{Y_{\delta_r}}{m} - \frac{Y_\beta}{m} \frac{\bar{N}_{\delta_r}}{I_{zz}} \right) K_B + \left(\frac{\bar{N}_\beta}{I_{zz}} \frac{Y_{\delta_r}}{m\bar{V}} - \frac{\bar{N}_{\delta_r}}{I_{zz}} \frac{Y_\beta}{m\bar{V}} \right) K'_R \right] X \\ &= \left[\frac{Y_\beta}{m\bar{V}} \frac{\bar{N}_R}{I_{zz}} + \frac{\bar{N}_\beta}{I_{zz}} + \frac{Y_{\delta_r}}{m\bar{V}} \frac{Y_\beta}{I_{zz}} \left(\frac{\bar{N}_\beta}{Y_\beta} - \frac{\bar{N}_{\delta_r}}{Y_{\delta_r}} \right) K_R + \frac{Y_{\delta_r}}{m} \frac{Y_\beta}{I_{zz}} \left(\frac{\bar{N}_\beta}{Y_\beta} - \frac{\bar{N}_{\delta_r}}{Y_{\delta_r}} \right) \left(1 + \frac{Y_\beta}{m\bar{V}} \right) K_B \right] X \\ &= \left[\frac{Y_\beta}{m\bar{V}} \frac{\bar{N}_R}{I_{zz}} + \frac{\bar{N}_\beta}{I_{zz}} \left(1 + \frac{Y_{\delta_r}}{m\bar{V}} \frac{Y_\beta}{\bar{N}_\beta} \left(\frac{\bar{N}_\beta}{Y_\beta} - \frac{\bar{N}_{\delta_r}}{Y_{\delta_r}} \right) K_R \right) + \frac{Y_{\delta_r}}{m} \frac{Y_\beta}{I_{zz}} \left(\frac{\bar{N}_\beta}{Y_\beta} - \frac{\bar{N}_{\delta_r}}{Y_{\delta_r}} \right) \left(1 + \frac{Y_\beta}{m\bar{V}} \right) K_B \right] X \\ &\approx \left[\frac{Y_\beta}{m\bar{V}} \frac{\bar{N}_R}{I_{zz}} + \frac{\bar{N}_\beta}{I_{zz}} + \frac{Y_{\delta_r}}{m} \frac{Y_\beta}{I_{zz}} \left(\frac{\bar{N}_\beta}{Y_\beta} - \frac{\bar{N}_{\delta_r}}{Y_{\delta_r}} \right) K_B \right] X \end{aligned} \quad (\text{B.187})$$

given the simplifying assumption of equation (B.123) and the constraints below,

$$\left| \frac{Y_R}{m} \frac{Y_{\delta_r}}{\bar{N}_{\delta_r}} \left(\frac{\bar{N}_R}{Y_R} - \frac{\bar{N}_{\delta_r}}{Y_{\delta_r}} \right) \frac{K_B}{K_R} \right| \ll 1 \quad (\text{B.188})$$

$$\left| \frac{Y_{\delta_r}}{m\bar{V}} \frac{Y_\beta}{\bar{N}_\beta} \left(\frac{\bar{N}_\beta}{Y_\beta} - \frac{\bar{N}_{\delta_r}}{Y_{\delta_r}} \right) K_R \right| \ll 1 \quad (\text{B.189})$$

These constraints become,

$$\left| \frac{K_B}{K_R} \right| \ll \left| \frac{m}{Y_R} \frac{l_F}{l_D - l_F} \right| \quad (\text{B.190})$$

$$\left| K_R \right| \ll \left| \frac{m\bar{V}}{Y_{\delta_r}} \frac{l_W}{l_W - l_F} \right| \quad (\text{B.191})$$

when the characteristic lengths of equations (5.55) to (5.57) are substituted. Given the desired directional dynamics characteristic equation,

$$\alpha_c(s) = s^2 + \alpha_1 s + \alpha_0 \quad (\text{B.192})$$

the coefficients of the characteristic polynomials of equations (B.183) and (B.192) can be matched,

$$\alpha_1 = - \left(\frac{Y_\beta}{m\bar{V}} + \frac{\bar{N}_R}{I_{zz}} - \frac{\bar{N}_{\delta_r}}{I_{zz}} K_R \right) X \quad (\text{B.193})$$

$$\alpha_0 = \left[\frac{Y_\beta}{m\bar{V}} \frac{\bar{N}_R}{I_{zz}} + \frac{\bar{N}_\beta}{I_{zz}} + \frac{Y_{\delta_r}}{m} \frac{Y_\beta}{I_{zz}} \left(\frac{\bar{N}_\beta}{Y_\beta} - \frac{\bar{N}_{\delta_r}}{Y_{\delta_r}} \right) K_B \right] X \quad (\text{B.194})$$

to yield the feedback gains,

$$K_R = \frac{I_{zz}}{\bar{N}_{\delta_r}} \left[\frac{Y_\beta}{m\bar{V}} + \frac{\bar{N}_R}{I_{zz}} + \alpha_1 \left(1 + K_B \frac{Y_{\delta_r}}{m} \right) \right] \quad (\text{B.195})$$

$$K_B = \frac{\frac{Y_\beta}{m\bar{V}} \frac{\bar{N}_R}{I_{zz}} + \frac{\bar{N}_\beta}{I_{zz}} - \alpha_0}{\frac{Y_{\delta_r}}{m} \left[\alpha_0 - \frac{Y_\beta}{I_{zz}} \left(\frac{\bar{N}_\beta}{Y_\beta} - \frac{\bar{N}_{\delta_r}}{Y_{\delta_r}} \right) \right]} \quad (\text{B.196})$$

Considering now the special case of the control law when the lateral specific acceleration feedback gain is manually set to zero. The closed loop characteristic equation becomes,

$$\alpha_c(s) = s^2 - \left(\frac{Y_\beta}{m\bar{V}} + \frac{\bar{N}_R}{I_{zz}} - \frac{\bar{N}_{\delta_R}}{I_{zz}} K_R \right) s + \left(\frac{Y_\beta \bar{N}_R}{m\bar{V} I_{zz}} + \frac{\bar{N}_\beta}{I_{zz}} \right) \quad (\text{B.197})$$

and the feedback gain K_R only influences the closed loop system's damping. Given the desired damping ratio ζ the feedback gains are,

$$K_R = \frac{I_{zz}}{\bar{N}_{\delta_R}} \left(\frac{Y_\beta}{m\bar{V}} + \frac{\bar{N}_R}{I_{zz}} + 2\zeta\omega_n \right) \quad (\text{B.198})$$

$$K_B = 0 \quad (\text{B.199})$$

with the natural frequency equal to its open loop value of,

$$\omega_n = \sqrt{\frac{Y_\beta \bar{N}_R}{m\bar{V} I_{zz}} + \frac{\bar{N}_\beta}{I_{zz}}} \quad (\text{B.200})$$

B.5.4 Steady state gain from rudder to lateral specific acceleration

With reference to equation (B.181), the closed loop dynamics after the stability augmentation control law has been implemented can be written as follows,

$$\dot{\mathbf{x}} = \mathbf{A}\mathbf{x} + \mathbf{B}\delta_{R_r} \quad (\text{B.201})$$

$$B_w = \mathbf{C}\mathbf{x} + D\delta_{R_r} \quad (\text{B.202})$$

where the state space matrices are,

$$\mathbf{A} = \begin{bmatrix} \frac{Y_\beta}{m\bar{V}} - K_B \frac{Y_\beta}{m} \frac{Y_{\delta_R}}{m\bar{V}} X & -1 - K'_R \frac{Y_{\delta_R}}{m\bar{V}} X \\ \frac{\bar{N}_\beta}{I_{zz}} - K_B \frac{Y_\beta}{m} \frac{\bar{N}_{\delta_R}}{I_{zz}} X & \frac{\bar{N}_R}{I_{zz}} - K'_R \frac{\bar{N}_{\delta_R}}{I_{zz}} X \end{bmatrix} \quad \mathbf{B} = \begin{bmatrix} \frac{Y_{\delta_R}}{m\bar{V}} X \\ \frac{\bar{N}_{\delta_R}}{I_{zz}} X \end{bmatrix} \quad (\text{B.203})$$

$$\mathbf{C} = \left[\frac{Y_\beta}{m} X \quad \left(\frac{Y_R}{m} - K_R \frac{Y_{\delta_R}}{m} \right) X \right] \quad D = \frac{Y_{\delta_R}}{m} X \quad (\text{B.204})$$

and the aileron and attitude angle couplings have been ignored. The steady state gain from the rudder input through to the lateral specific acceleration output can be written as follows,

$$K_{ss} = \frac{\text{Cadj}(-\mathbf{A})\mathbf{B} + D \det(-\mathbf{A})}{\det(-\mathbf{A})} \quad (\text{B.205})$$

The determinant in the above equation is simply obtained by substituting $s=0$ into equation (B.183). Calculating the first term in the numerator of equation (B.205) yields,

$$\begin{aligned}
\text{Cadj}(-\mathbf{A})\mathbf{B} &= -X^2 \begin{bmatrix} \frac{Y_\beta}{m} & \frac{Y_R}{m} - K_R & \frac{Y_{\delta_R}}{m} \end{bmatrix} \begin{bmatrix} \frac{\bar{N}_R}{I_{zz}} - K'_R \frac{\bar{N}_{\delta_R}}{I_{zz}} X & 1 + K'_R \frac{Y_{\delta_R}}{m\bar{V}} X \\ -\frac{\bar{N}_\beta}{I_{zz}} + K_B \frac{Y_\beta}{m} \frac{\bar{N}_{\delta_R}}{I_{zz}} X & \frac{Y_\beta}{m\bar{V}} - K_B \frac{Y_\beta}{m} \frac{Y_{\delta_R}}{m\bar{V}} X \end{bmatrix} \begin{bmatrix} \frac{Y_{\delta_R}}{m\bar{V}} \\ \frac{\bar{N}_{\delta_R}}{I_{zz}} \end{bmatrix} \\
&= -X^2 \begin{bmatrix} \frac{Y_\beta}{m} & \frac{Y_R}{m} - K_R & \frac{Y_{\delta_R}}{m} \end{bmatrix} \begin{bmatrix} \frac{Y_{\delta_R}}{m\bar{V}} \frac{\bar{N}_R}{I_{zz}} + \frac{\bar{N}_{\delta_R}}{I_{zz}} \\ \frac{\bar{N}_{\delta_R}}{I_{zz}} \frac{Y_\beta}{m\bar{V}} - \frac{Y_{\delta_R}}{m\bar{V}} \frac{\bar{N}_\beta}{I_{zz}} \end{bmatrix} \\
&= -X^2 \left[\frac{Y_\beta}{m} \left(\frac{Y_{\delta_R}}{m\bar{V}} \frac{\bar{N}_R}{I_{zz}} + \frac{\bar{N}_{\delta_R}}{I_{zz}} \right) + \left(\frac{Y_R}{m} - K_R \frac{Y_{\delta_R}}{m} \right) \left(\frac{\bar{N}_{\delta_R}}{I_{zz}} \frac{Y_\beta}{m\bar{V}} - \frac{Y_{\delta_R}}{m\bar{V}} \frac{\bar{N}_\beta}{I_{zz}} \right) \right] \\
&= X^2 \frac{Y_{\delta_R}}{m} \left[-\frac{Y_\beta}{m\bar{V}} \frac{\bar{N}_R}{I_{zz}} - \frac{Y_\beta}{I_{zz}} \frac{\bar{N}_{\delta_R}}{Y_{\delta_R}} + \frac{Y_\beta}{I_{zz}} \frac{Y_R}{m\bar{V}} \left(\frac{\bar{N}_\beta}{Y_\beta} - \frac{\bar{N}_{\delta_R}}{Y_{\delta_R}} \right) - \frac{Y_{\delta_R}}{m\bar{V}} \frac{Y_\beta}{I_{zz}} \left(\frac{\bar{N}_\beta}{Y_\beta} - \frac{\bar{N}_{\delta_R}}{Y_{\delta_R}} \right) K_R \right]
\end{aligned} \tag{B.206}$$

The complete numerator calculation is then,

$$\begin{aligned}
N &= X^2 \frac{Y_{\delta_R}}{m} \left[-\frac{Y_\beta}{m\bar{V}} \frac{\bar{N}_R}{I_{zz}} - \frac{Y_\beta}{I_{zz}} \frac{\bar{N}_{\delta_R}}{Y_{\delta_R}} + \frac{Y_\beta}{I_{zz}} \frac{Y_R}{m\bar{V}} \left(\frac{\bar{N}_\beta}{Y_\beta} - \frac{\bar{N}_{\delta_R}}{Y_{\delta_R}} \right) - \frac{Y_{\delta_R}}{m\bar{V}} \frac{Y_\beta}{I_{zz}} \left(\frac{\bar{N}_\beta}{Y_\beta} - \frac{\bar{N}_{\delta_R}}{Y_{\delta_R}} \right) K_R \right. \\
&\quad \left. + \frac{Y_\beta}{m\bar{V}} \frac{\bar{N}_R}{I_{zz}} + \frac{\bar{N}_\beta}{I_{zz}} + \frac{Y_{\delta_R}}{m\bar{V}} \frac{Y_\beta}{I_{zz}} \left(\frac{\bar{N}_\beta}{Y_\beta} - \frac{\bar{N}_{\delta_R}}{Y_{\delta_R}} \right) K_R + \frac{Y_{\delta_R}}{m} \frac{Y_\beta}{I_{zz}} \left(\frac{\bar{N}_\beta}{Y_\beta} - \frac{\bar{N}_{\delta_R}}{Y_{\delta_R}} \right) \left(1 + \frac{Y_R}{m\bar{V}} \right) K_B \right] \\
&= X^2 \frac{Y_{\delta_R}}{m} \left[\frac{Y_\beta}{I_{zz}} \left(\frac{\bar{N}_\beta}{Y_\beta} - \frac{\bar{N}_{\delta_R}}{Y_{\delta_R}} \right) + \frac{Y_\beta}{I_{zz}} \frac{Y_R}{m\bar{V}} \left(\frac{\bar{N}_\beta}{Y_\beta} - \frac{\bar{N}_{\delta_R}}{Y_{\delta_R}} \right) + \frac{Y_{\delta_R}}{m} \frac{Y_\beta}{I_{zz}} \left(\frac{\bar{N}_\beta}{Y_\beta} - \frac{\bar{N}_{\delta_R}}{Y_{\delta_R}} \right) \left(1 + \frac{Y_R}{m\bar{V}} \right) K_B \right] \\
&= X \frac{Y_{\delta_R}}{m} \frac{Y_\beta}{I_{zz}} \left(\frac{\bar{N}_\beta}{Y_\beta} - \frac{\bar{N}_{\delta_R}}{Y_{\delta_R}} \right) \left(1 + \frac{Y_R}{m\bar{V}} \right) \\
&\approx X \frac{Y_{\delta_R}}{m} \frac{Y_\beta}{I_{zz}} \left(\frac{\bar{N}_\beta}{Y_\beta} - \frac{\bar{N}_{\delta_R}}{Y_{\delta_R}} \right)
\end{aligned} \tag{B.207}$$

where the numerator has been denoted by N . Note that the determinant was substituted from equation (B.183) before any of the simplifying assumptions were made and thus the only simplifying assumption used to arrive at the result above is that of equation (B.123). Combining equations (B.207) and (B.192) gives the steady state gain,

$$K_{ss} = \frac{Y_{\delta_R}}{m} \frac{Y_\beta}{I_{zz}} \left(\frac{\bar{N}_\beta}{Y_\beta} - \frac{\bar{N}_{\delta_R}}{Y_{\delta_R}} \right) \frac{1}{\alpha_0} \left(1 + K_B \frac{Y_{\delta_R}}{m} \right)^{-1} \tag{B.208}$$

where the constraint of equation (B.191) is required if α_0 is to be used in the equation above.

B.5.5 Deriving the NNDT directional dynamics

The normalising definitions of equations (5.88) to (5.91) and (4.68) can be written as follows,

$$\mathbf{x}' = \mathbf{T}_x \mathbf{x} \tag{B.209}$$

$$\delta'_R = T_u \delta_R \quad (\text{B.210})$$

$$B'_W = T_y B_W \quad (\text{B.211})$$

$$\bar{\mathbf{x}} = T_d \dot{\mathbf{x}} \quad (\text{B.212})$$

with,

$$\mathbf{x}' = \begin{bmatrix} \beta' \\ R' \end{bmatrix} \quad (\text{B.213})$$

and \mathbf{x} from equation (B.155) and with transformation matrices,

$$\mathbf{T}_x = \begin{bmatrix} 1 & 0 \\ 0 & \frac{b}{2\bar{V}_a} \end{bmatrix} \quad T_u = 1 \quad T_y = \frac{m}{qS} \quad T_d = \frac{m\bar{V}}{qS} \quad (\text{B.214})$$

Substituting the above relationships into the directional dynamics of equations (B.153) and (B.154) yields,

$$\mathbf{T}_x^{-1} T_d^{-1} \bar{\mathbf{x}}' = \mathbf{A} \mathbf{T}_x^{-1} \mathbf{x}' + \mathbf{B} T_u^{-1} \delta'_R + \mathbf{B}_1 \delta'_A + \mathbf{B}_2 e_{33}^{III} \quad (\text{B.215})$$

$$T_y^{-1} B'_W = \mathbf{C} \mathbf{T}_x^{-1} \mathbf{x}' + D T_u^{-1} \delta'_R \quad (\text{B.216})$$

where it has been noted that all transformation matrices are static relative to the normal dynamics. Rearranging above gives,

$$\bar{\mathbf{x}}' = \mathbf{A}' \mathbf{x}' + \mathbf{B}' \delta'_R + \mathbf{B}'_1 \delta'_A + \mathbf{B}'_2 e_{33}^{III} \quad (\text{B.217})$$

$$B'_W = \mathbf{C}' \mathbf{x}' + D' \delta'_R \quad (\text{B.218})$$

with,

$$\mathbf{A}' = T_d \mathbf{T}_x \mathbf{A} \mathbf{T}_x^{-1} \quad \mathbf{B}' = T_d \mathbf{T}_x \mathbf{B} T_u^{-1} \quad \mathbf{B}'_1 = T_d \mathbf{T}_x \mathbf{B}_1 \quad \mathbf{B}'_2 = T_d \mathbf{T}_x \mathbf{B}_2 \quad (\text{B.219})$$

$$\mathbf{C}' = T_y \mathbf{C} \mathbf{T}_x^{-1} \quad D' = T_y D T_u^{-1} \quad (\text{B.220})$$

where the definition for NNDT aileron deflection comes from equation (5.36). Multiplying the above matrices out gives,

$$\mathbf{A}' = \begin{bmatrix} C_{y\beta} & -k_R \\ k_z \bar{C}_{n\beta} & k_z \bar{C}_{n_R} \end{bmatrix} \quad \mathbf{B}' = \begin{bmatrix} C_{y\delta_R} \\ k_z \bar{C}_{n\delta_R} \end{bmatrix} \quad \mathbf{B}'_1 = \begin{bmatrix} 0 \\ k_z \bar{C}_{n\delta_A} \end{bmatrix} \quad \mathbf{B}'_2 = \begin{bmatrix} g' \\ 0 \end{bmatrix} \quad (\text{B.221})$$

$$\mathbf{C}' = \begin{bmatrix} C_{y\beta} & C_{y_R} \end{bmatrix} \quad D' = C_{y\delta_R} \quad (\text{B.222})$$

where,

$$k_R = 4m'_R \bar{V}' \quad (\text{B.223})$$

$$k_z = \frac{1}{2} \frac{\bar{V}'}{r'_z} \quad (\text{B.224})$$

with,

$$m'_R = \frac{m}{\rho S b} \quad (\text{B.225})$$

$$r'_z = \frac{r_z}{b} \quad (\text{B.226})$$

$$r_z = \sqrt{\frac{I_{zz}}{m}} \quad (\text{B.227})$$

and g' and \bar{V}' from equations (B.74) and (B.76) respectively. In equations (B.223) and (B.224), m'_R is the aircraft's mass normalised to a lateral reference air mass and r'_z is the normalised pitch radius of gyration. Note that it has been assumed that,

$$|C_{Y_R}| \ll |k_R| \quad (\text{B.228})$$

which is equivalent to the standard aircraft assumption of equation (B.123).

B.5.6 Characteristic equation for the NNDT poles

The poles of the system in equation (B.217) are the roots of the characteristic equation,

$$p(s') = \det(s'\mathbf{I} - \mathbf{A}') \quad (\text{B.229})$$

Expanding this equation,

$$\begin{aligned} p(s') &= \det \begin{bmatrix} s' - C_{y\beta} & k_R \\ -k_z \bar{C}_{n\beta} & s' - k_z \bar{C}_{n_R} \end{bmatrix} \\ &= (s')^2 - (C_{y\beta} + k_z \bar{C}_{n_R})s' + k_z (C_{y\beta} \bar{C}_{n_R} + k_R \bar{C}_{n\beta}) \end{aligned} \quad (\text{B.230})$$

B.5.7 Characteristic equation for the NNDT zeros

The zeros from rudder through to lateral specific acceleration are the roots of the characteristic equation,

$$z(s') = C' \text{adj}(s'\mathbf{I} - \mathbf{A}') \mathbf{B}' + D' \det(s'\mathbf{I} - \mathbf{A}') \quad (\text{B.231})$$

Expanding the first term in the above equation yields,

$$\begin{aligned}
T_1 &= \begin{bmatrix} C_{y\beta} & C_{yR} \\ C_{y\delta R} & C_{y\delta R} \end{bmatrix} \begin{bmatrix} s' - k_z \bar{C}_{nR} & -k_R \\ k_z \bar{C}_{n\beta} & s' - C_{y\beta} \end{bmatrix} \begin{bmatrix} C_{y\delta R} \\ k_z \bar{C}_{n\delta R} \end{bmatrix} \\
&= C_{y\beta} \left[C_{y\delta R} (s' - k_z \bar{C}_{nR}) - k_R k_z \bar{C}_{n\delta R} \right] + C_{yR} \left[k_z \bar{C}_{n\beta} C_{y\delta R} + k_z \bar{C}_{n\delta R} (s' - C_{y\beta}) \right] \\
&= C_{y\delta R} \left[\left(C_{y\beta} + C_{yR} k_z \frac{\bar{C}_{n\delta R}}{C_{y\delta R}} \right) s' - k_z \left(C_{y\beta} \bar{C}_{nR} - C_{yR} \bar{C}_{n\beta} + k_R C_{y\beta} \frac{\bar{C}_{n\delta R}}{C_{y\delta R}} + C_{y\beta} C_{yR} \frac{\bar{C}_{n\delta R}}{C_{y\delta R}} \right) \right]
\end{aligned} \tag{B.232}$$

where T_1 has been used to denote the first term. The determinant of the second term of equation (B.231) has already been calculated in equation (B.230) and so the characteristic equation for the zeros becomes,

$$\begin{aligned}
z(s') &= C_{y\delta R} \left[\left(C_{y\beta} + C_{yR} k_z \frac{\bar{C}_{n\delta R}}{C_{y\delta R}} \right) s' - k_z \left(C_{y\beta} \bar{C}_{nR} - C_{yR} \bar{C}_{n\beta} + k_R C_{y\beta} \frac{\bar{C}_{n\delta R}}{C_{y\delta R}} + C_{y\beta} C_{yR} \frac{\bar{C}_{n\delta R}}{C_{y\delta R}} \right) \right. \\
&\quad \left. + (s')^2 - (C_{y\beta} + k_z \bar{C}_{nR}) s' + k_z (C_{y\beta} \bar{C}_{nR} + k_R \bar{C}_{n\beta}) \right] \\
&= C_{y\delta R} \left[(s')^2 - k_z C_{yR} \left(\frac{\bar{C}_{nR}}{C_{yR}} - \frac{\bar{C}_{n\delta R}}{C_{y\delta R}} \right) s' + k_z C_{y\beta} \left(\frac{\bar{C}_{n\beta}}{C_{y\beta}} - \frac{\bar{C}_{n\delta R}}{C_{y\delta R}} \right) (k_R + C_{yR}) \right] \\
&\approx C_{y\delta R} \left[(s')^2 - k_z C_{yR} \left(\frac{\bar{C}_{nR}}{C_{yR}} - \frac{\bar{C}_{n\delta R}}{C_{y\delta R}} \right) s' + k_R k_z C_{y\beta} \left(\frac{\bar{C}_{n\beta}}{C_{y\beta}} - \frac{\bar{C}_{n\delta R}}{C_{y\delta R}} \right) \right]
\end{aligned} \tag{B.233}$$

where equation (B.228) has been used to simplify the result. Since only the roots of equation (B.233) are desired the characteristic equation can be simplified to,

$$z(s') = (s')^2 - k_z C_{yR} \left(\frac{\bar{C}_{nR}}{C_{yR}} - \frac{\bar{C}_{n\delta R}}{C_{y\delta R}} \right) s' + k_R k_z C_{y\beta} \left(\frac{\bar{C}_{n\beta}}{C_{y\beta}} - \frac{\bar{C}_{n\delta R}}{C_{y\delta R}} \right) \tag{B.234}$$

B.5.8 NNDT directional stability augmentation

Define the stability augmentation control law,

$$\delta'_R = -K'_R R' - K'_B B'_W + \delta'_{R_R} \tag{B.235}$$

Substituting for the lateral specific acceleration from equation (B.218) gives,

$$\delta'_R = X' \left(\begin{bmatrix} -K'_B C_{y\beta} & -\bar{K}'_R \end{bmatrix} \begin{bmatrix} \beta' \\ R' \end{bmatrix} + \delta'_{R_R} \right) \tag{B.236}$$

with,

$$X' = \left(1 + K'_B C_{y\delta R} \right)^{-1} \tag{B.237}$$

$$\bar{K}'_R = K'_R + K'_B C_{yR} \tag{B.238}$$

Substituting the control law into the directional dynamics of equation (B.217) gives,

$$\begin{bmatrix} \bar{\beta}' \\ \bar{R}' \end{bmatrix} = \begin{bmatrix} C_{y\beta} - K'_B C_{y\beta} C_{y\delta_R} X' & -k_R - \bar{K}'_R C_{y\delta_R} X' \\ k_z \bar{C}_{n\beta} - K'_B C_{y\beta} k_z \bar{C}_{n\delta_R} X' & k_z \bar{C}_{n_R} - \bar{K}'_R k_z \bar{C}_{n\delta_R} X' \end{bmatrix} \begin{bmatrix} \beta' \\ R' \end{bmatrix} + \begin{bmatrix} C_{y\delta_R} X' \\ k_z \bar{C}_{n\delta_R} X' \end{bmatrix} \delta'_{R_R} \quad (\text{B.239})$$

The closed loop poles are the roots of the characteristic equation,

$$\alpha_c(s') = \det \left(\begin{bmatrix} s - C_{y\beta} + K'_B C_{y\beta} C_{y\delta_R} X' & k_R + \bar{K}'_R C_{y\delta_R} X' \\ -k_z \bar{C}_{n\beta} + K'_B C_{y\beta} k_z \bar{C}_{n\delta_R} X' & s - k_z \bar{C}_{n_R} + \bar{K}'_R k_z \bar{C}_{n\delta_R} X' \end{bmatrix} \right) = 0 \quad (\text{B.240})$$

Expanding the determinant above yields,

$$\alpha_c(s') = (s')^2 + a_1 s' + a_0 \quad (\text{B.241})$$

where,

$$a_1 = -(C_{y\beta} + k_z \bar{C}_{n_R}) + (k_z \bar{C}_{n\delta_R} \bar{K}'_R + C_{y\beta} C_{y\delta_R} K'_B) X' \quad (\text{B.242})$$

$$a_0 = k_z (C_{y\beta} \bar{C}_{n_R} + k_R \bar{C}_{n\beta}) + k_z \left((\bar{C}_{n\beta} C_{y\delta_R} - \bar{C}_{n\delta_R} C_{y\beta}) \bar{K}'_R - (\bar{C}_{n_R} C_{y\beta} C_{y\delta_R} + k_R C_{y\beta} \bar{C}_{n\delta_R}) K'_B \right) X' \quad (\text{B.243})$$

Expanding the above coefficients yields,

$$\begin{aligned} a_1 &= - \left[C_{y\beta} + k_z \bar{C}_{n_R} + k_z \bar{C}_{n_R} C_{y\delta_R} K'_B - k_z \bar{C}_{n\delta_R} \bar{K}'_R \right] X' \\ &= - \left(C_{y\beta} + k_z \bar{C}_{n_R} - k_z \bar{C}_{n\delta_R} K'_R \left(1 - C_{y_R} \frac{C_{y\delta_R}}{\bar{C}_{n\delta_R}} \left(\frac{\bar{C}_{n_R}}{C_{y_R}} - \frac{\bar{C}_{n\delta_R}}{C_{y\delta_R}} \right) \frac{K'_B}{K'_R} \right) \right) X' \\ &\approx - \left(C_{y\beta} + k_z \bar{C}_{n_R} - k_z \bar{C}_{n\delta_R} K'_R \right) X' \end{aligned} \quad (\text{B.244})$$

$$\begin{aligned} a_0 &= k_z \left[(C_{y\beta} \bar{C}_{n_R} + k_R \bar{C}_{n\beta}) + (k_R \bar{C}_{n\beta} C_{y\delta_R} - k_R C_{y\beta} \bar{C}_{n\delta_R}) K'_B + (\bar{C}_{n\beta} C_{y\delta_R} - \bar{C}_{n\delta_R} C_{y\beta}) \bar{K}'_R \right] X' \\ &= k_z \left[(C_{y\beta} \bar{C}_{n_R} + k_R \bar{C}_{n\beta}) + C_{y\delta_R} C_{y\beta} \left(\frac{\bar{C}_{n\beta}}{C_{y\beta}} - \frac{\bar{C}_{n\delta_R}}{C_{y\delta_R}} \right) K'_R + C_{y\delta_R} C_{y\beta} \left(\frac{\bar{C}_{n\beta}}{C_{y\beta}} - \frac{\bar{C}_{n\delta_R}}{C_{y\delta_R}} \right) (k_R + C_{y_R}) K'_B \right] X' \\ &= k_z \left[C_{y\beta} \bar{C}_{n_R} + \bar{C}_{n\beta} \left(k_R + C_{y\delta_R} \frac{C_{y\beta}}{\bar{C}_{n\beta}} \left(\frac{\bar{C}_{n\beta}}{C_{y\beta}} - \frac{\bar{C}_{n\delta_R}}{C_{y\delta_R}} \right) K'_R \right) + C_{y\delta_R} C_{y\beta} \left(\frac{\bar{C}_{n\beta}}{C_{y\beta}} - \frac{\bar{C}_{n\delta_R}}{C_{y\delta_R}} \right) (k_R + C_{y_R}) K'_B \right] X' \\ &\approx k_z \left[C_{y\beta} \bar{C}_{n_R} + k_R \bar{C}_{n\beta} + k_R C_{y\delta_R} C_{y\beta} \left(\frac{\bar{C}_{n\beta}}{C_{y\beta}} - \frac{\bar{C}_{n\delta_R}}{C_{y\delta_R}} \right) K'_B \right] X' \end{aligned} \quad (\text{B.245})$$

given the simplifying assumption of equation (B.228) and the constraints below,

$$\left| C_{y_R} \frac{C_{y\delta_R}}{\bar{C}_{n\delta_R}} \left(\frac{\bar{C}_{n_R}}{C_{y_R}} - \frac{\bar{C}_{n\delta_R}}{C_{y\delta_R}} \right) \frac{K'_B}{K'_R} \right| \ll 1 \quad (\text{B.246})$$

$$\left| C_{y\delta_R} \frac{C_{y\beta}}{\bar{C}_{n\beta}} \left(\frac{\bar{C}_{n\beta}}{C_{y\beta}} - \frac{\bar{C}_{n\delta_R}}{C_{y\delta_R}} \right) K'_R \right| \ll |k_R| \quad (\text{B.247})$$

These constraints become,

$$\left| \frac{K'_B}{K'_R} \right| \ll \left| \frac{1}{C_{y\beta}} \frac{l'_F}{l'_D - l'_F} \right| \quad (\text{B.248})$$

$$\left| K'_R \right| \ll \left| \frac{k_R}{C_{y\delta_R}} \frac{l'_W}{(l'_W - l'_F)} \right| \quad (\text{B.249})$$

when the characteristic lengths of equations (5.102) to (5.104) are substituted. Given the desired directional dynamics characteristic equation,

$$\alpha_c(s') = (s')^2 + \alpha_1 s' + \alpha_0 \quad (\text{B.250})$$

the coefficients of the characteristic polynomials of equations (B.241) and (B.250) can be matched,

$$\alpha_1 = -\left(C_{y\beta} + k_z \bar{C}_{n_R} - k_z \bar{C}_{n_{\delta_R}} K'_R \right) X' \quad (\text{B.251})$$

$$\alpha_0 = k_z \left[C_{y\beta} \bar{C}_{n_R} + k_R \bar{C}_{n_\beta} + k_R C_{y\delta_R} C_{y\beta} \left(\frac{\bar{C}_{n_\beta}}{C_{y\beta}} - \frac{\bar{C}_{n_{\delta_R}}}{C_{y\delta_R}} \right) K'_B \right] X' \quad (\text{B.252})$$

to yield the feedback gains,

$$K'_R = \frac{1}{k_z \bar{C}_{n_{\delta_R}}} \left[C_{y\beta} + k_z \bar{C}_{n_R} + \alpha_1 \left(1 + K'_B C_{y\delta_R} \right) \right] \quad (\text{B.253})$$

$$K'_B = \frac{k_z C_{y\beta} \bar{C}_{n_R} + k_z k_R \bar{C}_{n_\beta} - \alpha_0}{C_{y\delta_R} \left[\alpha_0 - k_R k_z C_{y\beta} \left(\frac{\bar{C}_{n_\beta}}{C_{y\beta}} - \frac{\bar{C}_{n_{\delta_R}}}{C_{y\delta_R}} \right) \right]} \quad (\text{B.254})$$

Considering now the special case of the control law when the lateral specific acceleration feedback gain is manually set to zero. The closed loop characteristic equation becomes,

$$\alpha_c(s') = (s')^2 - \left(C_{y\beta} + k_z \bar{C}_{n_R} - k_z \bar{C}_{n_{\delta_R}} K'_R \right) s' + k_z \left(C_{y\beta} \bar{C}_{n_R} + k_R \bar{C}_{n_\beta} \right) \quad (\text{B.255})$$

and the feedback gain K'_R only influences the closed loop system's damping. Given the desired damping ratio ζ the feedback gains are,

$$K'_R = \frac{1}{k_z \bar{C}_{n_{\delta_R}}} \left(C_{y\beta} + k_z \bar{C}_{n_R} + 2\zeta \omega_n \right) \quad (\text{B.256})$$

$$K'_B = 0 \quad (\text{B.257})$$

with the natural frequency equal to its open loop value of,

$$\omega'_n = \sqrt{k_z \left(C_{y\beta} \bar{C}_{n_r} + k_R \bar{C}_{n_\beta} \right)} \quad (\text{B.258})$$

B.5.9 NNDT rudder to lateral specific acceleration steady state gain

The closed loop dynamics after the stability augmentation control law has been implemented can be written as follows,

$$\bar{\mathbf{x}}' = \mathbf{A}' \mathbf{x}' + \mathbf{B}' \delta'_{R_r} \quad (\text{B.259})$$

$$\mathbf{B}'_W = \mathbf{C}' \mathbf{x}' + \mathbf{D}' \delta'_{R_r} \quad (\text{B.260})$$

where the state space matrices are,

$$\mathbf{A}' = \begin{bmatrix} C_{y\beta} - K'_B C_{y\beta} C_{y\delta_r} X' & -k_R - \bar{K}'_R C_{y\delta_r} X' \\ k_z \bar{C}_{n_\beta} - K'_B C_{y\beta} k_z \bar{C}_{n_{\delta_r}} X' & k_z \bar{C}_{n_r} - \bar{K}'_R k_z \bar{C}_{n_{\delta_r}} X' \end{bmatrix} \quad \mathbf{B}' = \begin{bmatrix} C_{y\delta_r} X' \\ k_z \bar{C}_{n_{\delta_r}} X' \end{bmatrix} \quad (\text{B.261})$$

$$\mathbf{C}' = \left[C_{y\beta} X' \quad \left(C_{y_r} - K'_R C_{y\delta_r} \right) X' \right] \quad \mathbf{D}' = C_{y\delta_r} X' \quad (\text{B.262})$$

and the aileron and attitude angle couplings have been ignored. The steady state gain from the rudder input through to the lateral specific acceleration can be written as follows,

$$K'_{ss} = \frac{\mathbf{C}' \text{adj}(-\mathbf{A}') \mathbf{B}' + \mathbf{D}' \det(-\mathbf{A}')}{\det(-\mathbf{A}')} \quad (\text{B.263})$$

The determinant in the above equation is simply obtained by substituting $s' = 0$ into equation (B.241). Calculating the first term in the numerator of equation (B.263) yields,

$$\begin{aligned} \mathbf{C} \text{adj}(-\mathbf{A}) \mathbf{B} &= -(X')^2 \begin{bmatrix} C_{y\beta} & C_{y_r} - K'_R C_{y\delta_r} \end{bmatrix} \begin{bmatrix} k_z \bar{C}_{n_r} - \bar{K}'_R k_z \bar{C}_{n_{\delta_r}} X' & k_R + \bar{K}'_R C_{y\delta_r} X' \\ -k_z \bar{C}_{n_\beta} + K'_B C_{y\beta} k_z \bar{C}_{n_{\delta_r}} X' & C_{y\beta} - K'_B C_{y\beta} C_{y\delta_r} X' \end{bmatrix} \begin{bmatrix} C_{y\delta_r} \\ k_z \bar{C}_{n_{\delta_r}} \end{bmatrix} \\ &= -k_z (X')^2 \begin{bmatrix} C_{y\beta} & C_{y_r} - K'_R C_{y\delta_r} \end{bmatrix} \begin{bmatrix} C_{y\delta_r} \bar{C}_{n_r} + k_R \bar{C}_{n_{\delta_r}} \\ \bar{C}_{n_{\delta_r}} C_{y\beta} - C_{y\delta_r} \bar{C}_{n_\beta} \end{bmatrix} \\ &= -k_z (X')^2 \left[C_{y\beta} \left(C_{y\delta_r} \bar{C}_{n_r} + k_R \bar{C}_{n_{\delta_r}} \right) + \left(C_{y_r} - K'_R C_{y\delta_r} \right) \left(\bar{C}_{n_{\delta_r}} C_{y\beta} - C_{y\delta_r} \bar{C}_{n_\beta} \right) \right] \\ &= k_z (X')^2 C_{y\delta_r} \left[-C_{y\beta} \bar{C}_{n_r} - k_R C_{y\beta} \frac{\bar{C}_{n_{\delta_r}}}{C_{y\delta_r}} + C_{y_r} C_{y\beta} \left(\frac{\bar{C}_{n_\beta}}{C_{y\beta}} - \frac{\bar{C}_{n_{\delta_r}}}{C_{y\delta_r}} \right) - C_{y\delta_r} C_{y\beta} \left(\frac{\bar{C}_{n_\beta}}{C_{y\beta}} - \frac{\bar{C}_{n_{\delta_r}}}{C_{y\delta_r}} \right) K'_R \right] \end{aligned} \quad (\text{B.264})$$

The complete numerator calculation is then,

$$\begin{aligned}
N &= k_z (X')^2 C_{y\delta_R} \left[\begin{aligned} &-C_{y\beta} \bar{C}_{n_R} - k_R C_{y\beta} \frac{\bar{C}_{n\delta_R}}{C_{y\delta_R}} + C_{y\beta} C_{y_R} \left(\frac{\bar{C}_{n\beta}}{C_{y\beta}} - \frac{\bar{C}_{n\delta_R}}{C_{y\delta_R}} \right) - C_{y\delta_R} C_{y\beta} \left(\frac{\bar{C}_{n\beta}}{C_{y\beta}} - \frac{\bar{C}_{n\delta_R}}{C_{y\delta_R}} \right) K'_R \\ &+ C_{y\beta} \bar{C}_{n_R} + k_R \bar{C}_{n\beta} + C_{y\delta_R} C_{y\beta} \left(\frac{\bar{C}_{n\beta}}{C_{y\beta}} - \frac{\bar{C}_{n\delta_R}}{C_{y\delta_R}} \right) K'_R + C_{y\delta_R} C_{y\beta} \left(\frac{\bar{C}_{n\beta}}{C_{y\beta}} - \frac{\bar{C}_{n\delta_R}}{C_{y\delta_R}} \right) (k_R + C_{y_R}) K'_B \end{aligned} \right] \\
&= k_z (X')^2 C_{y\delta_R} \left[\begin{aligned} &k_R C_{y\beta} \left(\frac{\bar{C}_{n\beta}}{C_{y\beta}} - \frac{\bar{C}_{n\delta_R}}{C_{y\delta_R}} \right) + C_{y\beta} C_{y_R} \left(\frac{\bar{C}_{n\beta}}{C_{y\beta}} - \frac{\bar{C}_{n\delta_R}}{C_{y\delta_R}} \right) + C_{y\delta_R} C_{y\beta} \left(\frac{\bar{C}_{n\beta}}{C_{y\beta}} - \frac{\bar{C}_{n\delta_R}}{C_{y\delta_R}} \right) (k_R + C_{y_R}) K'_B \end{aligned} \right] \quad (\text{B.265}) \\
&= k_z X' C_{y\delta_R} C_{y\beta} \left(\frac{\bar{C}_{n\beta}}{C_{y\beta}} - \frac{\bar{C}_{n\delta_R}}{C_{y\delta_R}} \right) (k_R + C_{y_R}) \\
&\approx k_R k_z X' C_{y\delta_R} C_{y\beta} \left(\frac{\bar{C}_{n\beta}}{C_{y\beta}} - \frac{\bar{C}_{n\delta_R}}{C_{y\delta_R}} \right)
\end{aligned}$$

where the numerator has been denoted by N . Note that the determinant was substituted from equation (B.241) before any of the simplifying assumptions were made and thus the only simplifying assumption used to arrive at the result above is that of equation (B.228). Combining equations (B.265) and (B.250) gives the steady state gain,

$$K'_{ss} = k_R k_z C_{y\delta_R} C_{y\beta} \left(\frac{\bar{C}_{n\beta}}{C_{y\beta}} - \frac{\bar{C}_{n\delta_R}}{C_{y\delta_R}} \right) \frac{1}{\alpha_0} (1 + K'_B C_{y\delta_R})^{-1} \quad (\text{B.266})$$

where the constraint of equation (B.249) is required if α_0 is to be used in the equation above.

Appendix C

Example Aircraft Data

The geometric, inertial, aerodynamic and propulsion parameters of the three example aircraft used in Chapter 8 are provided in this appendix.

C.1 Aerobatic aircraft

The aerobatic aircraft is a CAP 232 0.90 size model aircraft fitted with a GMS 1.20 cubic inch methanol engine. The parameters for this UAV were extracted from [13]. They are summarised below.

Inertia:

$$m = 5.0 \text{ kg} \quad (\text{C.1})$$

$$\mathbf{I}_B = \begin{bmatrix} 0.200 & 0 & 0 \\ 0 & 0.360 & 0 \\ 0 & 0 & 0.525 \end{bmatrix} \text{ kgm}^2 \quad (\text{C.2})$$

Geometry:

$$\bar{c} = 0.30 \text{ m} \quad (\text{C.3})$$

$$b = 1.73 \text{ m} \quad (\text{C.4})$$

$$S = 0.50 \text{ m}^2 \quad (\text{C.5})$$

$$A = 5.97 \quad (\text{C.6})$$

Aerodynamic:

$$e = 0.85 \quad C_{D_0} = 0.0200 \quad (\text{C.7})$$

$$C_{L_0} = 0.0 \quad C_{L_\alpha} = 5.1309 \quad C_{L_Q} = 7.7330 \quad C_{L_{\delta_E}} = 0.7126 \quad (\text{C.8})$$

$$C_{m_0} = 0.0 \quad C_{m_\alpha} = -0.2954 \quad C_{m_Q} = -10.281 \quad C_{m_{\delta_E}} = -1.5852 \quad (\text{C.9})$$

$$C_{Y_\beta} = -0.2777 \quad C_{Y_p} = 0.0102 \quad C_{Y_R} = 0.2122 \quad C_{Y_{\delta_A}} = -0.0077 \quad C_{Y_{\delta_R}} = 0.2303 \quad (\text{C.10})$$

$$C_{I_\beta} = -0.0331 \quad C_{I_p} = -0.4248 \quad C_{I_R} = 0.0450 \quad C_{I_{\delta_A}} = -0.3731 \quad C_{I_{\delta_R}} = 0.0080 \quad (\text{C.11})$$

$$C_{n_\beta} = 0.0860 \quad C_{n_p} = -0.0251 \quad C_{n_R} = -0.1250 \quad C_{n_{\delta_A}} = -0.0065 \quad C_{n_{\delta_R}} = -0.1129 \quad (\text{C.12})$$

Propulsion:

$$\tau_T = 0.25 \text{ s} \quad (\text{C.13})$$

$$T_{\max} = 70 \text{ N} \quad (\text{C.14})$$

C.2 Variable stability aircraft

The variable stability aircraft is an electrically powered, blended-wing-body UAV with an in flight adjustable centre of mass. Varying the centre of mass position changes the longitudinal static stability of the aircraft. Consequently the longitudinal aerodynamic stability and control derivatives listed below are a function of the centre of mass position. The parameters for this aircraft were obtained from [48].

Inertia:

$$m = 3.2 \text{ kg} \quad (\text{C.15})$$

$$\mathbf{I}_B = \begin{bmatrix} 0.192 & 0 & 0 \\ 0 & 0.055 & 0 \\ 0 & 0 & 0.251 \end{bmatrix} \text{ kgm}^2 \quad (\text{C.16})$$

Geometry:

$$\bar{c} = 0.25 \text{ m} \quad (\text{C.17})$$

$$b = 1.70 \text{ m} \quad (\text{C.18})$$

$$S = 0.385 \text{ m}^2 \quad (\text{C.19})$$

$$A = 7.50 \quad (\text{C.20})$$

Aerodynamic:

$$e = 0.85 \quad C_{D_0} = 0.0183 \quad (\text{C.21})$$

$$C_{L_0} = 0.0633 \quad C_{L_\alpha} = f_{L_\alpha}(\Delta_{cg}) \quad C_{L_Q} = f_{L_Q}(\Delta_{cg}) \quad C_{L_{\delta_E}} = f_{L_{\delta_E}}(\Delta_{cg}) \quad (\text{C.22})$$

$$C_{m_0} = 0.0 \quad C_{m_\alpha} = f_{m_\alpha}(\Delta_{cg}) \quad C_{m_Q} = f_{m_Q}(\Delta_{cg}) \quad C_{m_{\delta_E}} = f_{m_{\delta_E}}(\Delta_{cg}) \quad (\text{C.23})$$

$$C_{y_\beta} = -0.5404 \quad C_{y_p} = -0.2136 \quad C_{y_R} = 0.2399 \quad C_{y_{\delta_A}} = -0.0945 \quad C_{y_{\delta_R}} = 0.3682 \quad (\text{C.24})$$

$$C_{l_p} = -0.2381 \quad C_{l_r} = -0.4851 \quad C_{l_R} = 0.1694 \quad C_{l_{\delta_A}} = -0.3521 \quad C_{l_{\delta_R}} = 0.1058 \quad (\text{C.25})$$

$$C_{n_p} = 0.0654 \quad C_{n_r} = -0.0020 \quad C_{n_R} = -0.0350 \quad C_{n_{\delta_A}} = 0.0023 \quad C_{n_{\delta_R}} = -0.0477 \quad (\text{C.26})$$

where,

$$f_{L_a}(\Delta_{cg}) = 4.3000 + (1.2828\Delta_{cg} - 8.7407\Delta_{cg}^2) \quad (\text{C.27})$$

$$f_{L_q}(\Delta_{cg}) = 4.0543 + (-34.9717\Delta_{cg}) \quad (\text{C.28})$$

$$f_{L_{\delta_E}}(\Delta_{cg}) = 1.6524 + (0.6603\Delta_{cg} - 5.0574\Delta_{cg}^2) \quad (\text{C.29})$$

$$f_{m_z}(\Delta_{cg}) = -0.1286 + (17.0453\Delta_{cg}) \quad (\text{C.30})$$

$$f_{m_q}(\Delta_{cg}) = -1.6945 + (16.5444\Delta_{cg} - 133.2634\Delta_{cg}^2) \quad (\text{C.31})$$

$$f_{m_{\delta_E}}(\Delta_{cg}) = -0.4582 + (6.4093\Delta_{cg}) \quad (\text{C.32})$$

with Δ_{cg} the change in the centre of mass position relative to the nominal, most forward centre of mass position. The centre of mass change is controlled to lie in the range,

$$\Delta_{cg} \in [0.0, 0.02] \text{ m} \quad (\text{C.33})$$

Notice that the variation in the lateral parameters with the centre of mass position has been ignored in the model due to its weak dependency. The functions of equations (C.27) to (C.32) are all least squared fits of an appropriate order to the longitudinal aerodynamic data over centre of mass position.

Propulsion:

$$\tau_T = 0.2 \text{ s} \quad (\text{C.34})$$

$$T_{\max} = 20 \text{ N} \quad (\text{C.35})$$

C.3 VTOL aircraft

The Vertical Takeoff and Landing (VTOL) aircraft is an experimental custom made tail-sitter UAV. The aircraft has two electric motors mounted on the wings and a number of aerodynamic actuators to allow for control in both hover and forward flight states. The aircraft parameters were obtained from [16].

Inertia:

$$m = 9.0 \text{ kg} \quad (\text{C.36})$$

$$\mathbf{I}_B = \begin{bmatrix} 0.888 & 0 & 0 \\ 0 & 0.421 & 0 \\ 0 & 0 & 1.243 \end{bmatrix} \text{kgm}^2 \quad (\text{C.37})$$

Geometry:

$$\bar{c} = 0.37 \text{ m} \quad (\text{C.38})$$

$$b = 1.57 \text{ m} \quad (\text{C.39})$$

$$S = 0.57 \text{ m}^2 \quad (\text{C.40})$$

$$A = 4.29 \quad (\text{C.41})$$

Aerodynamic:

$$e = 0.85 \quad C_{D_0} = 0.0272 \quad (\text{C.42})$$

$$C_{L_0} = 0.0 \quad C_{L_\alpha} = 4.1877 \quad C_{L_Q} = 8.1626 \quad C_{L_{\delta E}} = C_{L_{\delta ET}} + k_E C_{L_{\delta FH}} \quad (\text{C.43})$$

$$C_{m_0} = 0.0 \quad C_{m_\alpha} = -1.6147 \quad C_{m_Q} = -7.6367 \quad C_{m_{\delta E}} = C_{m_{\delta ET}} + k_E C_{m_{\delta FH}} \quad (\text{C.44})$$

$$C_{Y_\beta} = -1.7190 \quad C_{Y_p} = 0.2557 \quad C_{Y_R} = 1.1875 \quad C_{Y_{\delta A}} = 0.0009 \quad C_{Y_{\delta R}} = C_{Y_{\delta RF}} + k_R C_{Y_{\delta FV}} \quad (\text{C.45})$$

$$C_{l_\beta} = -0.0043 \quad C_{l_p} = -0.6566 \quad C_{l_R} = 0.1039 \quad C_{l_{\delta A}} = -0.2193 \quad C_{l_{\delta R}} = C_{l_{\delta RF}} + k_R C_{l_{\delta FV}} \quad (\text{C.46})$$

$$C_{n_\beta} = 0.4745 \quad C_{n_p} = -0.0689 \quad C_{n_R} = -0.3359 \quad C_{n_{\delta A}} = 0.0186 \quad C_{n_{\delta R}} = C_{n_{\delta RF}} + k_R C_{n_{\delta FV}} \quad (\text{C.47})$$

with,

$$C_{L_{\delta ET}} = 1.2434 \quad C_{L_{\delta FH}} = 0.7479 \quad (\text{C.48})$$

$$C_{m_{\delta ET}} = -1.8088 \quad C_{m_{\delta FH}} = -0.0827 \quad (\text{C.49})$$

$$C_{Y_{\delta RF}} = 1.0078 \quad C_{Y_{\delta FV}} = 0.3113 \quad (\text{C.50})$$

$$C_{l_{\delta RF}} = -0.0410 \quad C_{l_{\delta FV}} = -0.0033 \quad (\text{C.51})$$

$$C_{n_{\delta RF}} = -0.3885 \quad C_{n_{\delta FV}} = -0.0173 \quad (\text{C.52})$$

and,

$$k_E = -1 \quad (\text{C.53})$$

$$k_R = -2.5 \quad (\text{C.54})$$

Propulsion:

$$\tau_T = 0.25 \text{ s} \quad (\text{C.55})$$

$$T_{\max} = 120 \text{ N} \quad (\text{C.56})$$

Bibliography

- [1] M.T. DeGarmo. *Issues Concerning Integration of Unmanned Aerial Vehicles in Civil Airspace*. The MITRE Corporation MP 04W0000323, November 2004.
- [2] J.M. Sullivan. “Evolution or Revolution? The Rise of UAVs”. *IEEE Technology and Society Magazine*, 2006.
- [3] M.J. Jordan. *Merging the Tribes: Streamlining DOD’s Acquisition of Unmanned Aerial Systems*. Masters thesis, U.S. Army War College, March 2006.
- [4] A.M.G. Walan. *Application of Maneuver-Based Control in Variable Autonomy Unmanned Combat Aerial Vehicles*. Air Force Institute of Technology, March 2003.
- [5] Office of the Secretary of Defence. *Unmanned Aerial Vehicles Roadmap 2000 – 2025*. April 2001.
- [6] N. Carstens. *Development of a Low-Cost and Low-Weight Flight Control System for an Electrically Powered Free-Flying Model Helicopter*. Masters thesis, Stellenbosch University, April 2005.
- [7] I.K. Peddle. *Autonomous Flight of a Model Aircraft*. Masters thesis, Stellenbosch University, April 2005.
- [8] I.K. Peddle, G.W. Milne. “Development of a Low Cost Waypoint Navigation Autopilot for an Unmanned Aerial Vehicle”. *SAIMechE R&D Journal*, 23(2), July 2007.
- [9] S. Groenewald. *Development of a Rotary-Wing Test Bed for Autonomous Flight*. Masters thesis, Stellenbosch University, April 2006.
- [10] J. Venter. *Development of an Experimental Tilt-Wing VTOL Unmanned Aerial Vehicle*. Masters thesis, Stellenbosch University, April 2006.
- [11] J.C. Roos. *Autonomous Take-Off and Landing of a Fixed Wing Unmanned Aerial Vehicle*. Masters thesis, Stellenbosch University, March 2007.
- [12] J.C. Roos, I.K. Peddle. “Autonomous Take-Off and Landing of a Low Cost Unmanned Aerial Vehicle”, *Submitted to Control Engineering Practice (in review)*, January 2008.
- [13] W.J. Hough. *Autonomous Aerobatic Flight of a Fixed Wing Unmanned Aerial Vehicle*. Masters thesis, Stellenbosch University, March 2007.

- [14] L.E. Rossouw. *Autonomous Flight of an Unmanned Helicopter*. Masters thesis, Stellenbosch University, March 2008.
- [15] C. Van Schalkwyk. *Full State Control of a Fury X-Cell Unmanned Helicopter*. Masters thesis, Stellenbosch University, To be submitted.
- [16] S.C. Kriel. *A Comparison of Control Systems for the Flight Transition of VTOL Unmanned Aerial Vehicles*, Masters thesis, Stellenbosch University, March 2008.
- [17] J.E. Wilson. *Hover Control for a Vertical Take-Off and Landing Vehicle*. Masters thesis, Stellenbosch University, To be submitted.
- [18] I.K. Peddle, T. Jones, J. Treurnicht. "Practical Near Hover Flight Control of a Ducted Fan (SLADe)". *Accepted at Control Engineering Practice*, November 2007.
- [19] J.H. Blakelock. *Automatic Control of Aircraft and Missiles, Second Edition*. John Wiley and Sons, New York, 1991.
- [20] A.E. Bryson Jr. *Control of Spacecraft and Aircraft*. Princeton University Press, NJ, 1994.
- [21] J.H. Kim, S. Wishart, S. Sukkarieh. "Real-time Navigation, Guidance and Control of a UAV using Low-cost Sensors". *International Conference of Field and Service Robotics (FSR03)*, Japan, July 2003.
- [22] D. Kingston, R. Beard, T. McLain, M. Larsen, W. Ren. "Autonomous Vehicle Technologies for Small Fixed-wing UAVs". *AIAA 2nd Unmanned Unlimited Systems, Technologies and Operations Conference*, San Diego, CA, September 2003.
- [23] B. Taylor, C. Bil, S. Watkins, G. Egan. "Horizon Sensing Attitude Stabilisation: A VMC Autopilot". *In the 18th International UAV Systems Conference*, Bristol, UK, 2003.
- [24] S. Park. *Avionics and Control Systems Development for Mid-Air Rendezvous of Two Unmanned Aerial Vehicles*. PhD dissertation, Massachusetts Institute of Technology, 2004
- [25] D.J. Leith, W.E. Leithead. "Survey of Gain Scheduling Analysis & Design". *International Journal of Control*, 1999.
- [26] J.E. Slotine, W. Li. *Applied Nonlinear Control*. Prentice Hall, NJ, 1991.
- [27] S.H. Lane, R.F. Stengel. "Flight Control Design Using Non-Linear Inverse Dynamics". *Automatica*, 24(4), 471-483, 1988.
- [28] D.J. Bugajski, D.F. Enns. "Nonlinear Control Law with Application to High Angle-of-Attack Flight". *Journal of Guidance, Control and Dynamics*, 15(3), 761-767, 1992.

- [29] S.A. Snell, D.F. Enns, W.L. Garrard. "Nonlinear Inversion Flight Control for a Supermaneuverable Aircraft". *Journal of Guidance, Control and Dynamics*, 15(4), 976-984, 1992.
- [30] J. Reiner, G.J. Balas, W.L. Garrard. "Flight Control Design Using Robust Dynamic Inversion and Time-scale Separation". *Automatica*, 32(11), 1493-1504, 1996.
- [31] J. Buffington, R. Adams, S. Banda. "Robust, Nonlinear, High Angle-of-Attack Control Design for a Supermaneuverable Vehicle". *Proceedings of the AIAA Guidance, Navigation and Control Conference*, Monterey, CA (pp. 690-700), 1993.
- [32] J. Hauser, S. Sastry, G. Meyer. "Nonlinear Control Design for Slightly Non-Minimum Phase Systems: Application to V/STOL Aircraft". *Automatica*, 28(4), 665-679, 1992.
- [33] S.A. Al-Hiddabi, N.H. McClamroch. "Aggressive Longitudinal Aircraft Trajectory Tracking Using Nonlinear Control". *Journal of Guidance, Control and Dynamics*, 25(1), 26-32, 2002.
- [34] R.B. Miller, M. Pachter. "Maneuvering Flight Control with Actuator Constraints". *Journal of Guidance, Control and Dynamics*, 20(4), 729-735, 1997.
- [35] M. Pachter, P.R. Chandler, L. Smith. "Maneuvering Flight Control". *Journal of Guidance, Control and Dynamics*, 21(3), 368-374, 1998.
- [36] R. Bhattacharya, G.J. Balas, M.A. Kaya, A. Packard. "Nonlinear Receding Horizon Control of an F-16 Aircraft". *Journal of Guidance, Control and Dynamics*, 20(5), 924-931, 2002.
- [37] M.J. Kim, W.H. Kwon, Y.H. Kim, C. Song. "Autopilot Design for Bank-to-Turn Missiles Using Receding Horizon Predictive Control Scheme". *Journal of Guidance, Control and Dynamics*, 20(6), 1248-1254, 1997.
- [38] S.J. Qin, T.A. Badgwell. "A Survey of Industrial Model Predictive Control Technology". *Control Engineering Practice*, Vol 11, 733-764, 2003.
- [39] E.F. Camacho, C. Bordons. *Model Predictive Control*. Springer, London, 1999.
- [40] D.P. Boyle, G.E. Chamitoff. "Autonomous Maneuver Tracking for Self-Piloted Vehicles". *Journal of Guidance, Control and Dynamics*, 22(1), 58-68, 1999.
- [41] B. Etkin. *Dynamics of Atmospheric Flight*. John Wiley & Sons, 1972.
- [42] M.V. Cook. *Flight Dynamics Principles*. Elsevier Butterworth-Heinemann, 1997.
- [43] B. Etkin, L.D. Reid. *Dynamics of Flight, Stability and Control, 3rd Ed.* John Wiley & Sons, 1996.

- [44] J.S. Freudenberg, D.P. Looze. "Right-half Plane Poles and Zeros and Design Tradeoffs in Feedback Systems". *IEEE Transactions on Automatic Control*, 30(6), 555-565, 1985.
- [45] G.C. Goodwin, S.F. Graebe, M.E. Salgado. *Control System Design*. Prentice Hall, New Jersey, 2001.
- [46] H. Bode. *Network Analysis and Feedback Amplifier Design*. Van Nostrand, New York, 1945.
- [47] G.F. Franklin, J.D. Powell, A. Emami-Naeini. *Feedback Control of Dynamic Systems, 4th Ed.* Prentice Hall, NJ, 2002.
- [48] D. Blaauw. *Control of a Variable Stability Aircraft*. Masters Thesis, Stellenbosch University, To be Submitted.
- [49] D.C. Lay. *Linear Algebra and its Applications, 2nd Ed.* Addison-Wesley, Reading Massachusetts, 1997.
- [50] J. Wittenburg. *Dynamics of Systems of Rigid Bodies*. Teubner, Stuttgart, 1977.